Mineralogical Magazine (2020), **84**, 165–244
doi:10.1180/mgm.2020.13

CAMBRIDGE UNIVERSITY PRESS

Special category: Foundations in mineralogy and crystallography

A structure hierarchy for silicate minerals: chain, ribbon, and tube silicates

Maxwell C. Day and Frank C. Hawthorne*
Department of Geological Sciences, University of Manitoba, Winnipeg, Manitoba R3T 2N2 Canada

Abstract

A structure hierarchy is developed for chain-, ribbon- and tube-silicate based on the connectedness of one-dimensional polymerisations of $(TO_4)^{n-}$ tetrahedra, where T = Si^{4+} plus P^{5+}, V^{5+}, As^{5+}, Al^{3+}, Fe^{3+}, B^{3+}, Be^{2+}, Zn^{2+} and Mg^{2+}. Such polymerisations are described by a *geometrical repeat unit* (with n_g tetrahedra) and a *topological repeat unit* (or graph) (with n_t vertices). The connectivity of the tetrahedra (vertices) in the geometrical (topological) repeat units is denoted by the expression ${}^cT_r$ (${}^cV_r$) where c is the connectivity (degree) of the tetrahedron (vertex) and r is the number of tetrahedra (vertices) of connectivity (degree) c in the repeat unit. Thus ${}^cT_r = {}^1T_{r1}{}^2T_{r2}{}^3T_{r3}{}^4T_{r4}$ (${}^cV_r = {}^1V_{r1}{}^2V_{r2}{}^3V_{r3}{}^4V_{r4}$) represents all possible connectivities (degrees) of tetrahedra (vertices) in the geometrical (topological) repeat units of such one-dimensional polymerisations. We may generate all possible ${}^cT_r$ (${}^cV_r$) expressions for chains (graphs) with tetrahedron (vertex) connectivities (degrees) $c = 1$ to 4 where $r = 1$ to n by sequentially increasing the values of c and r, and by ranking them accordingly. The silicate (*sensu lato*) units of chain-, ribbon- and tube-silicate minerals are identified and associated with the relevant ${}^cT_r$ (${}^cV_r$) symbols. Following description and association with the relevant ${}^cT_r$ (${}^cV_r$) symbols of the silicate units in all chain-, ribbon- and tube-silicate minerals, the minerals are arranged into decreasing O:T ratio from 3.0 to 2.5, an arrangement that reflects their increasing structural connectivity. Considering only the silicate component, the compositional range of the chain-, ribbon- and tube-silicate minerals strongly overlaps that of the sheet-silicate minerals. Of the chain-, ribbon- and tube-silicates and sheet silicates with the same O:T ratio, some have the same ${}^cV_r$ symbols (vertex connectivities) but the tetrahedra link to each other in different ways and are topologically different. The abundance of chain-, ribbon- and tube-silicate minerals decreases as O:T decreases from 3.0 to 2.5 whereas the abundance of sheet-silicate minerals increases from O:T = 3.0 to 2.5 and decreases again to O:T = 2.0. Some of the chain-, ribbon- and tube-silicate minerals have more than one distinct silicate unit: (1) vinogradovite, revdite, lintisite (punkaruaivite) and charoite have mixed chains, ribbons and/or tubes; (2) veblenite, yuksporite, miserite and okenite have clusters or sheets in addition to chains, ribbons and tubes. It is apparent that some chain-ribbon-tube topologies are favoured over others as of the ~450 inosilicate minerals, ~375 correspond to only four topologically unique graphs, the other ~75 minerals correspond to ~46 topologically unique graphs.

Keywords: structure hierarchy, chain-silicate mineral, ribbon-silicate mineral, tube-silicate mineral, structural connectivity, stoichiometry

(Received 18 November 2019; accepted 23 February 2020; Accepted Manuscript published online: 26 February 2020; Associate Editor: Irina O Galuskina)

Introduction

The organisation of minerals based on their structural and chemical properties is central to the field of Mineralogy. In recent years, work has focused on developing structure hierarchies for mineral groups previously classified on the basis of chemical composition. In mathematical terms, a hierarchy is an ordered set of elements where the ordering reflects a natural hierarchical relation between the arrangements of elements. In mineralogical terms, a structure hierarchy is a set of structures ordered according to the polymerisation of coordination polyhedra of higher bond-valence (Hawthorne, 1983*a*, 2014) from lower to higher connectivity. Structure hierarchies have been developed for phosphates, arsenates and vanadates (Kostov and Breskovska, 1989), phosphates (Hawthorne, 1998; Huminicki and Hawthorne, 2002), arsenates (Majzlan *et al.*, 2014), vanadium bronzes (Evans and Hughes, 1990), sulfates (Sabelli and Trosti-Ferroni, 1985; Hawthorne *et al.*, 2000), tellurium oxycompounds (Christy *et al.*, 2016*b*), uranyl oxysalts (Burns, 1999, 2005, Lussier *et al.*, 2016), borates (Burns *et al.*, 1995; Hawthorne *et al.*, 1996; Grice *et al.*, 1999), aluminofluoride minerals (Hawthorne, 1984), and anion-centered structures (Filatov *et al.*, 1992; Krivovichev, 2008, 2009; Krivovichev and Filatov, 1999*a*,*b*; Krivovichev *et al.*, 1998, 2013). Such hierarchies (1) provide a framework to understand the factors controlling composition and structural variability of minerals, and (2) help link particular chemical compositions and structural arrangements with different crystallisation mechanisms (Hawthorne, 2014, 2018; Schindler *et al.*, 2000, 2006) and paragenetic sequences (Christy *et al.*, 2016*a*). Rather than a synthesis of previous experimental work, they should be viewed as a starting point for further theoretical work.

***Author for correspondence:** Frank C. Hawthorne, Email: frank.hawthorne@umanitoba.ca
Cite this article: Day M.C. and Hawthorne F.C. (2020) A structure hierarchy for silicate minerals: chain, ribbon, and tube silicates. *Mineralogical Magazine* **84**, 165–244. https://doi.org/10.1180/mgm.2020.13

© Mineralogical Society of Great Britain and Ireland 2020

https://doi.org/10.1180/mgm.2020.13 Published online by Cambridge University Press

Previous work on silicate minerals

Currently, there is no comprehensive structure hierarchy for silicate minerals. One might assume that the importance of silicates in crust and mantle processes would be sufficient incentive to develop a coherent structure hierarchy for silicate minerals. However, the large number (~1500 approved by the International Mineralogical Association) of silicate minerals makes this a difficult task.

Following a suggestion by Machatschki (1928), the earliest silicate classification was developed by Bragg (1930), who organised silicate minerals based on the type and degree of linkage of $(TO_4)^{n-}$ tetrahedra. This broad classification scheme is still used today and assigns silicate minerals to six groups: *neso* (ortho-), *soro-*, *cyclo* (ring-), *ino* (chain-), *phyllo* (sheet-), *tecto* (framework-) *silicates* (Bragg, 1930). A few extensions have been made to 'Bragg's classification of silicates' following the discovery and subsequent solution of new silicate structures. Berman (1937) first described $^{[4]}Be^{2+}$ replacing $^{[4]}Si^{4+}$, Strunz (1938) included $^{[4]}P^{5+}$, $^{[4]}As^{5+}$, $^{[4]}Ge^{4+}$, $^{[4]}Ti^{4+}$ and $^{[4]}Fe$, and Zoltai (1960) included most of the remaining ions that replace or show solid solution with $^{[4]}Si^{4+}$. The most significant later contribution to the classification of silicates was made by Belov (1961) who described the various modes of linkage between different coordination polyhedra, specifically in minerals containing large alkali and alkaline-earth cations (Voronkov *et al.*, 1974, 1975; Sandomirskii and Belov, 1984). Zoltai (1960) also described a *sharing-coefficient* between $(TO_4)^{n-}$ tetrahedra and organised silicate structures based on their *repeat units*. Liebau (1985) described silicate units (rings, chains, sheets etc.) using sets of variables including *linkedness, connectedness, branchedness, dimensionality* and *periodicity* and assigned names to such structures (e.g. zero-dimensional dreier double ring, one-dimensional *zweier* triple chain). This work provided detailed descriptions of silicate structures to date, and for many years has been the 'go to' source for crystallographers working on comparative aspects of silicate structures.

Hawthorne *et al.* (2019) dealt with the large number of silicate minerals by dividing them into four categories and considering them separately according to the dimensional polymerisation of their tetrahedra: (1) **cluster silicates** that do not show infinite polymerisation; (2) **chain, ribbon and tube silicates** that are infinitely polymerised in one dimension; (3) **sheet silicates** that are infinitely polymerised in two dimensions; and (4) **framework silicates** that are infinitely polymerised in three dimensions. Hawthorne (2015*a*) and Hawthorne *et al.* (2019) introduced the first comprehensive structure hierarchy for sheet-silicate minerals. Hawthorne (2015*a*) represented sheet structures as *n*-connected plane nets ($2 < n \leq 4$), and showed that combining such nets with topological building operations allows one to generate sheet-silicate structures. Hawthorne (2015*a*) also developed formula- and structure-generating functions to show how the chemical composition and structure of sheet silicates can be algebraically generated from such plane nets and associated building operations. We will use a similar approach for chain-, ribbon- and tube-silicate minerals. Here we develop a structure hierarchy for these minerals and will examine and provide a detailed mathematical description of the topology of chain-, ribbon- and tube-silicate units in a subsequent paper.

Terminology

With such a wide compositional range of minerals and large number of structures, the colour scheme for the various polyhedra is somewhat complicated; we list the general colour scheme in Table 1 and will not refer to this scheme in the figure captions. In some cases, other aspects of a structure need to be emphasised by using the colours that do not correspond to Table 1; where this is done, the colour scheme will be noted in the figure caption. The structure of a given mineral is typically shown in two or three different orientations. The relation between these orientations is shown by outlining the part of the structure in (a) that is shown in (b) or (c) using dashed black lines and the labels (b') and (c'), respectively. This labelling method is not described in the figure captions.

Table 1. Colour scheme for polyhedra and cations.

	Tetrahedra	RGB code*	Cations or polyhedra (CN > 4)	RGB code*
Si	Orange	255–170–85*		
Al	Pale blue	174–189–244	Pale brown	249–211–174
Be	Light green	117–255–117		
B	Blue	000–128–255		
V	Light violet	198–159–240		
As	Light red	240–100–128		
P	Light yellow	235–239–146		
Zn			Green–yellow	209–232–162
Mn			Light teal	187–239–247
Mg			Pale yellow	244–241–128
Na			Light green	152–228–148
Ca			Pale blue	171–172–231
Fe	Purple	200–140–200	Pale pink	247–185–211
Ti			Pale purple	201–164–202
Nb			Yellow–tan	237–239–148
Cu			Teal–green	185–225–210
Ba			Light brown	217–197–167
Li	Light purple	187–187–255	Pale yellow	227–230–136
K			Grey	170–170–170
Sr			Dark green	163–194–160
Sn			Brown–purple	203–156–154
Sc			Light red	239–173–185
Pb			Green	138–200–173
Zr			Light blue	180–180–255
U			Pale green	101–245–188
C			Dark grey	085–085–085
F			Bright green	000–255–000
H^+/H_2O			Red	255–000–000

*Colours are RGB codes from *ATOMS*© (from Shape Software); where colours differ from listed codes refer to the figure caption

Mineral names are written in bold font to aid comparison of different minerals throughout the text. In the tables, we have attempted to write each mineral as the principal end-member formula (Hawthorne, 2002), as this simplifies the connections between mineral composition and bond topology. In the tables, the *silicate unit* (i.e. the silicate part of the structure) is written in bold font and in square brackets, except where there is some question as to the formula of the silicate unit (e.g. where there is significant disorder of the constituents of that unit). Bond-valences were calculated with the parameters of Gagné and Hawthorne (2015). We have also gathered together all the information of Tables 3–9 in an Excel file, so that the information given here can be conveniently retrieved, searched and sorted with a macro that we have written. This file has been deposited as Supplementary material with the Principal Editors of *Mineralogical Magazine* (details below).

Silicate

Where we refer to a silicate unit (e.g. silicate chain, ribbon and/or tube), let it be understood that the unit must contain Si^{4+} but may

https://doi.org/10.1180/mgm.2020.13 Published online by Cambridge University Press

also contain other tetrahedrally coordinated cations: e.g. T = P^{5+}, V^{5+}, As^{5+}, Al^{3+}, Fe^{3+}, B^{3+}, Be^{2+}, Zn^{2+} and Mg^{2+}. For simplicity of expression, we refer to such compositions as silicates, whether or not the dominant tetrahedrally coordinated cation is Si^{4+}, as we require them to contain Si^{4+} as an essential constituent. Chains and ribbons that contain no Si^{4+}-tetrahedra will be discussed if such minerals provide insight into the relation between composition and structure; examples include the aluminate minerals **addibischoffite** and **warkite**. Synthetic compounds will be discussed if they contain chains, ribbons or tubes of Si^{4+}-tetrahedra that are topologically unique or intermediate between other chains in the hierarchy.

We will refer to a tetrahedron or any other higher coordination polyhedron by its central cation if the anions coordinating that cation are solely O^{2-} or if the identity of such anions is unclear. It follows that the expression *Si^{4+}-tetrahedron* (tetrahedrally coordinated Si^{4+}) or *Na^{+}-octahedron* (octahedrally coordinated Na^{+}) represents a $(Si^{4+}O_4)^{4-}$-tetrahedron or a $(Na^{+}O_6)^{11-}$-octahedron, respectively and a 'T-tetrahedron' represents a $(TO^4)^{n-}$ tetrahedron, where T is one or more unspecified tetrahedrally coordinated cation. If the anions that coordinate any given cation are anything other than O^{2-} (i.e. $(OH)^{-}$, (H_2O), F^{-}), the expanded notation for that cation-polyhedron will be given, e.g. $(Na^{+}O_4(OH)_2)^{9-}$-octahedron or $(SiO_3(OH))^{3-}$-tetrahedron. Where coordination number is not expressed in this notation, it will be appended to the central cation of the respective polyhedron or ion (e.g. $^{[7]}Na^{+}$-polyhedron or $^{[8]}Ba^{+}$ ion).

We define chains, ribbons, and tubes of T-tetrahedra as follows:

Chain: a silicate unit of $(TO_4)^{n-}$ tetrahedra that link infinitely in a single direction and that can be broken by eliminating a single linkage between adjacent $(TO_4)^{n-}$ tetrahedra (Fig. 1*a*).

Ribbon: a silicate unit of $(TO_4)^{n-}$ tetrahedra that link infinitely in a single direction and that cannot be broken by eliminating a single linkage between adjacent $(TO_4)^{n-}$ tetrahedra (Fig. 1*b*).

Tube: a silicate unit of $(TO_4)^{n-}$ tetrahedra that link infinitely in a single direction, and also link orthogonal to the direction of polymerisation to form a hollow cylinder. A silicate tube cannot be broken by eliminating a single linkage between adjacent $(TO_4)^{n-}$ tetrahedra (Fig. 1*c*).

For simplicity, we will refer to all chain-, ribbon- and tube-silicate minerals and structures as *chain silicates* and *chains*, respectively. A *layer* is a single planar or semi-planar array of ions. A *sheet* is a single planar or semi-planar array of linked polyhedra.

Low-acidity $^{[4]}$T cations: Alkali metals

There is some ambiguity about the [4]-coordinated ions Li^{+}, Na^{+}, K^{+}, Rb^{+} and Tl^{+}. These ions all have Lewis acidities (Gagné and Hawthorne, 2017) lower than the cut-off of 0.30 vu used by Hawthorne and Schindler (2008) to exclude ions from the structural unit, and using this criterion, we would exclude such ions from the chain. Conversely, from a topological perspective, one might wish to include all tetrahedrally coordinated cations. In some cases, the same structure types may incorporate different cations with a range of valence states at a tetrahedrally coordinated site; for example, in the **milarite** structure (Gagné and Hawthorne, 2016), the *T*2 site in the framework may be occupied by Li^{+} (e.g. berezanskite, Hawthorne *et al.*, 2016; sogdianite; Sokolova *et al.*, 2000), and various divalent (Be^{2+}, Mg^{2+}, Fe^{2+} and Zn^{2+}) and trivalent (B^{3+}, Al^{3+} or Fe^{3+}) cations. It seems undesirable to separate isostructural minerals on the basis of Lewis acidity of the *T* cation and we include such minerals in the same group here.

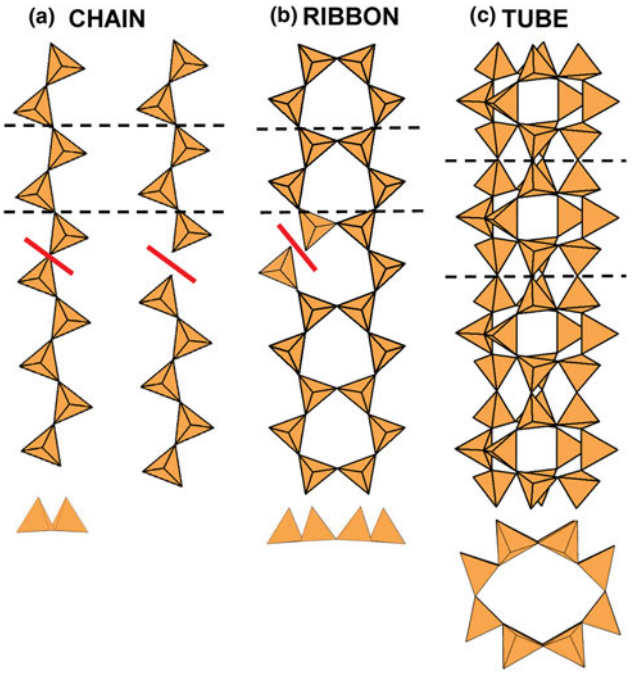

Fig. 1. Definitions of a silicate chain, ribbon and tube: (*a*) a chain: if the linkage between two tetrahedra is broken, the one-dimensional polymerisation is lost; (*b*) a ribbon: if the linkage between two tetrahedra is broken, the one-dimensional polymerisation is not lost; (*c*) a tube: if the linkage between two tetrahedra is broken, the one-dimensional polymerisation is not lost, and also the tetrahedra fold round on themselves perpendicular to the direction of polymerisation to form a hollow cylinder. Dashed black lines show the geometrical repeat unit of the chain, ribbon and tube.

Graphical (topological) and geometrical chain representations

Two- and three-dimensional graphs (or nets) are commonly used to describe and analyse the structures of sheet-silicate and framework-silicate minerals (e.g. Wells, 1962, 1977; Smith, 1977, 1978, 1988; Hawthorne, 2015*a*; Hawthorne and Smith, 1986*a*,*b*, 1988; Hawthorne *et al.*, 2019; Krivovichev, 2008, 2009) and some tubular chain silicates (Rozhdestvenskaya and Krivovichev, 2011). However, there is no complete description of silicate chains, ribbons and tubes as one-dimensional graphs. We will take this approach here as it: (1) leads to compact representations of the connectivity of silicate chains, ribbons and tubes; (2) simplifies comparison of different structures; and (3) facilitates theoretical analysis of all possible chain, ribbon and tube arrangements of polymerised tetrahedra. Here, chain-, ribbon- and tube-silicate structures are commonly shown in three representations: (1) polyhedron representations where $(TO_4)^{n-}$ groups are shown as tetrahedra and the original chain geometry is preserved (Fig. 2*a*); (2) *ball-and-stick* representations in which tetrahedra are represented by points and links between tetrahedra are represented by lines, and the original chain geometry is preserved (Fig. 2*b*); and (3) representations in which the chain is reduced to a graph in which tetrahedra are represented by vertices and linkages between tetrahedra are represented by edges, and the original chain

https://doi.org/10.1180/mgm.2020.13 Published online by Cambridge University Press

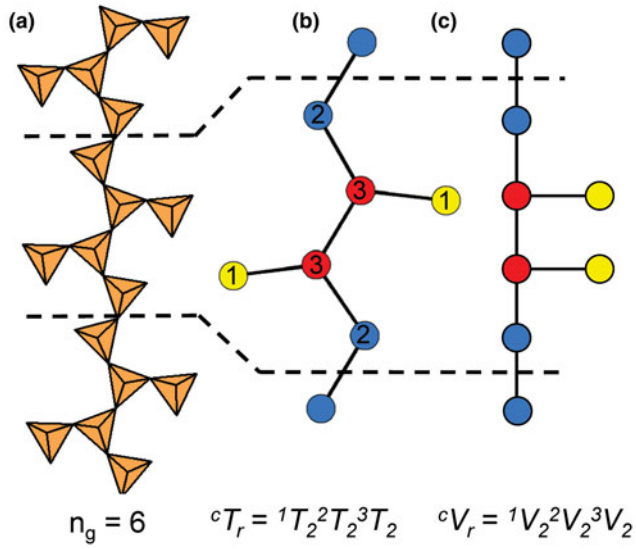

Fig. 2. (*a*) Tetrahedral, (*b*) ball-and-stick and (*c*) graphical representations of the chain in **sapphirine-supergroup** minerals viewed orthogonal to the **c**-axis. Each tetrahedron in (*a*) is represented by a point (ball) in (*b*) and a vertex in (*c*), and all linkages between tetrahedra in (*a*) are represented by lines (sticks) in (*b*) and edges in (*c*) that connect each ball or vertex. Red, blue and yellow points (circles) represent 3–, 2– and 1–connected vertices. Dashed black lines show the geometrical repeat unit in (*a*) and (*b*) and the topological repeat unit in (*c*).

geometry is not preserved (Fig. 2*c*). Throughout this paper, the geometry, topology and connectivity of each chain, ribbon and tube will be described by reducing each chain to a single *repeat unit* that can be linked infinitely by translation in a single direction to produce the chain.

The geometrical repeat unit and the ^cT_r expression

In the tetrahedron and ball-and-stick representations, we assign a *geometrical repeat unit* in which the geometry of the chain (lengths and angles of linkages between tetrahedra) is preserved. The geometrical repeat unit contains the minimum number of tetrahedra (n_g) required to generate the chain through translation operations. It is necessary to specify the numbers of 1-, 2-, 3- and 4-connected tetrahedra that comprise n_g to describe the geometrical repeat unit of a chain. To do this, we denote a tetrahedron by *T*, its connectivity by the superscript *c* (*c* = 1–4) and the number of such tetrahedra in the geometrical repeat unit by the subscript *r*. The expression $^cT_r = {}^1T_r{}^2T_r{}^3T_r{}^4T_r$ represents the possible connectivities of tetrahedra in the repeat unit, and the number of terms with r ≠ 0 in the ^cT_r expression is defined as its rank. The majority of chains contain only 2- and 3-connected vertices (i.e. ^cT_r has a rank of 2 as *r* = 0 for ^1T_r and ^4T_r), but some chains also contain 1- and/or 4-connected vertices. As an example, consider the tetrahedron (Fig. 2*a*) and ball-and-stick (Fig. 2*b*) representations of the $[Si_6O_{18}]^{12-}$ chain in **sapphirine-supergroup** minerals. The ball-and-stick representation shows three types of vertices: 3-connected (red circles), 2-connected (blue circles) and 1-connected (yellow circles) (Fig. 2*b*). The repeat unit contains two of each of these types of vertex ($n_g = 6$), and the ^cT_r expression for the **aenigmatite**-type chain is written as $^cT_r = {}^1T_2{}^2T_2{}^3T_2{}^4T_0 = {}^1T_2{}^2T_2{}^3T_2$ (rank = 3).

We can generate all possible ^cT_r expressions for chains with tetrahedron connectivities, c, of 1, 2, 3 and 4 where *r* = 1 to ∞ by sequentially increasing the values of *c* and *r*. There are various ways in which this may be done. However, the most useful way is to order these in terms of increasing rank of ^cT_r (i.e. the number of individual ^cT_r vaues). For a given rank, we sequentially increase the value of *c* for *r* = 1 to ∞; Table 2 shows the ^cT_r expressions produced in this way. For a rank of 1, where *c* = 1, a chain is not possible: $^1T_1$ corresponds to single tetrahedron; $^1T_2$ corresponds to a $[T_2O_7]$ dimer, and no further linkages are possible without changing the value of *c* (Table 2). Thus, $^2T_1$ is the simplest possible chain arrangement, followed by $^2T_2$, $^2T_3$, $^2T_4$ etc. For higher ranks, we order ^cT_r first in terms of *c* and then in terms of *r*, hence for a rank of 2: $^2T_r{}^3T_r$, we have $^2T_1{}^3T_r$, $^2T_2{}^3T_r$, $^2T_3{}^3T_r$……. etc. Thus we have a rationale for both generating all theoretical chains and ordering observed chains into a preliminary hierarchy.

Table 2. Hierarchical ordering of ^cT_r values where *r* = 1–∞ and *c* = 1–4.

Rank	1	2	3	4
c ↓	^1T_r ^2T_r ^3T_r ^4T_r	$^1T_r{}^2T_r$ $^1T_r{}^3T_r$ $^1T_r{}^4T_r$ $^2T_r{}^3T_r$ $^2T_r{}^4T_r$ $^3T_r{}^4T_r$	$^1T_r{}^2T_r{}^3T_r$ $^1T_r{}^3T_r{}^4T_r$ $^2T_r{}^3T_r{}^4T_r$	$^1T_r{}^2T_r{}^3T_r{}^4T_r$

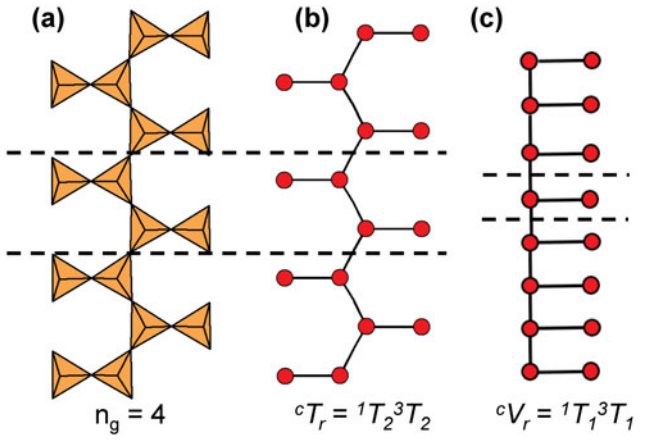

Fig. 3. (*a*) Tetrahedral, (*b*) ball-and-stick and (*c*) graphical representations of the chain in **astrophyllite-supergroup** minerals where $^cT_r \neq {}^cV_r$.

The topological repeat unit

Graphical representations of chains have a *topological repeat unit* in which only the topological properties are preserved. The topological repeat unit contains the minimum number of vertices (n_t) required to generate the chain through infinite linkage in a single direction. By analogy with the geometrical repeat unit, we may describe the topological repeat unit using the expression $^cV_r = {}^1V_r{}^2V_r{}^3V_r{}^4V_r$ where ^cV_r denotes the connectivity of vertices (*V*) rather than tetrahedra (*T*).

In many chains, tetrahedra are topologically identical but geometrically distinct. This often results in chains with geometrical and topological repeat units that contain different numbers of tetrahedra and vertices. Figures 3*a,b* show the tetrahedron and ball-and-stick representations of the chain in **astrophyllite-supergroup** minerals, where $^cT_r = {}^3T_2{}^1T_2$ is the connectivity of

https://doi.org/10.1180/mgm.2020.13 Published online by Cambridge University Press

the tetrahedra in the geometrical repeat unit. Figure 3*c* shows the graphical representation of the same chain with a topological repeat unit that contains two vertices rather than four as shown in the ball-and-stick representation (Fig. 3*b*); this is because the direction of branching of 1-connected vertices (or tetrahedra) does not affect the topology of the linkage. It follows that we may describe the topological repeat unit in **astrophyllite-supergroup** minerals as ${}^{c}V_r = {}^{3}V_1{}^{1}V_1$. Hence the ${}^{c}V_r$ expression for a topological repeat unit may be derived by multiplying the values of r in the respective ${}^{c}T_r$ expression by n_t/n_g. For some chains, ribbons and tubes, a graphical representation will not be given if such a representation further obscures the connectivity of vertices and/or if ${}^{c}T_r = {}^{c}V_r$ ($n_g = n_t$).

Group and class

In Mineralogy, a group is defined as two or more minerals with the same or similar structure and chemical composition, a group may belong to a single supergroup and/or have multiple subgroups, and supergroups may belong to a single class or subclass (Mills *et al.*, 2009). Here, we also use the words *group* and *class* in their general sense: [1] group indicates a collection of minerals with same ${}^{c}T_r$ and/or ${}^{c}V_r$ expression; [2] *class* organises minerals with ${}^{c}T_r$ expressions in which the tetrahedron connectivity is the same (*c*) but not necessarily the number of tetrahedra with that connectivity (*r*). For example, the hierarchy class ${}^{3}T_r$ contains the groups ${}^{3}T_4$, ${}^{3}T_6$, ${}^{3}T_8$, ${}^{3}T_{12}$, ${}^{3}T_{16}$, ${}^{3}T_{17}$, ${}^{3}T_{32}$ and ${}^{3}T_{56}$.

Structure hierarchy

Structure hierarchies for most mineral classes and subclasses are based on cation-coordination polyhedra with the highest bond-valences, examples of which include $(S^{6+}O_4)^{2-}$, $(P^{5+}O_4)^{3-}$ and $(As^{5+}O_4)^{3-}$ tetrahedra (Hawthorne, 2014). With respect to chain silicates, the relatively high bond-valence associated with the $(TO_4)^{n-}$-tetrahedron results in a strongly bonded, high-enthalpy tetrahedron. In chain silicates, such tetrahedra polymerise infinitely in a single direction to form the chain, ribbon or tube of the structure. Excess charge is balanced by lower-valence cations interstitial to the silicate unit. Most structure hierarchies follow the idea of *Binary Structural Representation* (Hawthorne, 1983*a*, 1985, 1986, 1990, 1992; Hawthorne and Schindler, 2008) in which structures are partitioned into a strongly bonded *structural unit* and a weakly bonded *interstitial complex*. The *Principle of Correspondence of Lewis-acidity–Lewis-basicity* (Hawthorne, 2012*a*,*b*) examines the controls on chemical composition and on the structural arrangement of both the structural unit and the interstitial complex (e.g.

Table 3. Minerals with ${}^{2}T_2$ chains.

${}^{c}T_r$	Mineral	Ideal structural formula	Unit stoichiometry	${}^{c}V_r$	Space group	O:T	Figs	Refs.
${}^{2}T_1$	Synthetic	------	$[GeO_3]$	${}^{2}V_1$		3.0	4	(1)
${}^{2}T_2$	Pyroxenes opx/cpx	XY**[Si_2O_6]**	$[SiO_3]$	${}^{2}V_1$	*C*2/*c* *Pbca*	3.0	5	(2)
		Lintisite group						
${}^{2}T_2$	Lintisite	Na_6Ti_4**[$Li_2Si_4O_{12}$][Si_2O_6]**$_2O_4(H_2O)_4$	$[SiO_3]$	${}^{2}V_1$	*C*2/*c*	2.4	6	(3)
${}^{4}T_4\,{}^{6}T_2{}^{*}$	〃 〃	〃 〃	$[Li_{0.33}Si_{0.67}O_2]$	${}^{4}V_2{}^{6}V_1$				
${}^{2}T_2$	Punkaruaivite	Ti_4**[$Li_2Si_4O_{10}(OH)_2$][Si_2O_6]**$_2(OH)_4(H_2O)_2$	$[SiO_3]$	${}^{2}V_1$	*C*2/*c*	2.4	6*d*,*e*	(4)
${}^{4}T_4\,{}^{6}T_2{}^{*}$	〃 〃	〃 〃	$[Li_{0.33}Si_{0.67}\ O_{1.67}(OH)_{0.33}]$	${}^{4}V_2{}^{6}V_1$				
${}^{2}T_2$	Eliseevite	$Na_{1.5}LiTi_2$**[$Si_4O_{10.5}(OH)_{1.5}$]**$O_2(H_2O)_2$	$[SiO_{2.63}(OH)_{0.37}]$	${}^{2}V_1$	*C*2/*c*	3.0	–	(5)
${}^{2}T_2$	Kukisvumite	Na_6Ti_4**[$ZnSi_4O_{12}$][Si_2O_6]**$_2O_4(H_2O)_4$	$[SiO_3]$	${}^{2}V_1$	*Pccn*	2.4	–	(6)
${}^{4}T_4\,{}^{6}T_2{}^{*}$	〃 〃	〃 〃	$[Zn_{0.2}Si_{0.8}O_{2.4}]$	${}^{4}V_2{}^{6}V_1$				
${}^{2}T_2$	Manganokukisvumite	Na_6Ti_4**[$MnSi_4O_{12}$][Si_2O_6]**$_2O_4(H_2O)_4$	$[SiO_3]$	${}^{2}V_1$	*Pccn*	2.4	–	(7)
${}^{4}T_4\,{}^{6}T_2{}^{*}$	〃 〃	〃 〃	$[Mn_{0.2}Si_{0.8}O_{2.4}]$	${}^{4}V_2{}^{6}V_1$				
		Carpholite group: $A_2BM_2Al_4[Si_4O_{12}]V_4W_4$						
${}^{2}T_2$	Carpholite	□Mn_2Al_4**[Si_2O_6]**$_2(OH)_4(OH)_4$	$[SiO_3]$	${}^{2}V_1$	*Ccca*	3.0	7*a*,*b*	(8)
${}^{2}T_2$	Balipholite	$BaMgLiAl_4$**[Si_2O_6]**$_2(OH)_4(OH)_4$	$[SiO_3]$	${}^{2}V_1$	*Ccca*	3.0	–	(9)
${}^{2}T_2$	Ferrocarpholite	□$(Fe^{2+},Mg)_2Al_4$**[Si_2O_6]**$_2(OH)_4(OH)_4$	$[SiO_3]$	${}^{2}V_1$	*Ccca*	3.0	–	(10)
${}^{2}T_2$	Magnesiocarpholite	□$(Mg,Fe^{2+})_2Al_4$**[Si_2O_6]**$_2(OH)_4(OH)_4$	$[SiO_3]$	${}^{2}V_1$	*Ccca*	3.0	–	(11)
${}^{2}T_2$	Vanadiocarpholite	□$Mn_2V_2Al_2$**[Si_2O_6]**$_2(OH)_4(OH)_4$	$[SiO_3]$	${}^{2}V_1$	*Ccca*	3.0	–	(12)
${}^{2}T_2$	Potassiccarpholite	$KMnLiAl_4$**[Si_2O_6]**$_2(OH)_4F_4$	$[SiO_3]$	${}^{2}V_1$	*Ccca*	3.0	–	(13)
${}^{2}T_2$	Nchwaningite	Mn_4**[Si_2O_6]**$(OH)_4(H_2O)_2$	$[SiO_3]$	${}^{2}V_1$	$Pca2_1$	3.0	7*c*,*d*	(14)
${}^{2}T_2$	Lorenzenite	Na_2Ti_2**[Si_2O_6]**O_3	$[SiO_3]$	${}^{2}V_1$	Pbcn	3.0	8*a*,*b*	(15)
${}^{2}T_2$	Shattuckite	Cu_5**[Si_2O_6]**$_2(OH)_2$	$[SiO_3]$	${}^{2}V_1$	Pcab	3.0	8*c*–*e*	(16)
${}^{2}T_2$	Capranicaite	(K,□)(Ca,Na)Al_4B_4**[Si_2O_6]**O_{12}	$[SiO_3]$	${}^{2}V_1$	$P2_1/m$	3.0	–	(17)
${}^{2}T_2$	Yegorovite	Na_4**[$Si_2O_4(OH)_2$]**$_2(H_2O)_7$	$[SiO_2(OH)]$	${}^{2}V_1$	$P2_1/c$	3.0	9*a*–*f*	(18)
${}^{2}T_2$	Aerinite	$Ca_6FeAl(Fe,Mg)_2(Al,Mg)_6$**[$Si_{12}O_{36}$]**$(OH)_{12}H(H_2O)_{12}(CO_3)$	$[SiO_3]$	${}^{2}V_1$	*P*3c1	3.0	10*a*–*d*	(19)
${}^{2}T_2$	Synthetic	Ba_2**[Si_2O_6]**	$[SiO_3]$	${}^{2}V_1$	$P2_12_12_1$	3.0	–	(20)
${}^{2}T_2$	Synthetic	Li_4**[Si_2O_6]**	$[SiO_3]$	${}^{2}V_1$	$Cmc2_1$	3.0	–	(21)
${}^{2}T_2$	Synthetic	Ag_4**[Si_2O_6]**	$[SiO_3]$	${}^{2}V_1$	$P2_12_12_1$	3.0	–	(22)
${}^{2}T_2$	Synthetic	Na_4**[Si_2O_6]**	$[SiO_3]$	${}^{2}V_1$	$Cmc2_1$	3.0	–	(23)
${}^{2}T_2$	Synthetic	Na_2Zn**[Si_2O_6]**	$[SiO_3]$	${}^{2}V_1$	*Fdd*2	3.0	–	(24)
${}^{2}T_2$	Synthetic	Na_2Ba**[Si_2O_6]**	$[SiO_3]$	${}^{2}V_1$	$P12_11$	3.0	–	(25)

References: (1) Krivovichev *et al.* (1998); (2) Warren and Bragg (1928); (3) Merlino *et al.* (1990), Yakovenchuk *et al.* (2012); (4) Yakovenchuk *et al.* (2010); (5) Yakovenchuk *et al.* (2011); (6) Merlino *et al.* (2000*b*); (7) Gault *et al.* (2004); (8) Naumova *et al.* (1974), Ghose *et al.* (1989); (9) Zhizhong *et al.* (1987); (10) MacGillavry *et al.* (1956), Viswanathan and Seidel (1979); (11) Viswanathan (1981), Fuchs *et al.* (2001); (12) Basso *et al.* (2005); (13) Tait *et al.* (2004); (14) Nyfeler *et al.* (1995); (15) Hang *et al.* (1969), Sundberg *et al.* (1987); (16) Evans and Mrose (1977), Newberg (1964), Evans and Mrose (1966); (17) Callegari *et al.* (2011); (18) Zubkova *et al.* (2009*b*), Pekov *et al.* (2010*b*); (19) Rius *et al.* (2009), Rius *et al.* (2004); (20) Grosse and Tillmanns (1974); (21) George *et al.* (1998); (22) Jansen *et al.* (1991); (23) McDonald and Cruickshank (1967); (24) Simonov *et al.* (1980); (25) Gunawardane *et al.* (1973).
*Indicates the ${}^{c}T_r$ expression of an additional structural unit including a chain, ribbon, tube, cluster or sheet of $[TO_4]^{n-}$ tetrahedra in the respective mineral.

https://doi.org/10.1180/mgm.2020.13 Published online by Cambridge University Press

Schindler and Hawthorne, 2001*a*,*b*,*c*, 2004, 2008; Schindler *et al.*, 2000, 2006). The development of a structure hierarchy for silicate minerals needs to focus solely on the polymerisation of the silicate unit (*sensu late*) at this stage as the polymerisation of tetrahedra is orders of magnitude more complicated than polymerisation of any other oxysalt polyhedron. Thus here we focus on silicate polymerisation and do not consider bonds to other higher-coordination cations that would normally be considered as part of a structural unit in other classes of oxysalt minerals. Hence here we divide the structure into a silicate unit and an interstitial structure (not complex) that contains the rest of the structure. The initial ordering of chains, ribbons and tubes follows the hierarchy of $^{c}T_{r}$ expressions listed in Table 2.

We plan to examine the interaction of the silicate unit with the interstitial cations and anions in our future work on chain-silicate minerals, and here we also describe the coordination of the interstitial cations and (H_2O), unless the details are obscured by positional disorder. We differentiate between Transformer $(H_2O)^{t}$, Non-Transformer $(H_2O)^{n}$, Inverse-Transformer $(H_2O)^{i}$ and solely hydrogen-bonded $(H_2O)^{z}$ groups where possible (Hawthorne, 1992; Hawthorne and Schindler, 2008; Hawthorne and Sokolova, 2012). Literature references to specific minerals are made in the tables (not the text) except where dealing with more general topics.

$^{2}T_{r}$ class

The number of 2-connected tetrahedra in the repeat unit of any $^{2}T_{r}$ chain is equal to the periodicity of that chain and is therefore the same in chain silicates with identical chain geometry. Here, the r value is used to subdivide all chain silicates with $^{2}T_{r}$ chains into ten groups where $r = 1$, 2, 3, 4, 5, 6, 7, 9, 12 and 24 (Tables 3–5). Belov (1961) showed how the size of the higher-coordinated cations can affect the geometry and periodicity of the

Table 4. Minerals with $^{2}T_{3}$ chains.

$^{c}T_{r}$	Mineral	Ideal structural formula	Chain stoichiometry	$^{c}V_{r}$	Space group	O:T	Figs	Refs.
		Wollastonite group: anhydrous: $M1_2M2_2M3M4[Si_3O_9]_2$						
$^{2}T_{3}$	Wollastonite (1*A*, 3*A*, 4*A*, 5*A*, 7*A*)	Ca_3**[Si_3O_9]**	[SiO_3]	$^{2}V_{1}$	$P\bar{1}$	3.0	11	(1)
$^{2}T_{3}$	Wollastonite (2*M*)	Ca_3**[Si_3O_9]**	[SiO_3]	$^{2}V_{1}$	$P2_1$	3.0	11	(1)
$^{2}T_{3}$	Dalnegorskite	Ca_2Ca_2MnCa**[Si_3O_9]$_2$**	[SiO_3]	$^{2}V_{1}$	$P\bar{1}$	3.0	–	(2)
$^{2}T_{3}$	Bustamite	$(Ca,Mn^{2+})_2Ca_2Mn^{2+}Ca$**[$Si_3O_9$]$_2$**	[SiO_3]	$^{2}V_{1}$	$P\bar{1}$	3.0	12*a*,*b*	(3)
$^{2}T_{3}$	Ferrobustamite	$(Ca,Fe^{2+})_2Ca_2Fe^{2+}Ca$**[$Si_3O_9$]$_2$**	[SiO_3]	$^{2}V_{1}$	$P\bar{1}$	3.0	12*c*,*d*	(4)
$^{2}T_{3}$	Mendigite	$Mn^{2+}_2Mn^{2+}Mn^{2+}Ca$**[$Si_3O_9$]$_2$**	[SiO_3]	$^{2}V_{1}$	$P\bar{1}$	3.0	12*e*,*f*	(5)
		Wollastonite group: hydrous: $M3(M1,M2)_2[Si_3O_8(OH)]$						
$^{2}T_{3}$	Pectolite	$NaCa_2$**[Si_3O_8(OH)]**	[$SiO_{2.7}(OH)_{0.3}$]	$^{2}V_{1}$	$P\bar{1}$	3.0	13*a*,*b*	(6)
$^{2}T_{3}$	Schizolite	$Na(Ca,Mn)_2$**[Si_3O_8(OH)]**	[$SiO_{2.7}(OH)_{0.3}$]	$^{2}V_{1}$	$P\bar{1}$	3.0	13*c*,*d*	(7)
$^{2}T_{3}$	Murakamiite	$LiCa_2$**[Si_3O_8(OH)]**	[$SiO_{2.7}(OH)_{0.3}$]	$^{2}V_{1}$	$P\bar{1}$	3.0	13*e*,*f*	(8)
$^{2}T_{3}$	Tanohataite	$LiMn^{2+}_2$**[Si_3O_8(OH)]**	[$SiO_{2.7}(OH)_{0.3}$]	$^{2}V_{1}$	$P\bar{1}$	3.0	13*g*,*h*	(9)
$^{2}T_{3}$	Serandite	$NaMn^{2+}_2$**[Si_3O_8(OH)]**	[$SiO_{2.7}(OH)_{0.3}$]	$^{2}V_{1}$	$P\bar{1}$	3.0	13*i*,*j*	(10)
$^{2}T_{3}$	Barrydawsonite-(Y)	$Na_2Ca_2(Na,Y)_2$**[Si_3O_8(OH)]$_2$**	[$SiO_{2.7}(OH)_{0.3}$]	$^{2}V_{1}$	$P2_1/a$	3.0	–	(11)
$^{2}T_{3}$	Vistepite	$SnMn_4$**[$B_2Si_4O_{16}$(OH)$_2$]**	[$(B_{0.3}Si_{0.7})O_{2.7}(OH)_{0.3}$]	$^{2}V_{1}$	$P\bar{1}$	3.0	14*a*,*b*	(12)
$^{2}T_{3}$	Cascandite	$CaSc$**[Si_3O_8(OH)]**	[$SiO_{2.7}(OH)_{0.3}$]	$^{2}V_{1}$	$C\bar{1}$	3.0	14c,d	(13)
		Hilairite group						
$^{2}T_{3}$	Hilairite	Na_2Zr**[Si_3O_9]**$(H_2O)_3$	[SiO_3]	$^{2}V_{1}$	*R*32	3.0	15	(14)
$^{2}T_{3}$	Calciohilairite	$CaZr$**[Si_3O_9]**$(H_2O)_3$	[SiO_3]	$^{2}V_{1}$	*R*32	3.0	–	(15)
$^{2}T_{3}$	Komkovite	$BaZr$**[Si_3O_9]**$(H_2O)_3$	[SiO_3]	$^{2}V_{1}$	*R*32	3.0	–	(16)
$^{2}T_{3}$	Sazykinaite-(Y)	Na_3YZr**[Si_6O_{18}]**$(H_2O)_6$	[SiO_3]	$^{2}V_{1}$	*R*32	3.0	–	(17)
$^{2}T_{3}$	Pyatenkoite-(Y)	Na_3YTi**[Si_6O_{18}]**$(H_2O)_6$	[SiO_3]	$^{2}V_{1}$	*R*32	3.0	–	(18)
$^{2}T_{3}$	Synthetic	$K_{1.81}Na_{0.09}H_{0.1}Zr$**[$Si_3O_9$]**	[SiO_3]	$^{2}V_{1}$	*R*3	3.0	–	(19)
$^{2}T_{3}$	Synthetic	$Rb_{1.8}Na_{0.2}Zr$**[Si_3O_9]**$(H_2O)_{0.35}$	[SiO_3]	$^{2}V_{1}$	*R*3	3.0	–	(19)
$^{2}T_{3}$	Synthetic	$Pb_{0.6}Na_{0.4}H_{0.4}Zr$**[$Si_3O_9$]**$(H_2O)_3$	[SiO_3]	$^{2}V_{1}$	*R*3	3.0	–	(19)
$^{2}T_{3}$	Synthetic	$SrZr$**[Si_3O_9]**$(H_2O)_{1.5}$	[SiO_3]	$^{2}V_{1}$	*R*3	3.0	–	(19)
$^{2}T_{3}$	Synthetic	$Na_{1.14}Cs_{0.55}H_{0.31}Zr$**[$Si_3O_9$]**$(H_2O)_{0.9}$	[SiO_3]	$^{2}V_{1}$	*R*32	3.0	–	(19)
$^{2}T_{3}$	Kamenevite	K_2Ti**[Si_3O_9]**(H_2O)	[SiO_3]	$^{2}V_{1}$	$P2_12_12_1$	3.0	–	(20)
$^{2}T_{3}$	Umbite	K_2Zr**[Si_3O_9]**(H_2O)	[SiO_3]	$^{2}V_{1}$	$P2_12_12_1$	3.0	16	(21)
$^{2}T_{3}$	Paraumbite	K_3HZr_2**[Si_6O_{18}]**$(H_2O)_3$	[SiO_3]	$^{2}V_{1}$	Orth	3.0	16	(22)
$^{2}T_{3}$	Kostylevite	K_2Zr**[Si_3O_9]**(H_2O)	[SiO_3]	$^{2}V_{1}$	$P2_1/a$	3.0	–	(23)
$^{2}T_{3}$	Synthetic	$(Cs_{1.37}K_{0.45}H_{0.18})_2$**[$Si_3O_9$]**$(H_2O)_{0.98}$	[SiO_3]	$^{2}V_{1}$	$P2_12_12_1$	3.0	–	(24)
$^{2}T_{3}$	Foshagite	Ca_4**[Si_3O_9]**$(OH)_2$	[SiO_3]	$^{2}V_{1}$	$P2_1/m$	3.0	17*a*,*b*	(25)
$^{2}T_{3}$	Hillebrandite	Ca_6**[Si_3O_9]**$(OH)_6$	[SiO_3]	$^{2}V_{1}$	*Cmcm*	3.0	–	(26)
$^{2}T_{3}$	Jennite	Ca_9**[Si_3O_9]$_2$**$(OH)_8(H_2O)_8$	[SiO_3]	$^{2}V_{1}$	$P\bar{1}$	3.0	17*c*,*d*	(27)
$^{2}T_{3}$	'Metajennite'	Ca_9**[Si_3O_9]$_2$**$(OH)_8(H_2O)_2$	[SiO_3]	$^{2}V_{1}$	–	3.0	–	(28)
$^{2}T_{3}$	Plombièrite (Tobermorite-14Å)	Ca_5**[Si_6O_{16}(OH)$_2$]**$(H_2O)_2{\cdot}(Ca(H_2O)_5)]$	[$SiO_{2.7}(OH)_{0.3}$]	$^{2}V_{1}$	*B*11*b*	3.0	17*e*,*f*	(29)
$^{2}T_{3}$	Riversideite MDO_1 (Tobermorite-9.3Å)	Ca_5**[Si_6O_{16}(OH)$_2$]**	[SiO_3]	$^{2}V_{1}$	*C*2/*c*	3.0	–	(30)
$^{2}T_{3}$	Riversideite MDO_2 (Tobermorite-9.3Å)	Ca_5**[Si_6O_{16}(OH)$_2$]**	[SiO_3]	$^{2}V_{1}$	$C\bar{1}$	3.0	–	(30)
$^{2}T_{3}$	Whelanite	Cu_2Ca_6**[Si_6O_{17}(OH)]**$(CO_3)(OH)_3(H_2O)_2]$	[$SiO_{2.83}(OH)_{0.17}$]	$^{2}V_{1}$	*Pnn*2	3.0	18*a*,*b*	(31)

References: (1) Hesse (1984), Henmi *et al.* (1983), Prewitt and Buerger (1963), Mamedov and Belov (1956); (2) Shchipalkina *et al.* (2018); (3) Peacor and Buerger (1962*a*), Peacor and Prewitt (1963), Aksenov *et al.* (2015), Shchipalkina *et al.* (2019*a*); (4) Yamanaka *et al.* (1977), Rapoport and Burnham (1973); (5) Chukanov *et al.* (2015*a*); (6) Takéuchi and Kudoh (1977), Prewitt (1967), Prewitt and Buerger (1963), Buerger (1956); (7) Ohashi and Finger (1978), Schaller (1955); (8) Imaoka *et al.* (2017); (9) Nagase *et al.* (2012); (10) Williams and Weller (2014), Rozhdestvenskaya and Vasilieva (2014); (11) Mitchell *et al.* (2015); (12) Hybler *et al.* (1997), Pautov *et al.* (1992); (13) Mellini and Merlino (1982), Mellini *et al.* (1982); (14) Grigorieva *et al.* (2009), Chao *et al.* (1974); (15) Boggs (1988), Pushcharovsky *et al.* (2002); (16) Voloshin *et al.* (1990); Sokolova *et al.* (1991); (17) Rastsvetaeva and Khomyakov (1992), Khomyakov *et al.* (1993); (18) Khomyakov *et al.* (1996), Rastsvetaeva and Khomyakov (1996); (19) Zubkova *et al.* (2009*a*), Pekov *et al.* (2010*a*); (20) Pekov *et al.* (2017); (21) Ilyushin *et al.* (1981), Sebastián *et al.* (2008); (22) Khomyakov *et al.* (1983*a*); (23) Ilyukhin *et al.* (1981), Khomyakov *et al.* (1983*c*); (24) Fewox *et al.* (2011); (25) Garbev (2004), Gard and Taylor (1958), Gard and Taylor (1960); (26) Dai and Post (1995), Xu and Boggs (1996); (27) Bonaccorsi *et al.* (2004), Gard *et al.* (1977), Carpenter *et al.* (1966); (28) Bonaccorsi *et al.* (2004); (29) Bonaccorsi *et al.* (2005), McConnell (1954); (30) Taylor (1953), Biagioni *et al.* (2015); (31) Kampf *et al.* (2012).

https://doi.org/10.1180/mgm.2020.13 Published online by Cambridge University Press

Table 5. Minerals with $^2T_{4-7}$, $^2T_9$, $^2T_{12}$ and $^2T_{24}$ chains.

^cT_r	Mineral	Ideal structural formula	Chain stoichiometry	^cV_r	Space group	O:T	Figs	Refs.
		Batisite group						
$^2T_4$	Batisite	$BaNa_2Ti_2$**[Si_4O_{12}]**O_2	[SiO_3]	$^2V_1$	*Imma*	3.0	19	(1)
$^2T_4$	Shcherbakovite	K_2NaTi_2**[Si_4O_{12}]**$(O,OH)_2$	[SiO_3]	$^2V_1$	*Imma*	3.0	–	(2)
$^2T_4$	Noonkanbahite	$BaKNaTi_2$**[Si_4O_{12}]**O_2	[SiO_3]	$^2V_1$	*Imma*	3.0	–	(3)
$^2T_4$	Haradaite	$Sr_2V_2^{4+}$**[Si_4O_{12}]**O_2]	[SiO_3]	$^2V_1$	*Cmcm*	3.0	20*a*,*b*	(4)
$^2T_4$	Suzukiite	$Ba_2V_2^{4+}$**[Si_4O_{12}]**O_2]	[SiO_3]	$^2V_1$	*Cmcm*	3.0	–	(5)
$^2T_4$	Ohmilite	$Sr_3(Ti,Fe^{3+})$**[Si_4O_{12}]**$(O,OH)(H_2O)_{2-3}$	[SiO_3]	$^2V_1$	$P2_1/m$	3.0	20*c*,*d*	(6)
$^2T_4$	Fukalite (MDO1)	Ca_8**[Si_4O_{12}]**$(OH)_4(CO_3)_2$	[SiO_3]	$^2V_1$	$P2_1/c$	3.0	21	(7)
$^2T_4$	Taikanite	$BaSr_2Mn_2^{3+}$**[Si_4O_{12}]**O_2	[SiO_3]	$^2V_1$	*C*2	3.0	22	(8)
$^2T_4$	Krauskopfite	Ba_2**[$Si_4O_8(OH)_4$]**$(H_2O)_4$	[SiO_2(OH)]	$^2V_1$	$P2_1/a$	3.0	23	(9)
			M_{42}**[T_4O_{12}]**$_4O_6(OH)_{40}$					
$^2T_4$	Balangeroite-2*M* (1*A*)	$(Mg,Fe^{2+},Fe^{3+})_{42}$**[$Si_4O_{12}$]**$_4O_6(OH)_{40}$	[SiO_3]	$^2V_1$	$P2/n$	3.0	24	(10)
$^2T_4$	Gageite-2*M* (1*A*)	$(Mn^{2+},Mg)_{42}$**[Si_4O_{12}]**$_4O_6(OH)_{40}$	[SiO_3]	$^2V_1$	$P2/n$	3.0	24	(11)
$^2T_4$	Synthetic	Ba_2U_2**[Si_4O_{12}]**O_4	[SiO_3]	$^2V_1$	*Cmcm*	3.0	–	(12)
$^2T_4$	Synthetic	Na_2Y_2**[Si_4O_{12}]**	[SiO_3]	$^2V_1$	$P2_1/c$	3.0	–	(13)
$^2T_4$	Synthetic	Cu_3Na_2**[Si_4O_{12}]**	[SiO_3]	$^2V_1$	*Pnma*	3.0	–	(14)
$^2T_4$	Synthetic	NaGd**[P_4O_{12}]**	[SiO_3]	$^2V_1$	$P2_1/n$	3.0	–	(15)
		Rhodonite group: $M_5M_{1-3}M_4$**[T_5O_{15}]**: **anhydrous**						
$^2T_5$	Rhodonite	$CaMn_4$**[Si_5O_{15}]**	[SiO_3]	$^2V_1$	$P\bar{1}$	3.0	25,26*c*,*d*	(16)
$^2T_5$	Vittinkiite	Mn_5**[Si_5O_{15}]**	[SiO_3]	$^2V_1$	$P\bar{1}$	3.0	26*a*,*b*	(17)
$^2T_5$	Ferrorhodonite	$CaMn_3Fe^{2+}$**[Si_5O_{15}]**	[SiO_3]	$^2V_1$	$P\bar{1}$	3.0	25*e*,*f*	(18)
		$M_5M_4M_{1-3}$**[T_5O_{14}(O,OH)] structures**						
$^2T_5$	Marsturite	$NaCaMn_3^{2+}$**[Si_5O_{14}(OH)]**	[$SiO_{2.8}(OH)_{0.2}$]	$^2V_1$	$P\bar{1}$	3.0	27*a*,*b*	(19)
$^2T_5$	Lithiomarsturite	$LiCa_2Mn_3^{2+}$**[Si_5O_{14}(OH)]**	[$SiO_{2.8}(OH)_{0.2}$]	$^2V_1$	$P\bar{1}$	3.0	27*c*,*d*	(20)
$^2T_5$	Nambulite	$(Li,Na)Mn_4^{2+}$**[Si_5O_{14}(OH)]**	[$SiO_{2.8}(OH)_{0.2}$]	$^2V_1$	$P\bar{1}$	3.0	27*e*,*f*	(21)
$^2T_5$	Natronambulite	$(Na,Li)Mn_4^{2+}$**[Si_5O_{14}(OH)]**	[$SiO_{2.8}(OH)_{0.2}$]	$^2V_1$	$P\bar{1}$	3.0	27*g*,*h*	(22)
$^2T_5$	Synthetic	Mn_5^{2+}**[Si_5O_{15}]**	[SiO_3]	$^2V_1$	$P\bar{1}$	3.0	–	(23)
$^2T_5$	Synthetic	$LiMn_4^{2+}$**[Si_5O_{14}(OH)]**	[SiO_3]	$^2V_1$	$P\bar{1}$	3.0	–	(23)
		Babingtonite group: $A_2M_1M_2$**[T_5O_{14}(OH)]**						
$^2T_5$	Babingtonite	$Ca_2(Fe^{2+},Mn^{2+})Fe^{3+}$**[$Si_5O_{14}$(OH)]**	[$SiO_{2.8}(OH)_{0.2}$]	$^2V_1$	$P\bar{1}$	3.0	28	(24)
$^2T_5$	Manganbabingtonite	$Ca_2(Mn^{2+},Fe^{2+})Fe^{3+}$**[$Si_5O_{14}$(OH)]**	[$SiO_{2.8}(OH)_{0.2}$]	$^2V_1$	$P\bar{1}$	3.0	28	(25)
$^2T_5$	Scandiobabingtonite	$Ca_2(Fe^{2+},Mn^{2+})Sc$**[Si_5O_{14}(OH)]**	[$SiO_{2.8}(OH)_{0.2}$]	$^2V_1$	$P\bar{1}$	3.0	–	(26)
$^2T_5$	Santaclaraite	$CaMn_4^{2+}$**[Si_5O_{14}(OH)]**$(OH)(H_2O)$]	[$SiO_{2.8}(OH)_{0.2}$]	$^2V_1$	$P\bar{1}$	3.0	–	(27)
$^2T_6$	Stokesite	Ca_2Sn_2**[Si_6O_{18}]**$(H_2O)_4$	[SiO_3]	$^2V_1$	*Pnna*	3.0	29	(28)
$^2T_6$	Gaidonnayite	Na_4Zr_2**[Si_6O_{18}]**$(H_2O)_4$	[SiO_3]	$^2V_1$	$P2_1nb$	3.0	–	(29)
$^2T_6$	Georgechaoite	$Na_2K_2Zr_2$**[Si_6O_{18}]**$(H_2O)_4$	[SiO_3]	$^2V_1$	$P2_1nb$	3.0	30	(30)
$^2T_6$	Synthetic	Cs_4Zr_2**[Si_6O_{18}]**$(H_2O)_4$	[SiO_3]	$^2V_1$	$P2_1nb$	3.0	–	(31)
$^2T_6$	Synthetic	K_8Sr_2**[Si_6O_{18}]**	[SiO_3]	$^2V_1$	*Ama*2	3.0	–	(32)
$^2T_7$	Pyroxferroite	Fe_7**[Si_7O_{21}]**	[SiO_3]	$^2V_1$	$P\bar{1}$	3.0	–	(33)
$^2T_7$	Pyroxmangite	Mn_7**[Si_7O_{21}]**	[SiO_3]	$^2V_1$	$P\bar{1}$	3.0	31	(34)
$^2T_7$	Synthetic	Mn_4Mg_3**[Si_7O_{21}]**	[SiO_3]	$^2V_1$	$P\bar{1}$	3.0	–	(35)
$^2T_9$	Synthetic Ferrosilite III	Fe_9**[Si_9O_{27}]**	[SiO_3]	$^2V_1$	$P\bar{1}$	3.0	32	(36)
$^2T_{12}$	Alamosite	Pb_{12}**[$Si_{12}O_{36}$]**	[SiO_3]	$^2V_1$	$P2/n$	3.0	33	(37)
$^2T_{24}$	Synthetic	$Na_{24}Y_8$**[$Si_{24}O_{72}$]**	[SiO_3]	$^2V_1$	$P2_12_12_1$	3.0	34	(38)

References: (1) Nikitin and Belov (1962), Schmahl and Tillmanns (1987), Rastsvetaeva *et al.* (1997*a*), Zolotarev *et al.* (2017); (2) Uvarova *et al.* (2003), Krivovichev *et al.* (2004*b*); (3) Prider (1965), Rastsvetaeva *et al.* (1997*a*), Uvarova *et al.* (2010); (4) Berger and Range (1996), Takéuchi and Joswig (1967), Watanabe *et al.* (1982), Basso *et al.* (1995); (5) Matsubara *et al.* (1982), Ito *et al.* (2014); (6) Mizota *et al.* (1983), Mizota *et al.* (1973), Komatsu *et al.* (1973); (7) Merlino *et al.* (2009), Henmi *et al.* (1977), Rastvetaeva *et al.* (2005); (8) Armbruster *et al.* (1993), Kalinin *et al.* (1985); (9) Coda *et al.* (1967), Alfors *et al.* (1965); (10) Bonaccorsi *et al.* (2012), Compagnoni *et al.* (1983), Ferraris *et al.* (1987), Belluso and Ferraris (1991); (11) Moore (1969*a*), Dunn (1979); (12) Plaisier *et al.* (1995); (13) Toebbens *et al.* (2005); (14) Kawamura and Kawahara (1976); (15) Amami *et al.* (2005); (16) Pertlik and Zahiri (1999), Peacor and Niizeki (1963), Peacor *et al.* (1978*a*), Pinckney and Burnham (1988); Leverett *et al.* (2008); (17) Pertlik and Zahiri (1999), Shchipalkina *et al.* (2019*b*); (18) Shchipalkina *et al.* (2017, 2019*a*); (19) Nagashima *et al.* (2014*a*), Peacor *et al.* (1978*b*), Kolitsch (2008); (20) Yang *et al.* (2011), Peacor *et al.* (1990); (21) Narita *et al.* (1975), Yoshii *et al.* (1972), Mukhopadhyay *et al.* (2005), Murakami *et al.* (1977); (22) Nagashima *et al.* (2014*a*), Matsubara *et al.* (1985); (23) Ito (1972); (24) Akasaka *et al.* (2013), Araki and Zoltai (1972), Kosoi (1975), Czank (1981), Armbruster, (2000), Nagashima *et al.* (2014*b*); (25) Vinogradova *et al.* (1966); (26) Orlandi *et al.* (1998); (27) Ohashi and Finger (1981), Erd and Ohashi (1984); (28) Vorma (1963), Gay and Rickson (1960), Yuan *et al.* (2017); (29) Chao and Watkinson (1974), Chao (1985), Donnay and Chao (1986), Larsen and Raade (1991), Celestian *et al.* (2019); (30) Ghose and Thakur (1985), Boggs and Ghose (1985); (31) Celestian *et al.* (2019); (32) Kahlenberg *et al.* (2007); (33) Burnham (1971), Lindsley and Burnham (1970), Shchipalkina *et al.* (2016*a*); (34) Narita *et al.* (1977), Liebau (1957), Zanazzi *et al.* (2008); (35) Finger and Hazen (1978) (36) Weber (1983), Liebau (1985); (37) Krivovichev and Burns (2004), Boucher and Peacor (1968); (38) Maksimov *et al.* (1980).

$[TO_3]^{n-}$ chains, and this is apparent in many of the figures illustrating these chains. We will examine the interaction between the silicate unit and the rest of the structure in detail in a later paper. All ^2T_r chains are topologically identical and hence have a topological repeat unit that contains a single 2-connected vertex: $^2V_1$.

$^2T_1$ chains

The metagermanate chain, [**GeO_3**] (Krivovichev *et al.*, 1998, fig. 4.C1), is the only known structure with $^2T_1$ chains (Figs 4*a*,*b*) in which each 2-connected $(GeO_4)^{4-}$-tetrahedron is geometrically and topologically identical (Fig. 4*c*). $^2T_1$ chains are the simplest possible chain-type and constitute the first group of the ^2T_r class where $r = 1$ (Tables 2 and 3).

$^2T_2$ chains

$^2T_2$ chains are extremely common and comprise one of the largest groups of minerals in the structure hierarchy (Table 3). The geometrical repeat unit of $^2T_2$ chains contains two $(TO_4)^{n-}$-tetrahedra ($n_g = 2$) that are linked to form $[T_2O_6]^{n-}$ groups that polymerise in a single direction to form the $^2T_2$ chain in

https://doi.org/10.1180/mgm.2020.13 Published online by Cambridge University Press

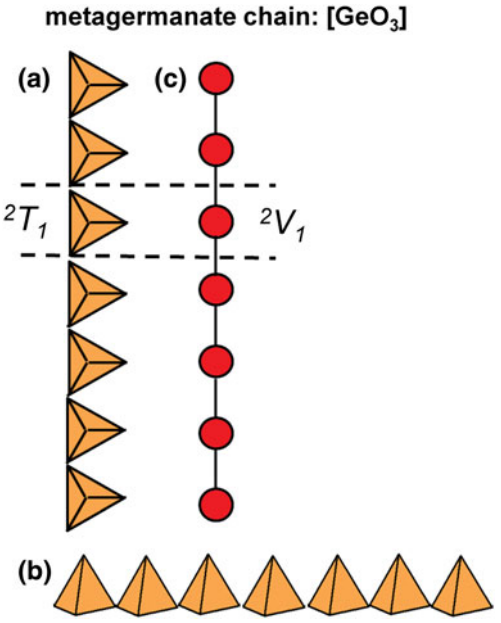

Fig. 4. (*a*, *b*) Tetrahedral representation of the $^{2}T_{1}$ **[GeO_3]** chain viewed orthogonal to the length of the chain; (*c*) a graphical representation of the chain where red points (vertices) represent Si^{4+}-tetrahedra and black lines (edges) represent linkages between adjacent Si^{4+}-tetrahedron. Dashed black lines show the geometrical and topological repeat unit of the chain.

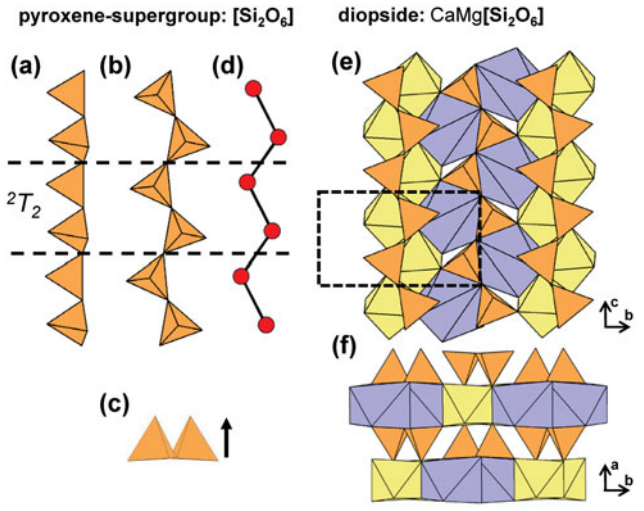

Fig. 5. (*a*, *b*, *c*) Tetrahedral representations of the $^{2}T_{2}$ chain in **pyroxenes** where both tetrahedra in the geometrical repeat unit point in the same direction and (*d*) a ball-and-stick representation of the chain. The structure of **diopside** projected (*e*) onto (100) and (*f*) along the **c**-axis. Dashed black lines show the geometrical repeat unit of the chain.

which both tetrahedra in the repeat unit may point in the same or opposing directions (Figs 5*a*–*d*). The topological repeat unit contains a single vertex that is topologically identical to all other vertices: $n_t = 1$, as is the case for all $^{2}T_{r}$ chains. The **pyroxene supergroup** are by far the most abundant minerals with this chain type; they have been described in considerable detail elsewhere (e.g. Papike *et al.*, 1973; Ohashi and Finger, 1974; Cameron and Papike, 1981; Bruno *et al.*, 1982; Rossi *et al.*, 1983; Tribaudino *et al.*, 1989; Redhammer *et al.*, 2006; Nestola *et al.*, 2007; Abdu and Hawthorne, 2013), and we will consider them here only briefly. Typically, $^{2}T_{2}$ chains extend along the **c**-axis and link to ribbons of edge-sharing octahedra; in **diopside**, there are alternating layers of $^{2}T_{2}$ chains and sheets of Mg^{2+}-octahedra and $^{[7]}Ca^{2+}$-polyhedra (Figs 5*e*,*f*). This general stacking sequence of chains of tetrahedra and sheets of octahedra (or higher-coordination polyhedra) is common in chain silicates that contain $^{2}T_{2}$ chains.

Lintisite-group minerals include **lintisite**, **punkaruaivite**, **eliseevite**, **kukisvumite** and **manganokukisvumite** (Table 3) all of which contain $^{2}T_{2}$ chains that occur in two distinct layers. **Lintisite** and **punkaruaivite** contain $^{[4]}Li^{+}$ and are of particular interest as Li^{+}-tetrahedra form chains of edge-sharing tetrahedra, and we will describe the structure here. Other minerals that contain silicate ribbons in addition to $^{2}T_{2}$ pyroxene-like chains, such as **vinogradovite** and **paravinogradovite** (see below), will be discussed in the $^{c}T_{r}$ section that corresponds to the ribbon rather than the $^{2}T_{2}$ chain. For all known chain-, ribbon- and tube-silicate minerals, tetrahedra link via corners through a common bridging anion. Such anions can link to a maximum of two Si^{4+}-tetrahedra, allowing a maximum Si^{4+}-connectivity of four. For a given $(SiO_4)^{4-}$-tetrahedron the average mean bond-valence is 1.0 vu and therefore the valence sum rule is satisfied at the O^{2-} bridging anion (Si–O–Si). However, if substitution of Si^{4+} by a cation with a smaller formal valence and a lower Lewis acidity (Gagné and Hawthorne, 2017) occurs, the mean bond-valence contribution to the bridging anion decreases which allows additional T–O linkages. This T-cation may have a connectivity of greater than four and form arrangements not observed in units composed predominately of Si^{4+}-tetrahedra. This situation occurs in **lintisite** (and **punkaruaivite**), in which Li^{+}-tetrahedra (mean bond-valence of 0.25 vu) have a connectivity of six and form $^{4}T_{4}{}^{6}T_{2}$ $[Li_2Si_4O_{12}]^{6-}$ ($[Li_2Si_4O_{10}(OH)_2]^{4-}$ in **punkaruaivite**) ribbons, the only example of this arrangement in chain-silicate minerals; the calculated bond-valence sum for $^{[4]}Li^{+}$ (*X*1 cation) in **lintisite** is 0.92 vu.

In **lintisite**, there are two distinct ways in which $^{2}T_{2}$ chains link to the rest of the structure (Fig. 6*a*): [1] $^{2}T_{2}$ chains link two adjacent sheets of Ti^{4+}-octahedra and $^{[8]}Na^{+}$-polyhedra (Na1) along the **a**-axis (Figs 6*b*); and [2] $^{2}T_{2}$ chains link sheets of Ti^{4+}-octahedra and $^{[8]}Na^{+}$-polyhedra (Na1) to chains of edge-sharing $(LiO_4)^{7-}$-tetrahedra (*X*1) (Figs 6*c*). This linkage of chains of $(SiO_4)^{4-}$- and $(LiO_4)^{7-}$-tetrahedra (*X*1) form $^{4}T_{4}{}^{6}T_{2}$ $[Li_2Si_4O_{12}]^{6-}$ ribbons (Figs 6*d*,*e*) that extend along the **c**-axis. In **lintisite**, channels extend along the **c**-axis and are occupied by Na^{+} that form $(NaO_2(H_2O)_4)^{3-}$-octahedra (Na2 and *W*1) (Fig. 6*a*). In **punkaruaivite**, $^{2}T_{2}$ chains and $^{4}T_{4}{}^{6}T_{2}$ $[Li_2Si_4O_{10}(OH)_2]^{4-}$ ribbons link to ribbons of edge-sharing $(TiO_4(OH)_2)^{6-}$-octahedra instead of sheets as the *Na*1 site is vacant. Channels are occupied solely by (H_2O) groups (*W*1) rather than Na2 cations as in **lintisite**, and the bond-valence sum at the *X*1-cation is 1.02 vu. **Eliseevite** contains only $^{2}T_{2}$ chains and no $^{4}T_{4}{}^{6}T_{2}$ ribbon as the *X*1 cation forms $(Li(H_2O)_4(OH)_2)^{-}$-octahedra rather than Li^{+}-tetrahedra. Here edge-sharing ribbons of $(Li(H_2O)_4(OH)_2)^{-}$-octahedra are linked along the **a**-axis to sheets of Ti^{4+}-octahedra and $^{[8]}Na^{+}$-polyhedra via $^{2}T_{2}$ chains. Although the bond-valence sums at the *X*1-cation in **lintisite** and **punkaruaivite** suggest Li^{+} is [4]-coordinated in this structure type, the bond-valence sums at the *X*1-cation in **eliseevite** for [4]- and [6]-coordinated Li^{+} are 0.75 and 0.90 vu, respectively. In **kukisvumite** and **manganokukisvumite**, Zn^{2+} and Mn^{2+} occupy the *X*1 site, respectively, and have both

https://doi.org/10.1180/mgm.2020.13 Published online by Cambridge University Press

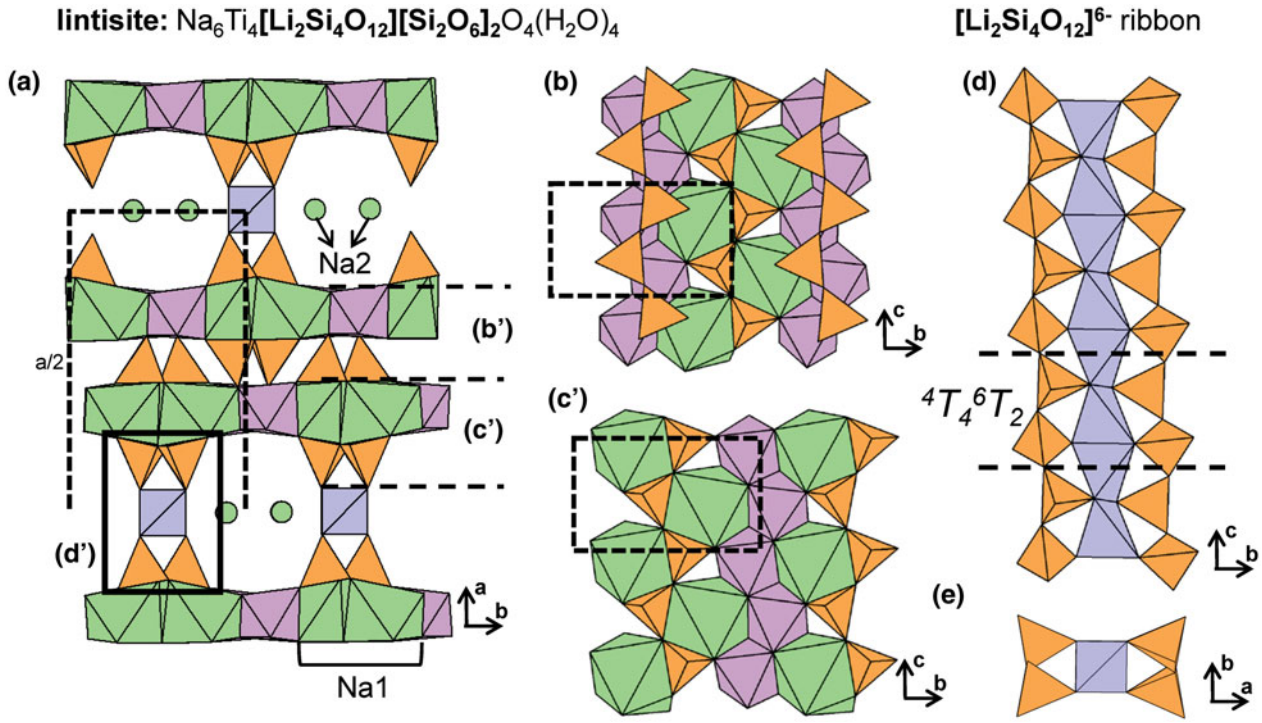

Fig. 6. The structure of **lintisite** projected (*a*) along the **c**-axis, (*b*, *c*) onto (100), and the $[Li_2Si_4O_{12}]^{6-}$ ribbon of $[SiO_4]^{4-}$ and $[LiO_4]^{7-}$ tetrahedra projected (*d*) onto (100) and (*e*) along the **c**-axis. Fine dashed black lines outline the unit cell which is halved along the **a**-axis in (*a*). The H atoms associated (H_2O) groups have been omitted for clarity.

been described as tetrahedrally coordinated cations. The incident bond-valence sum at the *X*1-cation for Zn^{2+} in **kukisvumite** is 1.16 vu, but there are no other anions close to Zn, and Zn must be tetrahedrally coordinated. This apparent bond-valence deficiency at the *X*1-cation is presumably the result of the half-occupancy of the site by Zn^{2+} with the real Zn^{2+}–O distances

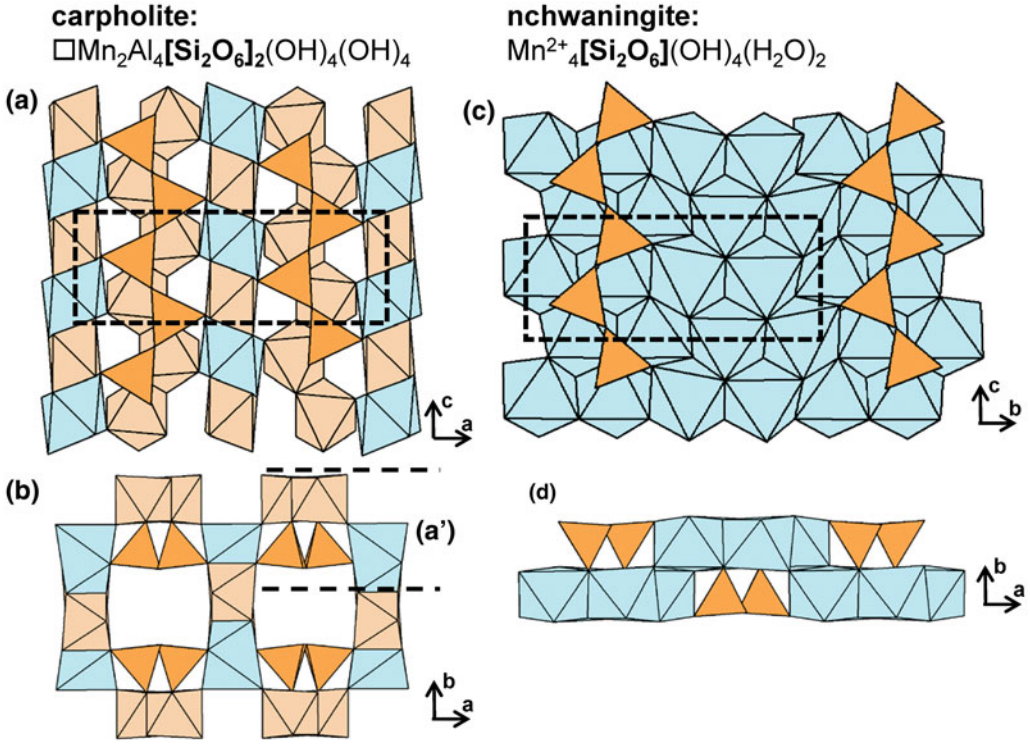

Fig. 7. The structure of **carpholite** projected (*a*) onto (010) and (*b*) along the **c**-axis. The structure of **nchwaningite** projected (*c*) onto (100) and (*d*) along the **c**-axis. Fine dashed black lines outline the unit cell and H atoms associated with $(OH)^-$ and (H_2O) groups have been omitted for clarity.

https://doi.org/10.1180/mgm.2020.13 Published online by Cambridge University Press

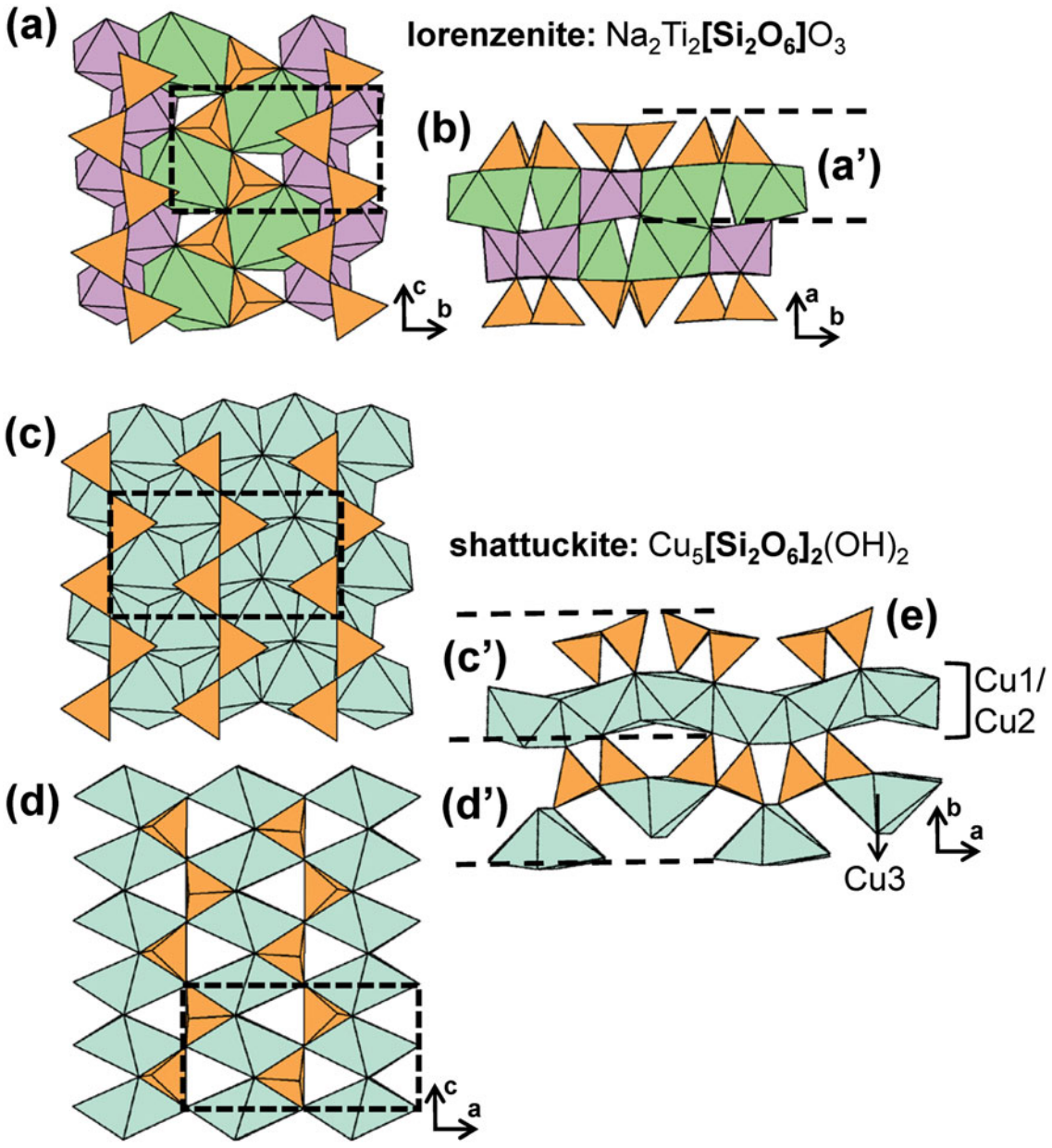

Fig. 8. The structure of **lorenzenite** projected (*a*) onto (100) and (*b*) along the **c**-axis. The structure of **shattuckite** projected (*c*, *d*) onto (010) and (*e*) along the **c**-axis. Fine dashed black lines outline the unit cell and H atoms associated with $(OH)^-$ groups have been omitted for clarity.

much shorter and the □–O distances much longer than the observed distances.

Although most chain silicates with $^2T_2$ chains contain alternating layers of chains of tetrahedra and sheets of octahedra (or higher-coordination polyhedra), there are different sequences of layer stacking that involve such chains. The **carpholite-group** minerals (Basso and Carbone, 2010) include **carpholite**, **balipholite, ferrocarpholite, magnesiocarpholite, vanadiocarpholite and potassiccarpholite** with the general formula $A_2BM_2Al_4[\mathbf{Si_4O_{12}}]V_4W_4$ (Tait *et al.*, 2004) (Table 3). In all group members, the *A* site is dominated by vacancy with minor Na^+ and the *B* site is also vacant in all members except **balipholite** and **potassiccarpholite** where it is occupied by Ba^{2+} and K^+, respectively. In **carpholite**, both *M*-octahedra are occupied by Mn^{2+} and share edges with Al^{3+}-octahedra, forming ribbons that extend along [001]. These ribbons are linked to each other along [100] by chains of Al^{3+}-octahedra, forming channels that are occupied by $^2T_2$ $[Si_2O_6]^{4-}$ chains (Figs 7*a*,*b*). In **magnesiocarpholite** and **ferrocarpholite**, Mg^{2+} and Fe^{2+} substitute for Mn^{2+} at one or both of the *M* sites. In **balipholite** and **potassiccarpholite**, Mg^{2+}/Li^+ and Mn^{2+}/Li^+ occupy the *M* sites, respectively and in **vanadiocarpholite** V^{3+} substitutes for Al^{3+}. In all **carpholite-group** minerals, the *V* and *W* sites are occupied by $(OH)^-$ groups except for **potassiccarpholite** where F^- occupies the *W* site.

The $^2T_2$ chains in **nchwaningite** link to sheets of $(MnO_2(OH)_3(H_2O))^{5-}$-octahedra along the **a**-axis and the **b**-axis (Fig. 7*c*). Each Si^{4+}–Mn^{2+} layer, shown in Fig. 7*d*, is linked to an identical layer along the **b**-axis via hydrogen bonding associated with (H_2O) and $(OH)^-$ groups that occupy interlayer

https://doi.org/10.1180/mgm.2020.13 Published online by Cambridge University Press

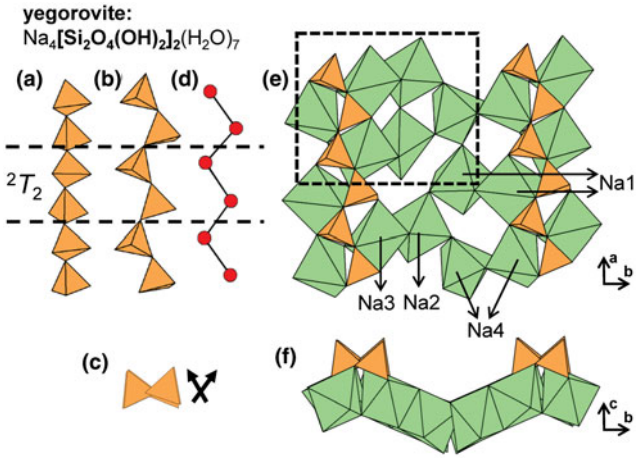

Fig. 9. (*a*, *b*, *c*) Tetrahedral representations of the $^2T_2$ chain in **yegorovite** where both tetrahedra in the geometrical repeat unit point in oblique directions, and (*d*) a ball-and-stick representation of the chain. The structure of **yegorovite** projected (*e*) onto (001) and (*f*) along the **a**-axis. Fine dashed black lines outline the unit cell and H atoms associated with $(OH)^-$ and (H_2O) groups have been omitted for clarity.

space and coordinate both Si^{4+} and Mn^{2+} ions. In **lorenzenite,** layers of $^2T_2$ chains link to a double-layer sheet of Ti^{4+}-octahedra and $^{[7]}Na^+$-polyhedra rather than a single-layer sheet (Figs 8*a*,*b*). In **shattuckite**, $^2T_2$ chains link to continuous, modulated single-layer sheets of $(CuO_4(OH)_2)^{8-}$-octahedra (Cu1 and Cu2) (Fig. 8*c*) and chains of Cu^{2+}-octahedra (Cu3) (Fig. 8*d*) that occur in layers parallel to the modulated sheets (001) (Fig. 8*e*). In **yegorovite,** both tetrahedra in the repeat unit are acid silicate (silanol) groups; $(SiO_3(OH))^{3-}$ and point in oblique directions with respect to each another (Figs 9*a*–*d*), a notable geometric difference from the more common $^2T_2$ minerals. Here, $^2T_2$ chains link to modulated single-layer sheets of $(NaO(H_2O)_3(OH)_2)^{3-}$-(Na1 and Na3) and $(NaO(H_2O)_4(OH))^{2-}$-octahedra (Na2 and Na4) that are parallel to (100) (Figs 9*e*,*f*). In **aerinite**, there are three distinct modes of linkage between $^2T_2$ chains and the rest of the structure. All $^2T_2$ chains link to chains of Fe^{3+}-octahedra that extend along and inside and outside of tubes of Al^{3+}-octahedra and $^{[7]}Ca^{2+}$-polyhedra and link such tubes to each other (Fig. 10*a*). Each chain of Fe^{3+}-octahedra links to three different $^2T_2$ chains (Fig. 10*b*). The way in which $^2T_2$ chains and chains of Fe^{3+}-octahedra link within tubes and between tubes of Al^{3+}-octahedra and $^{[7]}Ca^{2+}$-polyhedra is shown in Figs 10*c*,*d*, respectively. **Aerinite** also contains (H_2O), $(OH)^-$ and $(CO_3)^{2-}$ groups and we refer readers to Rius *et al.* (2009) for a more detailed structural description. Many synthetic compounds that contain $^2T_2$ $[Si_2O_6]^{4-}$ chains have been also been described, examples of which are listed in Table 3.

$^2T_3$ chains

In $^2T_3$ chains there are three geometrically distinct tetrahedra in the geometrical repeat unit, and all minerals that contain $^2T_3$ chains are listed in Table 4. There has been considerable work done on the effect of *M*-site substitutions on chain geometry, compositional limits and hydrogen bonding. In these minerals, *M*-site substitutions affect the periodicity, the geometrical aspects of the chain, and the stacking patterns of the structural elements. They are also affected by temperature (e.g. Ohashi and Finger, 1976, 1978; Liebau, 1980; Nagashima *et al.*, 2018; Prewitt and Peacor, 1964) but these effects will not be discussed in detail here.

Of the minerals that contain $^2T_3$ chains, **wollastonite-group** minerals are the most abundant and may be divided into two categories, anhydrous and hydrous, based on the absence or presence of $(OH)^-$ groups (Liebau, 1980) (Table 4). **Wollastonite** (*A* and *M* polytypes), **dalnegorskite**, **bustamite**, **mendigite** and **ferrobustamite** do not contain $(OH)^-$, whereas **pectolite**, **schizolite**, **murakamiite**, **tanohataite**, **serandite**, **berrydawsonite-(Y)** and **vistepite** contain $(OH)^-$ groups (Table 4). The geometry of the chain in **wollastonite-group** minerals is shown in Figs 11*a*–*d*. In general, these chains contain three distinct tetrahedra and consist of *c*-shaped trimers that link along the **b**-axis, parallel to ribbons of octahedra and/or other higher coordination polyhedra (Fig. 11*e*), These ribbons occur in layers that alternate with layers of $^2T_3$ chains (Fig. 11*f*). Thompson *et al.* (2016) examined the relations between pyroxenoids and pyroxenes in detail.

The most common **wollastonite** polytypes are 1*A* and 2*M*, with 3*A*, 4*A*, 5*A* and 7*A* polytypes being less common, resulting from different stacking sequences (Henmi *et al.*, 1983). **Wollastonite** contains three octahedrally coordinated sites that are fully occupied by Ca^{2+} (*M*1–*M*3) and form ribbons three octahedra wide (Figs 11*e*,*f*). The other *anhydrous* **wollastonite-group** minerals have the general formula $M1_2M2_2M3M4[Si_3O_9]_2$ and include **dalnegorskite**, **bustamite**, **ferrobustamite** and **mendigite** (Table 4). These minerals contain four sites *M*1–*M*4 occupied by Ca^{2+}, Mn^{2+} and Fe^{2+} where the *M*4 site is always occupied by Ca^{2+}. In **bustamite** (Figs 12*a*,*b*) and **ferrobustamite** (Figs 12*c*,*d*), the *M*1 site is occupied by $Ca^{2+} > Fe^{2+}$ and $Ca^{2+} > Mn^{2+}$, respectively and the *M*3 site is occupied by Mn^{2+} in **bustamite** and Fe^{2+} in **ferrobustamite**. In the structures of **bustamite**, **ferrobustamite** and **dalnegorskite**, the *M*2 sites are occupied dominantly by Ca^{2+}. In **mendigite**, the *M*1, *M*2 and *M*3 sites are dominated by Mn^{2+} (Figs 12*e*,*f*). **Dalnegorskite** represents the compositional limit of Ca^{2+} in the **bustamite-type** structure where *M*1, *M*2 and *M*4 are fully occupied by Ca^{2+} and *M*3 is occupied by Mn^{2+}.

The general formula of the *hydrous* **wollastonite-group** minerals can be written as $[M3(M1,M2)_2(Si_3O_8(OH)]$, where the *M*3 site is occupied either by Na^+ or Li^+, and *M*1 and *M*2 are occupied by Ca^{2+}, Mn^{2+}, Y^{3+}, Sn^{2+} and Sc^{3+} (Takéuchi *et al.*, 1976*a*,*b*; Mellini *et al.*, 1982; Hybler *et al.*, 1997; Nagashima *et al.*, 2018). The *M*1 and *M*2 octahedra are typically occupied by Ca^{2+} and Mn^{2+}, and form ribbons two polyhedra wide. Unlike the *anhydrous* varieties, ribbons of octahedra are linked to each other by *M*3 cations, forming sheets parallel to (101). In **pectolite**, *M*1 and *M*2 are occupied by Ca^{2+} and *M*3 is occupied by Na^+ (Figs 13*a*,*b*). In **barrydawsonite-(Y)**, *M*1 is occupied by Ca^{2+}, *M*2 is occupied by Na^+ and Y^{3+} (+*REE*), and *M*3 is occupied by Na^+. In **schizolite**, *M*1 and *M*2 are occupied by Ca^{2+} and Mn^{2+}, respectively, and *M*3 is occupied by Na^+ (Figs 13*c*,*d*). In **murakamiite** (Figs 13*e*,*f*) and **tanohataite** (Figs 13*g*,*h*) *M*1 and *M*2 are occupied by Ca^{2+} and Mn^{2+}, respectively, and *M*3 is occupied by Li^+. In **serandite**, *M*1 and *M*2 are occupied by Mn^{2+} and *M*3 is occupied by Na^+ (Figs 13*i*,*j*). In **vistepite**, the *T*3 site is occupied by B^{3+}, and ribbons are three octahedra wide. Unlike most *hydrous* **wollastonite-group** minerals, adjacent ribbons of octahedra are not linked by Na^+ or Li^+ to form sheets. It follows that the **vistepite** structure more closely resembles that of **bustamite** and **mendigite** despite containing $(OH)^-$ groups. Here, *M*1 and *M*2 are occupied by Mn^{2+}, *M*3 is occupied by Sn^{2+} and *M*4 is vacant (Figs 14*a*,*b*). In **cascandite,** *M*1 is occupied by Ca^{2+}, *M*2 is occupied by Sc^{3+} and *M*3 is vacant

https://doi.org/10.1180/mgm.2020.13 Published online by Cambridge University Press

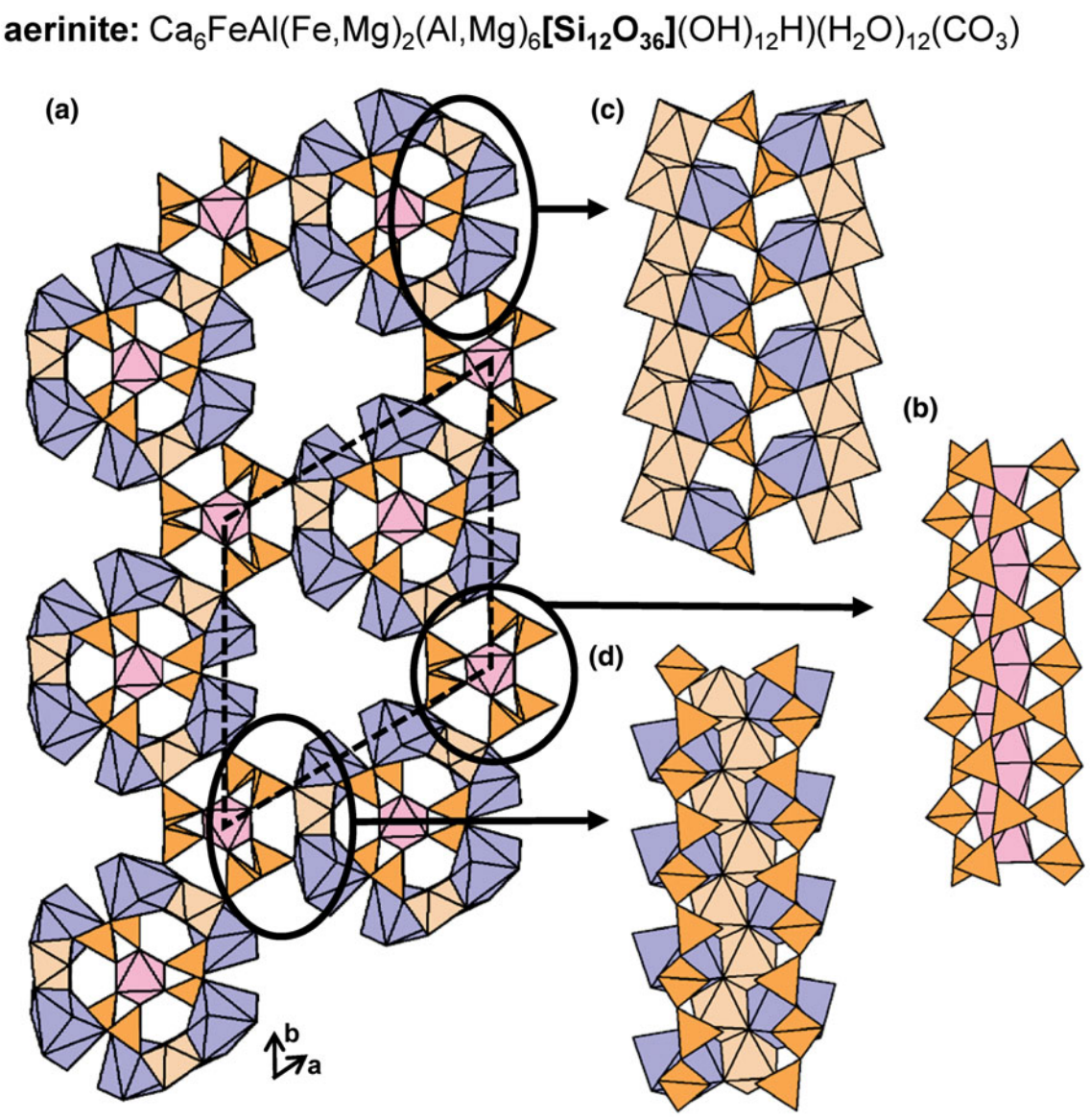

Fig. 10. The structure of **aerinite** projected (*a*) along the **c**-axis and (*b*, *c*, *d*) the structural modules that contain $^2T_2$ chains viewed orthogonal to the **c**-axis. Fine dashed black lines outline the unit cell and H atoms associated with $(OH)^-$ and (H_2O) groups and C atoms associated with (CO_3) groups have been omitted for clarity.

(Figs 14*c*,*d*). In general, *hydrous* **wollastonite-group** minerals contain one $(OH)^-$ group that acts as a bridging anion between $(SiO_3(OH)^-)^{3-}$ tetrahedra (*T*1) and $(CaO_5(OH^-))^{9-}$ octahedra (*M*1); a more detailed discussion of hydrogen bonding in these minerals is given by Nagashima *et al.* (2018).

In **hilairite**, $^2T_3$ chains extend along the **c**-axis and link to isolated Zr^{4+}-octahedra to form an open framework (Figs 15*a*, *b*). Zr^{4+}-octahedra occur in rows that extend along the **c**-axis, forming channels that are partly occupied by Na^+ (*Na*1 and *Na*2) and (H_2O) groups; these channels are labelled *1* in Fig. 15*a*. Figure 15*b* shows the position of Na1 atoms and channels labelled *2* that contain Na2 atoms and (H_2O) groups. Other members of the **hilairite group** include **calciohilairite**, **komkovite**, **sazykinaite-(Y)**, **pyatenkoite-(Y)** and synthetic K^+-, Rb^+-, Pb^{2+}-, Sr^{2+}-, Ba^{2+}-, Ca^{2+}- and Cs^+-exchanged analogues of **hilairite** (Pekov *et al.*, 2003, 2010*a*; Zubkova *et al.*, 2007, 2009*a*) (Table 4).

The $^2T_3$ chain in **umbite** is geometrically distinct from the $^2T_3$ chain in **wollastonite-** and the **hilairite-group** minerals. In **umbite**, chains extend along the **c**-axis and link to isolated Zr^{4+}-octahedra (Fig. 16*a*), forming an open framework that contains channels that also extend along the **c**-axis, resembling **hilairite-group** minerals (Figs 15*a*–*b*). In **umbite**, K2 atoms and (H_2O) groups occur in channels labelled *1* and K1 atoms occur within channels labelled *2* in Fig. 16*b*. In **paraumbite**, the H^+-exchanged variety of **umbite**, the K1 site is partly occupied by H^+ and in synthetic Cs^+-exchanged **umbite,** Cs^+ partly occupies the K1 site (Khomyakov *et al.*, 1983*a*; Fewox *et al.*, 2011). **Kamenevite** is the Ti^{4+}-analogue of **umbite** and **kostylevite** is a monoclinic polymorph of **umbite**.

Foshagite, **hillebrandite**, **jennite**, '**metajennite**', **plombièrite (tobermorite-14Å)**, **riversideite (tobermorite-9.3Å)** and **whelanite** can be chemically classified as calcium–silicate–hydrates (C–S–H minerals) (Table 4) and have received considerable

https://doi.org/10.1180/mgm.2020.13 Published online by Cambridge University Press

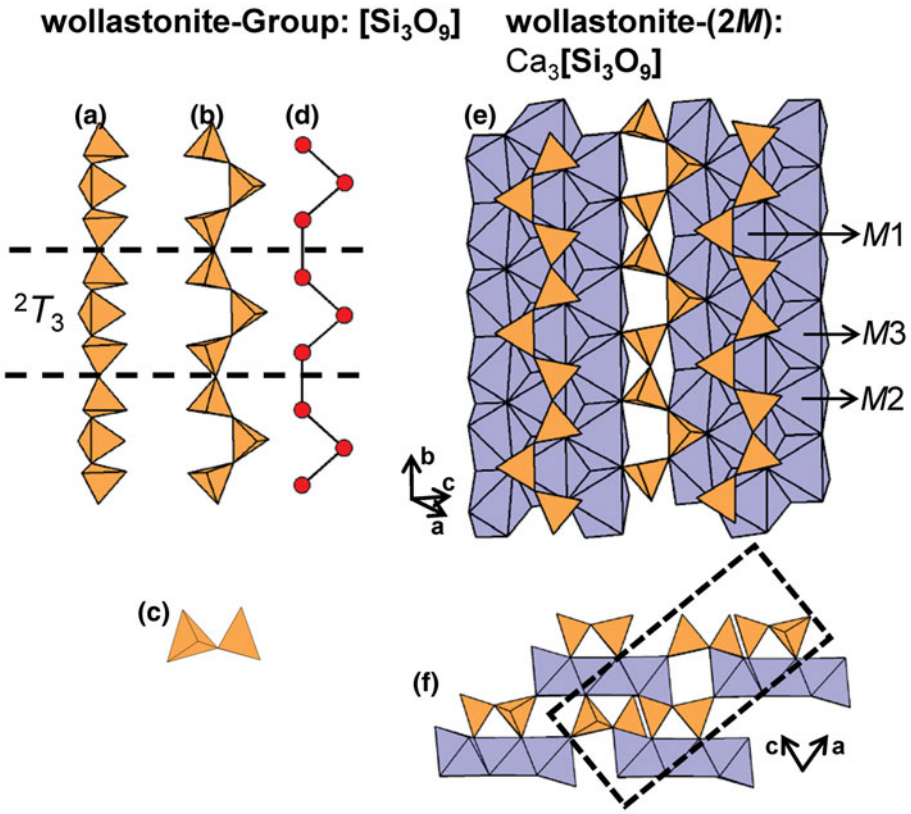

Fig. 11. (*a*, *b*, *c*) Tetrahedral representations of the $^2T_3$ chain in **wollastonite-group** minerals and (*d*) a ball-and-stick representation of the chain. The structure of **wollastonite-2*M*** viewed (*e*) orthogonal to the **b**-axis and (*f*) along the **b**-axis. Dashed black lines show the geometrical repeat unit of the chain and fine dashed black lines outline the unit cell.

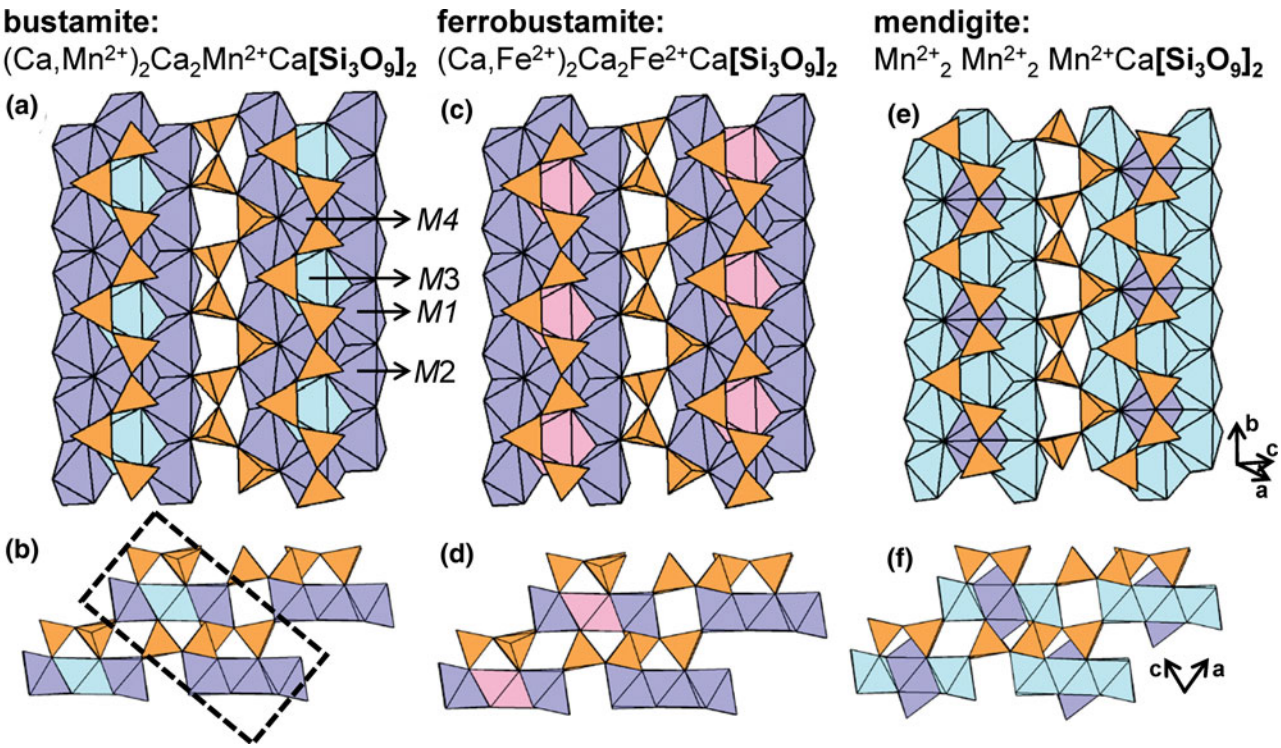

Fig. 12. The structure of (*a*, *b*) **bustamite**, (*c*, *d*) **ferrobustamite** and (*e*, *f*) **mendigite** viewed (*a*, *c*, *e*) orthogonal to the **b**-axis and (*b*, *d*, *f*) along the **b**-axis. *M*-site labels in (*a*) are also applicable to (*c*) and (*e*). Fine dashed black lines outline the unit cell.

https://doi.org/10.1180/mgm.2020.13 Published online by Cambridge University Press

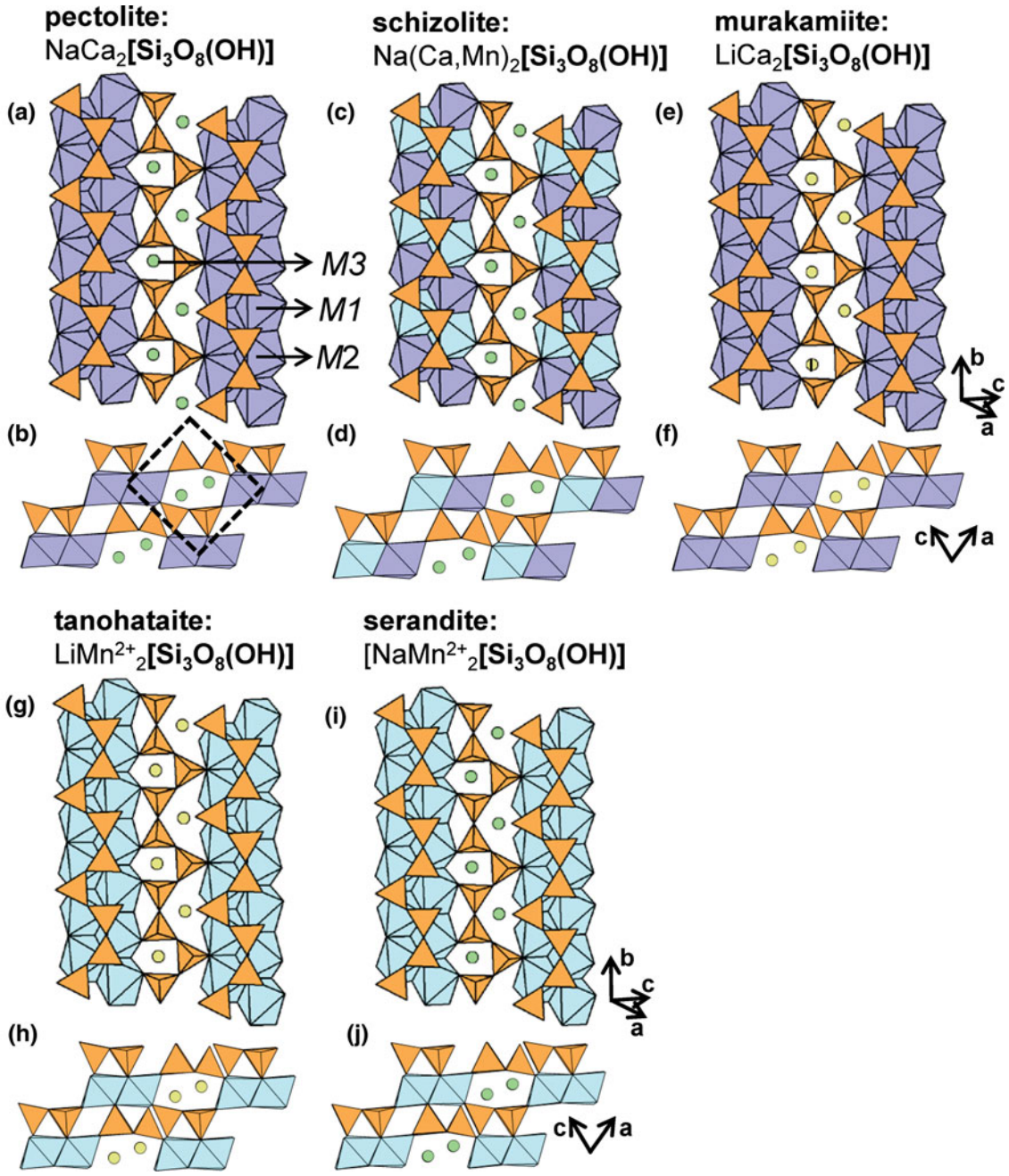

Fig. 13. The structure of (*a*, *b*) **pectolite**, (*c*, *d*) **schizolite**, (*e*, *f*) **murakamiite**, (*g*, *h*) **tanohataite** and (*i*, *j*) **serandite** viewed (*a*, *c*, *e*, *g*, *i*) orthogonal to the **b**-axis and (*b*, *d*, *f*, *h*, *j*) along the **b**-axis. *M*-site labels in (*a*) are also applicable to (*c*), (*e*), (*g*) and (*i*) and fine dashed black lines outline the unit cell. The H atoms associated with $(OH)^{-}$ groups have been omitted for clarity.

attention due to their structural and compositional similarities to the **tobermorite-group** minerals and their role in the hydration of Portland cement (Vigfusson, 1931; Gard and Taylor, 1976; Taylor, 1992; Cong and Kirkpatrick, 1996; Richardson, 2008; Meller *et al.*, 2009). Synthetic C–S–H phases produced by cement chemists are often poor quality and not suitable for X-ray diffraction analysis. Consequently, natural analogues of such phases are studied instead which correspond to many of the $^{2}T_{3}$, C–S–H minerals described here. In **foshagite,** $^{2}T_{3}$ chains link to ribbons of $(CaO_4(OH)_2)^{8-}$- and $(CaO_5(OH))^{9-}$-octahedra (Ca1–Ca4) (Fig. 17*a*). Ribbons four octahedra wide occur in layers parallel to (101) that alternate with layers of $^{2}T_{3}$ chains (Fig. 17*b*), an arrangement that is similar to that of the **wollastonite-group** minerals (Figs 11*e*–*f*). In **hillebrandite**, $^{2}T_{3}$ chains occupy and extend along tunnels in a framework of $(Ca(O,OH)_6)$-octahedra and $(Ca(O,(OH))_7)$-polyhedra.

In **jennite**, $^{2}T_{3}$ chains extend along the **b**-axis and link to a framework of Ca^{2+}-octahedra and $^{[7]}Ca^{2+}$-polyhedra (Ca1–Ca5). This framework consists of ribbons of $(CaO_4(OH)_2)^{8-}$-octahedra that extend along the **b**-axis (Ca1 and Ca3) and are cross-linked

https://doi.org/10.1180/mgm.2020.13 Published online by Cambridge University Press

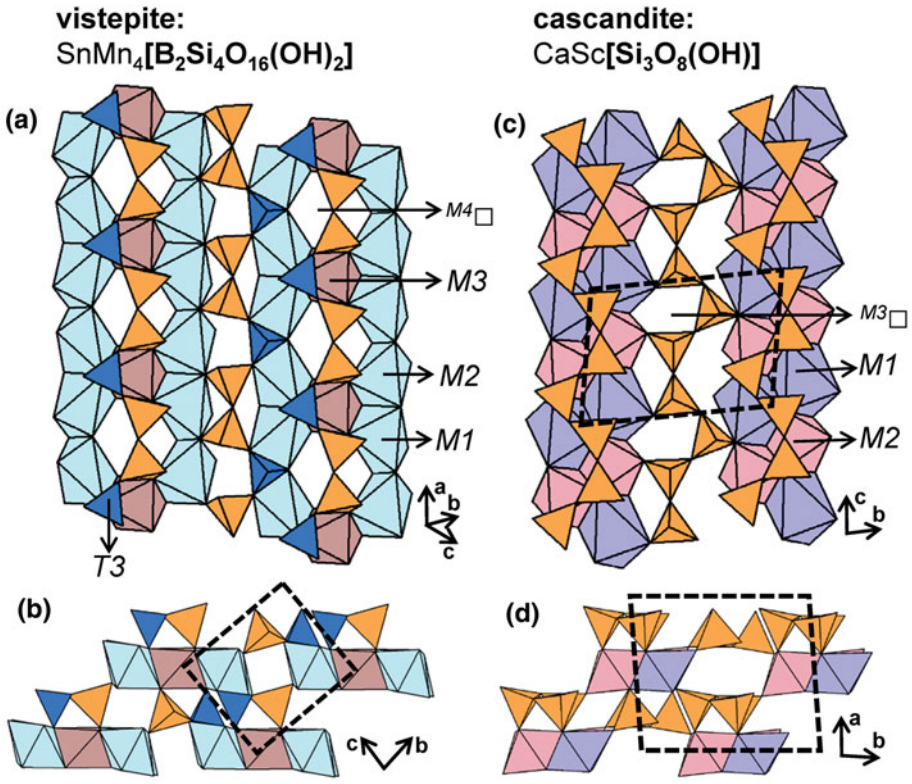

Fig. 14. The structure of **vistepite** viewed (*a*) orthogonal to the **a**-axis and (*b*) along the **a**-axis, $^{T3}[BO_4]$ tetrahedra are shown in dark blue. The structure of **cascandite** projected (*c*) onto (100) and (*d*) along the **c**-axis. Fine dashed black lines outline the unit cell and H atoms associated with $(OH)^-$ groups have been omitted for clarity.

to adjacent ribbons by isolated $(CaO^z(H_2O)_4)^{2-}$-octahedra (Ca5), forming sheets parallel to (001) (Fig. 17*c*). These sheets link along the **a**-axis via ribbons of $(CaO_3(OH)_2(H_2O))^{6-}$- and $(CaO_4(OH)_2(H_2O))^{8-}$-polyhedra (Ca2 and Ca4, respectively) (Fig. 17*d*). **Jennite** contains four *transformer* $(H_2O)^t$ groups and three $(OH)^-$ groups.

The $^2T_3$ $[Si_3O_8(OH)]^{5-}$ chains in **plombièrite** (**tobermorite-14Å**) link to sheets of $(CaO_6(OH))^{11-}$- (Ca1) and $(CaO_6(H_2O))^{10-}$-polyhedra (Ca2) that are parallel to (100), forming layers with the composition $[Ca_4Si_6O_{16}(OH)_2(H_2O)_2]^{2-}$ (Fig. 17*e*). These layers link along the **c**-axis via chains of $(CaO_2(H_2O)_4)$-octahedra (Ca3) that extend along the **b**-axis, parallel to $^2T_3$ chains (Fig 17*f*). **Plombièrite** contains one $(OH)^-$ group that bridges $(SiO_3(OH)^-)^{3-}$-tetrahedra and $(CaO_6(OH))^{11-}$-polyhedra (Ca1). **Plombièrite** also contains three $(H_2O)^t$ and two $(H_2O)^z$ groups that bond to interlayer Ca3 atoms, a layer that separates adjacent $^2T_3$ chains and prevents them from polymerising and forming $^2T_2{}^3T_4$ $[Si_6O_{16}]^{8-}$ ribbons as in **tobermorite-11Å** (see below). In **riversideite (tobermorite-9.3Å)**,$^2T_3$ $[Si_3O_8(OH)]^{5-}$ chains link to similar sheets of $(CaO_6(OH))^{11-}$-polyhedra, Ca^{2+}-octahedra and $^{[7]}Ca^{2+}$-polyhedra but occur within a structure that is much more condensed due to a lower H_2O content. For a more detailed description of hydrated C–S–H minerals, refer to the section on **tobermorite-11Å**. In both **plombièrite** and **riversideite** (**tobermorite-group** minerals), the following stacking sequence is observed; OTITOTIT, where 'O' represents a layer of Ca^{2+}-polyhedra, 'T' a layer containing $^2T_3$ chains and 'I', an interstitial layer of (H_2O) groups and Ca^{2+}-polyhedra that may or may not be present depending on the hydration state (Fig. 17*f*). In **whelanite**, the stacking sequence is OTCTOTCT (Fig. 18*a*), where 'O' represents a layer of $(CaO_6(OH,H_2O))$-polyhedra, 'T' is a layer containing $^2T_3$ chains, and 'C' is a layer of $(Cu(O,(OH))_6)$- and $(Ca(O,(OH))_6)$-octahedra. In **whelanite**, the TCT block has OD character with two overlapping, half-occupied $^2T_3$ chains in which all *T* sites (*Si*1a, *Si*1b and *Si*2) and anions involved in Si–O–Si linkages are half occupied; anions associated with Si^{4+}-tetrahedra but not involved in Si–O–Si linkages are half occupied by O^{2-} and half-occupied either by $(OH)^-$ or by (H_2O). Despite chemical, spectroscopic and structural evidence for $(CO_3)^{2-}$ groups in **whelanite**, its position in the structure has yet to be determined due to problems of disorder. Kampf *et al.* (2012) provide a detailed description of both MDO polytypes and their OD characteristics. Figure 18*b* shows the structure of **whelanite** in which both overlapping, $^2T_3$ chains are shown, one in red and the other in orange.

$^2T_4$ chains

The $^2T_4$ $[Si_4O_{12}]^{8-}$ chain in **batisite-group** minerals (Table 5) contains four distinct Si^{4+}-tetrahedra that form *c-shaped* tetramers (Figs 19*a–d*). In **batisite-group** minerals, $^2T_4$ chains extend along the **a**-axis and link to chains of corner-sharing Ti^{4+}-octahedra (Fig. 19*e*). Each Ti^{4+}-octahedra links to four distinct $^2T_4$ chains, and chains of octahedra and tetrahedra occur in layers that alternate along the **a**-axis. **Batisite-group** minerals also contain three sites *A*1, *A*2 and *A*3. In **batisite,** these sites are occupied by Ba^{2+}, Na^+ and Na^+, respectively (Fig. 19*f*). In **scherbakovite**, *A*1 and *A*2 are occupied by K^+ and *A*3 is occupied by Na^+. In **noonkanbahite**, *A*1, *A*2 and *A*3 are occupied by Ba^{2+}, K^+ and Na^+, respectively. Although the presence of $(OH)^-$ is only included in the ideal formula of **scherbakovite** (Table 5), there is evidence for partial occupancy of one O^{2-} site by $(OH)^-$ in **batisite** and **noonkanbahite** (Uvarova *et al.*, 2010; Zolotarev *et al.*, 2017).

The $^2T_4$ $[Si_4O_{12}]^{8-}$ chains in **haradaite** extend along the **c**-axis and are linked to each other along the **b**-axis by sheets

https://doi.org/10.1180/mgm.2020.13 Published online by Cambridge University Press

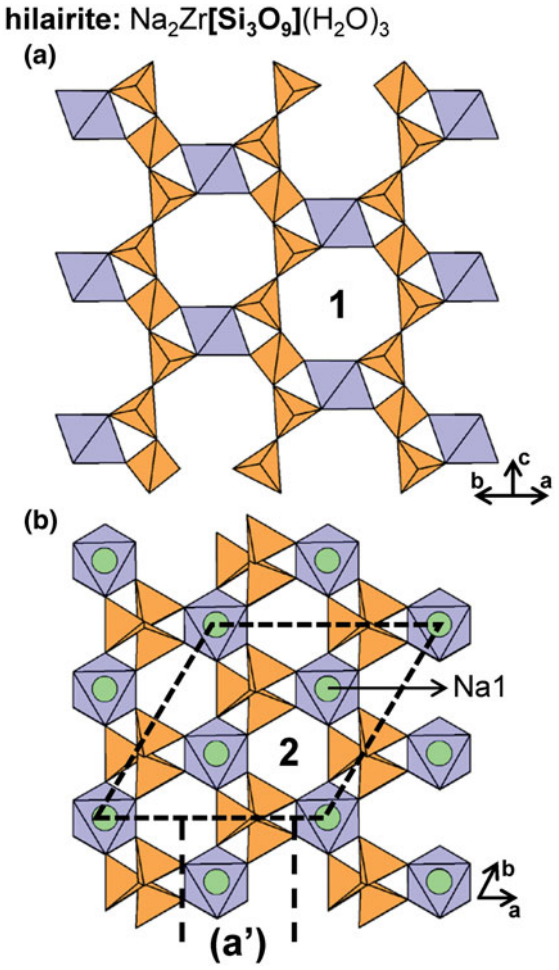

Fig. 15. The structure of **hilairite** projected (*a*) orthogonal to the **c**-axis and (*b*) along the **c**-axis. Channel *1* in (*a*) is occupied by Na1, Na2 and (H_2O) groups and channel *2* in (*b*) is occupied by Na2 and (H_2O) groups. The (H_2O) groups, Na1 and Na2 in (*a*) and (H_2O) groups and Na2 in (*b*) have been omitted for clarity. Fine dashed black lines outline the unit cell.

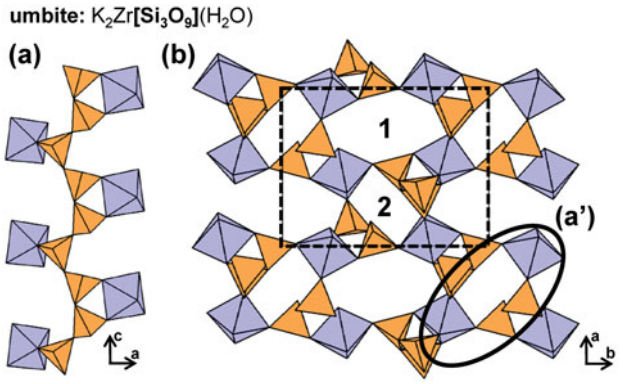

Fig. 16. The structure of **umbite** projected (*a*) onto (010) and (*b*) along the **c**-axis. In (*b*), channel *1* is occupied by K2 and (H_2O) groups and channel *2* is occupied by K1. The (H_2O) groups, K1 and K2 atoms have been omitted for clarity. Fine dashed black lines outline the unit cell.

of Sr^{2+}-polyhedra (Sr1) (Fig. 20*a*). Chains are also linked along the **c**-axis by $^{[5]}V^{4+}$-polyhedra. Sheets of $^{2}T_4$ chains and $^{[5]}V^{4+}$-polyhedra and sheets of Sr^{2+}-polyhedra are parallel to (001) and alternate along the **b**-axis (Fig. 20*b*). In **suzukiite**, the Ba^{2+}-analogue of **haradaite**, $^{2}T_4$ chains are linked to each other by sheets of $^{[11]}Ba^{2+}$-polyhedra. In **ohmilite**, $^{2}T_4$ chains extend along the **b**-axis and link to a complex layer of Ti^{4+}-octahedra (*M*1) and Sr^{2+}-polyhedra (Fig. 20*c*). Corner-sharing Ti^{4+}-octahedra form chains that extend along the **b**-axis and link to two $^{2}T_4$ chains, forming $[Si_8O_{24}(Ti_2O_2)]^{12-}$ ribbons. These ribbons link to each other along the **a**-axis by $(SrO_8(H_2O))^{14-}$- (Sr1), $(SrO_6(H_2O)_2)^{10-}$- (Sr2) and $(SrO_7(H_2O))^{12-}$-polyhedra (Sr3) (Fig. 20*d*). **Ohmilite** contains one $(H_2O)^n$ and two $(H_2O)^t$ groups. Mizota *et al.* (1983) have suggested that the substitution $Ti^{4+} + O^{2-} \leftrightarrow Fe^{3+} + OH^-$ may be responsible for the partial occupancy of the *M*1 site by Fe^{3+} and the OH-stretch in the IR spectrum of **ohmilite.**

In the OD structure of **fukalite**, six MDO polytypes are known; here we describe the **fukalite** structure based on the MDO1 polytype. Here, $^{2}T_4$ chains are strongly modulated, resembling chains in **batisite**, **haradaite** and **ohmilite**. In **fukalite**, there are two types of layers that are parallel to (100) and alternate along the **b**-axis (Fig. 21*a*). Layer *1* consists of planar sheets of $(CaO_6(OH))^{11-}$-polyhedra (Ca1–Ca4) and layer *2* consists of ribbons of $(CaO_4(OH)_2)^{8-}$- and $(CaO_5(OH)_2)^{10-}$-polyhedra (Ca5–Ca8) that link along the **c**-axis to form a modulated sheet. Layers are linked along the **b**-axis by $(CO_3)^{2-}$ groups and $^{2}T_4$ chains that extend along the **a**-axis (Fig. 21*b*). There are four $(OH)^-$ groups that bridge Ca^{2+}-polyhedra of layer *1* to Ca^{2+}-polyhedra of layer *2*.

The $^{2}T_4$ chain in **taikanite** (Figs 22*a–d*) is geometrically distinct from the $^{2}T_4$ chain in the **batisite-group** minerals. In **taikanite,** Si^{4+}-tetrahedra form chains that extend along the **b**-axis and link to chains of edge-sharing $^{[8]}Sr^{2+}$-polyhedra that also extend along the **b**-axis (Fig. 22*e*). These chains link along the **a**-axis via chains of edge-sharing Mn^{2+}-octahedra that extend along the **c**-axis and via $^{[8]}Ba^{2+}$-polyhedra. In **taikanite**, $^{[8]}Sr^{2+}$- and $^{[8]}Ba^{2+}$-polyhedra and $^{2}T_4$ chains occur in layers that alternate along the **c**-axis (Fig. 22*f*). The $^{2}T_4$ $[Si_4O_{10}(OH)_2]^{6-}$ chain in **krauskopfite** contains $(Si(O,OH)_4)$-tetrahedra but does not consist of *c*-shaped tetramers like the chains in **batisite-group** minerals (Fig. 19*b*); instead chains are more extended (linear) (Figs 23*a–d*). In **krauskopfite**, chains link to chains of edge-sharing $^{[8]}Ba^{2+}$-polyhedra (Fig. 23*e*) that occur in layers parallel to (001) and alternate with layers of $^{2}T_4$ chains (Fig. 23*f*). **Krauskopfite** contains six H^+ ions, two of which are associated with $(OH)^-$ groups and form acid silicate groups and four are associated with (H_2O) groups bonded to $^{[8]}Ba^{2+}$-polyhedra.

Balangeroite and **gageite** are asbestiform minerals that have monoclinic (2*M*) and triclinic (1*A*) polytypes due to their OD character (Bonaccorsi *et al.*, 2012) (Table 5). Both minerals contain $^{2}T_4$ chains that show a higher degree of chain extension than other $^{2}T_4$ chains (Figs 24*a–d*). Chains extend along the **b**-axis and link to a framework of predominately Mg^{2+}-, Mn^{2+}- and Fe^{2+}-octahedra. **Balangeroite** and **gageite** contain twenty-four distinct octahedrally coordinated *M*-sites that polymerise to form [1] a ribbon of edge-sharing octahedra, and [2] a column of edge-sharing octahedra. These units extend along the **b**-axis and each occurs in two crystallographically distinct orientations: sites *M*1–*M*12 comprise the ribbon and sites *M*13–*M*24 comprise the column (Fig. 24*e*). Here, there are eight distinct Si^{4+}-tetrahedra that form $^{2}T_4$ chains that occupy channels in the framework of octahedra. Each $^{2}T_4$ chain links to two crystallographically distinct columns (Fig. 24*f*) and to one ribbon (Fig. 24*g*). **Balangeroite** and **gageite** contain 20 $(OH)^-$ groups that each link to three *M*-site cations. The Ni–Fe analogue of

https://doi.org/10.1180/mgm.2020.13 Published online by Cambridge University Press

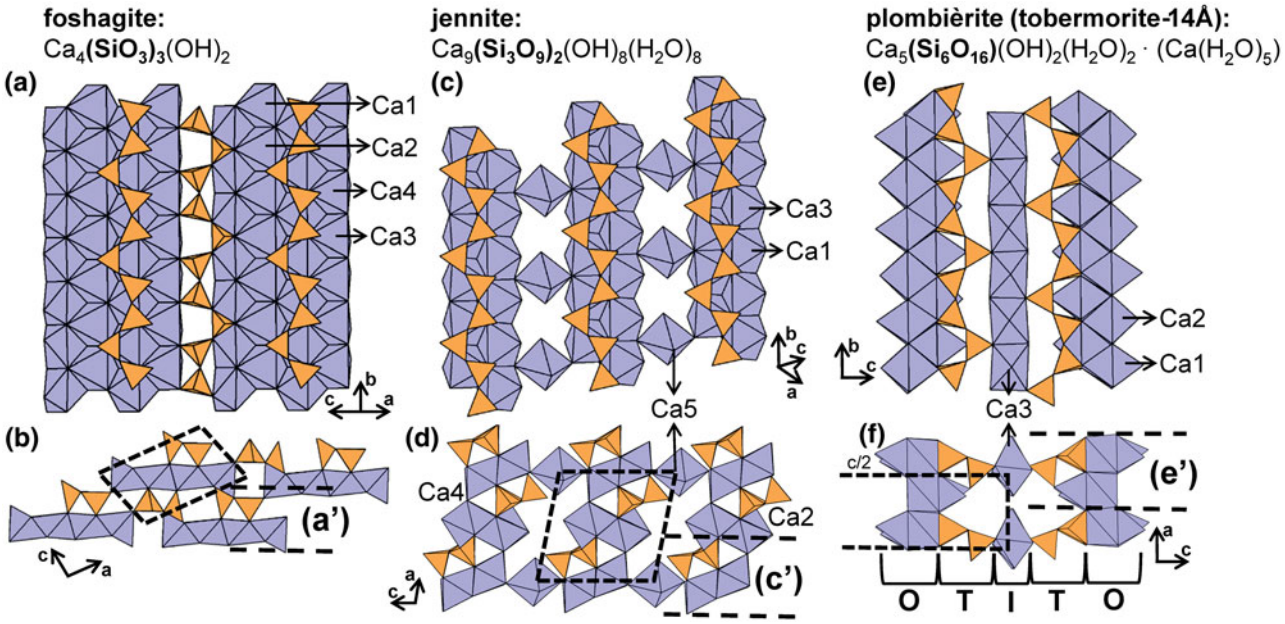

Fig. 17. The structure of (*a*, *b*) **foshagite** and (*c*, *d*) **jennite** viewed (*a*, *c*) orthogonal to the **b**-axis and (*b*, *d*) along the **b**-axis. The structure of **plombièrite (tobermorite-14Å)** projected (*e*) onto (100) and (*f*) along the **b**-axis. In (*f*), layers that contain $^2T_3$ chains are labelled T, layers that contain sheets of Ca^{2+}-polyhedra are labelled O and layers that contain interstitial Ca^{2+}-polyhedra and (H_2O) groups are labelled I. Fine dashed black lines outline the unit cell which is halved along the **c**-axis in (*f*). The H atoms associated with $(OH)^-$ and (H_2O) groups have been omitted for clarity.

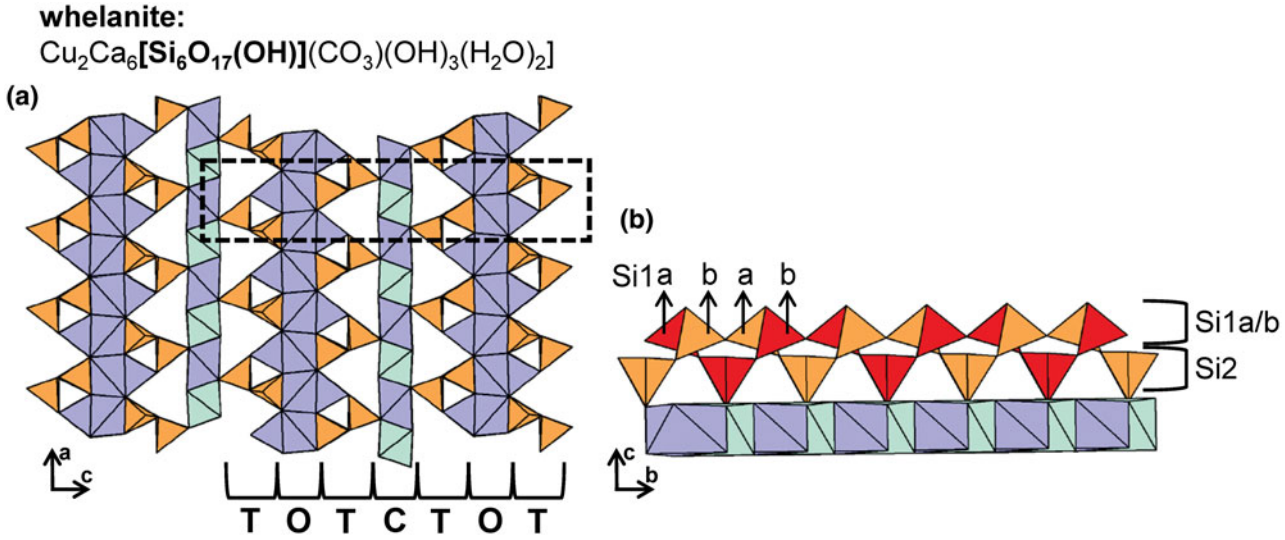

Fig. 18. The structure of **whelanite** projected (*a*) along the **b**-axis and (*b*) onto (100). In (*a*), the TOTCTOT stacking sequence is labelled and in (*b*) one of the overlapping, half-occupied $^2T_3$ chains is shown as orange tetrahedra on the other chain is shown as red tetrahedra. Fine dashed black lines outline the unit cell and H atoms associated with $(OH)^-$ and (H_2O) groups and C atoms associated with (CO_3) groups have been omitted for clarity.

balangeroite occurs as intergrowths in antigorite serpentinite (Evans and Kuehner, 2011).

Many novel, synthetic compounds contain $^2T_4$ chains such as **$BaUO_2[Si_2O_6]$** (Plaisier *et al.*, 1995), **$NaY[Si_2O_6]$** (Toebbens *et al.*, 2005), **$Cu_3Na_2[Si_4O_{12}]$** (Kawamura and Kawahara, 1976), **$Ca_3Mn_2O_2[Si_4O_{12}]$** (Moore and Araki, 1979) and **$NaGd[P_4O_{12}]$** (Amami *et al.*, 2005).

$^2T_5$ chains

The **rhodonite-group** minerals **rhodonite**, **ferrorhodonite** and **vittinkiite** (Table 5) contain $^2T_5$ chains in which Si^{4+}-tetrahedra link to form *c-shaped* trimers that are linked by $[Si_2O_7]^{6-}$ dimers (Figs 25*a*–*d*). Here, $^2T_5$ chains and ribbons of higher coordination polyhedra (*M*1–*M*5) occur in alternating layers that are parallel to (100).

https://doi.org/10.1180/mgm.2020.13 Published online by Cambridge University Press

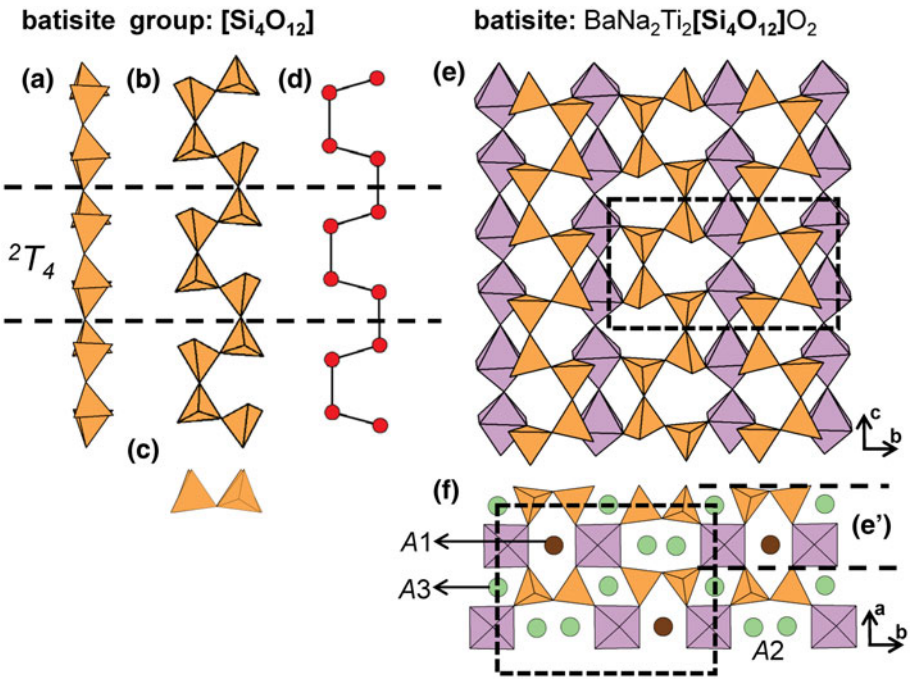

Fig. 19. (*a*, *b*, *c*) Tetrahedral representations of the $^2T_4$ chain in **batisite-group** minerals and (*d*) a ball-and-stick representation of the chain. The structure of **batisite** projected (*e*) onto (100) and (*f*) along the **c**-axis. Dashed black lines outline the geometrical repeat unit of the chain and fine dashed black lines outline the unit cell.

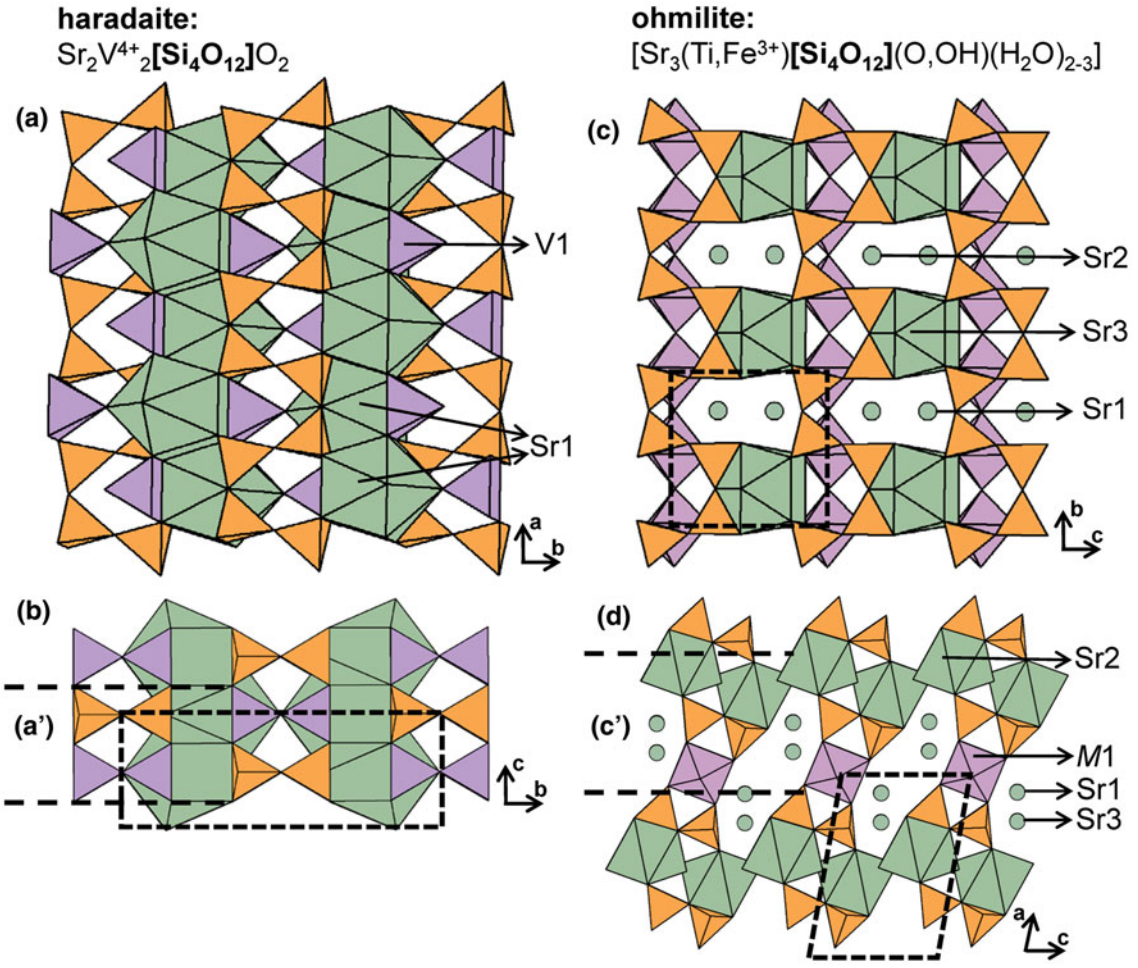

Fig. 20. The structure of **haradaite** projected (*a*) onto (001) and (*b*) along the **a**-axis (*b*). The structure of **ohmilite** projected (*c*) onto (100) and (*d*) along the **b**-axis (*c*) and into the **b**-axis. Fine dashed black lines outline the unit cell and H atoms associated with $(OH)^-$ and (H_2O) groups have been omitted for clarity.

https://doi.org/10.1180/mgm.2020.13 Published online by Cambridge University Press

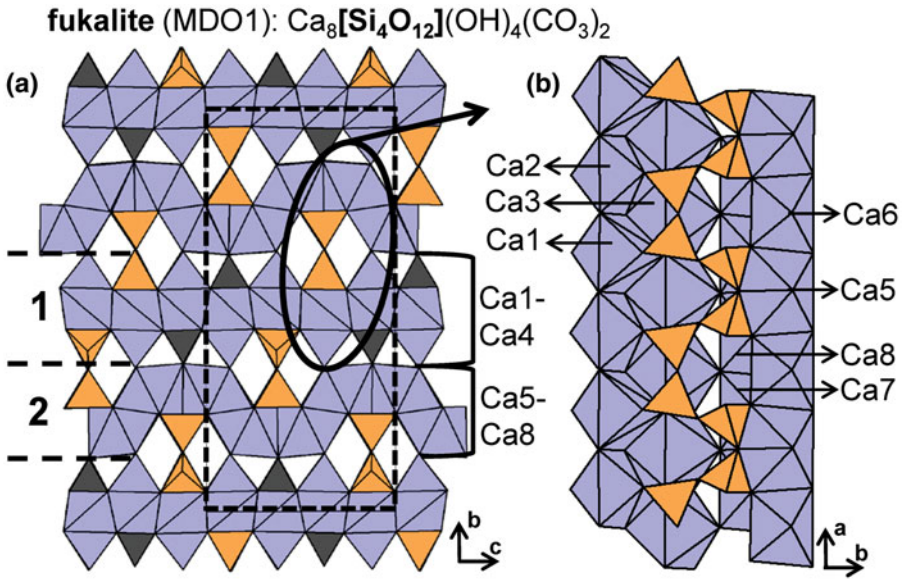

Fig. 21. The structure of **fukalite** projected (*a*) along the **a**-axis and (*b*) onto (001). In (*a*), (CO_3) groups are shown in dark grey and H atoms associated with $(OH)^-$ groups are omitted for clarity. Fine dashed black lines outline the unit cell.

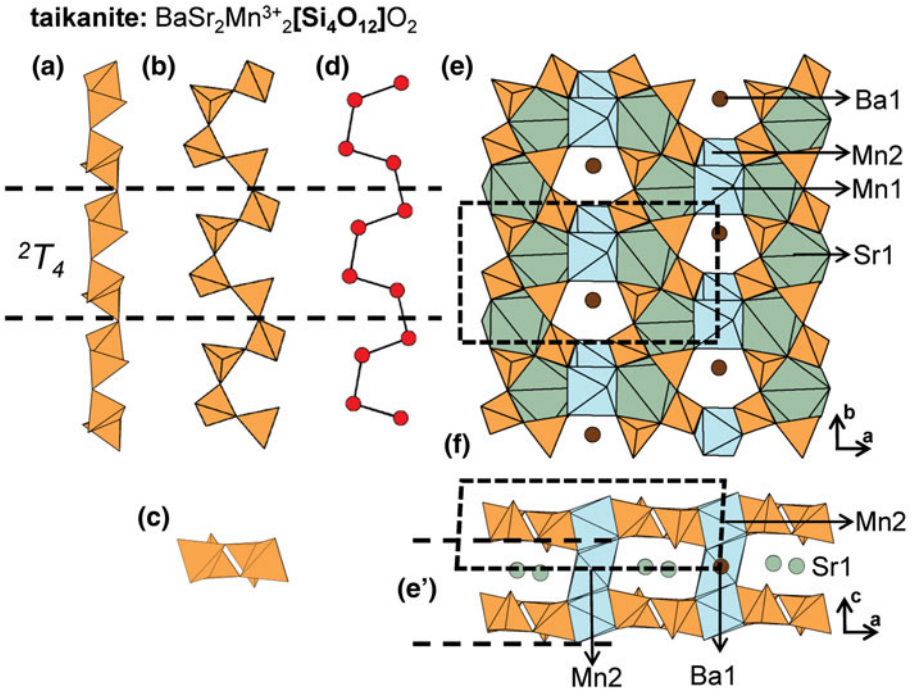

Fig. 22. (*a*, *b*, *c*) Tetrahedral representations of the $^2T_4$ chain in **taikanite** and (*d*) a ball-and-stick representation of the chain. The structure of **taikanite** projected (*e*) onto (001) and (*f*) along the **b**-axis. Dashed black lines outline the geometrical repeat unit of the chain and fine dashed black lines outline the unit cell.

The general formula for **rhodonite-group** minerals may be written as $M_5M_{1-3}M_4[\boldsymbol{T_5O_{15}}]$, and a new nomenclature scheme was recently provided by Shchipalkina *et al.* (2019*b*). In these structures, $^2T_5$ chains extend along [110] and link adjacent ribbons of higher-coordination polyhedra. In **vittinkiite**, ideally $Mn_5[\boldsymbol{Si_5O_{15}}]$, all *M* sites are occupied by Mn^{2+}. However, such compositions are uncommon, as most **rhodonite-group** minerals show considerable chemical variability over the *M sites* (Mason, 1975), incorporating Ca^{2+}, Fe^{2+}, Mg^{2+} and Zn^{2+} in addition to Mn^{2+}. The [7]-coordinated *M*5-site in **rhodonite** is dominated by Ca^{2+} (Figs 25*e*,*f*) and as a result, the formula for **rhodonite** is ideally $CaMn_4[\boldsymbol{Si_5O_{15}}]$. In **ferrorhodonite,** *M*4 is occupied by Fe^{2+}, *M*1–*M*3 are occupied by Mn^{2+}, and *M*5 is occupied by Ca^{2+}. Figures 26*a*–*f* highlights *M*-site substitution in these three minerals. **Rhodonite-group** minerals with significant Zn^{2+} and Mg^{2+} have been reported and details on the ordering of *M*-site cations and the effects of composition on **rhodonite** structures are given by Peacor and Niizeki (1963), Peacor *et al.* (1978*a*), Ohashi and Finger (1975), Nelson and Griffen (2005), Leverett *et al.* (2008) and Shchipalkina *et al.* (2017). The compositional range of the **rhodonite-group** minerals overlaps strongly with that of the **bustamite-group** minerals and in a minor way with that of **pyroxmangite** (Shchipalkina *et al.*, 2019*b*).

The general formula of **lithiomarsturite, marsturite, nambulite** and **natronambulite** can be written as $M_5M_4M_{1-3}[\boldsymbol{T_5O_{14}(O,OH)}]$ (Table 5). The *T*1 tetrahedra in **lithiomarsturite** and **marsturite**

https://doi.org/10.1180/mgm.2020.13 Published online by Cambridge University Press

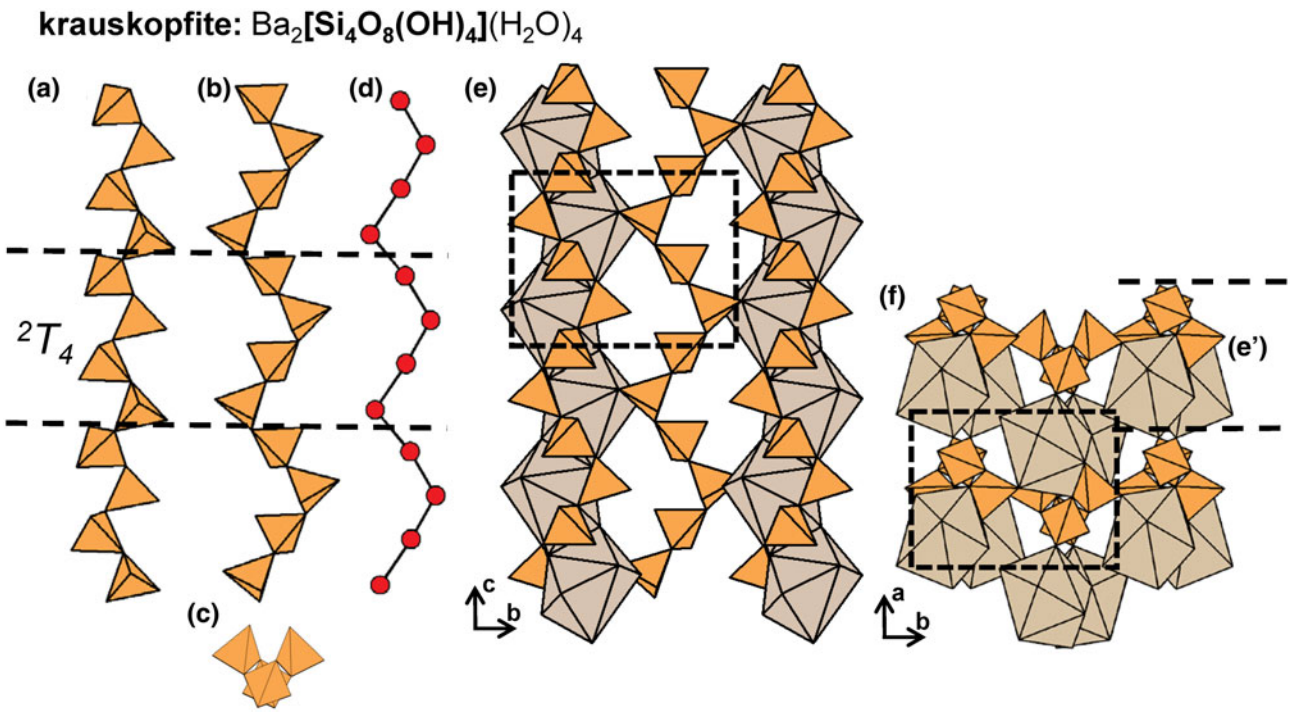

Fig. 23. (*a*, *b*, *c*) Tetrahedral representations of the $^2T_4$ chain in **krauskopfite** and (*d*) a ball-and-stick representation of the chain. The structure of **krauskopfite** projected (*e*) onto (100) and (*f*) along the **c**-axis. Dashed black lines outline the geometrical repeat unit of the chain and fine dashed black lines outline the unit cell. The H atoms associated with $(OH)^-$ and (H_2O) groups have been omitted for clarity.

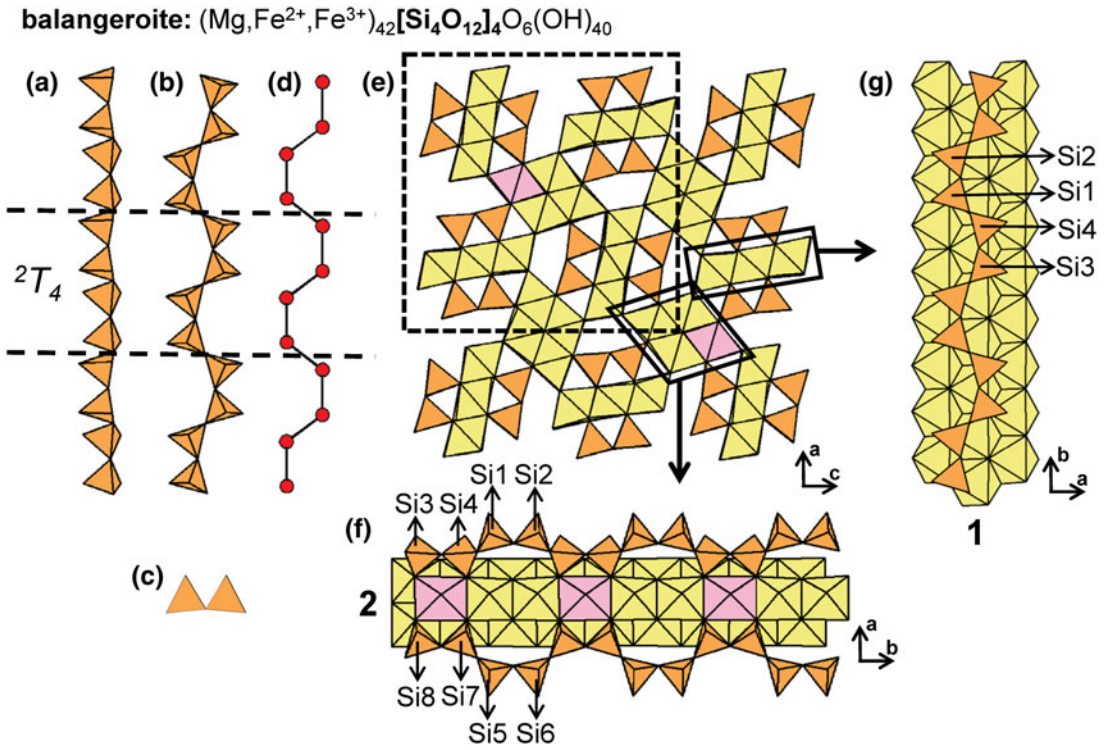

Fig. 24. (*a*, *b*, *c*) Tetrahedral representations of the $^2T_4$ chain in **balangeroite** and (*d*) a ball-and-stick representation of the chain. The structure of **balangeroite** projected (*e*) along the **b**-axis and (*f*, *g*) the two modes of linkage between $^2T_4$ chains and the interstitial structure projected onto (001). Dashed black lines outline the geometrical repeat unit of the chain and fine dashed black lines outline the unit cell. The H atoms associated with $(OH)^-$ groups have been omitted for clarity.

and the *T*4 tetrahedra in **natronambulite** and **nambulite** are acid silicate groups; $(SiO_3(OH))^{3-}$, and $^2T_5$ chains extend along [110]. The *M*1–*M*3 sites in **marsturite** and the *M*1 and *M*3 sites in **lithiomarsturite** are occupied by Mn^{2+}, the *M*5 site is occupied by Na^+ and Li^+, respectively, and the *M*4 site is occupied by Ca^{2+} in both minerals. In **marsturite**, $^{[7]}Ca^{2+}$-polyhedra (*M*4)

https://doi.org/10.1180/mgm.2020.13 Published online by Cambridge University Press

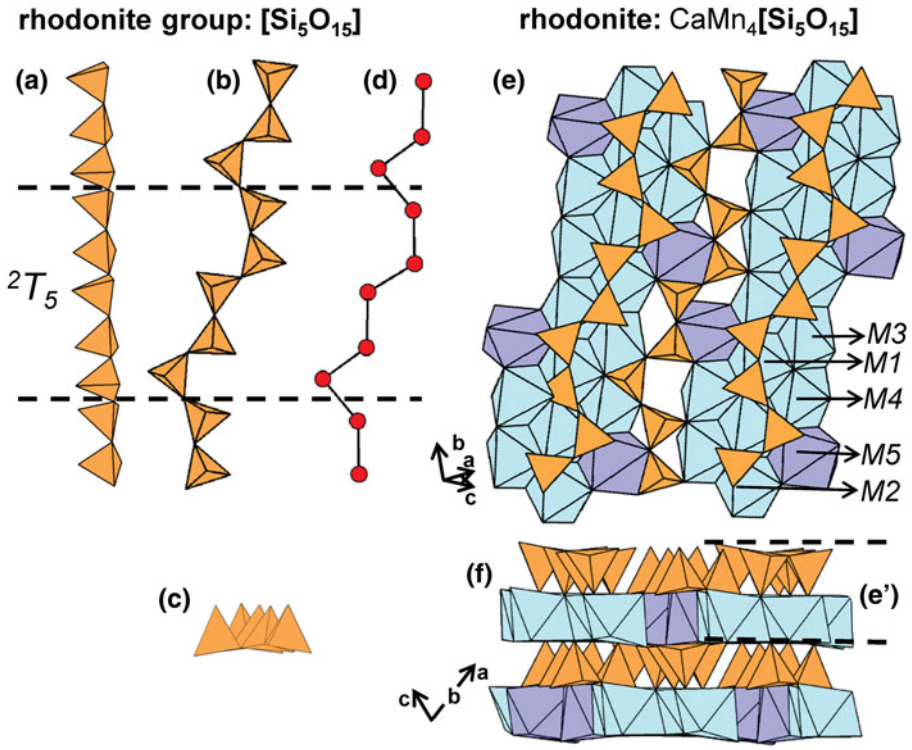

Fig. 25. (*a*, *b*, *c*) Tetrahedral representations of the $^{2}T_{5}$ chain in **rhodonite-group** minerals and (*d*) a ball-and-stick representation of the chain. The structure of **rhodonite** viewed (*e*) orthogonal to [110] and (*f*) along [110]. Dashed black lines outline the geometrical repeat unit of the chain.

and $(NaO_7(OH))^{14-}$-polyhedra (*M*5) link adjacent ribbons of *M*1–*M*3-octahedra to form sheets that alternate with layers of $^{2}T_{5}$ chains (Figs 27*a*,*b*). In **lithiomarsturite**, the *M*5 site is occupied by Li^{+} that forms $(LiO_4(OH))^{8-}$-polyhedra and the *M*2 site is occupied by Ca^{2+} that forms $(CaO_5(OH))^{9-}$-octahedra (Figs 27*c*, *d*). Although the coordination of Li^{+} in **lithiomarsturite**, **nambulite** and **natronambulite** is not yet agreed upon, Nagashima *et al.* (2014*a*) used bond-valence arguments to show that Li^{+} is probably [5]-coordinated; here we show Li^{+} as a [5]-coordinated cation (Fig. 27*c*). In **nambulite** and **natronambulite**, the octahedrally coordinated *M*1–*M*3 sites are occupied by Mn^{2+}, the *M*4 site is occupied by $^{[7]}Mn^{2+}$ and the *M*5 site is occupied by Li^{+} that forms $(LiO_4(OH))^{8-}$-polyhedra in **nambulite** (Figs 27*e*,*f*), and by Na^{+} that forms $(NaO_7(OH))^{14-}$-polyhedra in **natronambulite** (Figs 27*g*,*h*). In **nambulite** and **natronambulite,** the *M*4 and *M*5 polyhedra link adjacent ribbons of *M*1–*M*3 octahedra to form a sheet similar to that in **marsturite** and **lithiomarsturite**. In **santaclaraite**, *T*1 is an $(SiO_3(OH))^{3-}$-tetrahedron and $^{2}T_{5}$

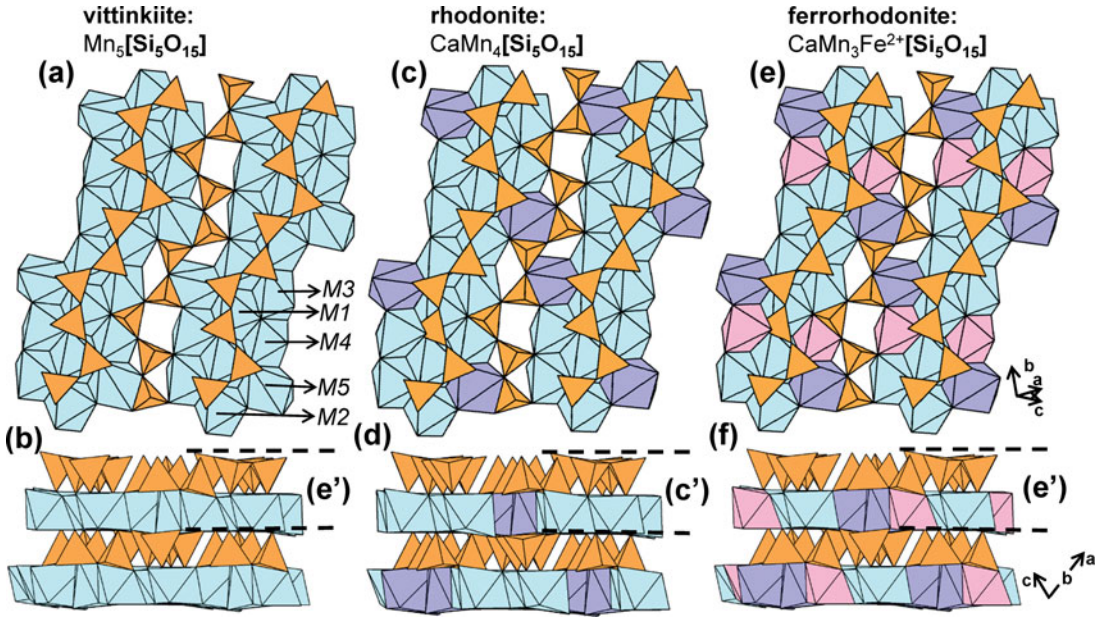

Fig. 26. The structure of (*a*, *b*) **vittinkiite**, (*c*, *d*) **rhodonite** and (*e*, *f*) **ferrorhodonite** viewed (*a*, *c*, *e*) orthogonal to [110] and (*b*, *d*, *f*) along [110]. *M*-site labels in (*a*) are also applicable to (*c*) and (*e*).

https://doi.org/10.1180/mgm.2020.13 Published online by Cambridge University Press

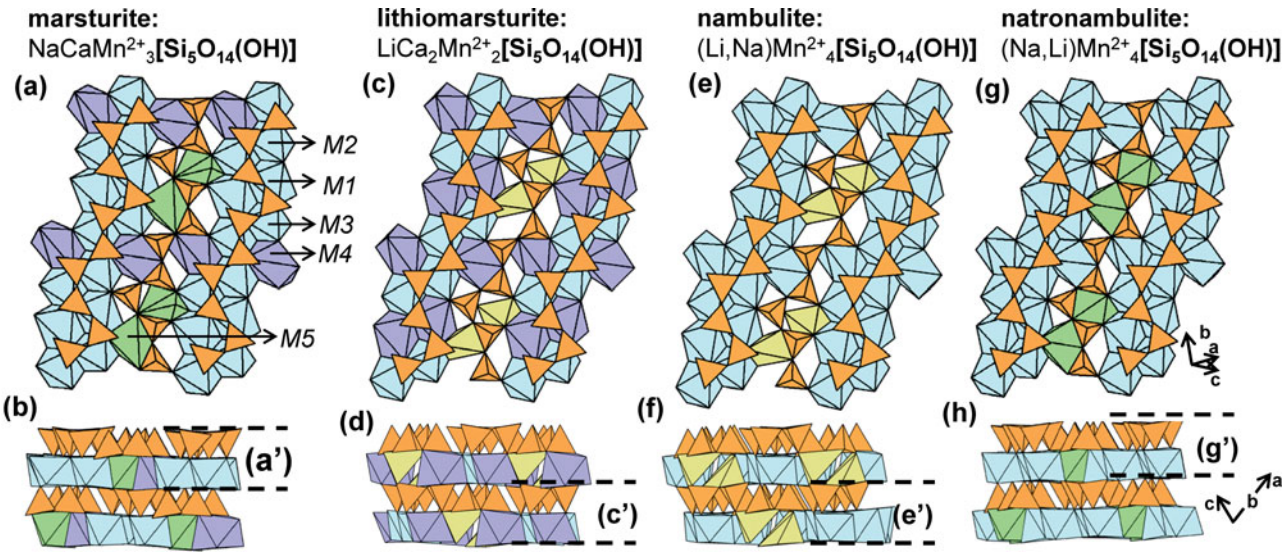

Fig. 27. The structure of (*a*, *b*) **marsturite**, (*c*, *d*) **lithiomarsturite**, (*e*, *f*) **nambulite** and (*g*, *h*) **natronambulite** viewed (*a*, *c*, *e*, *g*) orthogonal to [110] and (*b*, *d*, *f*, *h*) along [110]. Here, *M*-site labels in (*a*) are also applicable to (*c*), (*e*) and (*g*) and H atoms associated with $(OH)^-$ groups have been omitted for clarity.

chains link to rhodonite-type ribbons of $(Mn^{2+}(O,(OH),H_2O)_6)$-octahedra and Ca^{2+}-polyhedra.

The general formula for the **babingtonite-group** minerals can be written as $A_2M_1M_2[\boldsymbol{T_5O_{14}(OH)}]$ (Table 5). The geometrical repeat unit of the $^2T_5$ $[Si_5O_{14}(OH)]^{9-}$ chain in **babingtonite** contains four Si^{4+}-tetrahedra and one $(SiO_3(OH))^{3-}$-tetrahedron. These $^2T_5$ chains link to sheets of $^{[8]}Ca^{2+}$-polyhedra (Ca1 and Ca2) and Fe^{2+}-octahedra (*M*1 and *M*2) that are parallel to (110) (Figs 28*a*,*b*). In **manganbabingtonite**, the *M*1 site is occupied by Mn^{2+} and in **scandiobabingtonite** *M*2 is occupied by Sc^{3+}. Various synthetic compounds containing $^2T_5$ chains have been described including $\mathbf{Mn_5^{2+}[Si_5O_{15}]}$ (synthetic vittinkiite) and $\mathbf{LiMn_4^{2+}[Si_5O_{14}(OH)]}$ (synthetic nambulite) (Ito, 1972).

$^2T_6$ chains

The $^2T_6$ $[Si_6O_{18}]^{12-}$ chains in **stokesite**, **georgechaoite** and **gaidonnayite** are modulated in two directions and have been described geometrically as *spiral* chains (Vorma, 1963; Chao, 1985; Yuan *et al.*, 2017). These $^2T_6$ chains extend along the **b**-axis and are modulated along both the **c**-axis and the **a**-axis (Figs 29*a*–*d*). Chains of tetrahedra link to chains of Sn^{2+}-octahedra and $(CaO_4(H_2O)_2^T)^{6-}$-octahedra (Fig. 29e), and adjacent chains of octahedra are linked along the **c**-axis by $^2T_6$ chains (Fig. 29*f*). In **georgechaoite** and **gaidonnayite**, $^2T_6$ chains extend along [101] and are modulated along the **b**-axis (Figs 30*a*–*d*). Chains of tetrahedra link to chains of $(NaO_4(H_2O)_2^T)^{7-}$- and $(ZrO_6)^{8-}$-octahedra that are cross-linked by $(KO_4(H_2O)_2)^{7-}$-octahedra in **georgechaoite** (Figs 30*e*,*f*) and by $(NaO_4(H_2O)_2^T)^{7-}$-polyhedra in **gaidonnayite**. In **gaidonnayite**, Na sites contain minor amounts of K^+ that may be substituted by Cs^+ in synthetic Cs-exchanged varieties such as $\mathbf{Cs_4Zr_2[Si_6O_{18}](H_2O)_4}$ (Celestian *et al.*, 2019). **Synthetic** $\mathbf{K_8Sr_2[Si_6O_{18}]}$ also contains geometrically similar $^2T_6$ chains (Kahlenberg *et al.*, 2007).

$^2T_7$ chains

Pyroxferroite and **pyroxmangite** are of particular interest as they are the only minerals that contain $^2T_7$ chains (Figs 31*a*–*d*). Chains

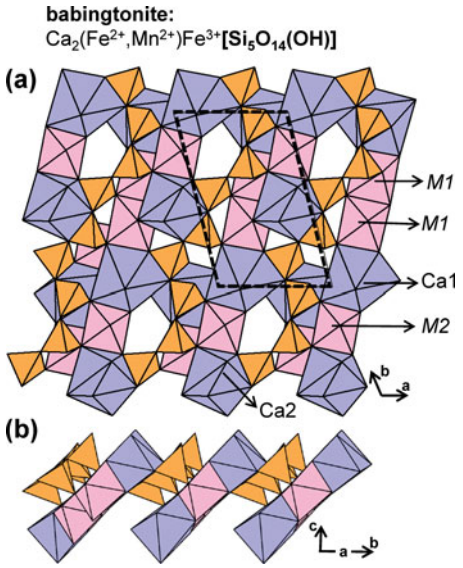

Fig. 28. The structure of **babingtonite** projected (*a*) onto (001) and (*b*) orthogonal to the **c**-axis. Fine dashed black lines outline the unit cell and H atoms associated with $(OH)^-$ groups have been omitted for clarity.

of tetrahedra link to sheets of octahedra and [7]-coordinated polyhedra (*M*1–*M*7) that occur in layers that alternate with layers of $^2T_7$ chains along [011] (Figs 31*e*,*f*). Compositions close to either end-member are rare; there is extensive Fe^{2+}–Mn^{2+} solid-solution that also can incorporate significant amounts of Mg^{2+}, Ca^{2+}, Na^+ and minor Al^{3+} and Cr^{3+}. In **pyroxmangite** and **pyroxferroite**, *M*1–*M*4 are octahedrally coordinated, *M*6 is [5]- or [6]-coordinated, and *M*5 and *M*7 are [7]-coordinated. In **pyroxmangite**, *M*1–*M*4 are typically occupied predominantly by Mn^{2+} with subordinate Mg^{2+} and Fe^{2+}; however, Mg^{2+} dominates at *M*2–*M*4 in synthetic Mg-rich **pyroxmangite** (Finger and Hazen, 1978). The *M*6 site is preferentially occupied by Mg^{2+} but may also be occupied by Mn^{2+} and/or Fe^{2+}, and *M*5 and *M*7 are occupied by Mn^{2+} with minor Mg^{2+} and Fe^{2+}. In

https://doi.org/10.1180/mgm.2020.13 Published online by Cambridge University Press

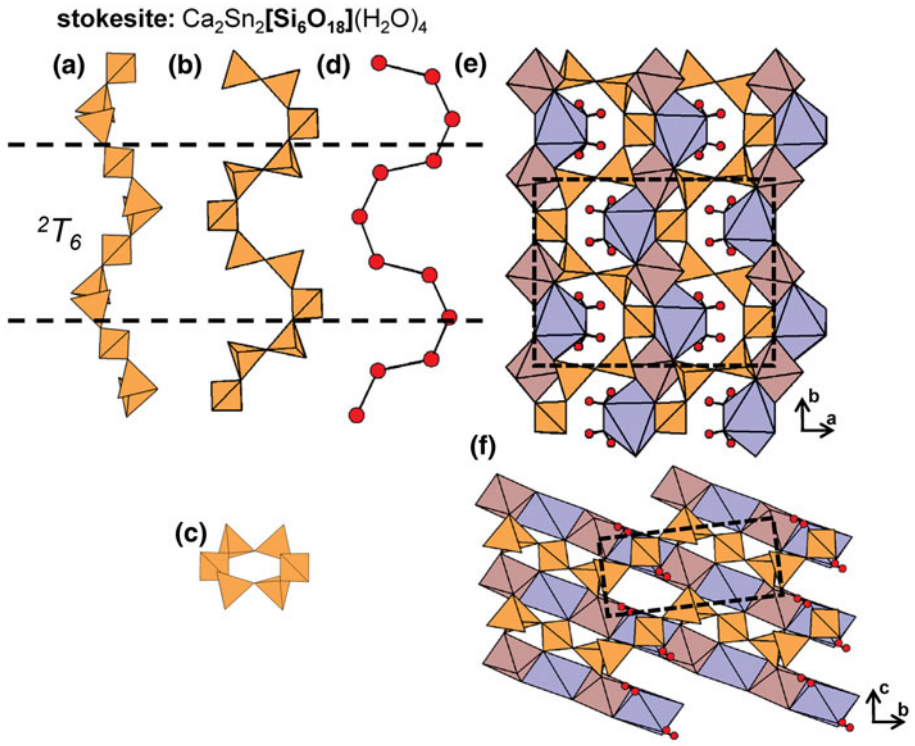

Fig. 29. (*a*, *b*, *c*) Tetrahedral representations of the $^2T_6$ chain in **stokesite** and (*d*) a ball-and-stick representation of the chain. The structure of **stokesite** projected (*e*) onto (001) and (*f*) along the **a**-axis. The H atoms of both (H_2O) groups are shown as red circles. Dashed black lines outline the geometrical repeat unit of the chain and fine dashed black lines outline the unit cell.

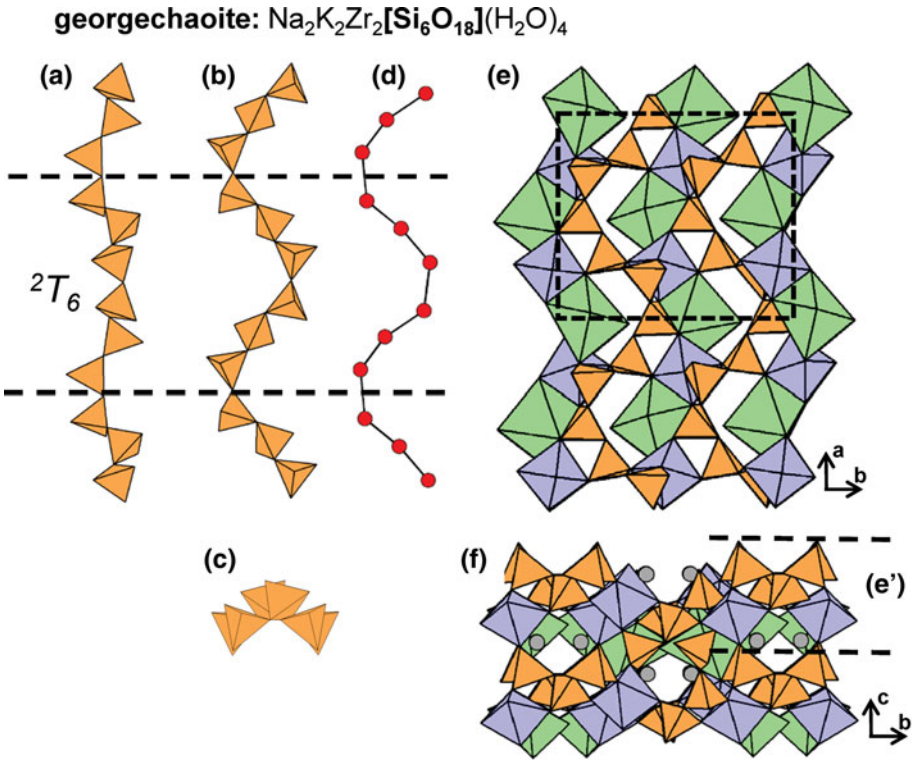

Fig. 30. (*a*, *b*, *c*) Tetrahedral representations of the $^2T_6$ chain in **georgechaoite** and (*d*) a ball-and-stick representation of the chain. The structure of **georgechaoite** projected (*e*) onto (001) and (*f*) along the **a**-axis. Dashed black lines outline the geometrical repeat unit of the chain and fine dashed black lines outline the unit cell. The H atoms associated (H_2O) groups have been omitted for clarity.

pyroxferroite, Ca^{2+} preferentially occupies the [7]-coordinated *M*5 and *M*7 sites, the *M*1–*M*4 sites are occupied by Fe^{2+} with subordinate Mn^{2+} and Ca^{2+}, and the *M*6 site is preferentially occupied by Mg^{2+} but may also contain Mn^{2+} and/or Fe^{2+}.

$^2T_9$ chains

The $^2T_9$ chain occurs only in **synthetic ferrosilite III** (Table 5) where it extends along the **c**-axis (Figs 32*a*–*d*). There are nine octahedrally coordinated sites (*M*1–*M*9) that are occupied by

https://doi.org/10.1180/mgm.2020.13 Published online by Cambridge University Press

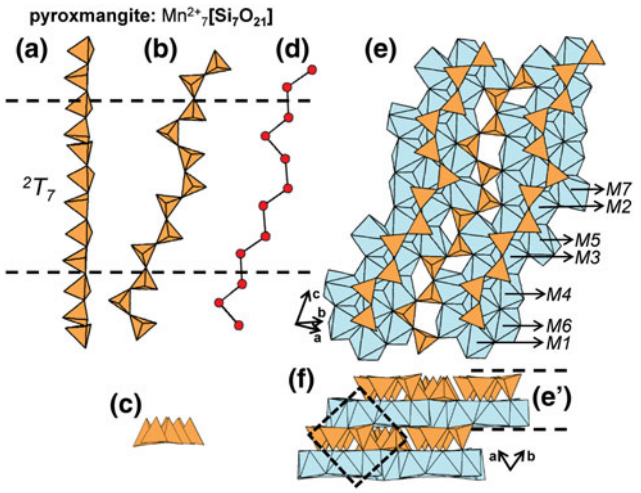

Fig. 31. (*a*, *b*, *c*) Tetrahedral representations of the $^2T_7$ chain in **pyroxmangite** and (*d*) a ball-and-stick representation of the chain. The structure of **pyroxmangite** viewed (*e*) orthogonal to the **c**-axis and (*f*) along the **c**-axis. Dashed black lines outline the geometrical repeat unit of the chain and fine dashed black lines outline the unit cell.

Fe^{2+} and form ribbons that extend parallel to [001]. The $^2T_9$ chains and ribbons of Fe^{2+}-octahedra occur in alternating layers (Figs 32*e*,*f*), comparable to the structures of **pyroxmangite** (Figs 31*e*,*f*) **pyroxferroite** and the **rhodonite-group** minerals (Figs 25*e*,*f* and 26*a*–*f*).

$^2T_{12}$ chains

The geometrical repeat unit of the chain in **alamosite** contains twelve Si^{4+}-tetrahedra that polymerise to form $^2T_{12}$ chains that extend parallel to [101]. The $^2T_{12}$ chains are modulated in two directions, resulting in a *spiral* chain (Figs 33*a*–*d*) resembling the $^2T_6$ chains in **stokesite** (Figs 29*a*–*d*). In **alamosite,** $^2T_{12}$ chains link to *spiral* ribbons of [5]-, [7]- and [6]-coordinated Pb^{2+}-polyhedra that occupy three sites: *Pb*1, *Pb*2 and *Pb*3 (Figs 33*e*,*f*).

$^2T_{24}$ chains

The $^2T_{24}$ chain occurs only in **synthetic** $\mathbf{Na_{24}Y_8(Si_{24}O_{72})}$. The geometrical repeat unit of this chain contains twenty-four Si^{4+}-tetrahedra that polymerise to form a *spiral* chain modulated along the **a**- and **c**-axes (Figs 34*a*–*d*). A complete structure description is given by Maksimov *et al.* (1980).

^3T_r class

$^3T_4$ ribbons

The geometrical repeat unit of the ribbons in **vinogradovite, paravinogradovite** and **bigcreekite** (Table 6) contains four distinct tetrahedra that polymerise to form $^3T_4$ ribbons (Figs 35*a*–*c*). Topologically, these $^3V_2$ ribbons (Fig. 35*d*) are identical to many of the ^3T_r ribbons described in the following sections. **Vinogradovite** and **paravinogradovite** contain $^2T_2$ pyroxene-like chains in addition to $^3T_4$ ribbons. **Vinogradovite** contains two

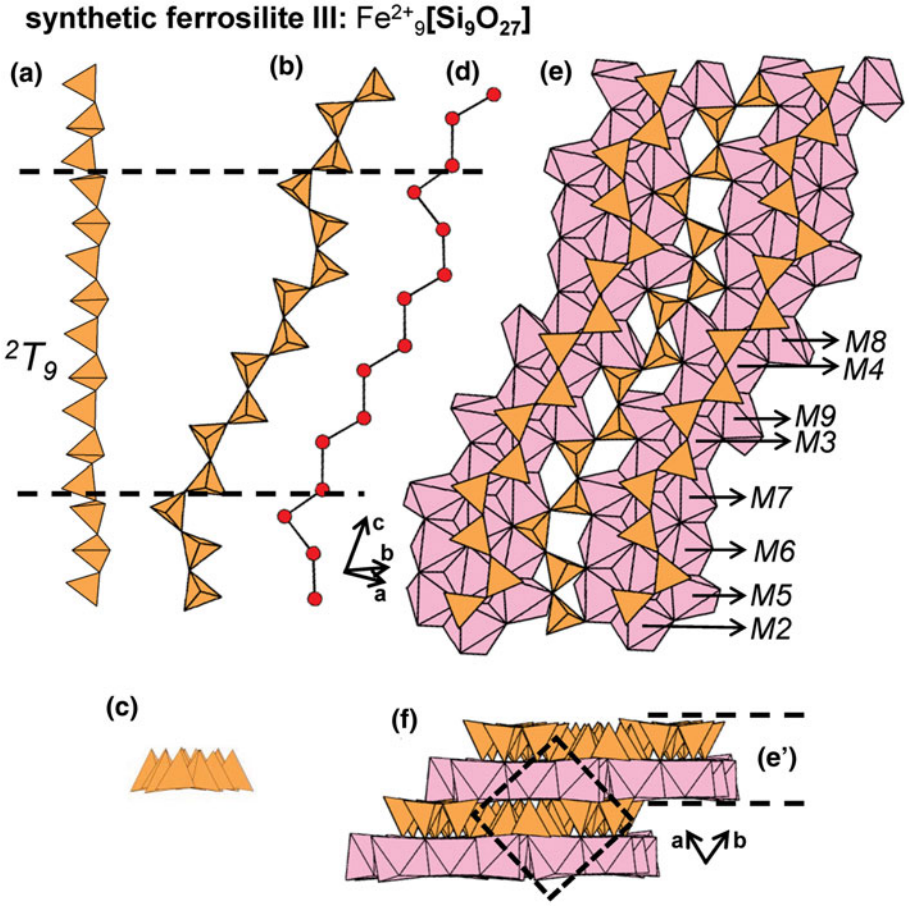

Fig. 32. (*a*, *b*, *c*) Tetrahedral representations of the $^2T_9$ chain in **synthetic ferrosilite III** and (*d*) a ball-and-stick representation of the chain. The structure of **synthetic ferrosilite III** viewed (*e*) orthogonal to the **c**-axis and (*f*) along the **c**-axis. Dashed black lines outline the geometrical repeat unit of the chain and fine dashed black lines outline the unit cell.

https://doi.org/10.1180/mgm.2020.13 Published online by Cambridge University Press

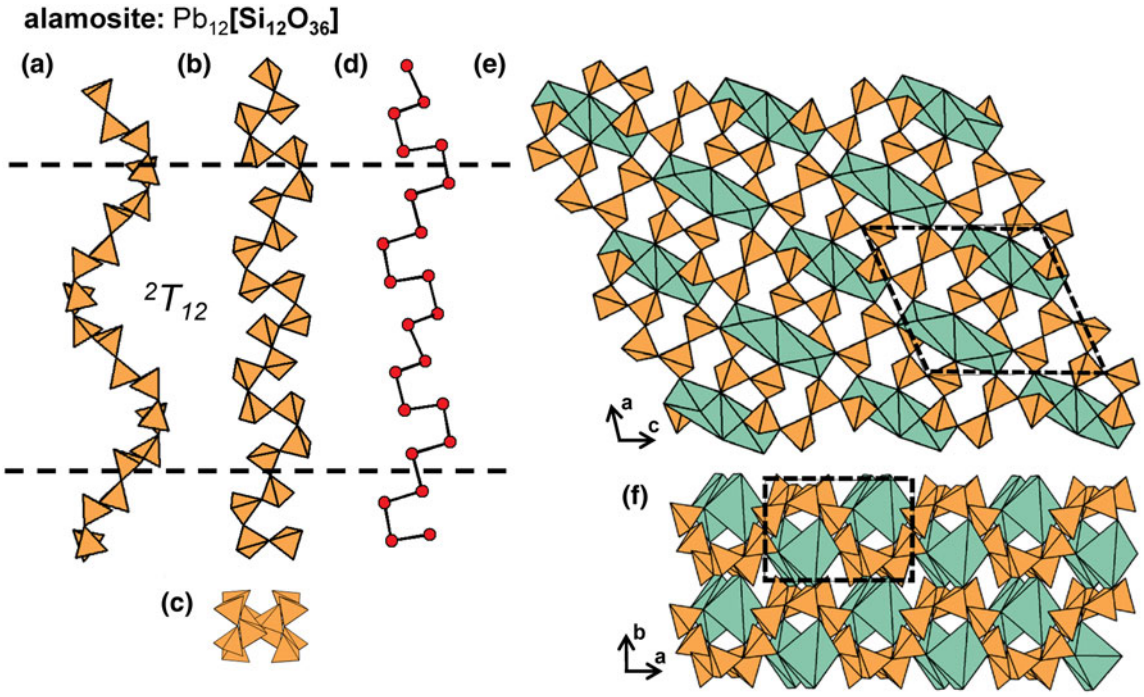

Fig. 33. (*a*, *b*, *c*) Tetrahedral representations of the $^2T_{12}$ chain in **alamosite** and (*d*) a ball-and-stick representation of the chain. The structure of **alamosite** projected (*e*) onto (010) and (*f*) along the **c**-axis. Pb1 and Pb2 atoms have been omitted for clarity. Dashed black lines outline the geometrical repeat unit of the chain and fine dashed black lines outline the unit cell.

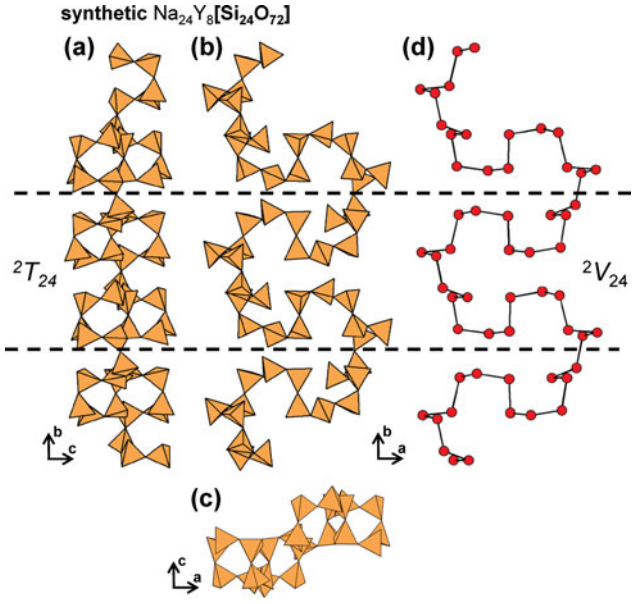

Fig. 34. (*a*, *b*, *c*) Tetrahedral representations of the $^2T_{24}$ chain in **synthetic $Na_{24}Y_8[Si_{24}O_{72}]$** projected (*a*) onto (100), (*b*) onto (001), (*c*) along the **b**-axis and (*d*) a ball-and-stick representation of the chain. Dashed black lines outline the geometrical repeat unit of the chain.

distinct tetrahedra: *T*1 and *T*2; the *T*1 tetrahedra form the $^2T_2$ chains and the *T*2 tetrahedra form the $^3T_4$ ribbons. **Paravinogradovite** contains seven distinct Si^{4+}-tetrahedra (*T*1–*T*7) and one Al^{3+}-tetrahedra (*T*8): *T*1–*T*4 tetrahedra form the $^2T_2$ chains and *T*5–*T*8 tetrahedra form the $^3T_4$ ribbons. In **vinogradovite**, $^2T_2$ chains and $^3T_4$ ribbons extend along the **c**-axis and link to sheets of Ti^{4+}-octahedra (*M*1) and $^{[8]}Na^+$-polyhedra (*X*1) that extend parallel to [001] (Fig. 36*a*). In Fig. 36*b*, channel *1* is occupied by Na^+(and K^+) ions (*A*1) and (H_2O) groups (*W*1 and *W*2). In **paravinogradovite**, chains and ribbons of tetrahedra extend along the **a**-axis and link to sheets of $[TiO_4(OH)_2]^{6-}$- (*M*1–*M*4) and $[NaO_5(OH)]^{10-}$-octahedra (*X*1–*X*2) that extend parallel to (100) (Fig. 36*c*). Due to its OD character, there are several partly occupied sites in **paravinogradovite**. As shown in Fig. 36*d*, channel *1* is partly occupied by Na^+ (*X*3), resulting in a discontinuous sheet. Multiple partly occupied sites occur within channel *2*, including *W*1–*W*3, *A*1–*A*4 (Na^+) and *A*5 (K^+). **Paravinogradovite** contains four H^+ sites associated with $(OH)^-$ groups (Fig. 36*d*).

The $^3T_4$ ribbon in **bigcreekite** extends along the **a**-axis and links to modulated sheets of $(BaO_2(H_2O)_7)^{2-}$-polyhedra that are parallel to (100) (Fig. 37*a*). $^3T_4$ ribbons and sheets of Ba^{2+}-polyhedra alternate along the **b**-axis (Fig. 37*b*). This type of $^3T_4$ ribbon occurs in several synthetic compounds including **$Li_4(SiGe_3O_{10})$** and **$Cs_2H_2(Si_4O_{10})$** (Völlenkle *et al.*, 1968; Dörsam *et al.*, 2003).

$^3T_6$ ribbons

The **epididymite group** includes **epididymite**, **eudidymite**, **elpidite** and **yusupovite** (Table 6), all of which contain $^3T_6$ $[Si_6O_{15}]^{6-}$ ribbons with the vertex degree $^3V_2$ (Figs 38*a*–*d*). In the two dimorphs, **epididymite** and **eudidymite**, ribbons extend along [001] and are linked to adjacent chains along [100] and [010] by pairs of edge-sharing Be^{2+}-tetrahedra, forming an open-framework of tetrahedra. Cavities within this framework are occupied by (H_2O) and Na^+ that forms $(NaO_6(H_2O))^{11-}$- and $(NaO_5(H_2O)_2)^{9-}$-polyhedra in **epididymite** and **eudidymite**, respectively. Although both minerals contain frameworks of

https://doi.org/10.1180/mgm.2020.13 Published online by Cambridge University Press

Table 6. Minerals with $^{3}T_{r}$ ribbons and tubes.

$^{c}T_{r}$	Mineral	Ideal structural formula	Unit stoichiometry	$^{c}V_{r}$	Space group	O:T	Figs	Refs.
$^{3}T_{4}$	Vinogradovite	Na_4Ti_4**[Si_2O_6]$_2$[Si_4O_{10}]**$O_4(H_2O,Na,K)_3$	[$SiO_{2.5}$]	$^{3}V_{2}$	*B*2/*b*	2.75	35,36*a*,*b*	(1)
$^{2}T_{2}$*	〃 〃	〃 〃	[SiO_3]	$^{2}V_{1}$				
$^{3}T_{4}$	Paravinogradovite	$(Na,\square)_2(Ti^{4+},Fe^{3+})_4$**[$Si_2O_6$]$_2$[$Si_3AlO_{10}$]**$(OH)_4(H_2O)$	[$Si_{0.75}Al_{0.25}O_{2.5}$]	$^{3}V_{2}$	*P*1	2.75	35,36*c*,*d*	(2)
$^{2}T_{2}$*	〃 〃	〃 〃	[SiO_3]	$^{2}V_{1}$				
$^{3}T_{4}$	Bigcreekite	Ba_2**[Si_4O_{10}]**$(H_2O)_8$	[$SiO_{2.5}$]	$^{3}V_{2}$	*Pnma*	2.50	37	(3)
$^{3}T_{4}$	Synthetic	Li_4**[$SiGe_3O_{10}$]**	[($Si_{0.25}Ge_{0.75}$)$O_{2.5}$]	$^{3}V_{2}$	*Abm*2	2.50	–	(4)
$^{3}T_{4}$	Synthetic	Cs_2H_2**[Si_4O_{10}]**	[$SiO_{2.5}$]	$^{3}V_{2}$	*Pnma*	2.50	–	(5)
		Epididymite group						
$^{3}T_{6}$	Epididymite	Na_2Be_2**[Si_6O_{15}]**(H_2O)	[$SiO_{2.5}$]	$^{3}V_{2}$	*Pnma*	2.50	38	(6)
$^{3}T_{6}$	Eudidymite	Na_2Be_2**[Si_6O_{15}]**(H_2O)	[$SiO_{2.5}$]	$^{3}V_{2}$	*C*2/*c*	2.50	38	(7)
$^{3}T_{6}$	Elpidite	Na_2Zr**[Si_6O_{15}]**$(H_2O)_3$	[$SiO_{2.5}$]	$^{3}V_{2}$	*Pbcm*	2.50	38,39	(8)
$^{3}T_{6}$	Yusupovite	Na_2Zr**[Si_6O_{15}]**$(H_2O)_3$	[$SiO_{2.5}$]	$^{3}V_{2}$	*C*2/*m*	2.50	38	(9)
$^{3}T_{6}$	Synthetic	Rb_2Zr**[Si_6O_{15}]**(H_2O)	[$SiO_{2.5}$]	$^{3}V_{2}$	*Cmce*	2.50	–	(10)
$^{3}T_{6}$	Synthetic	K_2Zr**[Si_6O_{15}]**(H_2O)	[$SiO_{2.5}$]	$^{3}V_{2}$	*Cmce*	2.50	–	(11)
$^{3}T_{8}$	Caysichite-(Y)	$Y_4(Ca,REE)_4$**[Si_8O_{20}]**$(CO_3)_6(OH)(H_2O)_7$]	[$SiO_{2.5}$]	$^{3}V_{2}$	*Ccmm*	2.50	40,41	(12)
		Litidionite group						
$^{3}T_{8}$	Litidionite	KNaCu**[Si_4O_{10}]**	[$SiO_{2.5}$]	$^{3}V_{8}$	$P\bar{1}$	2.50	42,43*a*,*b*	(13)
$^{3}T_{8}$	Fenaksite	KNaFe**[Si_4O_{10}]$_2$**	[$SiO_{2.5}$]	$^{3}V_{8}$	$P\bar{1}$	2.50	42	(14)
$^{3}T_{8}$	Manaksite	KNaMn**[Si_4O_{10}]**	[$SiO_{2.5}$]	$^{3}V_{8}$	$P\bar{1}$	2.50	42	(15)
$^{3}T_{8}$	Calcinaksite	KNa[$Ca(H_2O)$]**[Si_4O_{10}]**	[$SiO_{2.5}$]	$^{3}V_{8}$	$P\bar{1}$	2.50	42	(16)
$^{3}T_{8}$	Agrellite	$NaCa_2$**[Si_4O_{10}]**(F)	[$SiO_{2.5}$]	$^{3}V_{8}$	$P\bar{1}$	2.50	42,43*c*,*d*	(17)
$^{3}T_{8}$	Synthetic	K_2Ca**[Si_4O_{10}]**	[$SiO_{2.5}$]	$^{3}V_{8}$	$P\bar{1}$	2.50	–	(18)
$^{3}T_{8}$	Synthetic	KNa*M*[Si_4O_{10}] *M* = Cu^{2+}, Mn^{2+}, Fe^{2+}	[$SiO_{2.5}$]	$^{3}V_{8}$	$P\bar{1}$	2.50	–	(19)
$^{3}T_{8}$	Synthetic	Na_2M[Si_4O_{10}] *M* = Co^{2+}, Ni^{2+}, Cu^{2+}, Mn^{2+}	[$SiO_{2.5}$]	$^{3}V_{8}$	$P\bar{1}$	2.50	–	(20)
$^{3}T_{8}$	Narsarsukite	$Na_4(Ti,Fe)_2$**[Si_8O_{20}]**$(O,OH,F)_2$	[$SiO_{2.5}$]	$^{3}V_{8}$	*I*4/*m*	2.50	44,45	(21)
$^{3}T_{8}$	Synthetic	K_2Sc**[Si_4O_{10}]**F	[$SiO_{2.5}$]	$^{3}V_{8}$	*I*4/*m*	2.50	–	(22)
$^{3}T_{8}$	Synthetic	Pb_6O**[$Si_6Al_2O_{20}$]**	[$Si_{0.75}Al_{0.25}O_{2.5}$]	$^{3}V_{8}$	*I*4/*m*	2.50	–	(23)
$^{3}T_{8}$	Synthetic	K_2In**[Si_4O_{10}]**(OH)	[$SiO_{2.5}$]	$^{3}V_{8}$	$P2_1/m$	2.50	–	(24)
		Tuhualite group						
$^{3}T_{12}$	Tuhualite	$(Na,K)_2Fe^{3+}_2Fe^{2+}_2$**[$Si_{12}O_{30}$]**$(H_2O)$	[$SiO_{2.5}$]	$^{3}V_{2}$	*Cmca*	2.50	46,47	(25)
$^{3}T_{12}$	Emeleusite	$Na_4Li_2Fe^{3+}_2$**[$Si_{12}O_{30}$]**	[$SiO_{2.5}$]	$^{3}V_{2}$	Pnna	2.50	46	(26)
$^{3}T_{12}$	Zektzerite	Na_2Li_2Zr2**[$Si_{12}O_{30}$]**	[$SiO_{2.5}$]	$^{3}V_{2}$	Cmca	2.50	46	(27)
		Canasite group						
$^{3}T_{12}$	Canasite	$K_3Na_3Ca_5$**[$Si_{12}O_{30}$]**$(OH)_4$	[$SiO_{2.5}$]	$^{3}V_{12}$	*C*2/*m*	2.50	48	(28)
$^{3}T_{12}$	Fluorcanasite	$K_3Na_3Ca_5$**[$Si_{12}O_{30}$]**$F_3(OH)(H_2O)$	[$SiO_{2.5}$]	$^{3}V_{12}$	*Cm*	2.50	48,49*a*,*b*	(29)
$^{3}T_{12}$	Frankamenite	$K_3Na_3Ca_5$**[$Si_{12}O_{30}$]**$F_3(OH)(H_2O)$	[$SiO_{2.5}$]	$^{3}V_{12}$	*P*1	2.50	48	(30)
$^{3}T_{12}$	Miserite	$K_2(Ca,Y,REE)_{10}$**[Si_6O_{15}]$_2$[Si_2O_7]$_2$**$(OH,F)_4(H_2O)_2$	[$SiO_{2.5}$]	$^{3}V_{12}$	$P\bar{1}$	2.75	48,49*c*,*d*	(31)
$^{1}T_{2}$*	〃 〃	〃 〃	[$SiO_{3.5}$]	$^{1}V_{2}$				
$^{3}T_{12}$	Denisovite	$K_{15}(Ca,Na)_{48}$**[$Si_{60}O_{162}(F_{16}O_2(OH)_2$]**$(H_2O)_2$	[$SiO_{2.5}$]	$^{3}V_{12}$	*P*2/*a*	2.70	–	(32)
$^{2}T_{4}$	〃 〃	〃 〃	[$SiO_{2.83}$]	$^{2}V_{4}$				
$^{3}T_{2}$*				$^{3}V_{2}$				
$^{3}T_{16}$	Synthetic	Cs_4Y_2**[Si_8O_{20}]**F_4	[$SiO_{2.5}$]	$^{3}V_{8}$	*Pnma*	2.50	50	(33)
$^{3}T_{16}$	Synthetic	K_4In_2**[Si_8O_{20}]**$(OH)_2$	[$SiO_{2.5}$]	$^{3}V_{16}$	$P2_1/m$	2.50	51	(34)
$^{3}T_{16}$	Synthetic	K_4Lu_2**[Si_8O_{20}]**$(OH)_2$	[$SiO_{2.5}$]	$^{3}V_{16}$	$P2_1/m$	2.50	–	(35)
$^{3}T_{16}$	Synthetic	Ru_4Lu_2**[Si_8O_{20}]**F_2	[$SiO_{2.5}$]	$^{3}V_{16}$	$P2_1/m$	2.50	–	(35)
$^{3}T_{17}$	Charoite	$(K,Sr)_{15-16}(Ca,Na)_{32}$**[$Si_6O_{11}(O,OH)_6$]$_2$ [$Si_{12}O_{18}(O,OH)_{12}$]$_2$[$Si_{17}O_{25}(O,OH)_{18}$]$_2$**$(OH,F)_4(H_2O)_3$	[$SiO_{1.45}(O,OH)_{1.05}$]	$^{3}V_{17}$	$P2_1/m$	2.56	52*a*–*c*,53	(36)
$^{3}T_{12}$*	〃 〃			$^{3}V_{12}$			52*d*–*f*,53	
$^{2}T_{4}{}^{3}T_{2}$*	〃 〃	〃 〃	[$SiO_{1.5}(O,OH)$]	$^{2}V_{4}$			52*g*–*i*,53	
			[$SiO_{1.83}(O,OH)$]	$^{3}V_{2}$				
$^{3}T_{32}$	Synthetic	Na_{16}**[$Si_{32}O_{64}(OH)_{16}$]**	[$SiO_2(OH)_{0.5}$]	$^{3}V_{2}$	$Pna2_1$	2.50	–	(37)
$^{3}T_{56}$	Ashcroftine-(Y)	$K_{10}Na_{10}(Y,Ca)_{24}(OH)_4(CO_3)_{16}$**[$Si_{56}O_{140}$]**$(H_2O)_{16}$	[$SiO_{2.5}$]	$^{3}V_{56}$	I4/mmm	2.50	54	(38)

References: (1) Kalsbeek and Rønsbo (1992), Rastsvetaeva *et al.* (1968), Rastsvetaeva and Andrianov (1984); (2) Khomyakov *et al.* (2003); (3) Basciano *et al.* (2001); (4) Völlenkle *et al.* (1968); (5) Dörsam *et al.* (2003); (6) Robinson and Fang (1970); (7) Gatta *et al.* (2008), Fang *et al.* (1972); (8) Cannillo *et al.* (1973), Zubkova *et al.* (2011); (9) Agakhanov *et al.* (2015); (10) Grigor'eva *et al.* (2011); (11) Grigor'eva *et al.* (2011); (12) Mellini and Merlino (1978), Hogarth *et al.* (1974); (13) Brandão *et al.* (2009), Pozas *et al.* (1975); (14) Golovachev *et al.* (1971), Rozhdestvenskaya *et al.* (2004); (15) Khomyakov *et al.* (1992), Karimova and Burns (2007); (16) Aksenov *et al.* (2014), Chukanov *et al.* (2015*b*); (17) Rozhdestvenskaya and Nikishova (1998), Ghose and Wan (1979); (18) Schmidmair *et al.* (2018); (19) Brandão *et al.* (2009); (20) Kornev *et al.* (1972), Kawamura and Kawahara (1977), Durand *et al.* 1997, Cadoni and Ferraris (2011); (21) Peacor and Buerger (1962*b*), Pyatenko and Pudovkina (1960), Wagner *et al.* (1991), Kolitsch and Tillmanns (2004), Schingaro *et al.* (2017); (22) Kolitsch and Tillmanns (2004); (23) Siidra *et al.* (2009); (24) Hung *et al.* (2003); (25) Merlino (1969), Bagiński *et al.* (2018), Merlino and Biagioni (2018); (26) Johnsen *et al.* (1978), Upton *et al.* (1978); (27) Dunn *et al.* (1977), Ghose and Wan (1978); (28) Rastsvetaeva *et al.* (2003), Dorfman *et al.* (1959), Rozhdestvenskaya *et al.* (1987); (29) Rastsvetaeva *et al.* (2003), Khomyakov *et al.* (2009); (30) Rozhdestvenskaya *et al.* (1996), Nikishova *et al.* (1996); (31) Rozhdestvenskaya and Evdokimov (2006), Scott (1976), Rozhdestvenskaya *et al.* (1987), Kaneva *et al.* (2014); (32) Men'shikov (1984), Konev *et al.* (1987), Rozhdestvenskaya *et al.* (2017); (33) Schafer and Schleid (2007); (34) Hung *et al.* (2003); (35) Kahlenberg and Manninger (2014); (36) Rozhdestvenskaya *et al.* (2011), Chiragov and Shirinova (2004), Matesanz *et al.* (2008), Rozhdestvenskaya *et al.* (2010), Rozhdestvenskaya *et al.* (2009); (37) Sassi *et al.* (2003); (38) Moore *et al.* (1987).
*Indicates the $^{c}T_{r}$ expression of an additional structural unit including a chain, ribbon, tube, cluster or sheet of $[TO_4]^{n-}$ tetrahedra in the respective mineral.

tetrahedra rather than ribbons of tetrahedra, they have been added to Table 6 for purposes of comparison. In **elpidite**, $^{3}T_{6}$ ribbons extend along [100] and are linked to each other along [010] and [001] by Zr^{4+}- and $(NaO_4(H_2O)_2)^{7-}$-octahedra rather than Be^{2+}-tetrahedra, forming an open-framework that contains $^{3}T_{6}$ ribbons. Cavities within this framework are occupied by (H_2O)

https://doi.org/10.1180/mgm.2020.13 Published online by Cambridge University Press

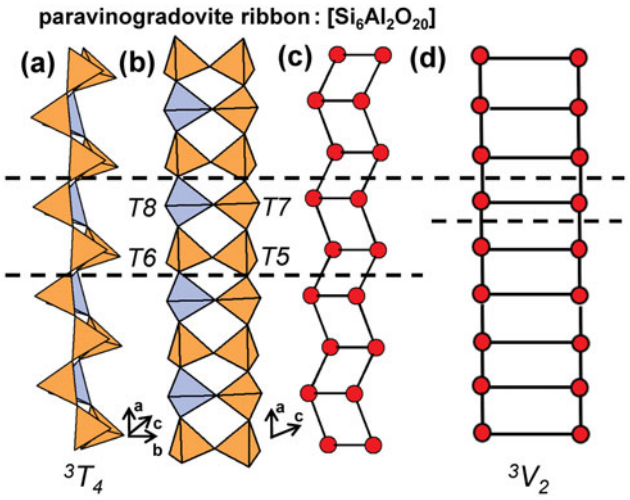

Fig. 35. (*a*, *b*) Tetrahedral representation of the $^3T_4$ ribbon in **paravinogradovite** projected (*a*) orthogonal to the **a**-axis (*b*) onto (010), (*c*) a ball-and-stick and (*d*) a graphical representation of the ribbon. The *T*8 site is occupied by Al^{3+}. Dashed black lines outline the geometrical and topological repeat unit of the ribbon.

and Na^+ that forms $(NaO_6(H_2O))^{11-}$-polyhedra (Figs 39*a*,*b*). In **yusupovite**, the monoclinic dimorph of **elpidite**, $^3T_6$ ribbons extend along [010] and there are six *T* sites rather that three as in the other **epididymite-group** minerals. Various synthetic, K^+- and Rb^+-exchanged analogues of **elpidite** (**$K_2Zr[Si_6O_{15}](H_2O)$** and **$Rb_2Zr[Si_6O_{15}](H_2O)$**) have been described by Grigor'eva *et al.* (2011).

$^3T_8$ ribbons and tubes

The $^3T_8$ $[Si_8O_{20}]^{8-}$ ribbon in **caysichite-(Y)** has a geometrical repeat unit that contains a pair of four-membered rings that are geometrically distinct from each another (Figs 40*a*–*c*). This $^3V_2$ ribbon (Fig. 40*d*) is topologically identical to the ribbon in **epididymite-group** minerals (Fig. 38*d*) **paravinogradovite, vinogradovite** and **bigcreekite** (Fig. 35*d*). In **caysichite-(Y)**, $[Si_8O_{20}]^{8-}$ ribbons extend along the **c**-axis and are linked to ribbons of (Ca, *REE*)- and Y-polyhedra (*Ca*1 and *Y*1) which are coordinated by oxygen atoms from $(CO_3)^{2-}$ groups, (H_2O) groups and $(OH)^-$ groups (Fig. 41*a*). Each $[Y_4(Ca,REE)_4(CO_3)_6(OH)(H_2O)_7]$ ribbon extends along the **c**-axis and is linked to four other ribbons along the **a**-axis and **b**-axis, forming an open framework. The $^3T_8$

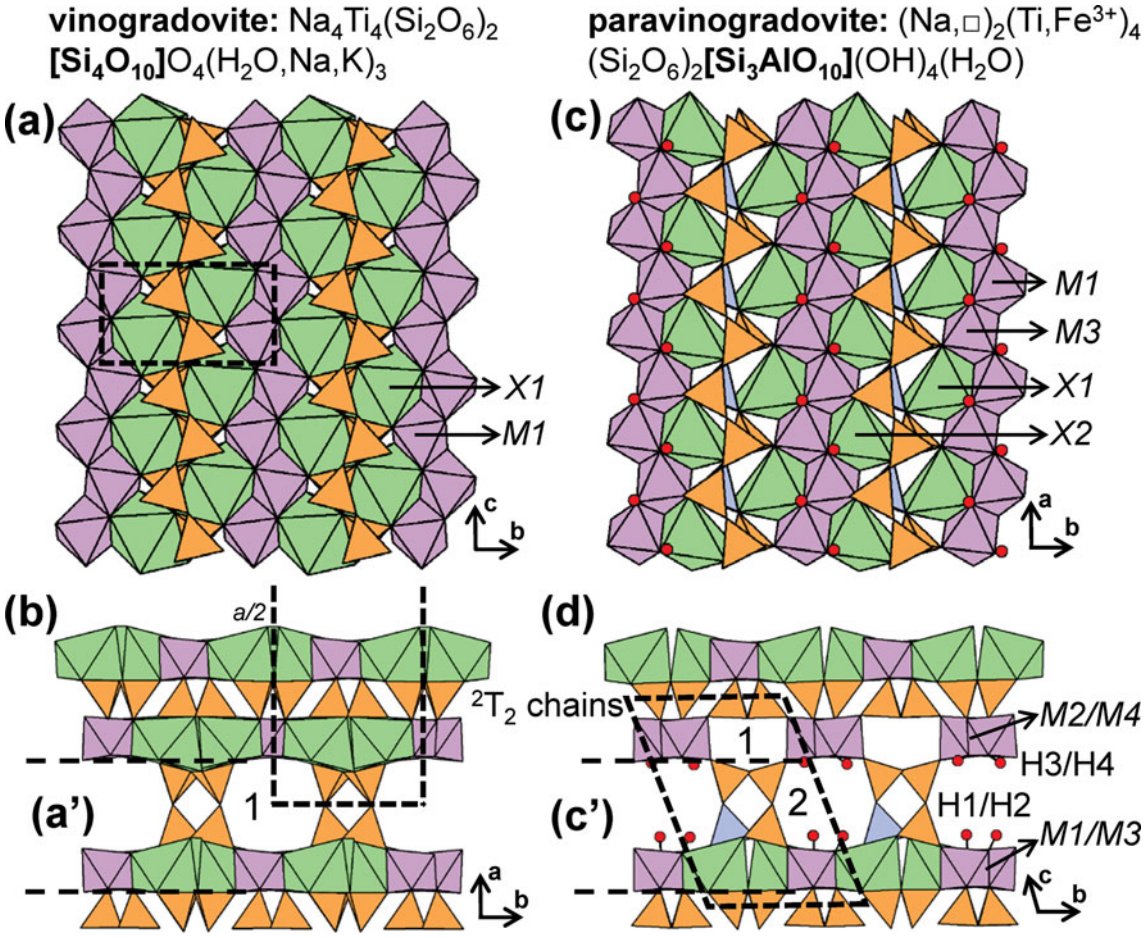

Fig. 36. The structure of **vinogradovite** projected (*a*) onto (100) and (*b*) along the **c**-axis. In (*b*), channel *1* is occupied by $Na(K)^+$-polyhedra and H atoms associated with (H_2O) groups have been omitted for clarity. The structure of **paravinogradovite** projected (*c*) onto (001) and (*d*) along the **a**-axis. In (*d*), channel *1* is partly occupied by Na^+-polyhedra and channel *2* is occupied by Na^+-polyhedra and (H_2O) groups which have been omitted for clarity. **Paravinogradovite** contains four H sites (H1–H4) associated with $(OH)^-$ that are shown as red circles. Fine dashed black lines outline the unit cell which is halved along the **a**-axis in (*b*).

https://doi.org/10.1180/mgm.2020.13 Published online by Cambridge University Press

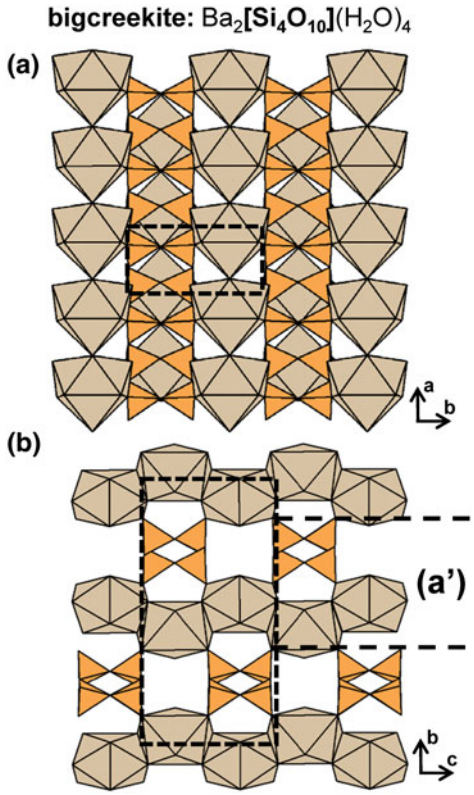

Fig. 37. The structure of **bigcreekite** projected (*a*) onto (001) and (*b*) along the **a**-axis. Fine dashed black lines outline the unit cell and H atoms associated with (H_2O) groups have been omitted for clarity.

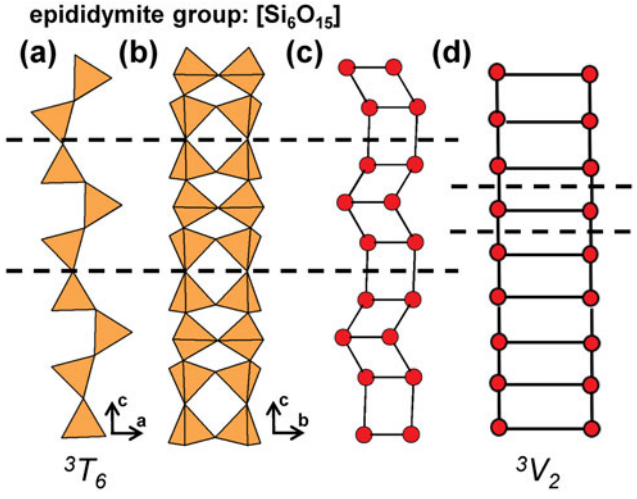

Fig. 38. (*a*, *b*) Tetrahedral representation of the $^3T_6$ ribbon in **epididymite group** projected (*a*) onto (010), (*b*) onto (100), (*c*) a ball-and-stick and (*d*) a graphical representation of the ribbon. Dashed black lines outline the geometrical and topological repeat unit of the ribbon.

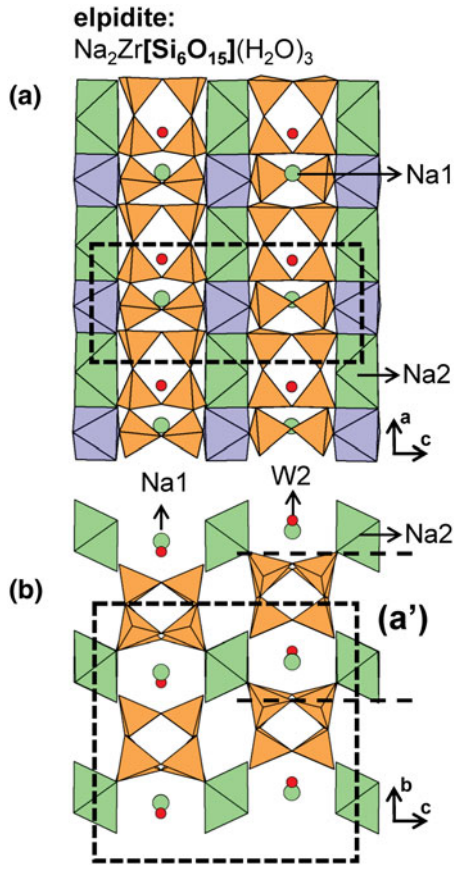

Fig. 39. The structure of **elpidite** projected (*a*) onto (010) and (*b*) onto (100). The $[NaO_4(H_2O)_2]^{7-}$-octahedra (Na2) are associated with the *W*1 site and $[NaO_6(H_2O)]^{11-}$-polyhedra (Na1) are shown as green circles and are associated with the *W*2 site. The Zr^{4+}-octahedra in (*b*) have been omitted for clarity. Fine dashed black lines outline the unit cell.

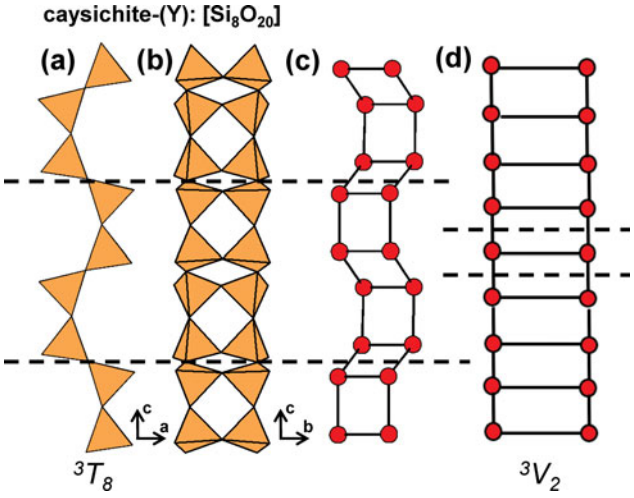

Fig. 40. (*a*, *b*) Tetrahedral representation of the $^3T_8$ ribbon in **caysichite-(Y)** projected (*a*) onto (010), (*b*) onto (100), (*c*) a ball-and-stick and (*d*) a graphical representation of the ribbon. Dashed black lines outline the geometrical and topological repeat unit of the ribbon.

ribbons extend along the tunnels of this framework and each links to four of these ribbons (Fig. 41*b*).

The $^3T_8$ $[Si_8O_{20}]^{8-}$ tube in **litidionite-group** minerals extends along the **a**-axis and consists of two linked chains of four-membered rings, each topologically identical to the $^3T_2{}^2T_2$ chain in **revdite** (see below) and the $^3T_4{}^2T_4$ chain in **vlasovite** (see below). In **litidionite**, adjacent four-membered rings of opposing chains link to each other across the tube via two tetrahedra, forming eight-membered rings that link along the **a**-axis

https://doi.org/10.1180/mgm.2020.13 Published online by Cambridge University Press

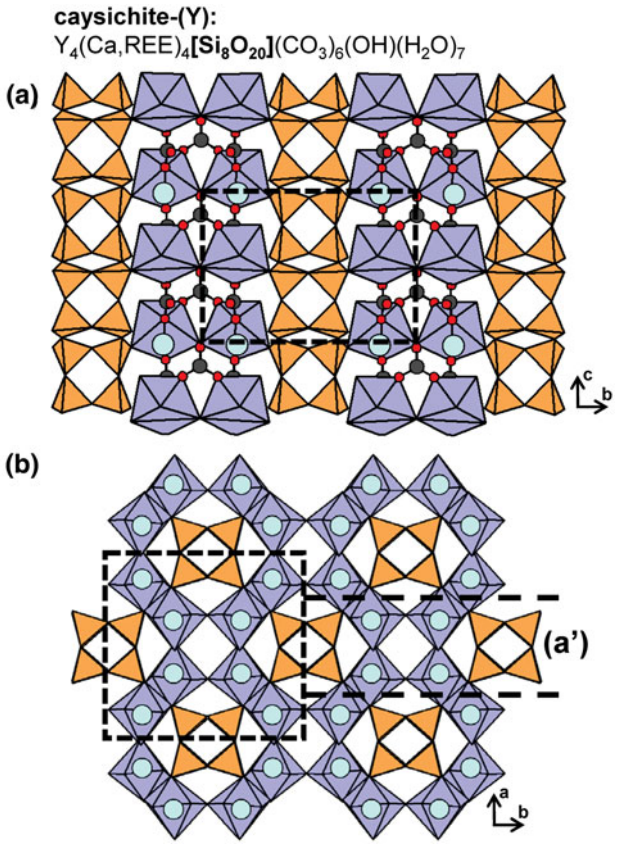

Fig. 41. The structure of **caysichite-(Y)** projected (*a*) onto (100) and (*b*) along the **c**-axis. In (*a*), the C and O atoms of the (CO_3) groups are shown as dark grey and red circles, respectively. In (*a*) and (*b*), Y^{3+} ions are shown as teal circles. In (*a*), H atoms associated with (H_2O) and $(OH)^-$ groups are omitted and in (*b*) C atoms associated with (CO_3) groups are also omitted for clarity. Fine dashed black lines outline the unit cell.

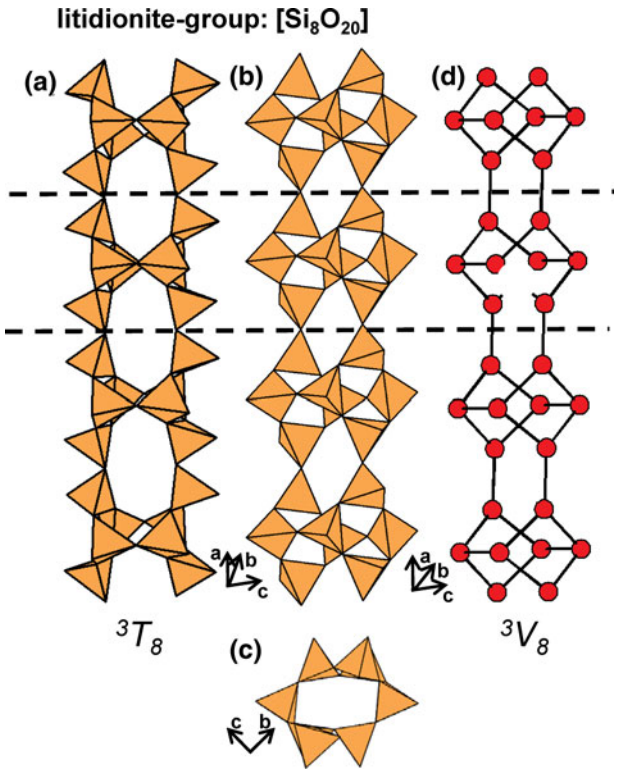

Fig. 42. (*a*, *b*, *c*) Tetrahedral representation of the $^3T_8$ tube in **litidionite** projected (*a*, *b*) orthogonal to the **a**-axis and (*c*) along the **a**-axis, (*d*) a ball-and-stick (graphical) representation of the tube. Dashed black lines outline the geometrical and topological repeat unit of the tube.

(Figs 42*a*,*b*), and a six-membered ring that can be viewed into the **a**-axis (Fig. 42*c*). In this tube $n_g = n_t$ as shown in Fig. 42*d*.

Members of the **litidionite group** include **manaksite**, **fenaksite** and **calcinaksite**, and there are isostructural synthetic structures such as $\mathbf{K_2Ca[Si_4O_{10}]}$ (Schmidmair *et al.*, 2018), $\mathbf{KNa}M\mathbf{[Si_4O_{10}]}$ ($M = Cu^{2+}$, Mn^{2+} and Fe^{2+}) (Brandão *et al.*, 2009) and $\mathbf{Na_2}M\mathbf{[Si_4O_{10}]}$ ($M = Co^{2+}$, Ni^{2+}, Cu^{2+} and Mn^{2+}) (Kornev *et al.*, 1972, Kawamura and Kawahara, 1977, Durand *et al.*, 1997, Cadoni and Ferraris, 2011). **Agrellite** (Table 6) is not isostructural with the **litidionite-group** minerals but contains a tube that is topologically identical. In **litidionite**, $^3T_8$ tubes link along the **c**-axis via ribbons of $^{[5]}Cu^{2+}$- and $^{[7]}Na^+$-polyhedra and $^{[8]}K^+$ ions occupy cavities within the tube (Figs 43*a*,*b*). In **agrellite,** tubes of tetrahedra extend along the **c**-axis and link along the **b**-axis via sheets of $(CaO_5F_2)^{10-}$-polyhedra (Ca1 and Ca4) and $(CaO_5F)^{9-}$-octahedra (Ca2 and Ca3). The *Ca*1 site may be partly occupied by *REE*s and Sr^{2+}, and cavities within the tube of tetrahedra are occupied by $^{[8]}Na^+$ ions (Figs 43*c*,*d*). In both structures, $^3T_8$ tubes and ribbons of higher coordination polyhedra occur in layers that alternate along [001] in **litidionite-group** minerals and along [010] in **agrellite**. **Fenaksite** and **manaksite** are the Fe^{2+}- and Mn^{2+}-analogues of **litidionite**, and **calcinaksite** is the Ca^{2+}-analogue of **litidionite** that also contains (H_2O).

The tube in **narsarsukite** extends along the **c**-axis and consists of four-membered rings of corner-sharing tetrahedra that link to adjacent tetrahedra, along [001], through two tetrahedra of each ring (Figs 44*a*–*c*). Topologically, this $^3V_8$ tube (Fig. 44*d*) is similar to the tube in **litidionite** but not identical (Fig. 42d). This tube extends parallel to chains of corner-sharing (TiO_5(O,OH,F)-octahedra that extend along the **c**-axis and each link to four $^3T_8$ tubes to form an open framework; channels in this framework are occupied by $^{[7]}Na^+$ ions (Figs 45*a*,*b*). Schingaro *et al.* (2017) report the partial substitution $Ti^{4+} + O^{2-} \leftrightarrow Fe^{3+} + F^-$, $(OH)^-$ at octahedrally coordinated sites. There are various synthetic compounds with $^3T_8$ ribbons and tubes: $\mathbf{K_2Sc[Si_4O_{10}]F}$ (Kolitsch and Tillmanns, 2004), $\mathbf{Pb_6O[Si_6Al_2]O_{20}}$ (Siidra *et al.*, 2009) and $\mathbf{K_2In[Si_4O_{10}](OH)}$ (Hung *et al.*, 2003) (Table 6).

$^3T_{12}$ ribbons and tubes

In **tuhualite**, $^3T_{12}$ ribbons extends along the **c**-axis and are modulated along the **b**-axis (Figs 46*a*–*d*). This $^3V_2$ ribbon (Fig. 46*e*) is topologically identical to the ribbons in **paravinogradovite**, **vinogradovite, bigcreekite**, (Fig. 35*d*) the **epididymite-group** minerals (Fig. 38*d*) and **caysichite-(Y)** (Fig. 40*d*). **Tuhualite** contains three octahedrally coordinated sites occupied by Fe^{2+}, Fe^{3+} (Fe1 and Fe2) and Na^+ (Na1); these octahedra polymerise to form sheets that link to $^3T_{12}$ ribbons. This linkage forms channels that extend along the **a**-axis and are occupied by octahedrally coordinated Na^+ and (H_2O) groups with subordinate K^+ (Fig. 47*a*). Sheets of octahedra and $^3T_{12}$ ribbons occur in layers that alternate along the **a**-axis (Fig. 47*b*). In **zektzerite** and **emeleusite**, the Li^+-analogues of **tuhualite,** $^3T_{12}$ ribbons link to sheets of Fe^{3+}-octahedra (Zr^{4+}-octahedra in **zektzerite**), Na^+-polyhedra and Li^+-tetrahedra. In both minerals, adjacent chains are linked to each other by Li^+-tetrahedra, forming a framework rather

https://doi.org/10.1180/mgm.2020.13 Published online by Cambridge University Press

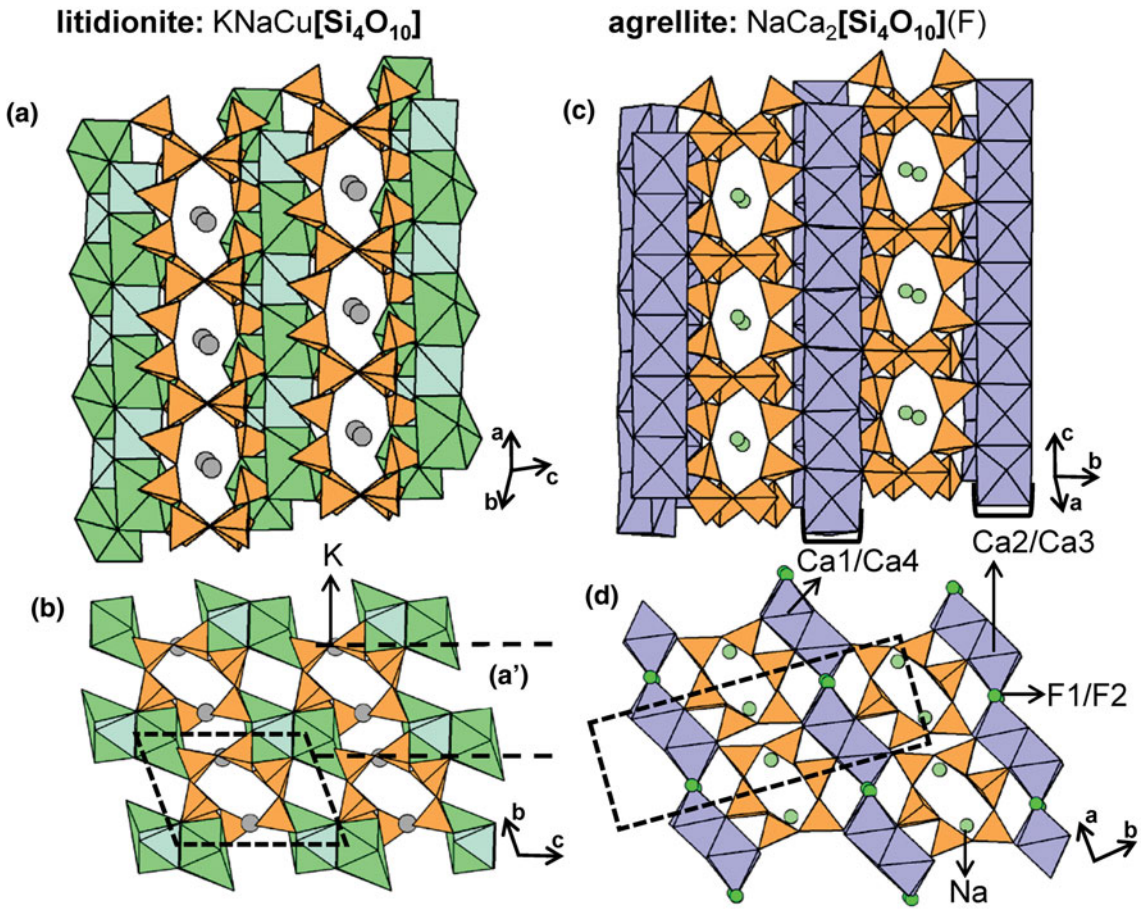

Fig. 43. The structure of **litidionite** viewed (*a*) orthogonal to the **a**-axis and (*b*) along the **a**-axis. The structure of **agrellite** viewed (*c*) orthogonal to the **c**-axis and (*d*) along the **c**-axis. In (*d*), F1 and F2 anions are shown as green circles. Fine dashed black lines outline the unit cell.

than a ribbon of tetrahedra. However, both minerals are included in Table 6 as they belong to the **tuhualite group**.

The $^3T_{12}$ $[Si_{12}O_{30}]^{12-}$ tubes in **canasite** and **fluorcanasite** extend along [010] and consist of two linked ribbons of six-membered rings (Figs 48*a*,*b*) that form a tube (Fig. 48*c*). Topologically, this $^3V_{12}$ tube (Fig. 48*d*) is similar to the $[Si_{12}O_{30}]^{12-}$ tube in **charoite** (see below). In both minerals, $^3T_{12}$ tubes link to corrugated sheets of Ca^{2+}- and Na^+-octahedra that are parallel to (100). Channels within each $^3T_{12}$ tube are occupied by K^+ ions (K1–K4) and by an additional (H_2O) group in **fluorcanasite**. In **canasite**, there are four $(OH)^-$ sites whereas in **fluorcanasite**, there are two F sites (F2 and F3), an (OH) site and a split site that typically contains F > (OH) (F1), all of which bond to Na^+- and Ca^{2+}-octahedra. In **fluorcanasite**, $^3T_{12}$ tubes and sheets of $(CaO_4(OH)F)^{8-}$-octahedra (Ca1–Ca3) and $(NaO_4F_2)^{9-}$-octahedra (Na1–Na3) occur in layers that alternate along the **c**-axis (Figs 49*a*,*b*). **Frankamenite** is the triclinic polymorph of **fluorcanasite**. In **miserite**, $^3T_{12}$ tubes extend along [001] and link to a more complicated slab that occurs in layers parallel (100). These slabs are composed of $(CaO_{7-x}F_x)$- and $(CaO_{6-x}F_x)$-polyhedra (where $x = 1$–2) and $[Si_2O_7]^{6-}$ dimers. Cavities are occupied by K^+ ions (K1–K2) and (H_2O) groups (Figs 49*c*,*d*).

Other ^3T_n tubes

There are several synthetic compounds that contain $^3T_{16}$ tubes and ribbons that are topologically distinct, with the vertex connectivity $^3T_8$ or $^3T_{16}$. Figures 50*a*–*d* show the $^3T_{16}$ ribbon in **synthetic $Cs_4Y_2[Si_8O_{20}]F_4$** that consists of four- and eight-membered rings of Si^{4+}-tetrahedra that link along [010]; this ribbon has a vertex degree $^3V_8$ (Fig. 50*e*). Although this ribbon somewhat resembles that of a tube (Fig. 50*c*), it does not form a contiguous hollow cylinder (Figs 50*b*,*d*) and is therefore a ribbon. One can also more rigorously differentiate ribbons and tubes on the basis of topology. All ribbon-graphs can be represented in 2-dimensions in which no edges cross and no vertices overlap (Fig. 50*e*); this is not possible for tube-graphs. This distinction represents an important topological divide in 1-dimensional graphs and will be discussed in detail in a subsequent paper. In **synthetic $Cs_4Y_2[Si_8O_{20}]F_4$**, $^3T_{16}$ ribbons link to each other via chains of $(YO_4F_2)^{7-}$-octahedra to form an open framework in which cavities are occupied by Cs^+ ions (Schäfer and Schleid, 2007). **Synthetic $K_4In_2[Si_8O_{20}](OH)_2$** contains $^3T_{16}$ tubes that consist of four-, six- and eight-membered rings of Si^{4+}-tetrahedra that link along [010] (Figs 51*a*,*b*); this tube has a vertex degree $^3V_{16}$ (Fig. 51*c*). The structure of **synthetic $K_4In_2[Si_8O_{20}](OH)_2$** is similar to that of **synthetic $Cs_4Y_2[Si_8O_{20}]F_4$** where $(YO_4F_2)^{7-}$-octahedra are replaced by $(InO_4(OH)_2)^{7-}$-octahedra and Cs^+ is replaced by K^+ (Hung *et al.*, 2003). The other synthetic compounds isostructural with **$K_4In_2[Si_8O_{20}](OH)_2$** are **$K_4Lu_2[Si_8O_{20}](OH)_2$** and **$Ru_4Lu_2[Si_8O_{20}]F_2$** (Kahlenberg and Manninger, 2014).

Charoite has several polytypes; for simplicity we briefly describe only one: **charoite-96**; for more detailed descriptions,

https://doi.org/10.1180/mgm.2020.13 Published online by Cambridge University Press

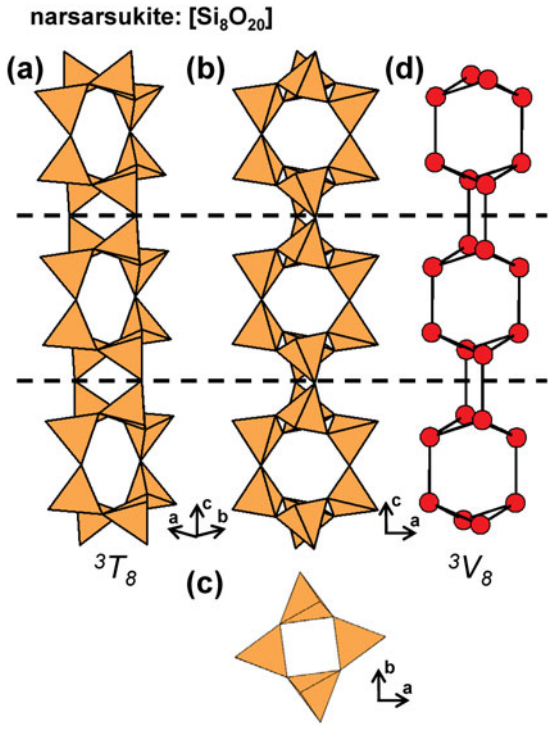

Fig. 44. (*a*, *b*, *c*) Tetrahedral representation of the $^{3}T_{8}$ tube in **narsarsukite** projected (*a*) orthogonal to the **c**-axis, (*b*) onto (010), (*c*) along the **c**-axis and (*d*) a ball-and-stick (graphical) representation of the tube. Dashed black lines outline the geometrical and topological repeat unit of the tube.

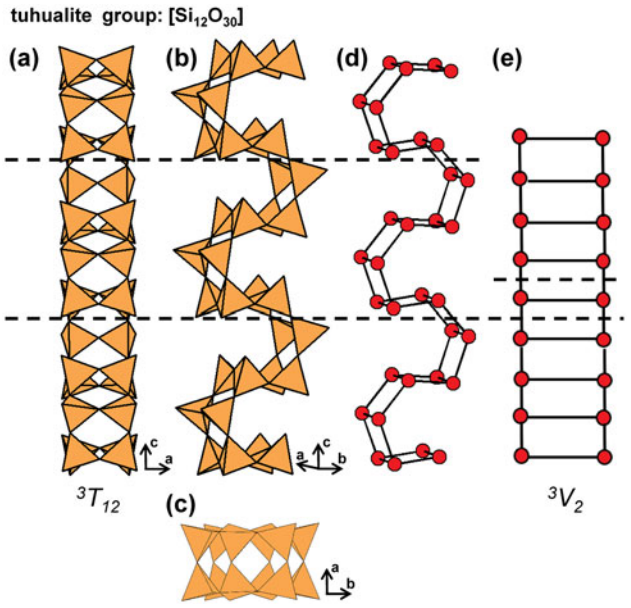

Fig. 46. (*a*, *b*, *c*) Tetrahedral representation of the $^{3}T_{12}$ ribbon in **tuhualite** projected (*a*) onto (010), (*b*) orthogonal to the **c**-axis, (*c*) along the **c**-axis, (*d*) a ball-and-stick and (*e*) a graphical representation of the ribbon. Dashed black lines outline the geometrical and topological repeat unit of the ribbon.

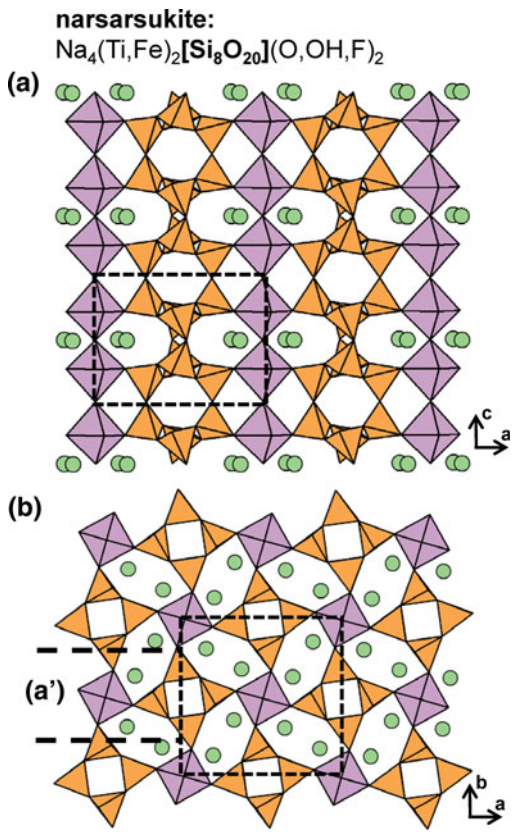

Fig. 45. The structure of **narsarsukite** projected (*a*) onto (010) and (*b*) along the **c**-axis. Fine dashed black lines outline the unit cell and H atoms associated with $(OH)^{-}$ groups have been omitted for clarity

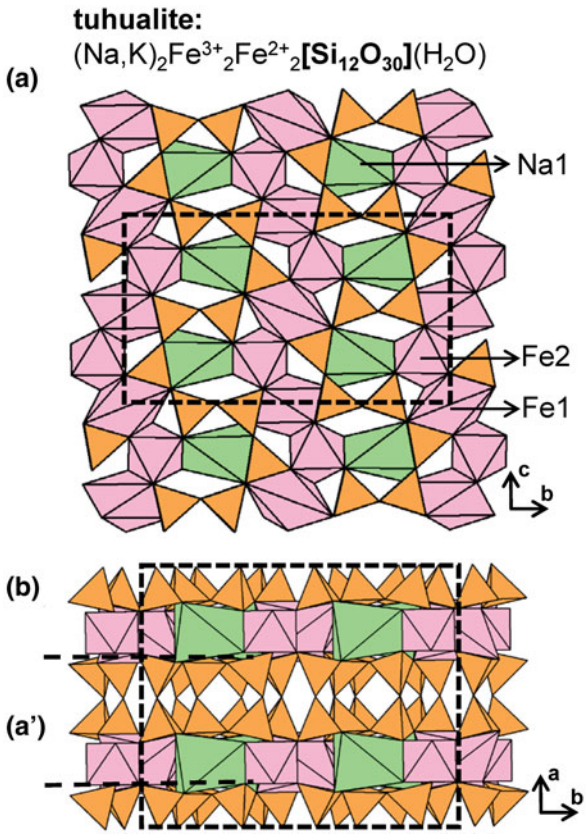

Fig. 47. The structure of **tuhualite** projected (*a*) onto (100) and (*b*) along the **c**-axis. Fine dashed black lines outline the unit cell and H atoms associated with (H_2O) groups have been omitted for clarity.

https://doi.org/10.1180/mgm.2020.13 Published online by Cambridge University Press

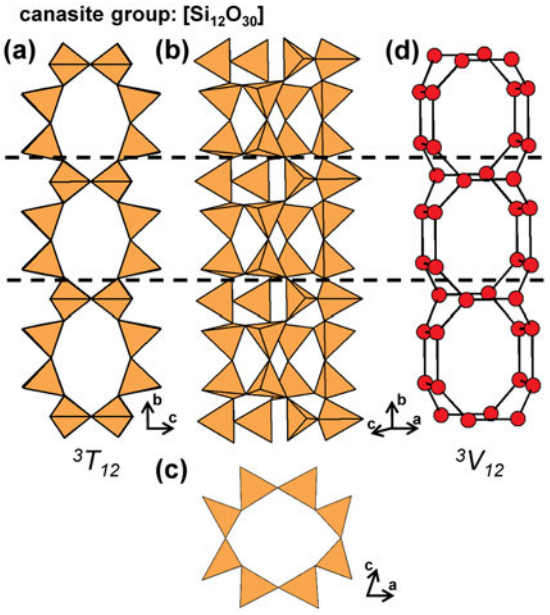

Fig. 48. (*a*, *b*, *c*) Tetrahedral representation of the $^3T_{12}$ tube in **canasite** projected (*a*) onto (100), (*b*) orthogonal to the **b**-axis, (*c*) along the **b**-axis and (*d*) a ball-and-stick (graphical) representation of the tube. Dashed black lines outline the geometrical and topological repeat unit of the tube.

see Rozhdestvenskaya *et al.* (2010, 2011). **Charoite** contains a $^3T_{17}$ tube (Figs 52*a*–*c*), a $^3T_{12}$ tube (Figs 52*d*–*f*) and a $^2T_4{}^3T_2$ ribbon (Figs 52*g*–*i*), all of which extend along [001]. Each tube and ribbon links to an open framework of $(NaO_5(OH))^{10-}$- and Ca^{2+}-octahedra. **Charoite** contains eleven sites occupied by alkali-metal and alkaline-earth-metal ions: *K*1–*K*7 (*K*7 is mostly vacant), *Sr*1 ions and *W*1–*W*3 groups occupy cavities within the $^3T_{17}$ and $^3T_{12}$ tubes and within the framework of octahedra (Fig. 53). The $(OH)^-$ groups are assumed to form $(Si(O,OH)_4)$, acid silicate groups and link to Na^+ ions to form $(NaO_5OH)^{10-}$-octahedra. **Denisovite** has a similar structure but contains only $^3T_{12}$ and $^2T_4{}^3T_2$ ribbons that extend along [001] and link to an open framework of Ca^{2+}- and Na^+-octahedra that are coordinated predominately by O^{2-} and subordinate F^- and $(OH)^-$. In **denisovite**, cavities within the $^3T_{12}$ tubes and within the framework of octahedra are occupied by K^+ ions and (H_2O) groups.

Synthetic $Na_{16}[Si_{32}O_{64}(OH)_{16}]$ contains $^3T_{32}$ ribbons that are topologically identical to the other ^3T_n, $^3V_2$ ribbons described above. These $^3T_{32}$ ribbons consist of four-membered rings of Si^{4+}- and $(SiO_3(OH))^{3-}$-tetrahedra that link along [102] to form planar ribbons. The $^3T_{32}$ ribbons occur in layers perpendicular to (010) and link to sheets of Na^+-polyhedra that are also perpendicular to (010) (Sassi *et al.*, 2003).

Ashcroftine-(Y) is the largest and most complicated inosilicate that is currently known. It contains $^3T_{56}$ tubes that consist of complex cages of Si^{4+}-tetrahedra that link to each other along [001] by

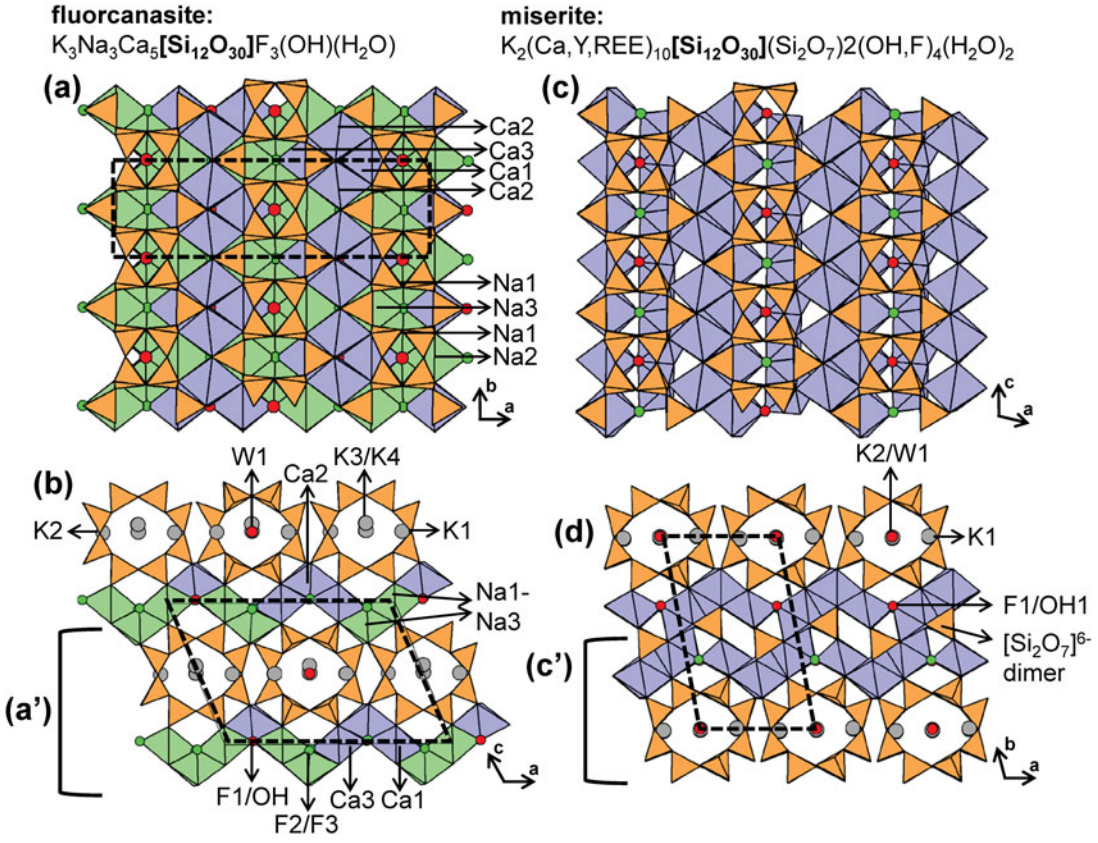

Fig. 49. The structure of **fluorcanasite** projected (*a*) onto (001) and (*b*) along the **b**-axis. The structure of **miserite** projected (*c*) onto (010) and (*d*) along the **c**-axis. In both structures, $(OH)^-$ and (H_2O) groups are shown as red circles and F anions are shown as green circles. Fine dashed black lines outline the unit cell.

https://doi.org/10.1180/mgm.2020.13 Published online by Cambridge University Press

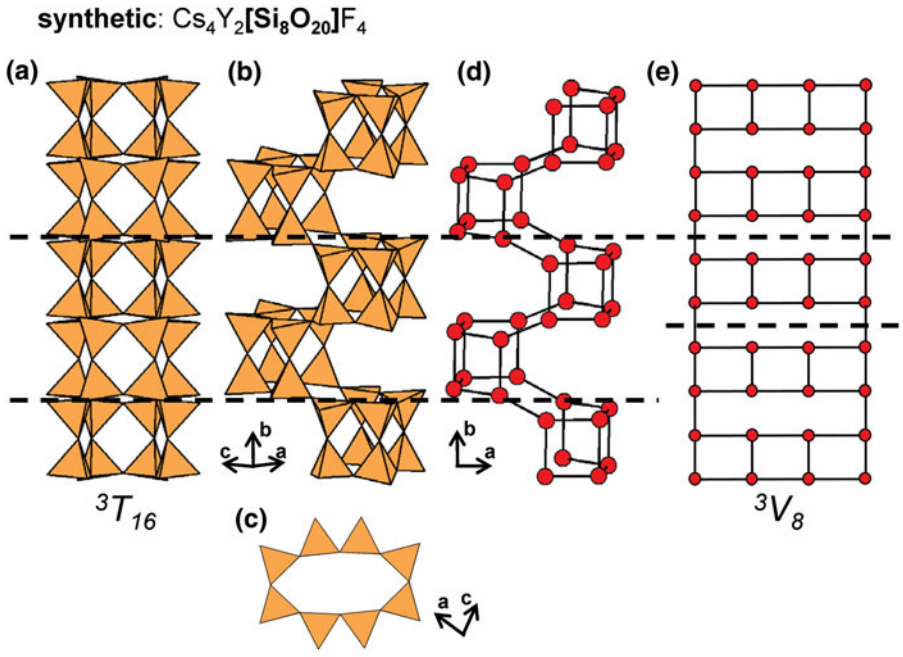

Fig. 50. (*a*, *b*, *c*) Tetrahedral representation of the $^3T_{16}$ ribbon in **synthetic $Cs_4Y_2[Si_8O_{20}]F_4$** projected (*a*) orthogonal to the **b**-axis, (*b*) onto (001), (*c*) along the **b**-axis, (*d*) a ball-and-stick and (*e*) a graphical representation of the ribbon. Dashed black lines outline the geometrical and topological repeat unit of the ribbon.

four $^3T_1$–$^3T_1$ linkages. Each cage consists of four-, seven- and eight-membered rings (Figs 54*a*–*e*). Due to the complicated nature of the **ashcroftine-(Y)** structure, we do not provide a total structure description or figure here and instead, refer readers to Moore *et al.* (1987).

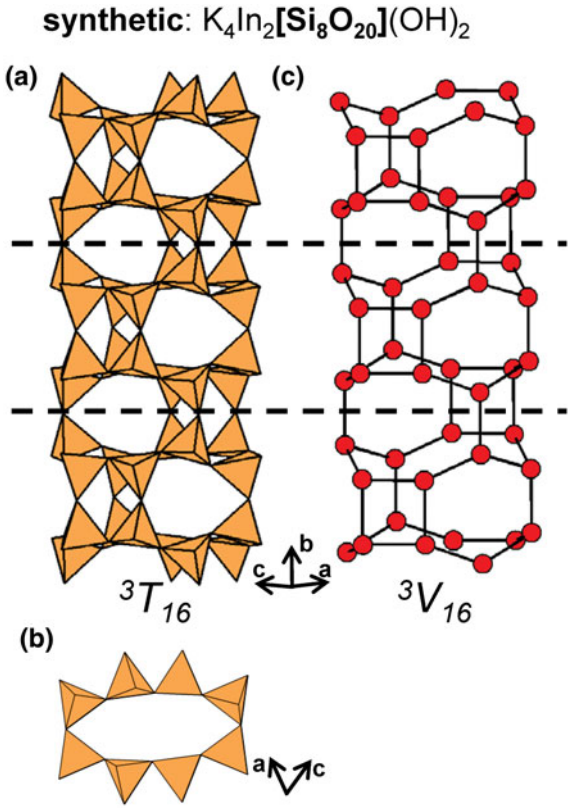

Fig. 51. (*a*, *b*, *c*) Tetrahedral representation of the $^3T_{16}$ tube in **synthetic $K_4In_2[Si_8O_{20}](OH)_4$** projected (*a*) orthogonal to the **b**-axis, (*b*) along the **b**-axis and (*c*) a ball-and-stick (graphical) representation of the tube. Dashed black lines outline the geometrical and topological repeat unit of the tube-ribbon.

$^1T_r{}^3T_r$ class

$^1T_2{}^3T_2$ chains

The **astrophyllite supergroup** includes minerals from the **astrophyllite**, **kupletskite** and **devitoite groups** (Table 7) (Sokolova *et al.*, 2017*a*), all of which contain $^1T_2{}^3T_2$ $[Si_4O_{12}]^{8-}$ chains that consist of a $^2T_2$ chain in which each tetrahedron is decorated by a 1-connected tetrahedron (Figs 55*a*–*d*). The geometrical repeat unit contains four tetrahedra whereas the topological repeat unit contains only two vertices ($^1V_1{}^3V_1$) (Fig. 55*e*). The $^1T_2{}^3T_2$ chains extend along the **a**-axis and link to adjacent chains along the **b**-axis via octahedrally or [5]-coordinated Ti^{4+}, Nb^{5+} or Fe^{3+} (plus minor other ions) occupying the *D* site to form the *H-sheet* (Fig. 56*a*). There are four octahedrally coordinated *M*-sites (*M*1–*M*4) that are occupied dominantly by Fe^{2+} (**astrophyllite group**) and Mn^{2+} (**kupletskite group**) although minor amounts of other cations (e.g. Zn^{2+}; Piilonen *et al.*, 2003*a*,*b*, 2006) can be incorporated. The resulting octahedra share edges to form a continuous sheet, called the O-sheet (Fig. 56*b*). The O-sheet is enclosed between two H-sheets to form an HOH block (Fig. 56*c*) (Sokolova, 2012; Sokolova *et al.*, 2017*a*), similar to the HOH block in **TS-block minerals** (Sokolova, 2006; Sokolova and Cámara, 2017). Species that occur between adjacent TS-blocks form the **I**-block. **Astrophyllite-supergroup** minerals that contain HOH blocks that link to one another directly (along the **c**-axis) through common vertices of the *D*-polyhedron are designated as *Type-1* structures and include the **astrophyllite-** and **kupletskite-group** minerals. **Astrophyllite-supergroup** minerals that contain HOH blocks that do not link directly are designated as *type-2 structures* and are members of the **devitoite group** (Table 7).

In **astrophyllite-group** minerals, the *A* and *B* sites are occupied by K^+ and Na^+, respectively (Figs 56*a*), except in

https://doi.org/10.1180/mgm.2020.13 Published online by Cambridge University Press

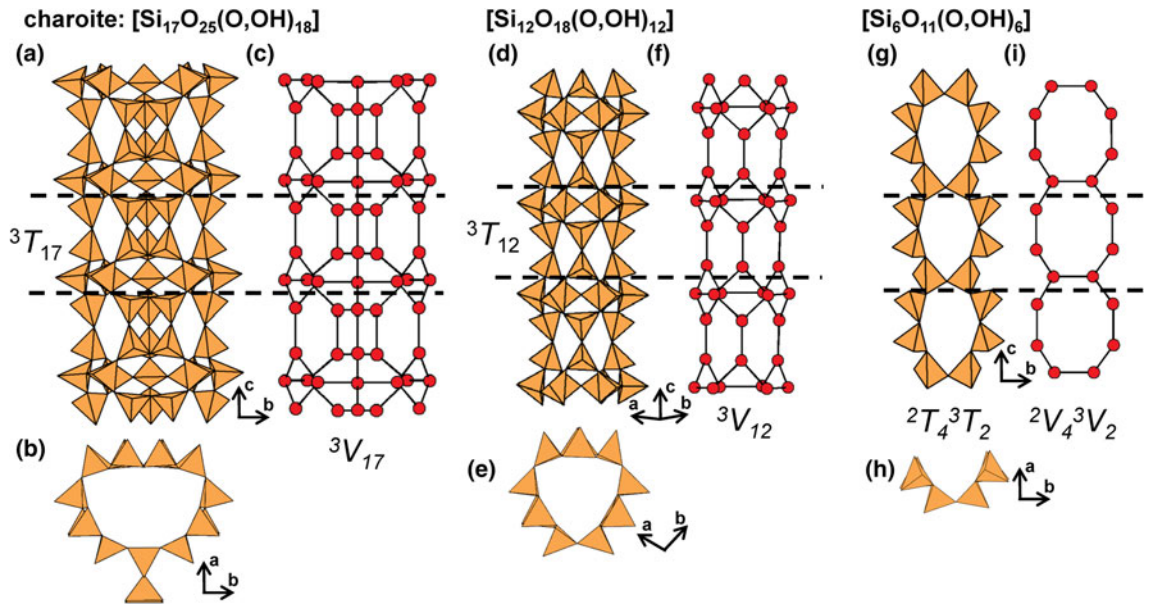

Fig. 52. (*a*, *b*, *c*) Tetrahedral representation of the $^{3}T_{17}$ tube in **charoite** projected (*a*) onto (100), (*b*) along the **c**-axis and (*c*) a ball-and-stick representation of this tube. (*d*, *e*, *f*) the $^{3}T_{12}$ tube in **charoite** projected (*d*) orthogonal to the **c**-axis, (*e*) along the **c**-axis and (*f*) a ball-and-stick representation of this tube. (*g*, *h*, *i*) the $^{2}T_{4}{}^{3}T_{2}$ ribbon in **charoite** projected (*g*) onto (100), (*h*) along the **c**-axis and (*i*) a ball-and-stick representation of this ribbon. Dashed black lines outline the geometrical and topological repeat unit of the tube or ribbon.

nalivkinite and **bulgakite** (in which the *A* site is occupied by Li^{+} with associated (H_2O) to complete its coordination), and in **tarbagatite** and **bulgakite** (in which the *B* site may contain dominant Ca^{2+}). In **kupletskite-group** minerals, the *A* and *B* sites are occupied by K^{+} and Na^{+}, respectively, except in **kupletskite-(Cs)** in which the *A* site is occupied by Cs^{+}. **Laverovite** is a **kupletskite-group** mineral but differs from the others in having Zr^{4+} occupying the *D* site. The **devitoite-group** minerals have much more diverse **I**-blocks, in accord with the absence of direct linkage between adjacent HOH blocks, and also more ordered O-sheets. Thus, **lobanovite** has (most importantly) Na^{+} at the *M*1 site and Mg^{2+} at the *M*4 site. **Sveinbergeite** has (H_2O) at the *A* site, Ca^{2+} at the *B* site, and 1 apfu Fe^{3+} at the *M* sites. **Devitoite** (Figs 57*a*,*b*) has Ba^{2+} at both the *A* and *B* sites, [5]-coordinated Fe^{3+} at the *D* site, and $(PO_4)_2^{3-}$ and $(CO_3)^{2-}$ groups in the **I**-block; in **heyerdahlite**, Mn^{2+} occupies the *M* sites.

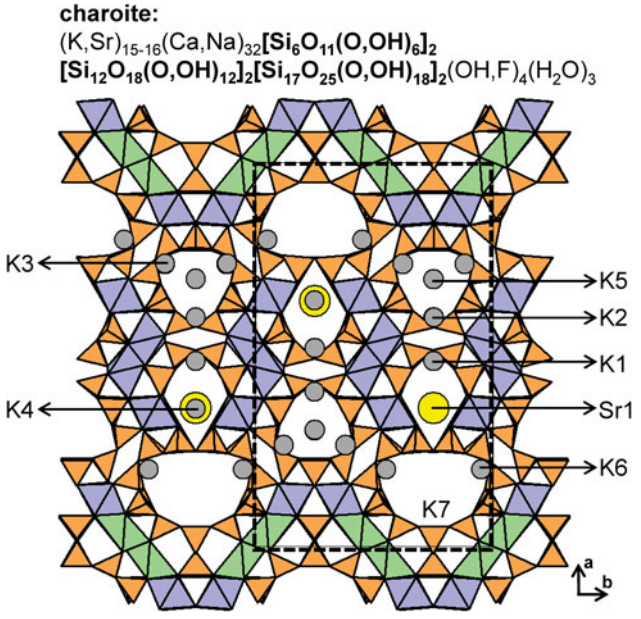

Fig. 53. The structure of **charoite** projected onto (001). Fine dashed black lines outline the unit cell and H atoms associated with (H_2O) and $(OH)^{-}$ groups have been omitted for clarity.

$^{1}T_{2}{}^{3}T_{4}$ ribbons

The $^{1}T_{2}{}^{3}T_{4}$ $[Si_6O_{17}]^{10-}$ ribbon in **nafertisite** consists of ribbons of edge-sharing hexagons, where each six-membered ring is decorated by two 1-connected tetrahedra (Figs 58*a*–*e*). The $^{1}T_{2}{}^{3}T_{4}$ ribbons extends along [100] and are linked along [001] to sheets of $(Fe^{2+}O_4(OH)_2)^{8-}$-octahedra (*M*1–*M*3) that are parallel to the **a**–**b** plane (110) (*O*-sheet) (Fig. 59*a*). Here, $^{1}T_{2}{}^{3}T_{4}$ ribbons occur in layers parallel to (110) and are linked to adjacent ribbons along [010] via $(ZrO_5F)^{7-}$-octahedra (*D* site), forming the *H*-sheet. The linkage of O- and H-sheets forms HOH blocks that are linked to adjacent blocks along [001] through common F^{-} anions of the *D*-site octahedra. Similar structure modules occur in **astrophyllite-supergroup** minerals (Sokolova *et al.*, 2017*a*) and **TS-block minerals** (Sokolova, 2006). In **nafertisite**, HOH blocks are separated by the *A*, *W*1, *B* and *C* sites that form the **I**-block (Fig. 59*b*). The *A* site is split into two disordered sites, *A*1 and *A*2, where K^{+} at *A*1 forms partly occupied $(KO_8F)^{16-}$-polyhedra, and Na^{+} at *A*2 forms $(NaO_4(H_2O)F)^{8-}$-octahedra. Due to the short distance between the *A*1 and *W*1 sites, they cannot both be locally occupied. Na^{+} fully occupies the *B* site forming $(NaO_8F_2)^{17-}$-polyhedra and the *C* site is occupied by Na^{+} with minor Rb^{+} and Cs^{+}. **Nafertisite** contains two $(OH)^{-}$ groups that are associated with the *M*1–*M*3 octahedra of the O-sheet.

https://doi.org/10.1180/mgm.2020.13 Published online by Cambridge University Press

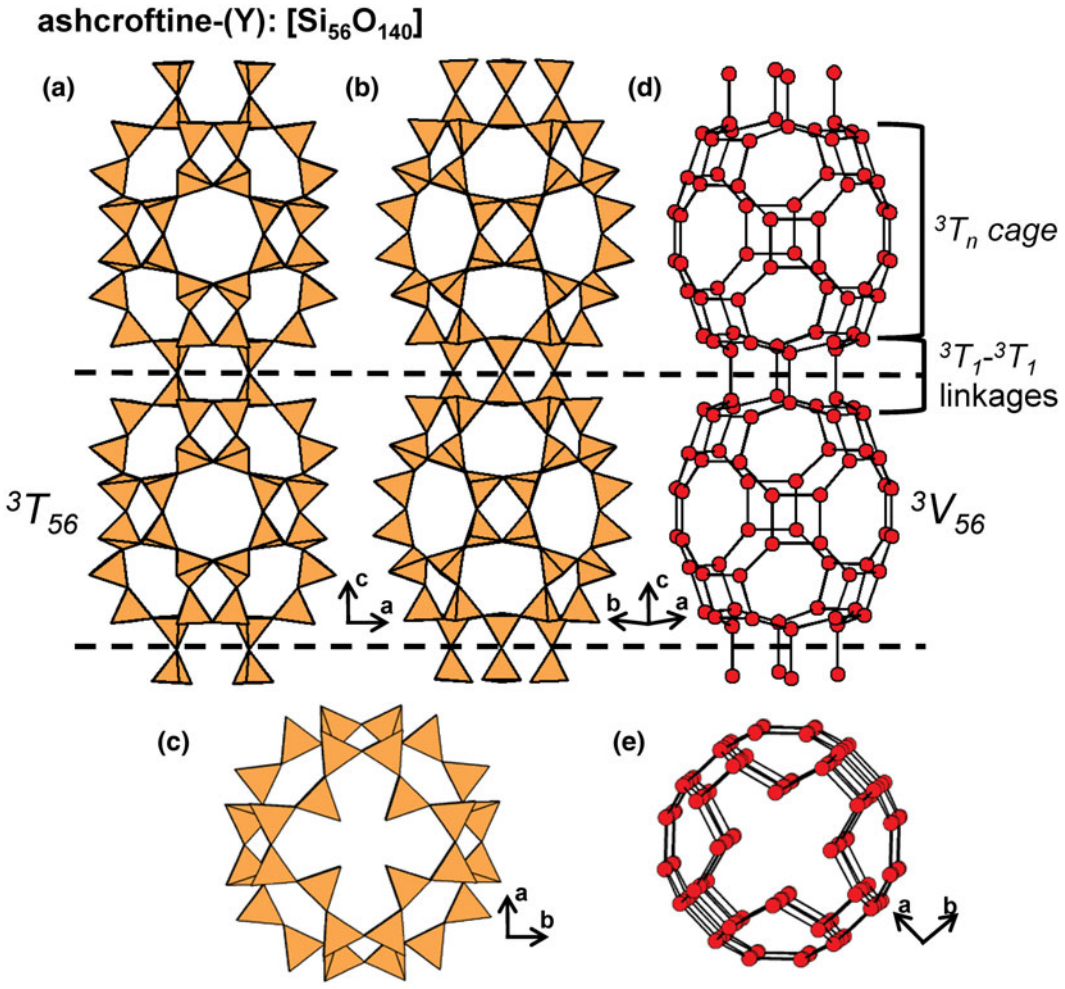

Fig. 54. (*a*, *b*, *c*) Tetrahedral representation of the $^{3}T_{56}$ tube in **ashcroftine** projected (*a*) onto (010), (*b*) orthogonal to the **c**-axis, (*c*) along the **c**-axis, and (*d*, *e*) a ball-and-stick (graphical) representation of the tube. Dashed black lines outline the geometrical and topological repeat unit of the tube.

$^{1}T_{2}{}^{3}T_{6}$ ribbons

The $^{1}T_{2}{}^{3}T_{6}$ $[Si_8O_{22}]^{12-}$ ribbon in **veblenite** consists of ribbons of edge-sharing hexagons of tetrahedra decorated by single, 1-connected tetrahedra along its periphery (Figs 60*a*–*d*). The ribbons link through dominantly Nb^{5+}-octahedra (*D* site) to form a discontinuous *H*-sheet, and adjacent *D*-octahedra are linked along [010] by $[Si_2O_7]^{6-}$ dimers. The $(Fe^{2+/3+}(O,OH)_6)$- and $(Mn^{2+}(O,OH)_6)$-octahedra share common edges to form a modulated O-sheet parallel to (001) (Fig. 61*a*). The H- and O-sheets link to form an HOH block (cf. **astrophyllite-supergroup** minerals, (Fig. 56). The HOH blocks are linked along [001] by an **I**-block that contains the *A1* and *A2* sites occupied by K^+, the *B* site which is dominantly vacant (with minor Na^+), and (H_2O) which occupies five sites (*W*1–*W*5) (Fig. 61*b*).

$^{2}T_{r}{}^{3}T_{r}$ class

$^{2}T_{2}{}^{3}T_{2}$ chains and ribbons

The general formula of the **amphibole-supergroup** minerals is $AB_2C_5T_8O_{22}W_2$ where A = □, Na^+, K^+ and Ca^{2+}; B = Na^+, Li^+, Ca^{2+}, Mn^{2+}, Fe^{2+} and Mg^{2+}; C = Mg^{2+}, Fe^{2+}, Mn^{2+}, Al^{3+}, Fe^{3+}, Mn^{3+}, Ti^{4+} and Li^+; T = Si^{4+}, Al^{3+} and Ti^{4+}; W = $(OH)^-$, F^-, Cl^- and O^{2-} (Hawthorne 1981, 1983*b*,*c*; Hawthorne and Oberti, 2007; Hawthorne *et al.*, 2012). The $^{2}T_{2}{}^{3}T_{2}$ ribbon in the **amphibole-supergroup** minerals has a geometrical repeat unit that contains four tetrahedra and consists of edge-sharing hexagons of tetrahedra that extend in the **c**-direction (Figs 62*a*–*d*). There is a strip of edge-sharing octahedra (*M*1–*M*3), occupied by the C-group cations, that links to $^{2}T_{2}{}^{3}T_{2}$ ribbons in the **a**- and **b**-directions (Fig. 63*a*). The *M*4 site is situated at the periphery of the strip of octahedra and is occupied by B-group cations; it is surrounded by eight oxygen atoms not all of which necessarily bond to the central cation. The *A* site occurs at the centre of a large cavity between the back-to-back $^{2}T_{2}{}^{3}T_{2}$ ribbons (Fig. 63*b*), but the A-group cations actually occupy the off-centered sites *A*(2) and *A*(*m*). There are (currently) six known structural variants of the amphibole arrangement. We may divide these structures into two types: (1) those that involve different stacking sequences in the **a**-direction (*C*2/*m*, *Pnma* and *Pnmn*), and (2) those that are derivatives of (1) and involve differences in coordination ($P2_1/m$) and/or topochemistry (*P*2/*a* or *C*1) (Hawthorne and Oberti, 2007). Complete details of the amphibole structure and chemistry are given in Hawthorne *et al.* (2007) and Oberti *et al.* (2007), and Hawthorne (2012*b*) has related the bond topologies and chemical compositions of the T–O–T (**pyroxene, amphibole, pyribole**

https://doi.org/10.1180/mgm.2020.13 Published online by Cambridge University Press

Table 7. Minerals with $^{1}T_{r}{}^{3}T_{r}$ and $^{2}T_{2}{}^{3}T_{r}$ ribbons.

$^{c}T_{r}$	Mineral	Ideal structural formula	Unit stoichiometry	$^{c}V_{r}$	Space group	O:T	Figs	Refs.
		Astrophyllite supergroup						
		Astrophyllite group						
$^{1}T_{2}{}^{3}T_{2}$	Astrophyllite	$K_2NaFe^{2+}_7Ti_2$**[Si_4O_{12}]$_2$**$O_2(OH)_4F$	[SiO_3]	$^{1}V_{1}{}^{3}V_{1}$	$P\bar{1}$	3.0	55,56	(1)
$^{1}T_{2}{}^{3}T_{2}$	Bulgakite	$Li_2(Ca,Na)Fe^{2+}_7Ti_2$**[Si_4O_{12}]$_2$**$O_2(OH)_4(F,O)(H_2O)_2$	[SiO_3]	$^{1}V_{1}{}^{3}V_{1}$	$P\bar{1}$	3.0	55	(2)
$^{1}T_{2}{}^{3}T_{2}$	Nalivkinite	$Li_2NaFe^{2+}_7Ti_2$**[Si_4O_{12}]$_2$**$O_2(OH)_4F$	[SiO_3]	$^{1}V_{1}{}^{3}V_{1}$	$P\bar{1}$	3.0	55	(3)
$^{1}T_{2}{}^{3}T_{2}$	Niobophyllite	$K_2NaFe^{2+}_7(Nb,Ti)_2$**[Si_4O_{12}]$_2$**$O_2(OH)_4(O,F)$	[SiO_3]	$^{1}V_{1}{}^{3}V_{1}$	$P\bar{1}$	3.0	55	(4)
$^{1}T_{2}{}^{3}T_{2}$	Tarbagataite	$(K,\square)CaFe^{2+}_7Ti_2$**[$Si_4O_{12}$]$_2$**$O_2(OH)_4(OH)$	[SiO_3]	$^{1}V_{1}{}^{3}V_{1}$	$P\bar{1}$	3.0	55	(5)
$^{1}T_{2}{}^{3}T_{2}$	Zircophyllite	$K_2NaFe^{2+}_7Zr_2$**[Si_4O_{12}]$_2$**$O_2(OH)_4F$	[SiO_3]	$^{1}V_{1}{}^{3}V_{1}$	$P\bar{1}$	3.0	55	(6)
		Kupletskite group						
$^{1}T_{2}{}^{3}T_{2}$	Kupletskite-1*A* (2*M*)	$K_2NaMn^{2+}_7Ti_2$**[Si_4O_{12}]$_2$**$O_2(OH)_4F$	[SiO_3]	$^{1}V_{1}{}^{3}V_{1}$	$P\bar{1}$ (*C*2/*c*)	3.0	55	(7)
$^{1}T_{2}{}^{3}T_{2}$	Kupletskite-(Cs)	$Cs_2NaMn^{2+}_7Ti_2$**[Si_4O_{12}]$_2$**$O_2(OH)_4F$	[SiO_3]	$^{1}V_{1}{}^{3}V_{1}$	$P\bar{1}$	3.0	55	(8)
$^{1}T_{2}{}^{3}T_{2}$	Niobokupletskite	$K_2NaMn_7(Nb,Ti)_2$**[Si_4O_{12}]$_2$**$O_2(OH)_4(O,F)$	[SiO_3]	$^{1}V_{1}{}^{3}V_{1}$	$P\bar{1}$	3.0	55	(9)
$^{1}T_{2}{}^{3}T_{2}$	Laverovite	$K_2NaMn_7Zr_2$**[Si_4O_{12}]$_2$**$O_2(OH)_4F$	[SiO_3]	$^{1}V_{1}{}^{3}V_{1}$	$P\bar{1}$	3.0	55	(10)
		Devitoite group						
$^{1}T_{2}{}^{3}T_{2}$	Devitoite	$(Ba_6(PO_4)_2(CO_3))Fe^{2+}_7Fe^{3+}_2$**[$Si_4O_{12}$]$_2$**$O_2(OH)_4$	[SiO_3]	$^{1}V_{1}{}^{3}V_{1}$	$P\bar{1}$	3.0	55,57	(11)
$^{1}T_{2}{}^{3}T_{2}$	Lobanovite	$K_2Na(Fe^{2+}_4Mg_2Na)Ti_2$**[$Si_4O_{12}$]$_2$**$O_2(OH)_4$	[SiO_3]	$^{1}V_{1}{}^{3}V_{1}$	*C*2/*m*	3.0	55	(12)
$^{1}T_{2}{}^{3}T_{2}$	Sveinbergeite	$(H_2O)_2(Ca(H_2O))(Fe^{2+}_6Fe^{3+})Ti_2$**[$Si_4O_{12}$]$_2$**$O_2(OH)_4((OH)H_2O))$	[SiO_3]	$^{1}V_{1}{}^{3}V_{1}$	$P\bar{1}$	3.0	55	(13)
$^{1}T_{2}{}^{3}T_{2}$	Heyerdahlite	$Na_3Mn_7Ti_2$**[Si_4O_{12}]$_2$**$O_2(OH)_4F(H_2O)_2$	[SiO_3]	$^{1}V_{1}{}^{3}V_{1}$	$P\bar{1}$	3.0	55	(14)
$^{1}T_{2}{}^{3}T_{4}$	Nafertisite	$Na_3Fe^{2+}_{10}Ti_2$**[Si_6O_{17}]$_2$**$O_2(OH)_6F(H_2O)_2$	[$SiO_{2.83}$]	$^{1}V_{2}{}^{3}V_{4}$	*A*2/*m*	2.83	58,59	(15)
$^{1}T_{2}{}^{3}T_{6}$	Veblenite	$KNa(Fe^{2+}_5Fe^{3+}_4Mn_7)Nb_3Ti$**[$Si_2O_7$]$_2$[$Si_8O_{22}$]$_2$**$O_6(OH)_{10}(H_2O)_3$	[$SiO_{2.75}$]	$^{1}V_{2}{}^{3}V_{6}$	$P\bar{1}$	2.90	60,61	(16)
$^{1}T_{2}$*	〃 〃	〃 〃	[$SiO_{3.5}$]	$^{1}V_{2}$				
		Amphibole supergroup						
$^{2}T_{2}{}^{3}T_{2}$	Amphiboles	$A_{0-1}B_2C_5$**[T_8O_{22}]**W_2	[$SiO_{2.75}$]	$^{2}V_{2}{}^{3}V_{2}$	mon/orth	2.75	62,63*a*,*b*	(17)
$^{2}T_{2}{}^{3}T_{2}$	Plancheite	Cu_{16}**[Si_8O_{22}]**$(OH)_8(H_2O)_2$	[$SiO_{2.75}$]	$^{2}V_{2}{}^{3}V_{2}$	*Pcnb*	2.75	62,63*c*,*d*	(18)
$^{2}T_{2}{}^{3}T_{2}$	Lavinskyite-2*O* (1*M*)	$K_2(LiCu^{2+})_2Cu^{2+}_{12}$**[$Si_8O_{22}$]**$(OH)_8$	[$SiO_{2.75}$]	$^{2}V_{2}{}^{3}V_{2}$	*Pcnb* (*P*2$_1$/c)	2.75	62	(19)
$^{2}T_{2}{}^{3}T_{2}$	Synthetic	Li_2Mg_2**[Si_4O_{11}]**	[$SiO_{2.75}$]	$^{2}V_{2}{}^{3}V_{2}$	$P\bar{1}$	2.75	64*a*,*b*,*e*,*f*	(20)
$^{2}T_{2}{}^{3}T_{2}$	Synthetic	Fe_3**[$BeSi_3O_9(OH)_2$]**	[$Be_{0.25}Si_{0.75}O_{0.82}OH_{0.18}$]	$^{2}V_{2}{}^{3}V_{2}$	*Pna*2$_1$	2.75	64*c*,*d*,*e*,*f*	(21)
		Jimthompsonite group						
$^{2}T_{2}{}^{3}T_{4}$	Jimthompsonite	$(Mg,Fe)_5$**[Si_6O_{16}]**$(OH)_2$	[$SiO_{2.67}$]	$^{2}V_{2}{}^{3}V_{4}$	*Pbca*	2.67	65,66	(22)
$^{2}T_{2}{}^{3}T_{4}$	Clinojimthompsonite	$(Mg,Fe)_5$**[Si_6O_{16}]**$(OH)_2$	[$SiO_{2.67}$]	$^{2}V_{2}{}^{3}V_{4}$	*C*2/*c*	2.67	65,66	(23)
$^{2}T_{2}{}^{3}T_{4}$	Synthetic	Na_2Mg_4**[Si_6O_{16}]**$(OH)_2$	[$SiO_{2.67}$]	$^{2}V_{2}{}^{3}V_{4}$	*C*2/*c*	2.67	–	(24)
$^{2}T_{2}{}^{3}T_{4}$	Synthetic	$NaMg_4$**[$Si_6O_{15}(OH)$]**$(OH)_2$	[$SiO_{2.5}(OH)_{0.17}$]	$^{2}V_{2}{}^{3}V_{4}$	*C*2/*c*	2.67	–	(24)
$^{2}T_{2}{}^{3}T_{4}$	Synthetic	Ba_4**[Si_6O_{16}]**	[$SiO_{2.67}$]	$^{2}V_{2}{}^{3}V_{4}$	*P*2$_1$/*c*	2.67	–	(25)
$^{2}T_{2}{}^{3}T_{4}$	Okenite	$Ca_2(H_2O)_9(H_2O)_3Ca_8$**[Si_6O_{16}][Si_6O_{15}]$_2$**$(H_2O)_6$	[$SiO_{2.67}$]	$^{2}V_{2}{}^{3}V_{4}$	$P\bar{1}$	2.56	67,68	(26)
$^{3}T_{12}$*	〃 〃	〃 〃	[$SiO_{2.5}$]	$^{3}V_{12}$				
$^{2}T_{2}{}^{3}T_{4}$	Yangite	$PbMn$**[Si_3O_8]**(H_2O)	[$SiO_{2.67}$]	$^{2}V_{2}{}^{3}V_{4}$	$P\bar{1}$	2.67	67	(27)
$^{2}T_{2}{}^{3}T_{6}$	Synthetic	$K_6Eu^{3+}_2$**[$Si_8O_{19}(OH)_2$]**$(OH)_2(H_2O)_{11}$	[$SiO_{2.38}(OH)_{0.25}$]	$^{2}V_{2}{}^{3}V_{6}$	*Pbam*	2.63	69*a*–*d*	(28)
$^{2}T_{2}{}^{3}T_{6}$	Synthetic	Ba_5**[Si_8O_{21}]**	[$SiO_{2.63}$]	$^{2}V_{2}{}^{3}V_{6}$	*C*2/*c*	2.63	69*e*–*h*	(29)
$^{2}T_{2}{}^{3}T_{8}$	Synthetic	Ba_6**[$Si_{10}O_{26}$]**	[$SiO_{2.6}$]	$^{2}V_{2}{}^{3}V_{8}$	*P*2$_1$/*c*	2.60	70*a*–*d*	(30)

References: (1) Cámara *et al.* (2010), Zhitova *et al.* (2017), Woodrow (1967), Shi *et al.* (1998), Piilonen *et al.* (2003*b*); (2) Agakhanov *et al.* (2016); (3) Uvarova *et al.* (2008), Agakhanov *et al.* (2008, 2016); (4) Nickel *et al.* (1964), Cámara *et al.* (2010); (5) Stepanov *et al.* (2012); (6) Kapustin (1973), Sokolova and Hawthorne (2016), Sokolova *et al.* (2018*a*); (7) Christiansen *et al.* (1998), Piilonen *et al.* (2001, 2006); (8) Cámara *et al.* (2010); (9) Cámara *et al.* (2010), Piilonen *et al.* (2000); (10) Sokolova *et al.* (2019); (11) Kampf *et al.* (2010); (12) Sokolova *et al.* (2017*b*), Sokolova and Cámara (2008), Shi *et al.* (1998); (13) Khomyakov *et al.* (2011); (14) Sokolova *et al.* (2018*b*); (15) Cámara *et al.* (2014), Ferraris *et al.* (1996); (16) Cámara *et al.* (2013); (17) Oberti *et al.* (1993); (18) Evans and Mrose (1966), Evans and Mrose (1977); (19) Yang *et al.* (2014), Kolitsch *et al.* (2018); (20) Czank and Bissert (1993); (21) Bakakin and Soloveva (1970); (22) Veblen and Burnham (1978*b*); (23) Konishi *et al.* (1993); (24) Tateyama *et al.* (1978), Ams *et al.* (2009); (25) Hesse and Liebau (1980), Filipenko *et al.* (1971); (26) Merlino (1983); (27) Downs *et al.* (2016); (28) Rastsvetaeva and Aksenov (2011); (29) Hesse and Liebau (1980), Wang *et al.* (2015); (30) Hesse and Liebau (1980).
*Indicates the $^{c}T_{r}$ expression of an additional structural unit including a chain, ribbon, tube, cluster or sheet of $[TO_4]^{n-}$ tetrahedra in the respective mineral.

and **mica supergroups**) and HOH (**astrophyllite, nafertisite, veblenite** and **mica supergroups**) minerals via (algebraic) generating functions.

Lavinskyite-2*O* (1*M*) and **plancheite** both contain $^{2}T_{2}{}^{3}T_{2}$ ribbons that link to both sides of a continuous sheet of (Cu(O,OH)$_6$)-octahedra (*M*1–*M*3), forming a T–O–T block. In **lavinskyite**, these blocks are linked to each other by K^+ ions (*A* site) that occupy cavities between back-to-back $^{2}T_{2}{}^{3}T_{2}$ ribbons. T–O–T blocks are also linked by $^{[5]}Cu^{2+}$- and Li^+-polyhedra (*M*4 site). **Plancheite** is isostructural with **lavinskyite-2*O*** where $^{2}T_{2}{}^{3}T_{2}$ ribbons link to sheets of $(CuO_4(OH)_2)^{8-}$-octahedra (Fig. 63*c*), (H_2O) groups replace K^+ at the *A* site, and $^{[5]}Cu^{2+}$ replaces Li^+ at the *M*4 site (Fig. 63*d*). These minerals contain $^{2}V_{2}{}^{3}V_{2}$ ribbons that are topologically identical to the ribbons in **amphibole-supergroup** minerals. For a more detailed description of **lavinskyite** and **plancheite** see Evans and Mrose (1966, 1977), Yang *et al.* (2014) and Kolitsch *et al.* (2018).

The $^{2}T_{2}{}^{3}T_{2}$ chains in **synthetic $Li_2Mg_2[Si_4O_{11}]$** and **$Fe_3[BeSi_3O_9(OH)]_2$** (Figs 64*a*–*f*) are topologically identical to the $[Si_8O_{22}]^{12-}$ chains in **vlasovite** (see below) and the $[Si_4O_6(OH)_5]^{1-}$ chain in **revdite** (see below) but not with the $^{2}V_{2}{}^{3}V_{2}$ ribbon in **amphibole-supergroup** minerals (Fig. 62*d*). In **synthetic $Li_2Mg_2[Si_4O_{11}]$**, *T*1–*T*4 are occupied by Si^{4+} (Figs 64*a*,*b*), and in **synthetic $Fe_3[BeSi_3O_9(OH)]_2$**, *T*1–*T*3 are occupied by Si^{4+} and *T*4 is occupied by Be^{2+} (Figs 64*c*,*d*). In **synthetic $Li_2Mg_2[Si_4O_{11}]$**, $^{2}T_{2}{}^{3}T_{2}$ chains extend along the **c**-axis and link to ribbons of Mg^{2+}-octahedra and Li^+-polyhedra that also extend along the **c**-axis; chains and ribbons occur in layers that alternate along [110]. In **synthetic $Fe_3[BeSi_3O_9(OH)]_2$**, each $^{2}T_{2}{}^{3}T_{2}$ chain links to several ribbons of Fe^{2+}-octahedra, both of

https://doi.org/10.1180/mgm.2020.13 Published online by Cambridge University Press

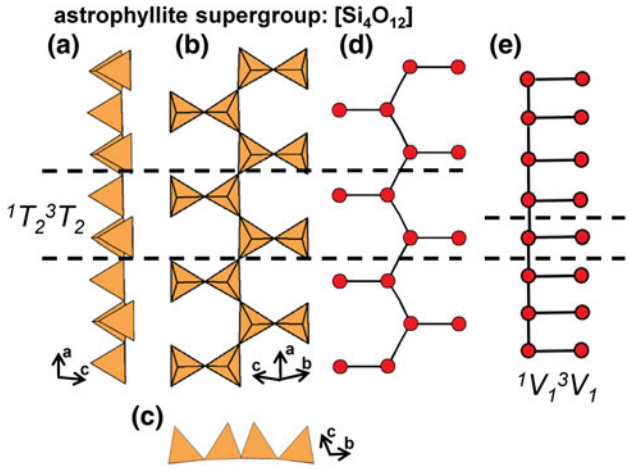

Fig. 55. (*a*, *b*, *c*) Tetrahedral representations of the $^{1}T_{2}{}^{3}T_{2}$ chain in **astrophyllite** projected (*a*) onto (010), (*b*) orthogonal to the **a**-axis, (*c*) along the **a**-axis, (*d*) a ball-and-stick and (*e*) a graphical representation of the chain. Dashed black lines outline the geometrical and topological repeat unit of the chain.

which extend along the **c**-axis, and chains of tetrahedra and ribbons of octahedra occur in layers that alternate along the **a**-axis. For a more detailed total structure description, see Czank and Bissert (1993) and Bakakin and Soloveva (1970).

$^{2}T_{2}{}^{3}T_{4}$ ribbons

The $^{2}T_{2}{}^{3}T_{4}$ ribbon in **jimthompsonite** and **clinojimthompsonite** has a geometrical repeat unit that contains three distinct tetrahedra. Each ribbon is planar and consists of three polymerised $^{2}T_{2}$ chains that form a ribbon that extends along the **c**-axis and consists of staggered edge-sharing hexagons (Figs 65*a*–*c*). The

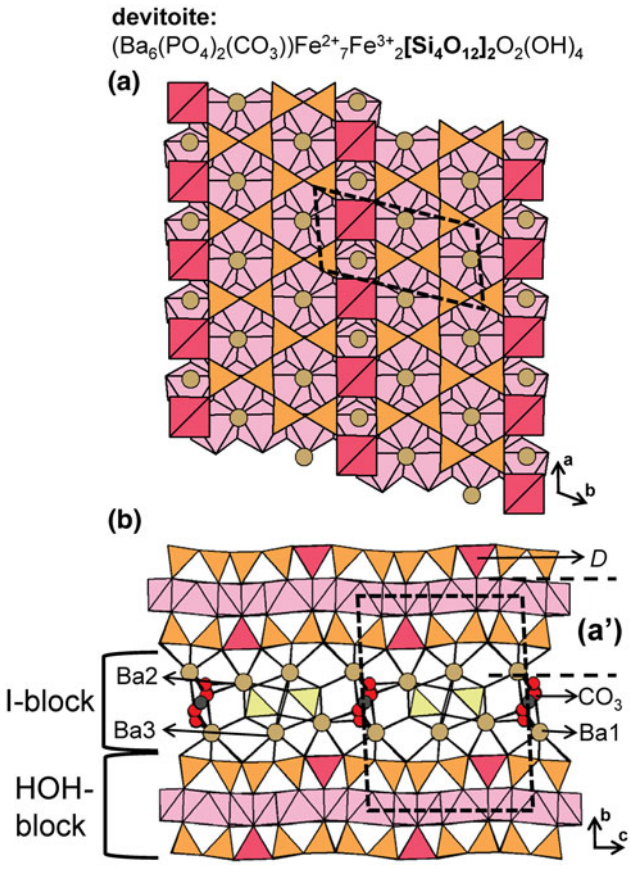

Fig. 57. The structure of **devitoite** highlighting the (*a*) *H*- and *O*-sheet projected onto (001) and the (*b*) HOH-block and **I**-block viewed along the **a**-axis. In (*b*), the C and O atoms of the (CO_3) groups are shown as dark grey and red circles, respectively. The **I**-block, [PO_4] groups are shown as yellow polyhedra and $^{[5]}Fe^{3+}$-polyhedra are shown in dark pink to differentiate them from Fe^{2+}-octahedra. Fine dashed black lines outline the unit cell and H atoms associated with $(OH)^{-}$ groups are omitted for clarity.

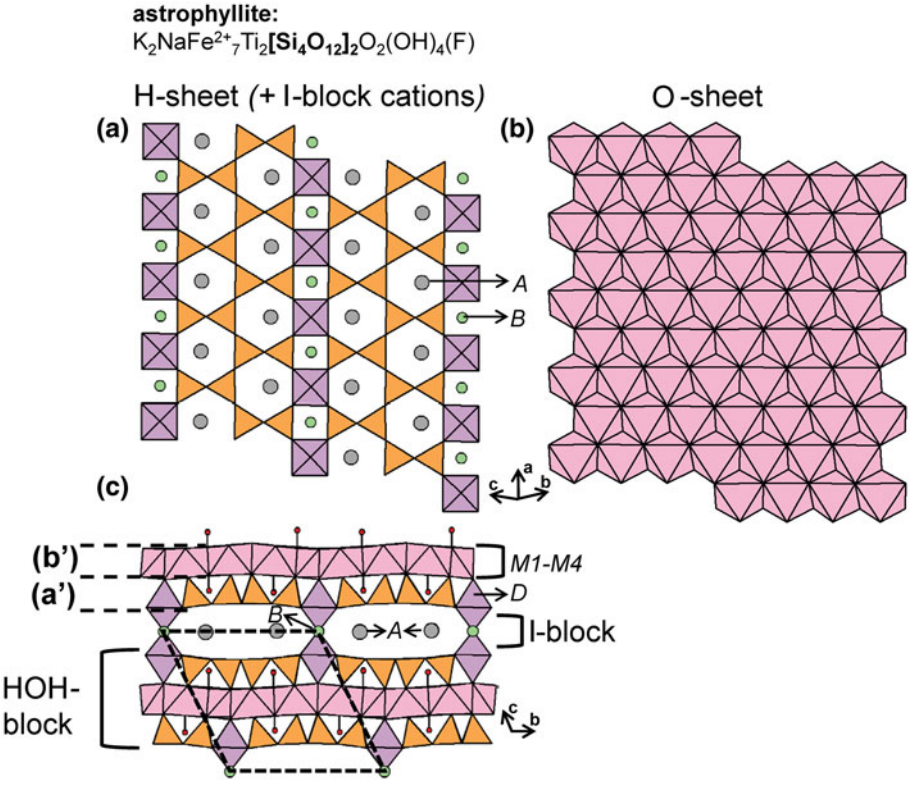

Fig. 56. The structure of **astrophyllite** highlighting the (*a*) H-sheet (and **I**-block cations) and (*b*) O-sheet projected orthogonal to the **a**-axis and (*c*) the HOH-block and **I**-block viewed along the **a**-axis. The *A* and *B*, **I**-block cations are labelled, and the H atoms associated with $(OH)^{-}$ groups are shown as red circles. Fine dashed black lines outline the unit cell.

https://doi.org/10.1180/mgm.2020.13 Published online by Cambridge University Press

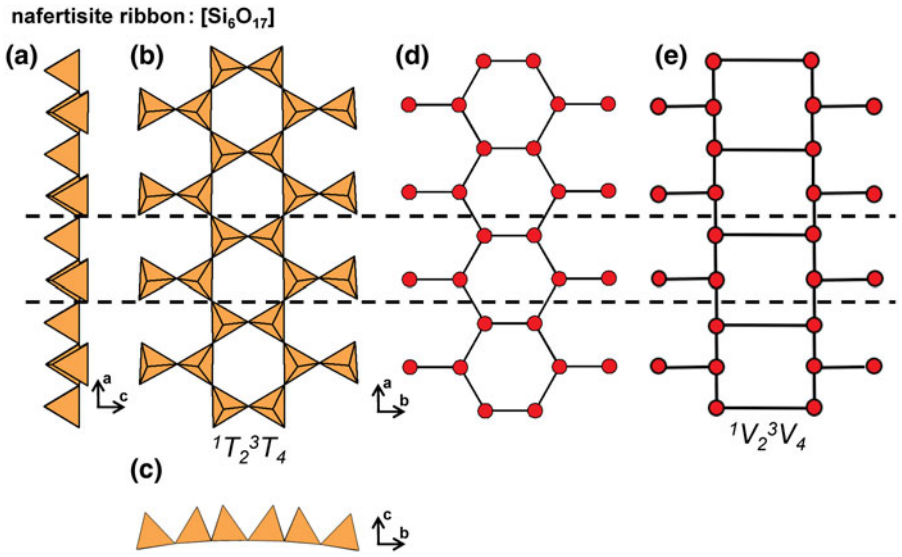

Fig. 58. (*a*, *b*, *c*) Tetrahedral representations of the $^{1}T_{2}{}^{3}T_{4}$ ribbon in **nafertisite** projected (*a*) onto (010), (*b*) onto (001), (*c*) along the **a**-axis, (*d*) a ball-and-stick and (*e*) a graphical representation of the ribbon. Dashed black lines outline the geometrical and topological repeat unit of the ribbon.

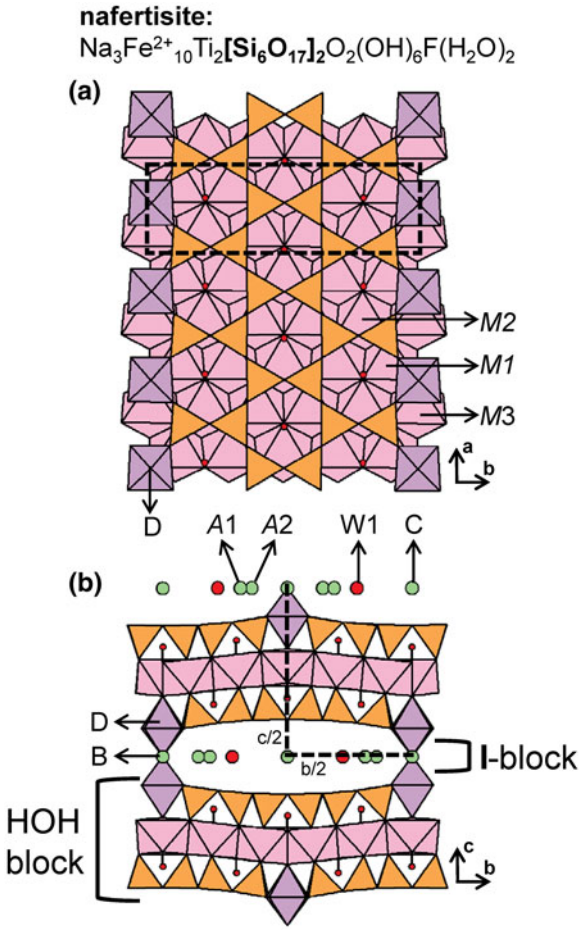

Fig. 59. The structure of **nafertisite** highlighting the (*a*) *H*- and *O*-sheets projected onto (001) and the (*b*) HOH-block and **I**-block viewed along the **a**-axis. The H atoms associated with $(OH)^{-}$ groups linked to octahedra of the O-sheet are shown as small red circles, (H_2O) groups (W1) are shown as larger red circles and **I**-block cations are shown as green circles. Fine dashed black lines outline the unit cell which is halved along the **c**- and **b**-axes in (*b*).

ribbon in **clinojimthompsonite** and **jimthompsonite** has the vertex degree $^{2}V_{2}{}^{3}V_{4}$ (Fig. 65*d*). The geometrical relations of the triple-chain in **jimthompsonite** and other biopyriboles such as **amphiboles** have been discussed in detail (e.g. Thompson, 1978; Papike and Ross, 1970; Law and Whittaker, 1980; Veblen and Burnham, 1978*a*,*b*; Cameron and Papike, 1979; Chisholm, 1981) and *M*-site substitutions and compositional limits are considered by Maresch *et al.* (2009) and Jenkins *et al.* (2012). In **clinojimthompsonite** and **jimthompsonite**, the *M*1–*M*5 sites are occupied by Mg^{2+} (and subordinate Fe^{2+}), these octahedra polymerise to form planar ribbons that extend along the **c**-axis. Mg^{2+} ions form $(MgO_4(OH)_2)^{8-}$-octahedra at the *M*1–*M*3 sites and Mg^{2+}-octahedra at the *M*4 and *M*5 sites. Each $^{2}T_{2}{}^{3}T_{4}$ ribbon links to three distinct ribbons of Mg^{2+}-octahedra and links such ribbons to each other along the **a**- and **b**-axes (Figs 66*a*,*b*).

Various synthetic compounds isostructural with **clinojimthompsonite** have also been reported: **$Na_2Mg_4[Si_6O_{16}](OH)_2$** and **$NaMg_4[Si_6O_{15}(OH)](OH)_2$** in which Na^{+} occupies the *A* site (vacant in **clinojimthompsonite** and **jimthompsonite**) and the *M*5 site (Tateyama *et al.*,1978; Ams *et al.*, 2009) (Table 7). This $^{2}T_{2}{}^{3}T_{4}$ ribbon also occurs in **synthetic $Ba_4[Si_6O_{16}]$** and links to sheets of Ba^{2+}-polyhedra.

The $^{2}T_{2}{}^{3}T_{4}$ $[Si_6O_{16}]^{8-}$ ribbons in **okenite** and **yangite** have a geometrical repeat unit that contain three distinct tetrahedra that polymerise to form planar ribbons of alternating four- and six-membered rings that extend along the **b**-axis (Figs 67*a*–*c*). Geometrically, this ribbon is related to ribbons in **tobermorite-11Å** (see below), **epididymite-group** minerals (Figs 38*a*–*c*) and related synthetic compounds such as **β-$Na_3Y[Si_6O_{15}]$** (Haile and Wuensch, 1997) as they all contain ribbons of two $^{2}T_{3}$ (**wollastonite**-like) chains with varying degrees of polymerisation between the tetrahedra of each chain. Topologically, this $^{2}V_{2}{}^{3}V_{4}$ ribbon is similar to the $^{2}V_{2}{}^{3}V_{2}$ ribbon in **amphibole-supergroup** minerals (Fig. 62*d*) but is not identical (Fig. 67*d*).

In addition to ribbons, **okenite** also contains planar $[Si_6O_{15}]^{6-}$ sheets that consist of five- and eight-membered rings of tetrahedra and correspond to a $(5^2.8)_2(5.8^2)_1$ net (Hawthorne *et al.*, 2019). **Okenite** contains six *Ca* sites (Ca1–Ca6), four of which are occupied by Ca^{2+} (Ca1–Ca4) that form planar ribbons of edge-sharing

https://doi.org/10.1180/mgm.2020.13 Published online by Cambridge University Press

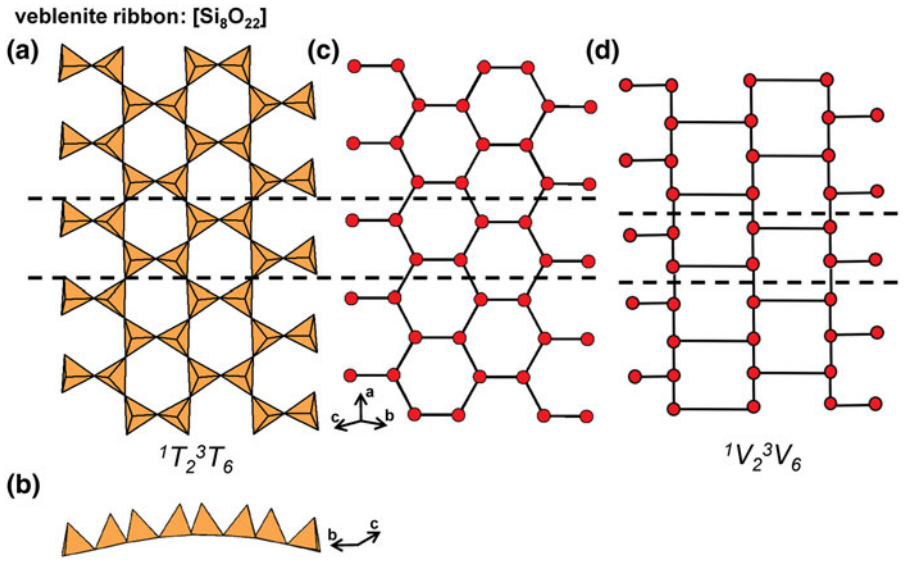

Fig. 60. (*a*, *b*) Tetrahedral representations of the $^{1}T_{2}{}^{3}T_{6}$ ribbon in **veblenite** projected (*a*) orthogonal to the **a**-axis, (*b*) along the **a**-axis, (*c*) a ball-and-stick and (*d*) a graphical representation of the ribbon. Dashed black lines outline the geometrical and topological repeat unit of the ribbon.

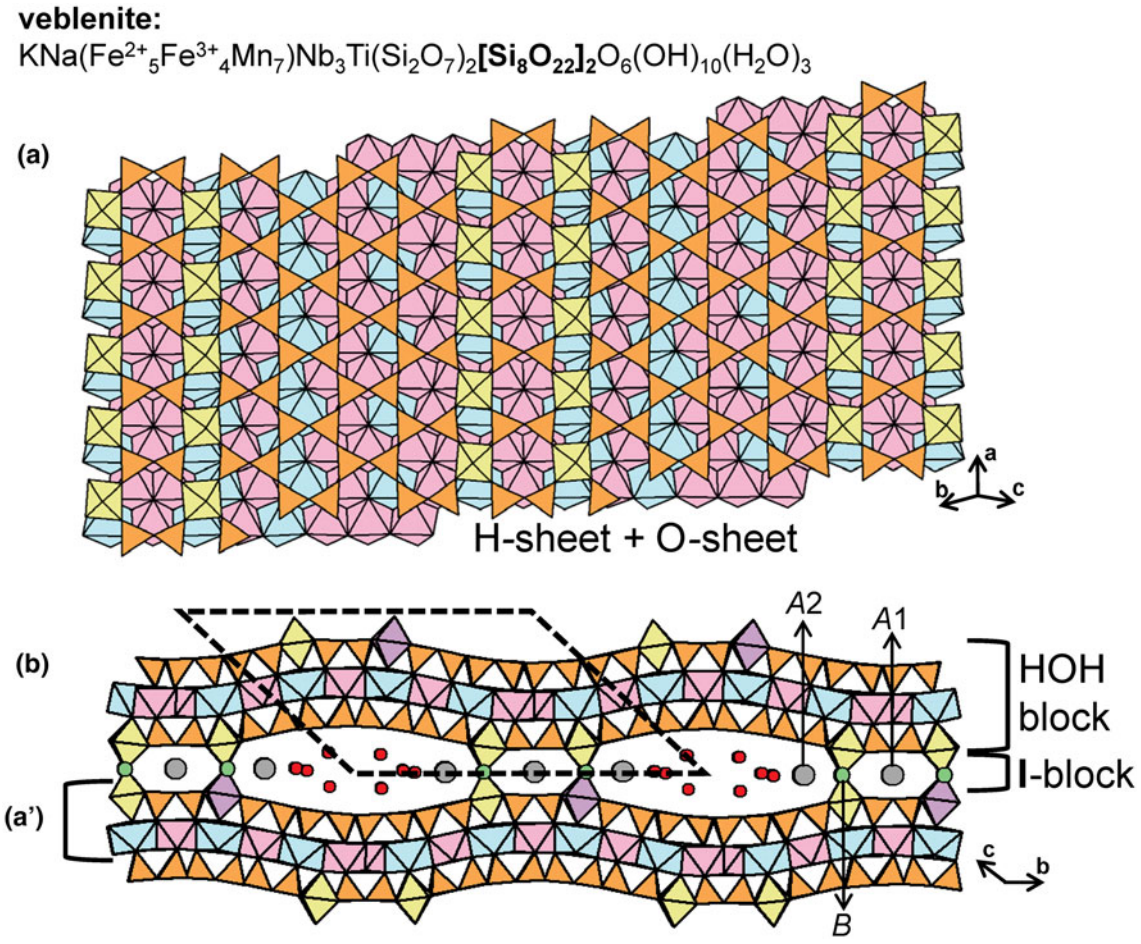

Fig. 61. The structure of **veblenite** highlighting the (*a*) H- and O-sheet projected onto (001) and the (*b*) HOH-block and **I**-block viewed along the **a**-axis. Here, **I**-block, (H_2O) groups are shown as red circles. Fine dashed black lines outline the unit cell and H atoms associated with $(OH)^{-}$ groups are omitted for clarity.

octahedra that extend along the **b**-axis and are linked to each other along the **a**-axis by $^{2}T_{2}{}^{3}T_{4}$ chains (Fig. 68*a*). A complicated $[Ca_2(H_2O)_{12}]^{4+}$ layer involving $(CaO_2(H_2O)_6)^{2-}$- (Ca5) and $(CaO_2(H_2O)_5)^{2-}$-polyhedra (Ca6) links adjacent sheets of tetrahedra along the **c**-axis. The stacking sequence, involving ribbons and sheets of tetrahedra, ribbons of Ca^{2+}-octahedra and

https://doi.org/10.1180/mgm.2020.13 Published online by Cambridge University Press

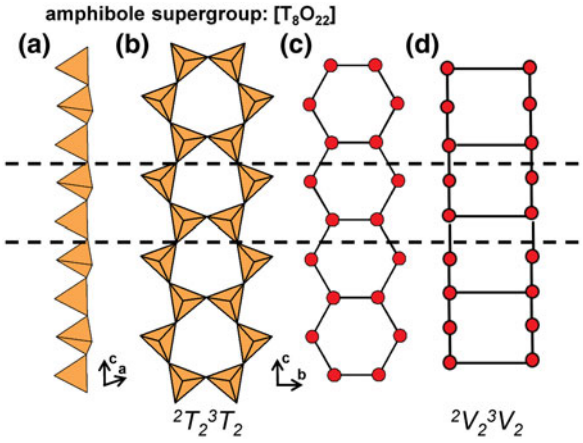

Fig. 62. (*a*, *b*) Tetrahedral representations of the $^{2}T_{2}{}^{3}T_{2}$ ribbon in **amphibole-supergroup** minerals projected (*a*) orthogonal to the **c**-axis, (*b*) onto (100), (*c*) a ball-and-stick and (*d*) a graphical representation of the ribbon. Dashed black lines outline the geometrical and topological repeat unit of the ribbon.

the $[Ca_2(H_2O)_{12}]^{4+}$ layer, is shown in Fig. 68*b*. The ribbon in **yangite** is topologically identical to that in **okenite**. However, the interstitial structure of **yangite** is relatively simple, containing one [5]- and one [6]-coordinated sites occupied by Pb^{2+} and Mn^{2+}, respectively, that form ribbons of edge-sharing octahedra. These ribbons and $^{2}T_{2}{}^{3}T_{4}$ chains occur in layers that alternate along the **c**-axis (Fig. 68*b*).

$^{2}T_{2}$ $^{3}T_{6}$ ribbons

Two topologically distinct variants of the $^{2}T_{2}{}^{3}T_{6}$ ribbon occur in **synthetic** $\mathbf{K_6Eu_2^{3+}[Si_8O_{19}(OH)_2](OH)_2(H_2O)_{11}}$ and $\mathbf{Ba_5[Si_8O_{21}]}$.

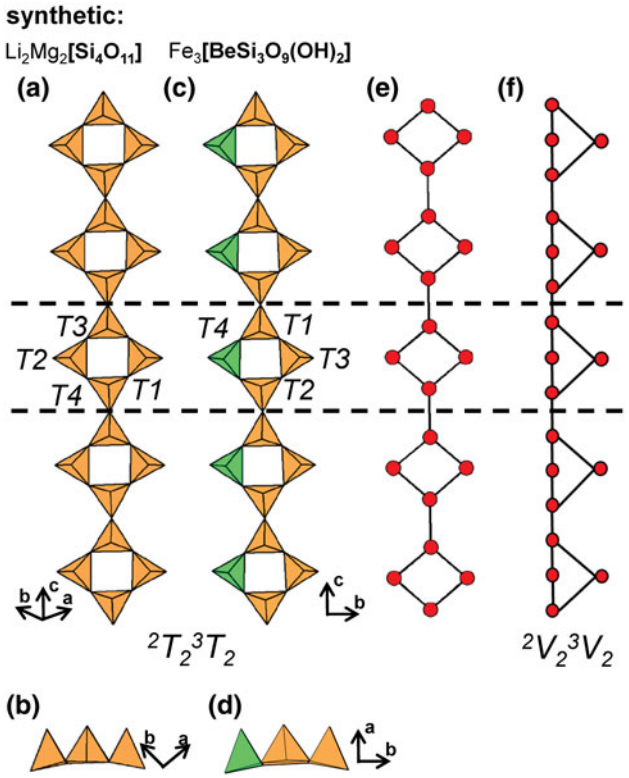

Fig. 64. Tetrahedral representations of the $^{2}T_{2}{}^{3}T_{2}$ chains in (*a*, *b*) **synthetic** $\mathbf{Li_2Mg_2[Si_4O_{11}]}$ and (*c*, *d*) $\mathbf{Fe_3[BeSi_3O_9OH]_2}$ projected (*a*) orthogonal to the **c**-axis, (*b*) along the **c**-axis, (*c*) onto (100), (*d*) along the **c**-axis, (*e*) a ball-and-stick and (*f*) a graphical representation of the both chains. The *T*4 site in **synthetic** $\mathbf{Fe_3[BeSi_3O_9OH]_2}$ is occupied by Be^{2+} and is shown as a dark green tetrahedron. Dashed black lines outline the geometrical and topological repeat unit of the chain.

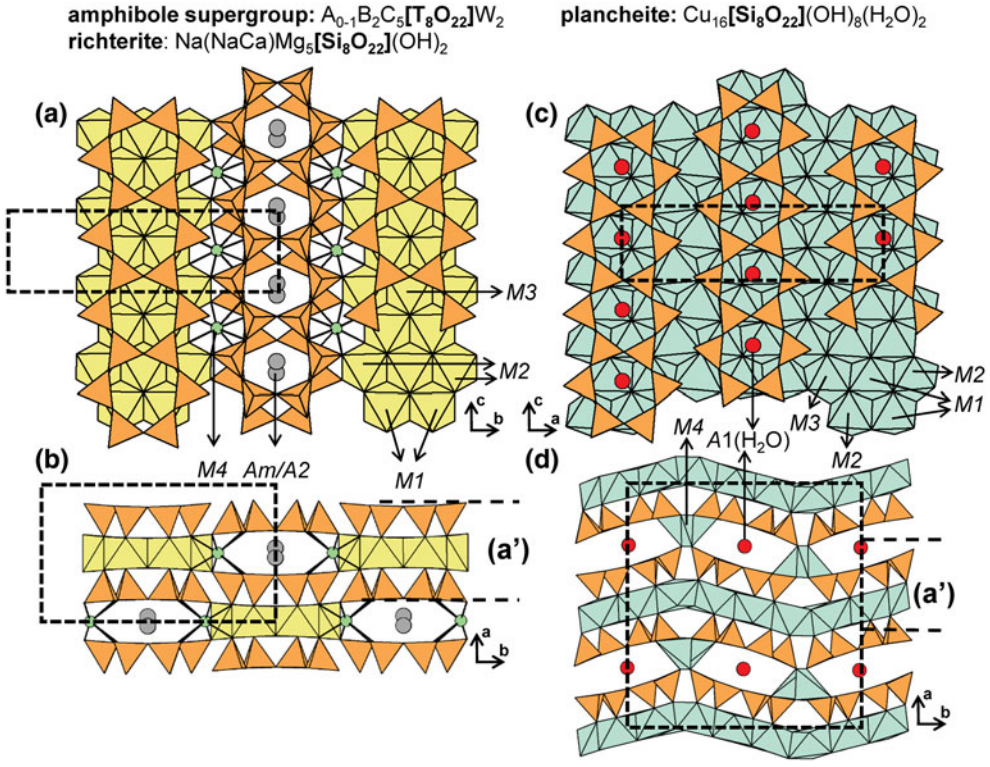

Fig. 63. The structure of **richterite** projected (*a*) onto (100) and (*b*) along the **c**-axis (*a*). The structure of **plancheite** projected (*c*) onto (100) and (*d*) along the **c**-axis. Fine dashed black lines outline the unit cell and H atoms associated with $(OH)^{-}$ groups are omitted for clarity

https://doi.org/10.1180/mgm.2020.13 Published online by Cambridge University Press

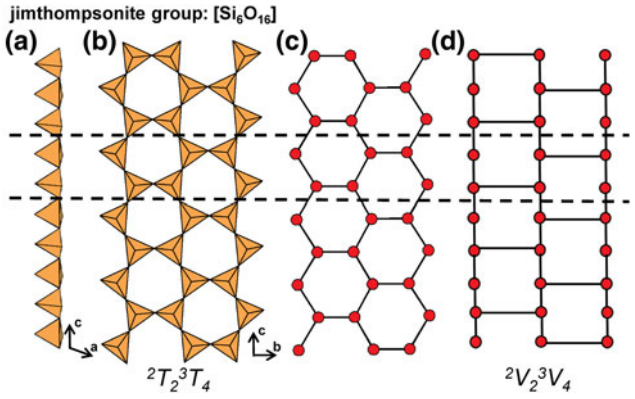

Fig. 65. (*a*, *b*) Tetrahedral representations of the $^{2}T_{2}{}^{3}T_{4}$ ribbon in **jimthompsonite** projected (*a*) orthogonal to the **c**-axis, (*b*) onto (100), (*c*) a ball-and-stick and (*d*) a graphical representation of the ribbon. Dashed black lines outline the geometrical and topological repeat unit of the ribbon.

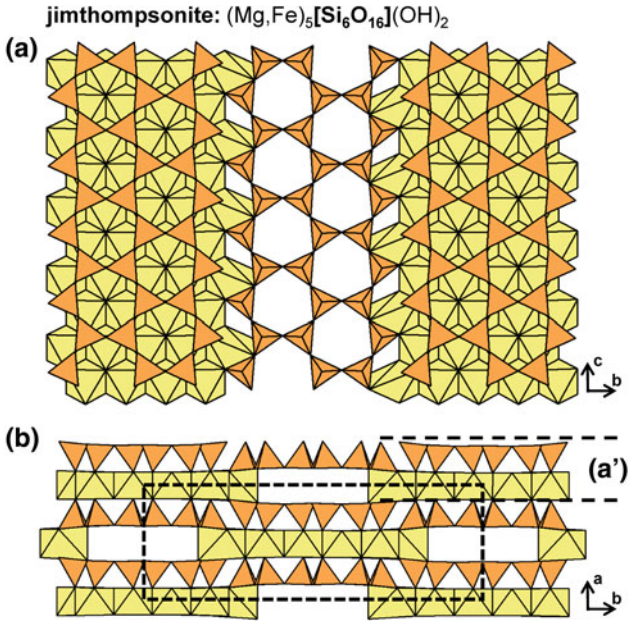

Fig. 66. The structure of **jimthompsonite** projected (*a*) onto (100) and (*b*) along the **c**-axis. Fine dashed black lines outline the unit cell and H atoms associated with $(OH)^{-}$ groups are omitted for clarity.

The geometrical repeat unit of the $^{2}T_{2}{}^{3}T_{6}$ ribbon in the former contains three distinct tetrahedra that polymerise to form ribbons that extend along the **c**-axis (Figs 69*a*–*d*). These ribbons consist of two linked $^{2}T_{2}{}^{3}T_{2}$ chains similar to those in **synthetic** $\mathbf{Li_2Mg_2[Si_4O_{11}]}$ (Figs 64*a*,*b*) and **vlasovite** (see below). The $^{2}T_{2}{}^{3}T_{6}$ ribbons link to each other via $(EuO_4(OH)_2)^{7-}$-octahedra, forming an open framework in which channels are occupied by $^{[8-9]}K^{+}$ ions and (H_2O) groups. The $^{2}T_{2}{}^{3}T_{6}$ ribbon in **synthetic** $\mathbf{Ba_5[Si_8O_{21}]}$ consists of two linked $^{2}T_{2}{}^{3}T_{2}$ amphibole-like ribbons (Figs 69*e*–*h*) and extends along the **b**-axis. These ribbons link to sheets of $^{[8]}Ba^{2+}$-polyhedra that are parallel to (010).

$^{2}T_{2}{}^{3}T_{8}$ ribbons

The geometrical repeat unit of the ribbon in **synthetic** $\mathbf{Ba_6[Si_{10}O_{26}]}$ contains ten distinct Si^{4+}-tetrahedra that polymerise

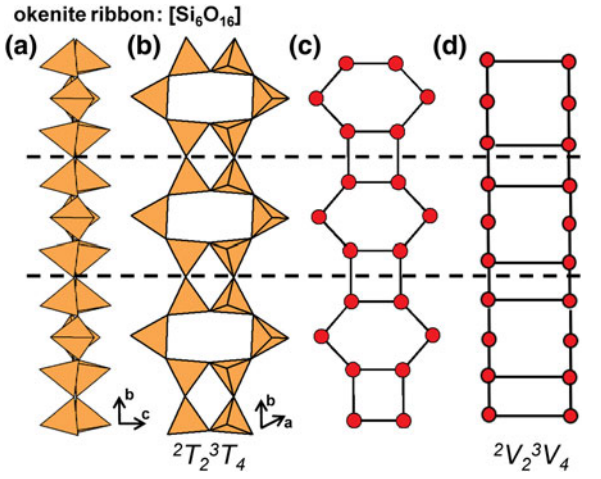

Fig. 67. (*a*, *b*) Tetrahedral representations of the $^{2}T_{2}{}^{3}T_{4}$ ribbon in **okenite** projected (*a*) onto (100), (*b*) onto (001), (*c*) a ball-and-stick and (*d*) a graphical representation of the ribbon. Dashed black lines outline the geometrical and topological repeat unit of the ribbon.

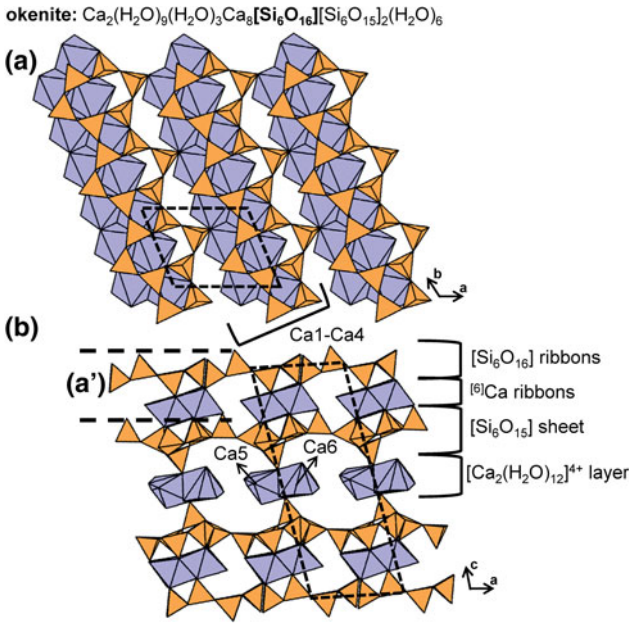

Fig. 68. The structure of **okenite** projected (*a*) onto (001) and (*b*) along the **b**-axis. Here, layers that contain $[Si_6O_{16}]^{8-}$ ribbons, $[Si_6O_{15}]^{6-}$ sheets and $[Ca_2(H_2O)_{12}]^{4+}$ dimers are labelled. Fine dashed black lines outline the unit cell and H atoms associated with (H_2O) groups are omitted for clarity.

to form $^{2}T_{2}{}^{3}T_{8}$ ribbons that extend parallel to [010] (Figs 70*a*–*d*). The structure of synthetic $\mathbf{Ba_6[Si_{10}O_{26}]}$ is closely related to those of synthetic $\mathbf{Ba_5[Si_8O_{21}]}$ (Figs 69*e*–*g*) and $\mathbf{Ba_4[Si_6O_{16}]}$ (Hesse and Liebau, 1980) in which ribbons of tetrahedra link to sheets of $^{[8]}Ba^{2+}$-polyhedra that are parallel to (010).

$^{2}T_{3}{}^{3}T_{4}$ ribbons

The $^{2}T_{3}{}^{3}T_{4}$ $[Si_7O_{18}(OH)]^{9-}$ ribbons in **tokkoite**, **senkevichite** and **tinaksite** (Table 8) have a geometrical repeat unit that contains seven distinct Si^{4+}-tetrahedra where *T*7 is an acid silicate group: $(SiO_3OH)^{3-}$. Each $^{2}T_{3}{}^{3}T_{4}$ ribbon consists of alternating four- and

https://doi.org/10.1180/mgm.2020.13 Published online by Cambridge University Press

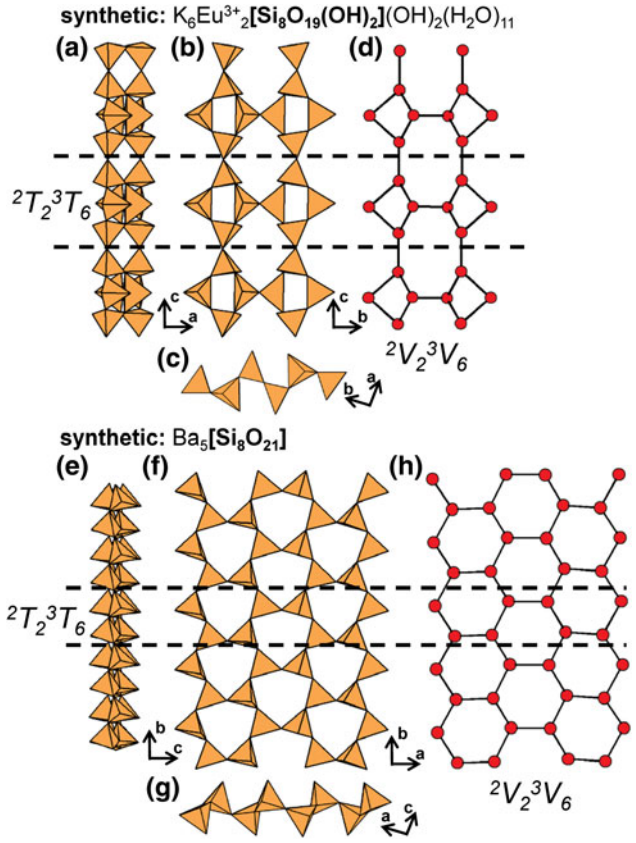

Fig. 69. (*a*, *b*, *c*) Tetrahedral representations of the $^2T_2{}^3T_6$ ribbon in **synthetic $K_6Eu_2^{3+}[Si_8O_{19}(OH)_2](OH)_2(H_2O)_9$** projected (*a*) onto (010), (*b*) onto (100), (*c*) along the **c**-axis and (*d*) a ball-and-stick (graphical) representation of the ribbon. (*e*, *f*, *g*) Tetrahedral representations of the $^2T_2{}^3T_6$ ribbon in **synthetic $Ba_5[Si_8O_{21}]$** projected (*e*) onto (100), (*f*) onto (001), (*g*) along the **b**-axis and (*h*) a ball-and-stick (graphical) representation of the ribbon. Dashed black lines outline the geometrical and topological repeat unit of the ribbon.

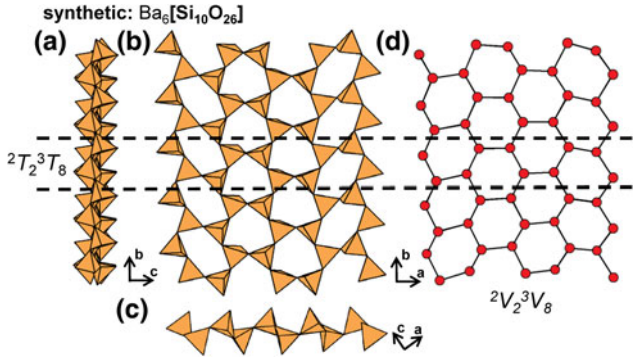

Fig. 70. (*a*, *b*, *c*) Tetrahedral representations of the $^2T_2{}^3T_8$ ribbon in **synthetic $Ba_6[Si_{10}O_{26}]$** projected (*a*) onto (100), (*b*) onto (001), (*c*) along the **b**-axis and (*d*) a ball-and-stick (graphical) representation of the ribbon. Dashed black lines outline the geometrical and topological repeat unit of the ribbon.

eight-membered rings (Figs 71*a*–*e*) and in **tokkoite**, extend along [001] and link to sheets of Ca^{2+}-octahedra (*M*1, *M*3–*M*4) and $^{[7]}Ca^{2+}$-polyhedra (*M*2) that extend parallel to the **b**–**c** plane (Figs 72*a*,*b*). These sheets are linked along [100] by $^2T_3{}^3T_4$ ribbons, forming large tunnels that are occupied by K^+ ions (*A*1–*A*2) (Fig. 72*c*). In **tinaksite** and **senkevichite**, Ti^{4+} and $^{[7]}Na^+$ occupy the *M*1 and *M*2 sites, respectively, and Cs^+ occupies the *A*1 site in **senkevichite**. The **tokkoite** → **tinaksite** (**senkevichite**) substitution: $2Ca^{2+}_{(M1+M2)} + (F,OH)^- \leftrightarrow Ti^{4+}_{(M1)} + Na^+_{(M2)} + O^-$ was suggested by Rozhdestvenskaya and Nikishova (2002).

$^2T_4{}^3T_2$ chains

The **howieite group** includes **deerite**, **johninnesite**, **taneyamalite** and **howieite,** all of which contain $^2T_4{}^3T_2$ $[Si_6(O,OH)_{17}]$ chains (Table 8). The geometrical repeat unit of each chain contains six-membered rings that link to one another through a single corner-sharing tetrahedra (Figs 73*a*–*c*). The structures of **howieite** (Figs 73*d*,*e*) and **taneyamalite** (Figs 73*f*,*g*) both contain six *T* sites fully occupied by Si^{4+} and twelve octahedrally coordinated *M* sites occupied dominantly by Fe^{2+} in **howieite** and Mn^{2+} in **taneyamalite**. In both minerals, octahedrally coordinated cations form $[M_{12}O_{30}]$ ribbons that are four octahedra wide (Figs 73*d*,*f*) and extend along the **c**-axis (Figs 73*e*,*g*), parallel to the $^2T_4{}^3T_2$ chains. These chains and ribbons of octahedra occur in layers that alternate along the **b**-axis, and adjacent ribbons of octahedra are linked along $[1\bar{2}0]$ by the 2-connected tetrahedra of each six-membered ring. Both minerals also contain 13 $(OH)^-$ sites, three of which are associated with the $[Si_6(O,OH)_{17}]$ chain and the rest with the $[M_{12}O_{30}]$ ribbon. These minerals also have a single large-cation site occupied by Na^+ in **howieite** and Na^+ with minor Ca^{2+} in **taneyamalite**. In both minerals, $^{[8]}Na^+$-polyhedra occur in layers with ribbons of octahedra and link adjacent $^2T_4{}^3T_2$ chains along the **b**-axis (Figs 73*d*–*g*).

The interstitial structure of **deerite** is closely related to that of **howieite** and **taneyamalite**, and **deerite** and **howieite** have been observed as intergrowths in the metasedimentary rocks of the Franciscan Formation, California (Fleet, 1977). The major difference in **deerite** is that ribbons of octahedra and $^2T_4{}^3T_2$ chains have more than one orientation, somewhat resembling wallpaper-borate structures (Moore and Araki, 1974; Cooper and Hawthorne, 1998), and hence do not occur in alternating layers as they do in **howieite** and **taneyamalite**. **Deerite** contains nine octahedrally coordinated *M*-sites occupied by Fe^{3+} (with minor Al^{3+}) and Fe^{2+} (with minor Mn^{2+}). The Fe^{2+}- and Fe^{3+}-octahedra form ribbons that are six octahedra wide (Fig. 74*a*) and extend along the **c**-axis, parallel to the $^2T_4{}^3T_2$ chains that each link to three interconnected ribbons (Figs 74*a*,*b*). **Deerite** contains five $(OH)^-$ groups that coordinate $Fe^{2+/3+}$-octahedra of the ribbon.

Johninnesite contains seven *T* sites (*T*1–*T*7), *T*1–*T*6 of are fully occupied by Si^{4+} forming $[Si_6O_{17}]^{10-}$ chains, and *T*7 is occupied by As^{5+} which does not link to the $^2T_4{}^3T_2$ chain. **Johninnesite** contains twelve octahedrally coordinated *M*-sites (*M*1–*M*12) occupied by Na^+, Mn^{2+}, Mg^{2+} and a vacancy. Edge-sharing $(MnO_6)^{10-}$- (*M*4), $(MnO_4(OH)_2)^{8-}$- (*M*5–*M*6) and $(MgO_4(OH)_2)^{8-}$-octahedra (*M*7–*M*9) link to form discontinuous sheets parallel to (010) (Fig. 74*c*). The vacant *M*-sites (*M*11–*M*12) in the sheet are capped by As^{5+}-tetrahedra on both sides of the sheet. Sheets of octahedra link to each other along the **a**-axis via ribbons of $(MnO_6)^{10-}$- (*M*1), $(MnO_5(OH))^{9-}$-(*M*2) and $(MnO_3(OH)_3)^{7-}$-octahedra (*M*3), forming channels that extend along the **c**-axis that are occupied by Na^+ ions (*M*10). The $^2T_4{}^3T_2$ chains link to both the sheet and ribbon, and occur in layers parallel to the **b**-axis (Figs 74*c*,*d*). In **johninnesite,** the tetrahedra of each chain in the same layer point in the same direction, in contrast to the tetrahedra in **howieite** (Figs 73*d*,*e*) and **taneyamalite** (Figs 73*f*,*g*) where

https://doi.org/10.1180/mgm.2020.13 Published online by Cambridge University Press

Table 8. Minerals with $^{2}T_{r}{}^{3}T_{r}$ ribbons.

$^{c}T_{r}$	Mineral	Ideal structural formula	Unit stoichiometry	$^{c}V_{r}$	Space group	O:T	Figs	Refs.
$^{2}T_{3}{}^{3}T_{4}$	Tokkoite	K_2Ca_4**[Si_7O_{18}(OH)]**(OH,F)	[$SiO_{2.57}(OH)_{0.14}$]	$^{2}V_{3}{}^{3}V_{4}$	$P\bar{1}$	2.71	71,72	(1)
$^{2}T_{3}{}^{3}T_{4}$	Senkevichite	(CsK)Ca_2NaTiO**[Si_7O_{18}(OH)]**	[$SiO_{2.57}(OH)_{0.14}$]	$^{2}V_{3}{}^{3}V_{4}$	$P\bar{1}$	2.71	71	(2)
$^{2}T_{3}{}^{3}T_{4}$	Tinaksite	K_2Ca_2NaTiO**[Si_7O_{18}(OH)]**	[$SiO_{2.57}(OH)_{0.14}$]	$^{2}V_{3}{}^{3}V_{4}$	$P\bar{1}$	2.71	71	(3)
		Howieite group						
$^{2}T_{4}{}^{3}T_{2}$	Howieite	Na(Fe,Mn)$_{10}$(Fe,Al)$_2$**[$Si_{12}O_{31}$(OH)$_3$]**$(OH)_{10}$	[$SiO_{2.58}(OH)_{0.25}$]	$^{2}V_{4}{}^{3}V_{2}$	$P1$	2.83	73*a–e*	(4)
$^{2}T_{4}{}^{3}T_{2}$	Taneyamalite	(Na,Ca)(Mn,Mg,Fe)$_{12}$**[$Si_{12}O_{31}$(OH)$_3$]**$(OH)_{10}$	[Si(OH,O)$_{2.83}$]	$^{2}V_{4}{}^{3}V_{2}$	$P1$	2.83	73*a–c,f,g*	(5)
$^{2}T_{4}{}^{3}T_{2}$	Deerite	(Fe,Mn)$_6$(Fe,Al)$_3$**[Si_6O_{17}]**$O_3(OH)_5$	[$SiO_{2.83}$]	$^{2}V_{4}{}^{3}V_{2}$	$P2_1/a$	2.83	74*a–b*	(6)
$^{2}T_{4}{}^{3}T_{2}$	Johninnesite	$Na_2Mn_3^{2+}Mg_7(AsO_4)_2$**[$Si_6O_{17}$]**$_2(OH)_8$	[$SiO_{2.83}$]	$^{2}V_{4}{}^{3}V_{2}$	$P\bar{1}$	2.83	74*c–d*	(7)
		Tobermorite group (C–S–H)						
		$Ca_{4+x}(Al_ySi_{6-y})O_{15+2x-y}(OH)_{2-2x+y}\cdot 5H_2O$, where $0 \le x \le 1$ and $0 \le y \le 1$, anomalous where $x \approx 0$						
$^{2}T_{4}{}^{3}T_{2}$	Kenotobermorite (11Å) 4*O* (anomalous)	Ca_4**[Si_6O_{15}(OH)$_2$]**$(H_2O)_2\cdot(H_2O)_3$	[$SiO_{2.5}(OH)_{0.33}$]	$^{2}V_{4}{}^{3}V_{2}$	*F*2*dd*	2.83	75*a,b,e,f*, 76*a,b*	(8)
$^{2}T_{4}{}^{3}T_{2}$	Tobermorite (11Å) 2*M* (normal)	Ca_4**[Si_6O_{17}]**$(H_2O)_2\cdot(Ca(H_2O)_3$	[$SiO_{2.83}$]	$^{2}V_{4}{}^{3}V_{2}$	*B*11*m*	2.83	75*a,b,e,f*, 76*c–d*	(9)
$^{2}T_{4}{}^{3}T_{2}$	Kenotobermorite (11Å) 2*M* (anomalous)	Ca_4**[Si_6O_{15}(OH)$_2$]**$(H_2O)_2\cdot(H_2O)_3$	[$SiO_{2.5}(OH)_{0.33}$]	$^{2}V_{4}{}^{3}V_{2}$	*B*11*m*	2.83	75*a,b,e,f*, 76*e,f*	(10)
$^{2}T_{4}{}^{3}T_{2}$	Clinotobermorite (11Å) 1*A*	Ca_4**[Si_6O_{17}]**$(H_2O)_2\cdot(Ca(H_2O)_3)$	[$SiO_{2.83}$]	$^{2}V_{4}{}^{3}V_{2}$	*C*$\bar{1}$	2.83	75*c–f*, 77*a,b*	(11)
$^{2}T_{4}{}^{3}T_{2}$	Clinotobermorite (11Å) 2*M*	Ca_4**[Si_6O_{17}]**$(H_2O)_2\cdot(Ca(H_2O)_3)$	[$SiO_{2.83}$]	$^{2}V_{4}{}^{3}V_{2}$	*Cc*	2.83	75*c–f*, 77*c,d*	(12)
$^{2}T_{4}{}^{3}T_{2}$	Kenoclinotobermorite (*theoretical*)	Ca_4**[Si_6O_{15}(OH)$_2$]**$(H_2O)_2\cdot(H_2O)_3$	[$SiO_{2.5}(OH)_{0.33}$]	$^{2}V_{4}{}^{3}V_{2}$	–	2.83	75*c–f*	(13)
$^{2}T_{4}{}^{3}T_{2}$	Tobermorite (10Å) 4*O*/2*M*	Ca_4**[Si_6O_{15}(OH)$_2$]**$\cdot(H_2O)$	[$SiO_{2.5}(OH)_{0.33}$]	$^{2}V_{4}{}^{3}V_{2}$	*C*2/*m*	2.83	–	(14)
$^{2}T_{4}{}^{3}T_{2}$	Kalitobermorite (*theoretical*)	Ca_4**[$AlSi_5O_{15}$(OH)$_2$]**$(H_2O)_2\cdot(K(H_2O)_3$	[$Al_{0.17}Si_{0.83}O_{2.5}(OH)_{0.33}$]	$^{2}V_{4}{}^{3}V_{2}$	–	2.83	–	(15)
		Xonotlite group						
$^{2}T_{4}{}^{3}T_{2}$	Xonotlite	Ca_6**[Si_6O_{17}]**$(OH)_2$	[$SiO_{2.83}$]	$^{2}V_{4}{}^{3}V_{2}$	*P*2/*a*	2.83	78	(16)
$^{2}T_{4}{}^{3}T_{2}$	Haineaultite	(Na,Ca)$_5$Ca(Ti,Nb)$_5$**[Si_6O_{17}]**$_2$(OH,F)$_8(H_2O)_5$	[$SiO_{2.83}$]	$^{2}V_{4}{}^{3}V_{2}$	*C*222	2.83	79*a–d*	(17)
$^{2}T_{4}{}^{3}T_{2}$	Zorite	Na_6Ti(Ti,Nb)$_4$**[Si_6O_{17}]**$_2(O,OH)_5(H_2O)_{11}$	[$SiO_{2.83}$]	$^{2}V_{4}{}^{3}V_{2}$	*Cmmm*	2.83	79*a,b,e,f*	(18)
$^{2}T_{4}{}^{3}T_{2}$	Yuksporite	$(Sr,Ba)_2K_4(Ca,Na)_{14}$(□,Mn,Fe){(Ti,Nb)$_4$	[$SiO_{2.83}$]	$^{2}V_{4}{}^{3}V_{2}$	*P*2$_1$/*m*	3.06	80	(19)
$^{1}T_{2}$*	〃 〃	$(O,OH)_4$**[Si_6O_{17}]**$_2$**[Si_2O_7]**$_3$}$(H_2O,OH)_3$	[$SiO_{3.5}$]	$^{1}V_{2}$				
$^{2}T_{4}{}^{3}T_{2}$	Synthetic	Pb_4Ti(Ti,Nb)$_4$**[Si_6O_{17}]**$_2(O,OH)_5(H_2O)_{10}$	[$SiO_{2.83}$]	$^{2}V_{4}{}^{3}V_{2}$	*Cmmm*	2.83	–	(20)
$^{2}T_{4}{}^{3}T_{2}$	Synthetic	K_8Na_2Ti(Ti,Nb)$_4$**[Si_6O_{17}]**$_2(O,OH)_5(H_2O)_{11}$	[$SiO_{2.83}$]	$^{2}V_{4}{}^{3}V_{2}$	*Cmmm*	2.83	–	(21)
$^{2}T_{4}{}^{3}T_{2}$	Synthetic	Cs_4Na_2Ti(Ti,Nb)$_4$**[Si_6O_{17}]**$_2(O,OH)_5(H_2O)_5$	[$SiO_{2.83}$]	$^{2}V_{4}{}^{3}V_{2}$	*Cmmm*	2.83	–	(21)
$^{2}T_{4}{}^{3}T_{2}$	Gilalite	Cu_5**[Si_6O_{17}]**$(H_2O)_7$	[$SiO_{2.83}$]	$^{2}V_{4}{}^{3}V_{2}$	Mon.	2.83	–	(22)
$^{2}T_{4}{}^{3}T_{4}$	Vlasovite	Na_2Zr**[Si_4O_{11}]**	[$SiO_{2.75}$]	$^{2}V_{2}{}^{3}V_{2}$	*B*2/*b*	2.75	81,82	(23)
$^{2}T_{4}{}^{3}T_{4}$	Synthetic	$HNb(H_2O)$**[Si_4O_{11}]**(H_2O)	[$SiO_{2.75}$]	$^{2}V_{2}{}^{3}V_{2}$	*P*2$_1$/*m*	2.75	83	(24)
$^{2}T_{4}{}^{3}T_{4}$	Synthetic	$Cs_{0.66}H_{0.33}Nb(H_2O)$**[$Si_4O_{11}$]**	[$SiO_{2.75}$]	$^{2}V_{2}{}^{3}V_{2}$	*P*2$_1$/*m*	2.75	83	(24)
$^{2}T_{4}{}^{3}T_{4}$	Synthetic	$Na_2H(NbO)$**[Si_4O_{11}]**$(H_2O)_{1.25}$	[$SiO_{2.75}$]	$^{2}V_{2}{}^{3}V_{2}$	*P*2$_1$/*m*	2.75	83	(24)
$^{2}T_{4}{}^{3}T_{8}$	Carlosturanite	$(Mg,Fe^{2+},Ti^{2+})_{21}$**[(Si,Al)$_{12}O_{28}(OH)_4$]**$(OH)_{30}(H_2O)$	[(Si,Al)$O_{2.34}(OH)_{0.33}$]	$^{2}V_{2}{}^{3}V_{4}$	*Cm*	2.67	84	(25)
$^{2}T_{6}{}^{3}T_{4}$	Inesite	$Ca_2(Mn,Fe)_7$**[$Si_{10}O_{28}$]**$(OH)_2(H_2O)_5$	[$SiO_{2.8}$]	$^{2}V_{6}{}^{3}V_{4}$	*P*$\bar{1}$	2.80	85	(26)
$^{2}T_{6}{}^{3}T_{4}$	Synthetic	K_6Gd_2**[$Si_{10}O_{28}$]**	[$SiO_{2.8}$]	$^{2}V_{6}{}^{3}V_{4}$	*Cmme*	2.80	86	(27)
$^{2}T_{6}{}^{3}T_{4}$	Haiweeite	$Ca_2(UO_2)_4$**[$Si_{10}O_{24}$(OH)$_4$]**$(H_2O)_{12}$	[$SiO_{2.4}(OH)_{0.4}$]	$^{2}V_{3}{}^{3}V_{2}$	*Pbcn*	2.80	87	(28)
$^{2}T_{14}{}^{3}T_{4}$	Liebauite	Ca_3Cu_5**[Si_9O_{26}]**	[$SiO_{2.89}$]	$^{2}V_{7}{}^{3}V_{2}$	*C*2/*c*	2.89	88,89	(29)

References: (1) Rozhdestvenskaya *et al.* (1989), Lacalamita *et al.* (2017); (2) Agakhanov *et al.* (2005), Uvarova *et al.* (2006); (3) Rogov *et al.* (1965), Bissert (1980); (4) Wenk (1974), Wenk (1973), Ghent *et al.* (1990); (5) Wenk (1974), Matsubara (1981), Aoki (1981); (6) Fleet (1977), Agrell *et al.* (1965), Wenk *et al.* 1976, Worthing (1987); (7) Grice and Dunn (1994), Dunn *et al.* (1986), Brugger and Berlepsch (1997); (8) Merlino *et al.* (2001); (9) Merlino *et al.* (2001), Hamid (1981); (10) Merlino *et al.* (2001), Churakov (2009); (11) Merlino *et al.* (2000*a*); (12) Merlino *et al.* (2000*a*), Henmi and Kusachi (1992), Hoffmann and Armbruster (1997); (13) Biagioni *et al.* (2015); (14) Biagioni *et al.* (2012*b*); (15) Biagioni *et al.* (2015); (16) Garbev (2004), Kudoh and Takéuchi (1979), Hejny and Armbruster (2001), Merlino and Bonaccorsi (2008), Churakov and Mandaliev (2008); (17) McDonald and Chao (2004); (18) Sandomirskii and Belov (1979), Belokoneva (2005), Zubkova *et al.* (2005), Zubkova *et al.* (2006), Cruciani *et al.* 1998; (19) Krivovichev *et al.* (2004*a*); (20) Zubkova *et al.* (2006); (21) Zubkova *et al.* (2005); (22) Cesbron and Williams (1980), López *et al.* (2014); (23) Sokolova *et al.* (2006), Voronkov and Pyatenko (1962), Gittins *et al.* (1973), Gobechiya *et al.* (2003), Kaneva *et al.* (2018); (24) Salvadó *et al.* (2001); (25) Compagnoni *et al.* (1985), Mellini *et al.* (1985), Deriu *et al.* (1994); (26) Wan and Ghose (1978), Ryall and Threadgold (1966), Richmond (1942); (27) Zhao *et al.* (2010); (28) Plášil *et al.* (2013), McBurney and Murdoch (1959), Rastsvetaeva *et al.* (1997*b*), Burns (2001); (29) Zöller *et al.* (1992).
*Indicates the $^{c}T_{r}$ expression of an additional structural unit including a chain, ribbon, tube, cluster or sheet of $(TO_4)^{n-}$ tetrahedra in the respective mineral.

adjacent chains have tetrahedra that point in opposite directions. **Johninnesite** contains eight $(OH)^{-}$ groups that are associated with the sheet and ribbon of octahedra.

$^{2}T_{4}{}^{3}T_{2}$ ribbons

Much work has been done developing classification schemes and nomenclature for **tobermorite-group** minerals as these species exhibit novel dehydration-hydration reactions, have a complex OD character, are used as cation-exchangers, and play a critical role in the hydration of Portland cement (Taylor, 1964, 1992; Gard and Taylor, 1976; Cong and Kirkpatrick, 1996; Garbev, 2004; Battocchio *et al.*, 2012). Here, we will describe only briefly the structure for selected group-members; see Mitsuda and Taylor (1978), Merlino *et al.* (1999, 2001), Merlino and Bonaccorsi (2008) and Biagioni *et al.* (2015) for more detailed descriptions. This group includes several calcium–silicate–hydrate (C–S–H) minerals such as **tobermorite-11Å** and **clinotobermorite-11Å** (Table 8) that contain $^{2}T_{4}{}^{3}T_{2}$ ribbons that consist of eight-membered rings that link along the **b**-axis through two Si^{4+}-tetrahedra (Figs 75*a–e*). These $^{2}V_{4}{}^{3}V_{2}$ ribbons (Fig. 75*f*) are topologically similar but not identical to the $^{2}V_{4}{}^{3}V_{2}$ chains in **howieite-group** minerals (Figs 73*c*, 75*f*).

Tobermorite-group minerals are broadly divided on the basis of their relative hydration states; note that the H_2O content typically shows a positive correlation with the basal spacing (d_{002}). Thus far, four groups have been distinguished based on basal spacing: 9Å (**riversideite**), 10Å, 11Å and 14Å (**plombièrite**), all with variable H_2O content. In all **tobermorite-group** minerals, $^{2}T_{3}$ chains of Si^{4+}-tetrahedra extend along the **b**-axis and link to sheets of $^{[7]}Ca^{2+}$-polyhedra. Depending on the hydration state (and the consequent basal spacing), adjacent chains may polymerise to form $^{2}T_{4}{}^{3}T_{2}$ ribbons as in **tobermorite-11Å** and **-10Å**. In **plombièrite**, where the H_2O content is relatively high, an interlayer of Ca^{2+} ions and (H_2O) groups forms (along (010)) and increases the spacing between adjacent $^{2}T_{3}$ chains (d_{002} = 14 Å), preventing chain condensation and the formation of $^{2}T_{4}{}^{3}T_{2}$ ribbons (Figs 17*e–f*). In **riversideite** (**tobermorite-9Å**), there is no H_2O, adjacent $^{2}T_{3}$ chains are forced closer to each other (d_{002} = 9.3 Å) and chain condensation does not occur. Multiple heating experiments have yielded the following dehydration reaction; **plombièrite** (**tobermorite-14Å**) →

https://doi.org/10.1180/mgm.2020.13 Published online by Cambridge University Press

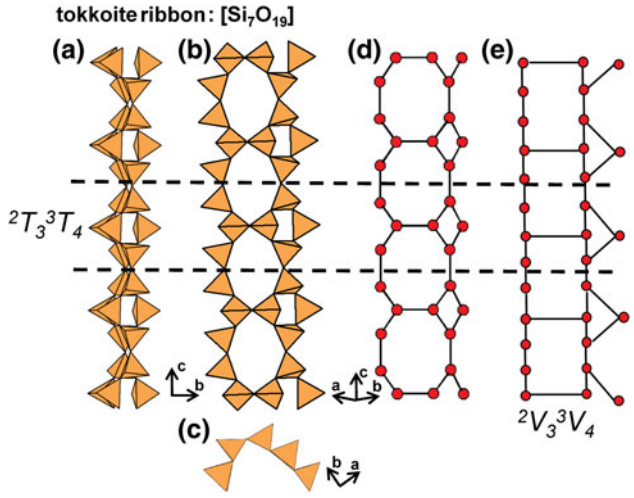

Fig. 71. (*a*, *b*, *c*) Tetrahedral representations of the $^2T_3{}^3T_4$ ribbon in **tokkoite** projected (*a*) onto (100), (*b*) orthogonal to the **c**-axis, (*c*) along the **c**-axis, (*d*) a ball-and-stick and (*e*) a graphical representation of the ribbon. Dashed black lines outline the geometrical and topological repeat unit of the ribbon.

tobermorite-11Å → riversideite (tobermorite-9Å) with increasing temperature. **Plombièrite** has also been produced through hydration of **tobermorite-11Å** (Merlino *et al.*, 2001; Biagioni *et al.*, 2012*a*; Biagioni *et al.*, 2016). Although **plombièrite** and **riversideite** are conventionally classified as **tobermorite-group** minerals, they contain $^2T_3$ chains rather than $^2T_4{}^3T_2$ ribbons and have therefore been included in a separate group (Table 4) along with other C–S–H minerals (also related to synthetic cement phases) that contain $^2T_3$ chains, such as **foshagite**, **hillebrandite** and **jennite** (Figs 17*a*–*f*).

Tobermorite-11Å occurs as both MDO_1, orthorhombic (4*O*), and MDO_2, monoclinic (2*M*) polytypes; each polytype is further differentiated on the basis of its thermal (dehydration) behaviour. **Tobermorite-11Å** is considered *anomalous* if the basal spacing is unaffected by heating and dehydration and is considered *normal* if the basal spacing decreases to 9 Å upon heating and dehydration, (Mitsuda and Taylor, 1978). The behaviour of a specific **tobermorite-11Å** specimen is a function of its composition within the solid solution between $Ca_4[\mathbf{Si_6O_{17}}](H_2O)_2)\cdot(Ca(H_2O)_3$ and $Ca_4[\mathbf{Si_6O_{15}(OH)_2}](H_2O)_2\cdot(H_2O)_3$, or more specifically the relative Ca^{2+} content, where an increase in Ca^{2+} (apfu) promotes *normal* behaviour (Merlino *et al.*, 2001). The general formula for **tobermorite-group** minerals is $Ca_{4+x}(Al_ySi_{6-y})O_{15+2x-y}(OH)_{2-2x+y}(H_2O)_5$, where $0 \le x \le 1$ and $0 \le y \le 1$, and *anomalous* behaviour corresponds to $x \approx 0$ (Biagioni *et al.*, 2015). In such *anomalous* species, the prefix '*keno*' is added to convey a relative Ca^{2+}-deficiency. **Clinotobermorite-11Å** is a dimorph of **tobermorite-11Å** that shows the same basal spacing and occurs as triclinic (1*A*) and monoclinic (2*M*) polytypes. Upon heating and dehydration of **clinotobermorite-11Å**, **tobermorite-9Å** is produced with $^2T_3$ $[Si_3O_8(OH)]^{5-}$ chains, similar to those in *hydrous* **wollastonite-group** minerals (Figs 27*a*–*h*) (Merlino *et al.*, 2000*a*). A detailed description of the OD relations between **tobermorite-11Å** and **clinotobermorite-11Å** is given by Merlino *et al.* (1999, 2000*a*). **Tobermorite-10Å** has also been produced through heating of **tobermorite-11Å**; such heating experiments also produced **clinotobermorite-11Å** as an intermediate biproduct (Biagioni *et al.*, 2012*a*,*b*). Various theoretical **tobermorite-group** minerals have been added to Table 8; **kenoclinotobermorite**, a Ca^{2+}-deficient **clinotobermorite-11Å** and **kalitobermorite**, a *normal* **tobermorite-11Å** in which interstitial Ca^{2+} is replaced by K^+ and Si^{4+} is partly replaced by Al^{3+} (Biagioni *et al.*, 2015).

The geometrical repeat unit of the $^2T_4{}^3T_2$ ribbon in **tobermorite-group** minerals contains three distinct Si^{4+}-tetrahedra in **tobermorite-11Å** and six distinct Si^{4+}-tetrahedra in **clinotobermorite-11Å**, and minor occupancy of these sites by Al^{3+} is often observed. Although both **tobermorite-11Å** and **clinotobermorite-11Å** contains chains that are topologically identical, ($^2V_4{}^3V_2$), they

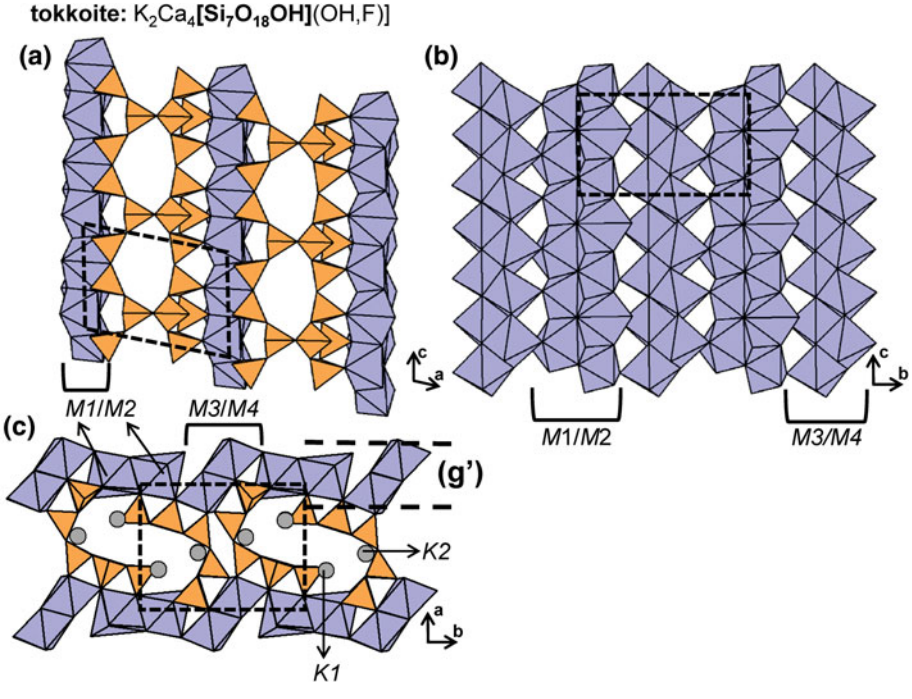

Fig. 72. The structure of **tokkoite** projected (*a*) onto (010) showing the linkage of $^2T_3{}^3T_4$ ribbons to sheets of Ca^{2+}-polyhedra, (*b*) sheets of Ca^{2+}-polyhedra projected onto (100) and (*c*) the alternating layers of $^2T_3{}^3T_4$ ribbons and sheets of Ca^{2+}-polyhedra projected along the **c**-axis. Fine dashed blacked lines outline the unit cell and H atoms associated with $(OH)^-$ groups are omitted for clarity

https://doi.org/10.1180/mgm.2020.13 Published online by Cambridge University Press

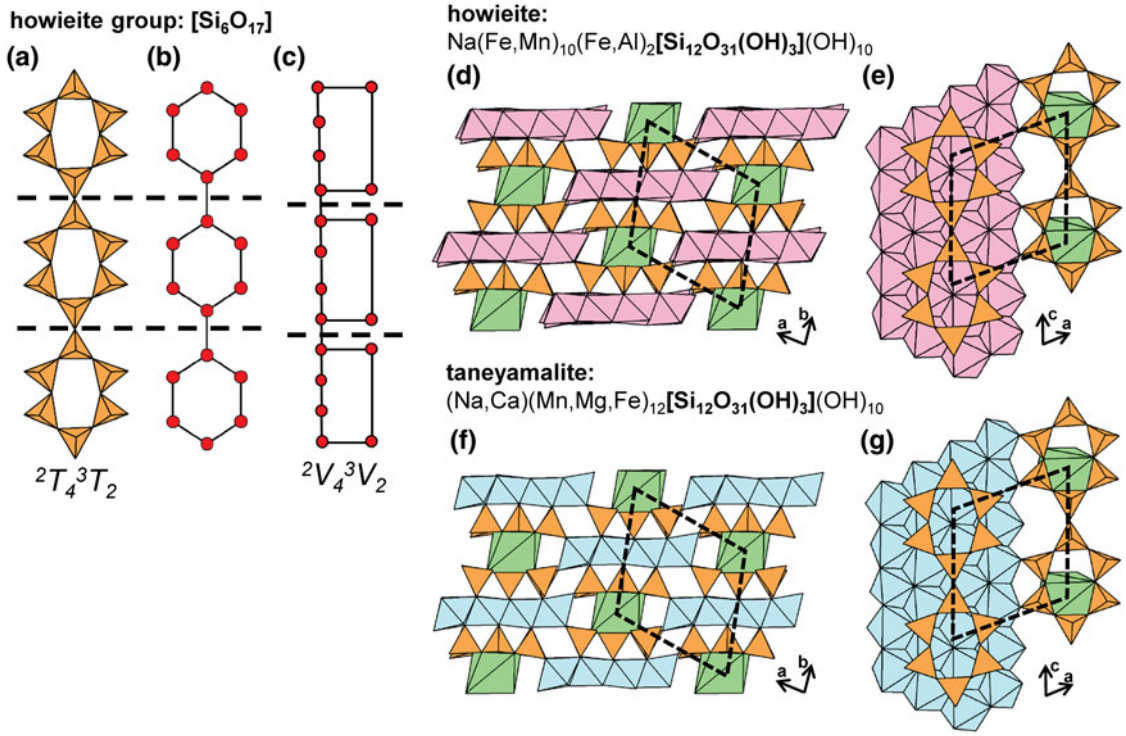

Fig. 73. (*a*, *b*, *c*) Tetrahedral representation of the $^{2}T_{4}{}^{3}T_{2}$ chain in **howeiite-group** minerals, (*b*) a ball-and-stick and (*c*) a graphical representation of this chain. The structure of **howeiite** projected (*d*) along the **c**-axis and (*e*) onto (010). The structure of **taneyamalite** projected (*f*) along the **c**-axis and (*g*) onto (010). Dashed black lines outline the geometrical and topological repeat unit of the ribbon and fine dashed black lines outline the unit cell. The H atoms associated with $(OH)^{-}$ groups are omitted for clarity

show major geometrical differences due to the response of the chains to accommodate structural differences (Figs 75*a*–*d*). All **tobermorite-group** minerals contain $[Si_6O_{17}]^{10-}$ ribbons, with the exception of the ribbons in **kenotobermorite-11Å** and **tobermorite-10Å** which contain acid silicate groups and have the stoichiometry $[Si_6O_{15}(OH)_2]^{8-}$. In all **tobermorite-group** minerals, each sheet of Ca^{2+}-polyhedra contains two [7]-coordinated sites, *Ca*1 and *Ca*2; there is a third site, *Ca*3, within cavities in the interlayer which is coordinated by (H_2O) and O^{2-} but is only occupied in *normal* **tobermorite-11Å, tobermorite-10Å** and **clinotobermorite-11Å**. The structures of *anomalous* orthorhombic **kenotobermorite-11Å** (Figs 76*a*,*b*), *normal* monoclinic **tobermorite-11Å** (Figs 76*c*,*d*) and *anomalous* monoclinic **kenotobermorite-11Å** (Figs 76*e*,*f*) show configurational differences of (H_2O) groups and Ca^{2+} ions (Ca3) in the interlayer space. The structures of triclinic and monoclinic **clinotobermorite** are shown in Figs 77*a*,*b* and 77*c*,*d*, respectively. Churakov (2009) and Merlino *et al.* (2000*a*, 2001) provide a detailed description of the hydrogen-bond model for **tobermorite-group** minerals.

The structures of the **xonotlite-group** minerals (Table 8) are closely related to those of the **tobermorite-group** minerals as both contain topologically identical $^{2}V_{4}{}^{3}V_{2}$ ($^{2}T_{4}{}^{3}T_{2}$) ribbons that link to hydrous sheets of higher-coordination Ca^{2+} polyhedra. **Xonotlite**, a bi-product of the hardening process of Portland cement, occurs as triclinic and monoclinic polytypes; here we describe the triclinic polytype. **Xonotlite** has a geometric repeat unit that contains three distinct Si^{4+}-tetrahedra that polymerise to form $^{2}T_{4}{}^{3}T_{2}$ ribbons (Fig. 78*a*,*b*) that extend along [010]. These ribbons link to sheets of $(CaO_5OH)^{9-}$-octahedra (*M*1) and $(CaO_6OH)^{11-}$-polyhedra (*M*2 and *M*3) that are parallel to the **a**–**b** plane (Fig. 78*c*), and chains of tetrahedra and ribbons of Ca^{2+}-polyhedra occur in layers that alternate along [001] (Fig. 78*d*). The geometric repeat unit of the $^{2}T_{4}{}^{3}T_{2}$ ribbons in **haineaultite** (Figs 79*a*,*b*) contains two distinct tetrahedra, one of which is an acid silicate group: $(SiO_3OH)^{3-}$. These ribbons extend along [001] and are linked along [010] to sheets of $(CaO_6(OH)_2)^{12-}$-polyhedra and $(Ti,Nb)^{4+}$-octahedra (Ti1) that are parallel to the **a**–**c** plane. Each $^{2}T_{4}{}^{3}T_{2}$ ribbon is also linked to adjacent ribbons along [100] by $(Ti(OH)_4(H_2O)_2)$ octahedra (Ti2), forming an open framework that contains channels that extend along [100] and [001]. These channels are occupied by (H_2O) groups and $(NaO_3(OH)_3)^{8-}$-octahedra (Figs 79*c*,*d*). The $[TiSi_4O_{15}]^{10-}$ block (Ti2) exhibits complicated OD behaviour: it is present only 50% of the time to allow the *T*2 tetrahedron of adjacent $^{2}T_{4}{}^{3}T_{2}$ ribbons to point in the same direction along [100] and link to a Ti^{4+}-octahedron (Ti2). Here, we have shown an *averaged* **haineaultite** structure in which the number of *T*2 tetrahedra are doubled to allow $[TiSi_4O_{15}]^{10-}$ blocks to occur in every channel (Fig. 79*d*).

The structure of **zorite** is similar to that of **haineaultite**: $^{2}T_{4}{}^{3}T_{2}$ ribbons (Figs 79*a*,*b*) extend along [001] and link to sheets of (Ti, Nb)$^{4+}$-octahedra (Ti1) and $(NaO_4(H_2O)_2)^{7-}$-octahedra (Na1 and W1) that are parallel to (011). **Zorite** shows the same OD character as **haineaultite** associated with the $[TiSi_4O_{15}]^{10-}$ block (Ti2); Figs 79*e*,*f* show a *non-averaged* representation of this disorder model in which half of the channels that extend along [001] are occupied by the $[Ti2Si_4O_{15}]^{10-}$ block and Na^{+}-polyhedra (Na2), and the other half by H_2O (*W*3 and *W*4) and $[NaO_5(H_2O)_2]^{9-}$ -polyhedra (Na2', *W*1 and *W*2). Na^{+} ions (Na2) in the channels with $[TiSi_4O_{15}]^{10-}$ blocks, have a different anion configuration

https://doi.org/10.1180/mgm.2020.13 Published online by Cambridge University Press

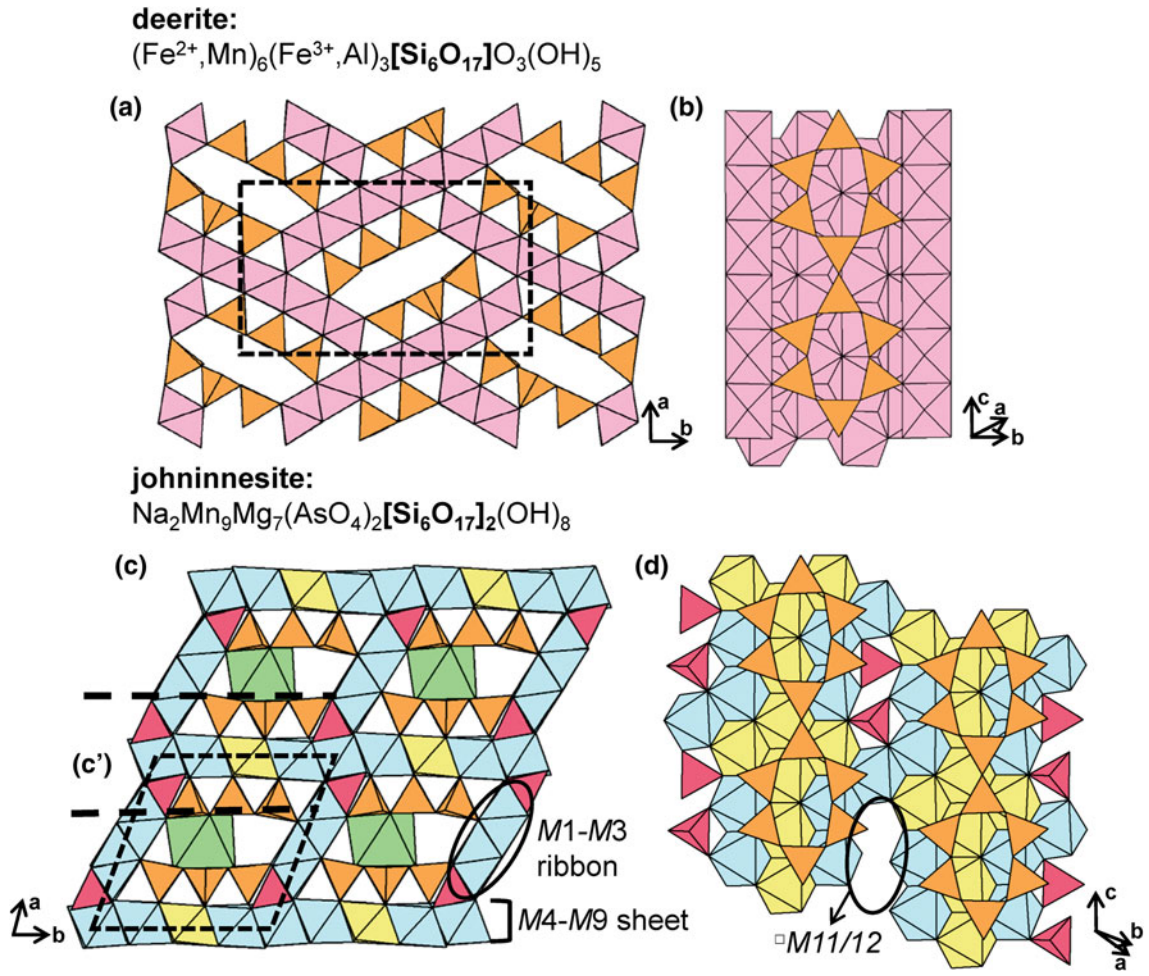

Fig. 74. The structure of **deerite** projected (*a*) along the **c**-axis and (*b*) orthogonal to the **c**-axis. The structure of **johninnesite** projected (*c*) along the **c**-axis and (*d*) orthogonal to the **c**-axis. Fine dashed black lines outline the unit cell and H atoms associated with $(OH)^{-}$ groups are omitted for clarity.

than the $(NaO_5(H_2O)_2)^{9-}$-polyhedra (Na2') occupying the channel without $[TiSi_4O_{15}]^{10-}$ blocks. Unlike the averaged OD model of **haineaultite**, the number of *T*2 tetrahedra does not need to be doubled in the OD model of **zorite** shown here; instead the **b**-axis is doubled. Several alternative OD models for **zorite** are described by Cruciani *et al.* (1998) and Belokoneva (2005). Due to the use of **zorite** as a molecular sieve, there has been much work on Pb^{2+}-, K^{+}- and Cs^{+}-exchanged forms of **zorite** (Zubkova *et al.*, 2006, 2005).

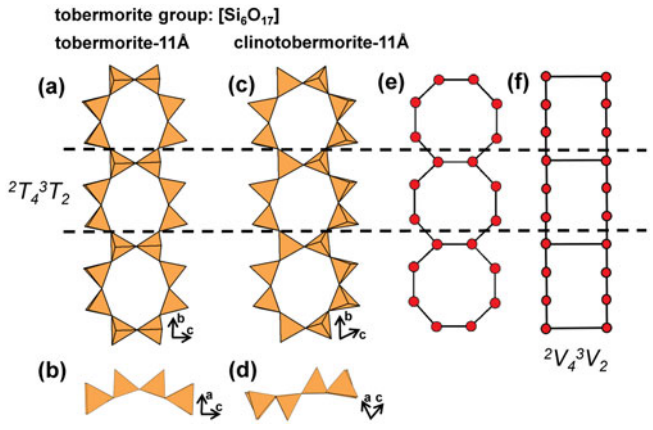

Fig. 75. (*a*, *b*, *c*) Tetrahedral representations of the $^{2}T_4{}^{3}T_2$ ribbon in (*a*, *b*) **tobermorite-11Å** and (*c*, *d*) **clinotobermorite-11Å** projected (*a*, *c*) onto (100) and (*b*, *d*) along the **b**-axis. (*e*) a ball-and-stick and (*f*) a graphical representation of the ribbon. Dashed black lines outline the geometrical and topological repeat unit of the ribbon.

Yuksporite contains nine distinct tetrahedra (*T*1–*T*9) that polymerise to form two distinct $^{1}T_2$ $[Si_2O_7]^{6-}$ dimers (*T*3–*T*7 and *T*9–*T*9) and two symmetrically distinct $^{2}T_4{}^{3}T_2$ ribbons, where the first ribbon involves the *T*1, *T*4 and *T*5 sites, and the second ribbon involves the *T*2, *T*6 and *T*8 sites (Figs 80*a*,*b*). In **yuksporite**, $^{2}T_4{}^{3}T_2$ ribbons link along [010] to sheets of Ca^{2+}-octahedra (Ca1 and Ca3) and $(CaO_6OH)^{11-}$-(Ca2 and Ca5), $(CaO_5(OH)_2)^{10-}$- (Ca4) and $(NaO_5(OH)_2)^{11-}$-polyhedra (*Na*3) that are parallel to the **a**–**c** plane (Figs 80*c*–*e*). Each $^{2}T_4{}^{3}T_2$ ribbon links to $[Si_2O_7]^{6-}$ dimers through $(Ti,Nb)^{4+}$-octahedra (*Ti*1 and *Ti*2) forming $[(Ti,Nb)_4(O,OH)_4[Si_6O_{17}]_2[Si_2O_7]_3]$ rods that extend along [100] (Fig. 80*f*). These rods contain channels that extend along [100] that are occupied by K^{+} ions, and channels that extend along [010] that are occupied by Na^{+} ions (Na1 and Na2) and Sr^{2+} (Ba^{2+}) ions (Sr1 and Sr2). Within these rods, the *M*1 site is partly occupied by Mn^{2+} and/or Fe^{2+} (Figs 80*d*,*f*). **Yuksporite** contains two $(OH)^{-}$ groups that are associated with cations occupying the

https://doi.org/10.1180/mgm.2020.13 Published online by Cambridge University Press

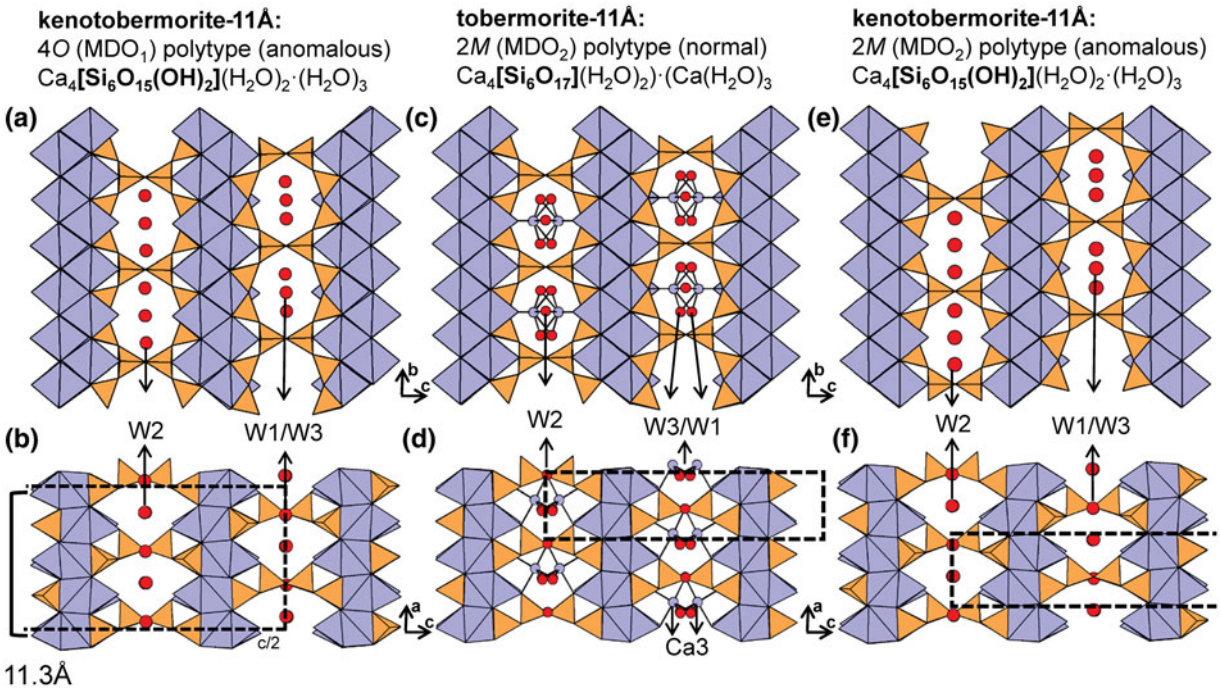

Fig. 76. The structure of (*a*, *b*) ***anomalous*** **kenotobermorite-11Å (MDO$_1$)**, (*c*, *d*) ***normal*** **tobermorite-11Å (MDO$_2$)** and (*e*, *f*) ***anomalous*** **kenotobermorite-11Å (MDO$_2$)** projected (*a*, *c*, *e*) onto (100) and (*b*, *d*, *f*) along the **b**-axis. Fine dashed black lines outline the unit cell and in (*b*) only half the unit cell along the **c**-axis is shown. The H atoms associated with $(OH)^-$ groups are omitted for clarity.

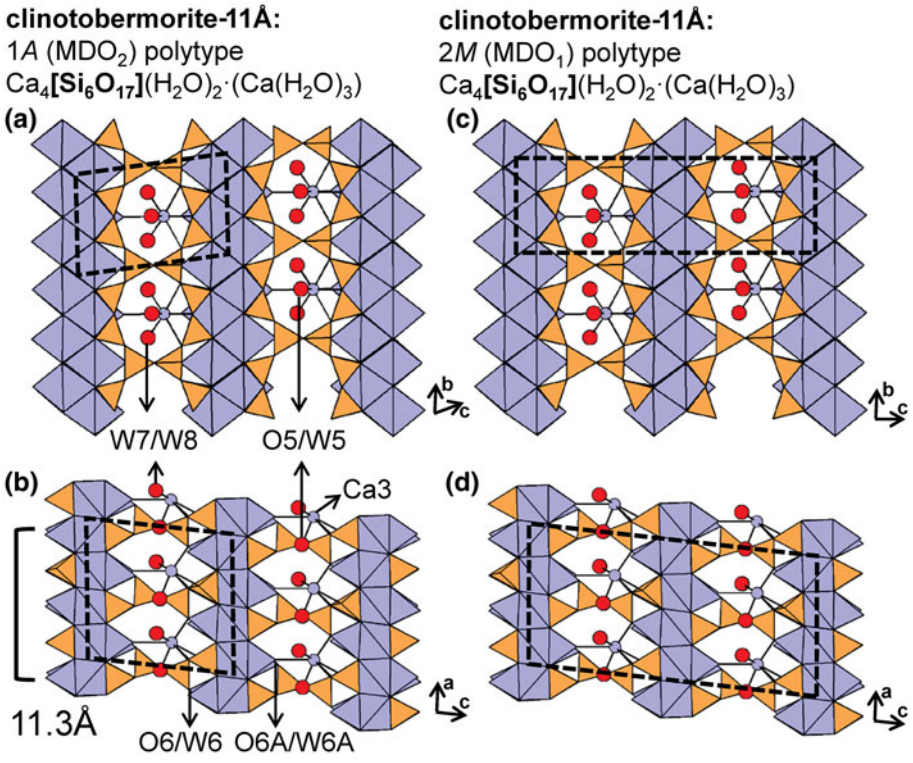

Fig. 77. The structure of (*a*, *b*) **clinotobermorite-11Å (MDO$_2$)** and (*c*, *d*) **clinotobermorite-11Å (MDO$_1$)** projected (*a*, *c*) onto (100) and (*b*, *d*) along the **b**-axis. Fine dashed black lines outline the unit cell.

Ca2, Ca4, Ca5 and Na1–Na3 sites, and two (H_2O) groups that are associated with cations occupying the *M*1, *K*3 and *Sr*1–*Sr*2 sites. **Gilalite** also contains $^2T_4{}^3T_2$ $[Si_6O_{17}]^{10-}$ ribbons but the structure is not yet known in detail. **Eveslogite** may also contain topologically identical $[Si_6O_{17}]^{10-}$ ribbons as it is structurally and chemically similar to **yuksporite,** but has not been listed in

https://doi.org/10.1180/mgm.2020.13 Published online by Cambridge University Press

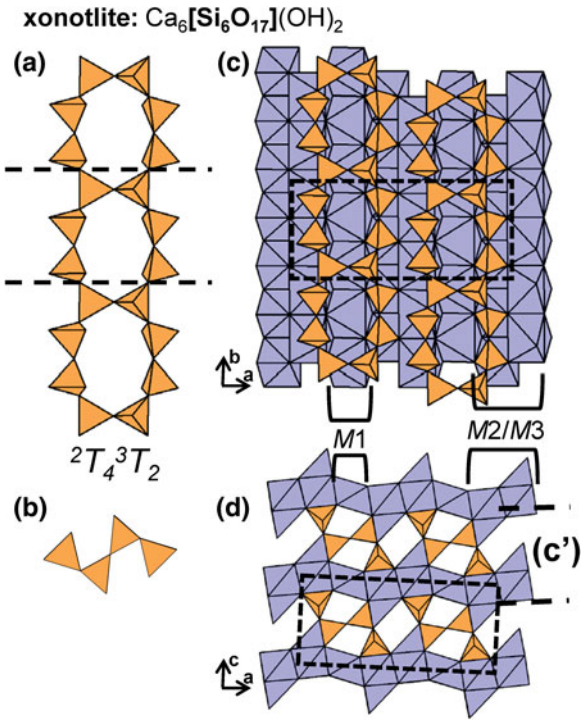

Fig. 78. (*a*, *b*) Tetrahedral representations of the $^2T_4{}^3T_2$ ribbon in **xonotlite**. The structure of **xonotlite** projected (*c*) onto (001) and (*d*) along the **b**-axis. Dashed black lines outline the geometrical repeat unit of the ribbon and fine dashed black lines outline the unit cell. The H atoms associated with $(OH)^-$ groups are omitted for clarity.

Table 8 as the silicate unit has not been described in detail. (Men'shikov *et al.*, 2003).

$^2T_4{}^3T_4$ chains and ribbons

The geometrical repeat unit of the $^2T_4{}^3T_4$ $[Si_8O_{22}]^{12-}$ chain in **vlasovite** contains two distinct Si^{4+}-tetrahedra that form four-membered rings that link to each other along [101]; alternate four-membered rings are geometrically equivalent (Figs 81*a*–*c*). In the geometrically similar $[Si_4O_6(OH)_5]^{1-}$ chain in **revdite** (see below), there is only one distinct four-membered ring. The $^2V_2{}^3V_2$ chain in **vlasovite** (Fig. 81*d*) and the $[Si_4O_6(OH)_5]^{1-}$ chain in **revdite** (see below) are therefore topologically identical but geometrically different.

In **vlasovite,** there is one distinct Zr^{4+}-octahedron and three distinct *Na*1, *Na*2A and *Na*2B sites. Each Zr^{4+}-octahedron links to four $^2T_4{}^3T_4$ chains, two of which are linked along the **b**-axis and the other two along $[\bar{1}01]$ (Figs 82*a*,*b*). These linkages form an open framework in which Na^+ ions occupy channels that extend along the **c**-axis (Fig. 82*c*). Spectroscopic evidence for bonded (H_2O) groups in **vlasovite** was reported by Gobechiya *et al.* (2003) and Sokolova *et al.* (2006), and Kaneva *et al.* (2018) suggested the presence of $(OH)^-$ groups and the associated substitution reaction $Na^+ + O^{2-} \leftrightarrow \square + (OH)^-$.

Synthetic $\mathbf{HNb(H_2O)[Si_4O_{11}](H_2O)}$, $\mathbf{Cs_{0.66}H_{0.33}Nb(H_2O)[Si_4O_{11}]}$ and $\mathbf{Na_2H(NbO)[Si_4O_{11}]\cdot(H_2O)_{1.25}}$contain $^2T_4{}^3T_4$ $[Si_8O_{22}]^{12-}$ ribbons that are geometrically and topologically different from the $^2T_4{}^3T_4$ chains in **vlasovite** (Figs 81*a*–*d*). In these synthetic compounds, ribbons consist of edge-sharing hexagons of Si^{4+}-tetrahedra that link along [010]. This ribbon type is geometrically similar to the $^2T_2{}^3T_2$ ribbon in **amphiboles** (Figs 62*b*,*c*)**;** however, every second six-membered ring is distorted so as to double n_g (Figs 83*a*–*d*). This $^2V_2{}^3V_2$ ribbon (Fig. 83*e*) is topologically identical to the ribbon in **amphibole-supergroup minerals** (Fig. 62*d*) and topologically different from the $^2V_2{}^3V_2$ chain in **vlasovite** (Fig. 81*d*) despite all three species having the vertex degree, $^2V_2{}^3V_2$. For a complete structure description and differentiation of these three synthetic compounds, see Salvadó *et al.* (2001).

$^2T_4{}^3T_8$ ribbons

The $^2T_4{}^3T_8$ $[(Si,Al)_{12}O_{28}(OH)_4]$, ribbon in **carlosturanite** (Figs 84*a*–*d*) is geometrically unique. It consists of three polymerised $^2T_4$ **batisite**-like chains (Figs 19*b*,*d*) and is geometrically similar to the ribbon in **jimthompsonite** (Figs 65*b*,*c*), **synthetic** $\mathbf{Ba_5[Si_8O_{21}]}$ (Figs 69*f*,*h*) and $\mathbf{Ba_6[Si_{10}O_{26}]}$ (Figs 70*b*,*d*). In **carlosturanite**, ribbons extend along the **b**-axis, and link to sheets of octahedra that are parallel to (010). The structure of **carlosturanite** closely resembles that of the **serpentine-group** minerals. Mellini *et al.* (1985) suggested that the substitution of some $[Si_2O_7]^{6-}$ groups for tetrahedrally arranged $[(OH)_6H_2O]^{6-}$ groups in **serpentine** results in *T*-site vacancies and breaks the sheet of tetrahedra into the $^3T_8{}^2T_4$ ribbons in **carlosturanite.**

$^2T_6{}^3T_4$ chains and ribbons

Inesite contains a $^2T_6{}^3T_4$ $[Si_{10}O_{28}]^{16-}$ ribbon that is unique to this mineral. The geometrical repeat unit contains ten tetrahedra that polymerise to form ribbons of alternating six- and eight-membered rings that extend along [001] (Figs 85*a*–*e*). Geometrically, this ribbon is similar to the $^2T_5$ chains in the **rhodonite-group** minerals (Figs 25*b*,*d*) as both of the centrosymmetrically equivalent single-chains that link to form the **inesite** ribbon have a geometrical repeat unit that contains five Si^{4+}-tetrahedra. This relation was first proposed by Richmond (1942) who transformed **inesite** to high-Ca **rhodonite** by thermal dehydration. The interstitial structure in **inesite** consists of ribbons of $(CaO_5(OH)(H_2O))^{9-}$-polyhedra and four distinct Mn^{2+}-octahedra: $(MnO_4(OH)_2)^{8-}$ (*M*1), $(MnO_6)^{10-}$ (*M*2), $(MnO_5(H_2O))^{8-}$ (*M*3) and $(MnO_4(OH)(H_2O))^{7-}$ (*M*4) that link along [100] via $^2T_6{}^3T_4$ ribbons (Figs 85*f*,*g*). **Inesite** contains three (H_2O) groups (*W*1–*W*3) and a single $(OH)^-$ group.

The geometrical repeat unit of the ribbon in **synthetic** $\mathbf{K_5Gd_5[Si_5O_{15}]_2}$ contains ten Si^{4+}-tetrahedra that polymerise to form ribbons of alternating four- and ten-membered rings that extend along the **b**-axis (Figs 86*a*–*e*). Each $^2T_6{}^3T_4$ ribbon links to ribbons of Gd^{3+}-octahedra and $^{[8]}Gd^{3+}$-polyhedra that extend along the **c**-axis and form an open framework in which channels are occupied with K^+ ions.

In **haiweeite**, the geometrical repeat unit of the $^2T_6{}^3T_4$ $[Si_{10}O_{24}(OH)_4]^{12-}$ chain contains ten Si^{4+}-tetrahedra that polymerise to form four-membered rings that link to one another along [010] through a single 2-connected corner-sharing tetrahedron. The geometrical repeat unit is double the topological repeat unit ($^2V_3{}^3V_2$) as every other four-membered ring of tetrahedra is rotated 180° with respect to [010] and is therefore geometrically distinct but topologically identical (Figs 87*a*–*e*). Four of the ten *T* sites form acid silicate groups: $(SiO_3OH)^{3-}$. **Haiweeite** contains two symmetrically distinct $^{[7]}U^{6+}$-polyhedra (U1 and U2) that share edges to form chains that extend along [010] and cross-link chains of tetrahedra to form uranyl-silicate sheets parallel to

https://doi.org/10.1180/mgm.2020.13 Published online by Cambridge University Press

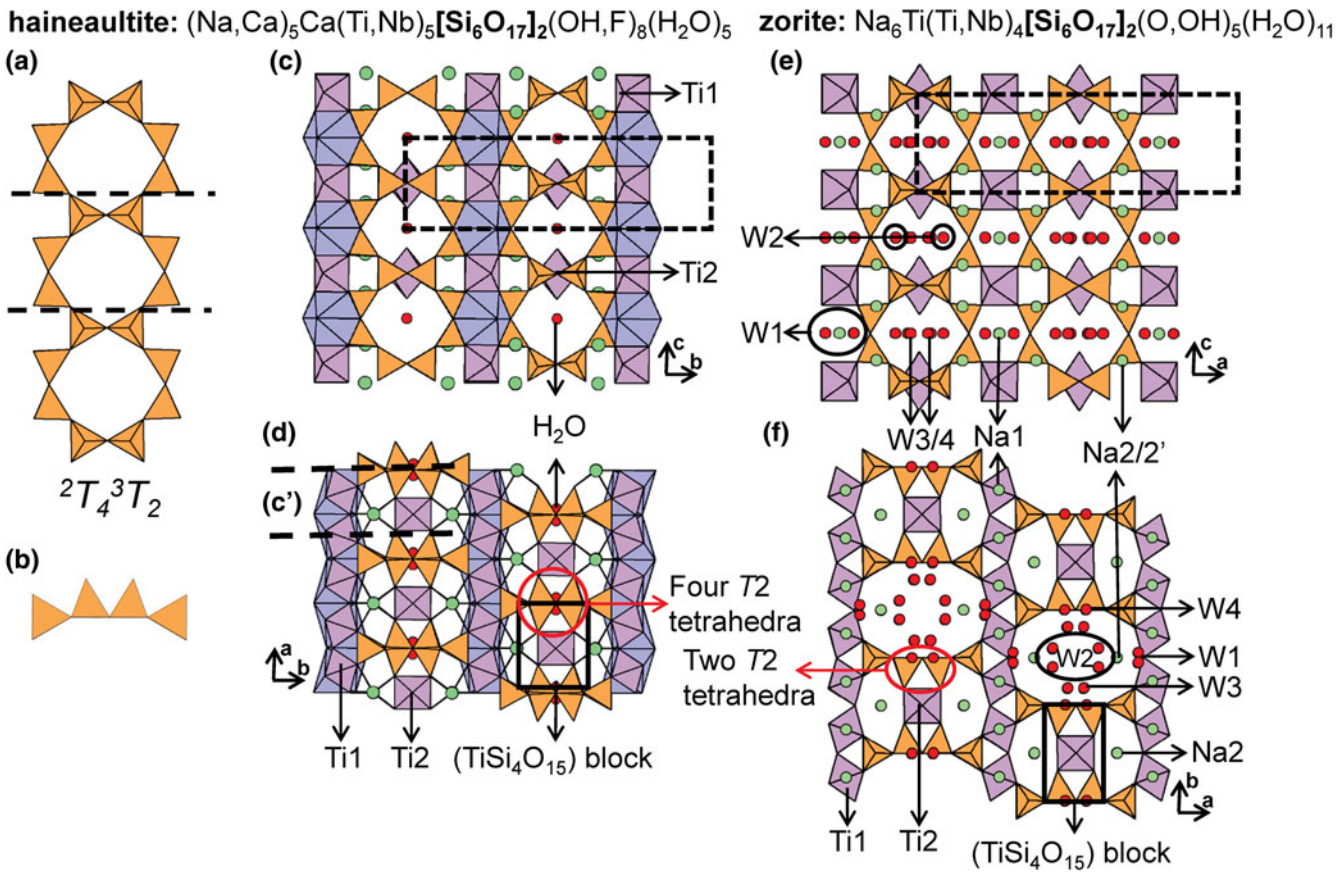

Fig. 79. (*a*, *b*) Tetrahedral representations of the $^{2}T_{4}{}^{3}T_{2}$ ribbon in **zorite and haineaultite**. The structure of **haineaultite** projected (*c*) onto (100) and (*d*) along the **c**-axis and the structure of **zorite** projected (*e*) onto (010) and (*f*) along the **c**-axis. In (*d*), an OD character is shown where there are four *T*2 sites to allow all channels to be occupied by $[TiSi_4O_{15}]$ blocks. In (*f*), an OD character is shown where there are two *T*2 sites to allow for $^{2}T_{4}{}^{3}T_{2}$ ribbons to occur and half of the channels to be occupied by $[TiSi_4O_{15}]$ blocks. Solid black lines outline the $[TiSi_4O_{15}]$ block in (*d*) and (*f*), dashed black lines outline the geometrical repeat unit of the ribbon and fine dashed black lines outline the unit cell. The H atoms associated with $(OH)^{-}$ groups are omitted for clarity.

(001). **Haiweeite** also contains $^{[11]}Ca^{2+}$-polyhedra that form $[Ca_2O_2(H_2O)_{12}]^{2-}$ dimers (Ca1) that link uranyl-silicate sheets along the **a**-axis (Figs 87*f*, *g*).

$^{2}T_{14}{}^{3}T_{4}$ chains

Liebauite contains $^{2}T_{14}{}^{3}T_{4}$ $[Si_{18}O_{52}]^{28-}$ chains that have a geometrical repeat unit that contains 18 Si^{4+}-tetrahedra that polymerise to form two six-membered rings of tetrahedra that link to each another via $^{2}T_{3}$ trimers of tetrahedra (Figs 88*a*–*d*). The chain in **liebauite** has a unique topology with the vertex degree $^{2}V_{7}{}^{3}V_{2}$ (Fig. 88*e*). The interstitial structure of **liebauite** consists of columns of Cu^{2+}-octahedra (Cu1 and Cu2) that extend along [001] and link to each other along [110] and [1$\bar{1}$0] via Cu^{2+}-pyramids (Cu3) (Fig. 89*a*). Adjacent Cu^{2+}-octahedra are also linked along [001] via $^{[8]}Ca^{2+}$-polyhedra (Ca1 and Ca2). The modulated $^{2}T_{14}{}^{3}T_{4}$ chains in **liebauite** extend along the **c**-axis and link to the both Cu^{2+}-octahedra and $^{[8]}Ca^{2+}$-polyhedra (Figs 89*b*,*c*).

$^{1}T_{r}{}^{2}T_{r}{}^{3}T_{r}$ class

$^{1}T_{1}{}^{2}T_{2}{}^{3}T_{3}$ chains

The geometrical repeat unit of the $^{1}T_{1}{}^{2}T_{2}{}^{3}T_{3}$ ribbon in **synthetic** $\mathbf{K_3Eu[Si_6O_{13}(OH)_4](H_2O)_2}$ (Table 9) contains three distinct Si^{4+}-tetrahedra, two singly acid $(SiO_3(OH))^{3-}$ groups, and one doubly acid $(SiO_2(OH)_2)^{2-}$ group (Figs 90*a*–*d*).The $^{1}T_{1}{}^{2}T_{2}{}^{3}T_{3}$ ribbons extend along [001] and are linked to adjacent ribbons by isolated Eu^{3+}-octahedra, forming sheets parallel to the **a**–**c** plane (101). These sheets are linked along [010] by interstital K^{+} ions and (H_2O) groups. Channels within these sheets are also occupied by K^{+} ions.

$^{1}T_{1}{}^{2}T_{3}{}^{3}T_{1}$ chains

The $^{1}T_{1}{}^{2}T_{3}{}^{3}T_{1}$ $[AlBeSi_3O_{15}]^{13-}$ chain in **surinamite** contains five distinct tetrahedra (*T*1–*T*5) in which *T*1 and *T*5 are occupied by Be^{2+} and Al^{3+}, respectively, and *T*2–*T*4 by Si^{4+}. Every fourth tetrahedron (*T*1) in this chain is decorated by a 1-connected Si^{4+}-tetrahedron (*T*3) (Figs 91*a*,*b*). The $^{1}V_{1}{}^{2}V_{3}{}^{3}V_{1}$ chain in **surinamite** is topologically similar to the chain in **aenigmatite**, **saneroite** and **terskite** (see below), all of which also have $^{2}V_{r}$ chains with 1-connected decorations (Fig. 91*c*). **Surinamite** contains nine octahedrally coordinated *M*-sites; the *M*1, *M*4, *M*5, *M*7 and *M*8 octahedra are larger and occupied by Mg^{2+} and Fe^{2+}, whereas the *M*2, *M*3, *M*6 and *M*9 octahedra are smaller and are occupied by Al^{3+} and Fe^{3+}. Figures 91*d*,*e* show the structure of **surinamite** in which all octahedra are shown as either Mg^{2+}- or Al^{3+}-octahedra for simplicity. Chains of tetrahedra and planar ribbons of edge-sharing octahedra are parallel to [100] and

https://doi.org/10.1180/mgm.2020.13 Published online by Cambridge University Press

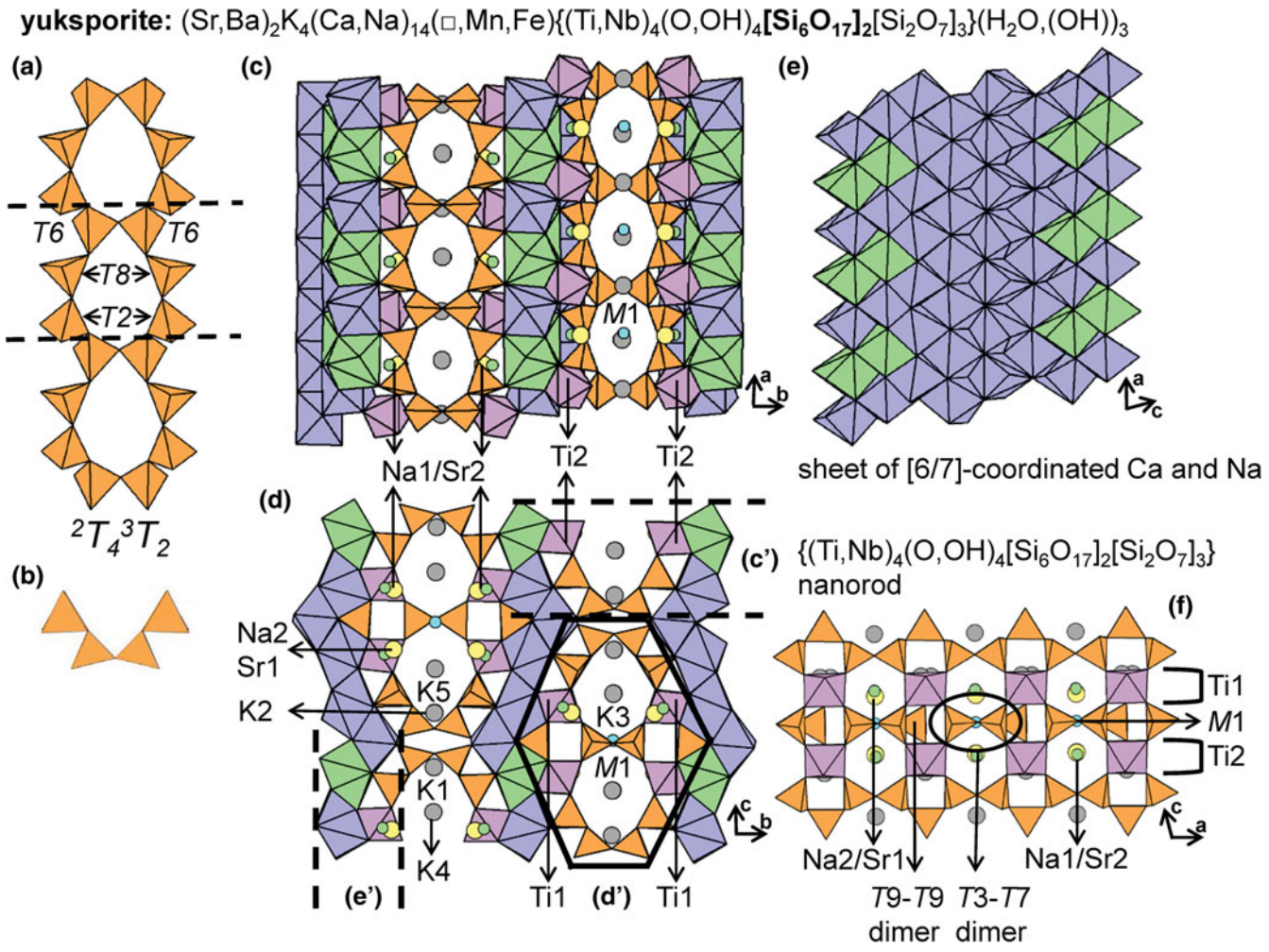

Fig. 80. (*a*, *b*) Tetrahedral representations of the $^{2}T_{4}\,^{3}T_{2}$ ribbon in **yuksporite**. The structure of **yuksporite** projected (*c*) onto (001) and (*d*) along the **a**-axis, (*e*) the sheet of [6/7]-coordinated Ca^{2+}- and Na^{+}-polyhedra projected onto (010) and (*f*) the $\{(Ti,Nb)_4(O,OH)_4[Si_6O_{17}]_2[Si_2O_7]_3\}$ rod projected onto (010). Dashed black lines outline the geometrical repeat unit of the ribbon and fine dashed black lines outline the unit cell. The H atoms associated with $(OH)^{-}$ and (H_2O) groups are omitted for clarity.

occur in layers that alternate along the **c**-axis. Adjacent ribbons of octahedra are linked to each other along the **b**-axis by $^{1}T_{1}\,^{2}T_{3}\,^{3}T_{1}$ chains and along the **c**-axis by *M*9 octahedra (Figs 91*d*,*e*). An unnamed analogue of **Be-free surinamite** has also been observed as lamellae in **sapphirine** (Christy and Putnis, 1988).

$^{1}T_{1}\,^{2}T_{4}\,^{3}T_{1}$ chains

The $^{1}T_{1}\,^{2}T_{4}\,^{3}T_{1}$ $[Si_5O_{14}(OH)(V,Si,As)O_3OH)]$ chain in **saneroite** (Figs 92*a*–*d*) is topologically similar to the chains in **surinamite, terskite** and the **sapphirine-supergroup** minerals (see below), and is geometrically similar to the chains in **scheuchzerite** (see below), **pyroxmangite** (Figs 31*b*,*d*) and most of the $^{2}T_{3}$ (Figs 11*b*,*d*) and $^{2}T_{5}$ (Figs 25*b*,*d*) **pyroxenoid** minerals (Tables 4 and 5). The geometrical repeat unit in **saneroite** contains six tetrahedra (*T*1–*T*6), where *T*1-tetrahedra are $(SiO_3(OH))^{3-}$, *T*2–*T*5-tetrahedra are Si^{4+}, and *T*6-tetrahedra are $(VO_3(OH))^{2-}$ but may also be partly occupied or dominated by Si^{4+} and As^{5+}. The chain in **saneroite** consists of alternating *c*-shaped trimers and dimers that link along [101], the *T*6 tetrahedron is 1-connected and links to the *T*4 tetrahedron to form a simple

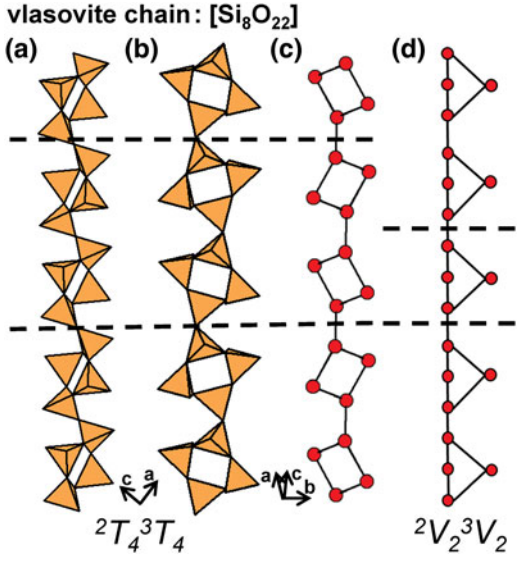

Fig. 81. (*a*, *b*) Tetrahedral representations of the chain in **vlasovite** projected approximately orthogonal to [101], (*c*) a ball-and-stick and (*d*) a graphical representation of the chain. Dashed black lines outline the geometrical and topological repeat unit of the chain.

https://doi.org/10.1180/mgm.2020.13 Published online by Cambridge University Press

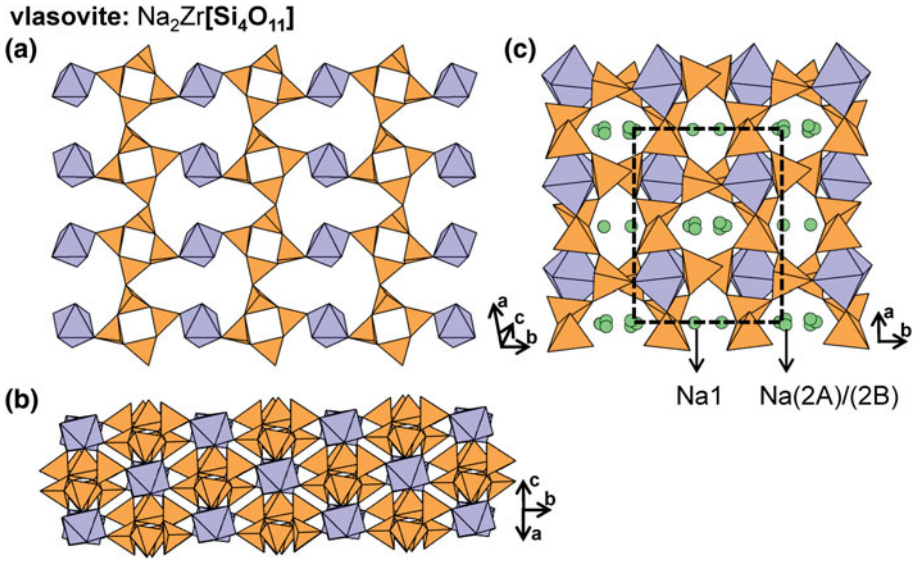

Fig. 82. The structure of **vlasovite** projected approximately (*a*) orthogonal to [101], (*b*) onto [101] where Na^+ ions have been omitted and (*c*) along the **c**-axis where Na^+ ions occur in channels parallel to the **c**-axis. Fine dashed black lines outline the unit cell.

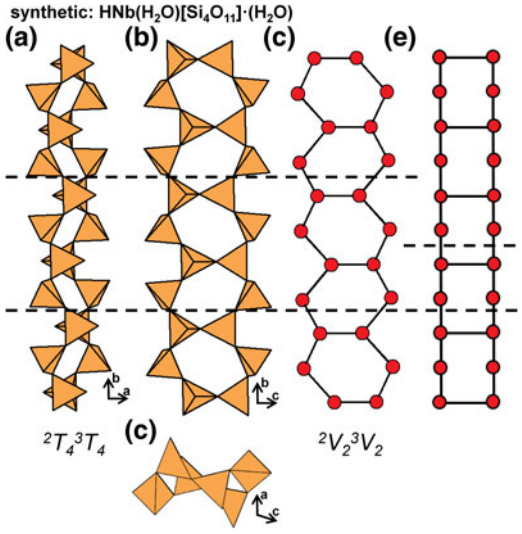

Fig. 83. (*a*, *b*, *c*) Tetrahedral representations of the $^2T_4{}^3T_4$ ribbon in **synthetic HNb $(H_2O)[Si_4O_{11}]\cdot(H_2O)$** projected (*a*) onto (001), (*b*) onto (100), (*c*) along the **b**-axis, (*d*) a ball-and-stick and (*e*) a graphical representation of the ribbon. Dashed black lines outline the geometrical and topological repeat unit of the ribbon.

decoration (Figs 92*a*–*c*). Two of the tetrahedra in the *c*-shaped trimer (*T*1 and *T*3) are linked via hydrogen bonding. The $^1T_1{}^2T_4{}^3T_1$ chains in **saneroite** are planar, occur in layers parallel to [110], and link to Mn^{2+}-octahedra (*M*1–*M*5) and $^{[8]}Na^+$-polyhedra (Na1 and Na2) that form sheets parallel to [110] (Figs 92*e*,*f*).

$^1T_1{}^2T_6{}^3T_3$ chains

The $^1T_1{}^2T_6{}^3T_3$ $[VSi_9O_{28}(OH)]^{18-}$ chain in **scheuchzerite** (Figs 93*a*–*c*) geometrically resembles the chain in **saneroite** (Fig. 92*b*, *c*) and **pyroxmangite** (Figs 31*b*,*d*) but is unique from a topological perspective (Fig. 93*d*). The geometrical repeat unit contains seven Si^{4+}-tetrahedra (*T*1, *T*3 and *T*5–*T*9), two $(SiO_3(OH))^{3-}$-tetrahedra (*T*2 and *T*4) and one V^{5+}-tetrahedron (*T*10). The chain consists of six-membered rings of tetrahedra linked to one another along [011] by *c*-shaped trimers of $(SiO_3(OH))^{3-}$ and Si^{4+}-tetrahedra. Each six-membered ring is decorated by a single 1-connected V^{5+} tetrahedron and two of the Si^{4+} tetrahedra (*T*2 and *T*4) in the trimer are linked by a hydrogen bond (Figs 93*a*,*b*). Here, chains are planar and occur in layers parallel to (211), and are linked along [111] to sheets of edge-sharing Mn^{2+}-octahedra (*M*1–*M*9) and $^{[7]}Na^+$-polyhedra (Figs 94*a*,*b*).

$^1T_2{}^2T_2{}^3T_2$ chains

The geometrical repeat unit of the $^1T_2{}^2T_2{}^3T_2$ chain in **terskite** (Figs 95*a*,*b*) contains two Si^{4+}-tetrahedra and four acid silicate tetrahedra: $(SiO_3OH)^{3-}$. **Terskite** contains two symmetrically inequivalent chains, both of which have the topology $^1V_1{}^2V_1{}^3V_1$ where every second vertex of the backbone $^2V_1$ chain is decorated with a 1-connected vertex (Fig. 95*c*). In **hydroterskite**, the geometrical repeat unit contains one distinct Si^{4+}-tetrahedron, one acid silicate tetrahedron: $(SiO_3OH)^{3-}$, and three doubly acid silicate groups: $(SiO_2(OH)_2)^{2-}$, and there is only one symmetrically distinct chain.

The $[Si_6O_{14}(OH)_4]^{8-}$ and $[Si_6O_{12}(OH)_6]^{6-}$ chains in **terskite** and **hydroterskite** extend along the **c**-axis and are strongly modulated (Fig. 95*a*,*b*). In both minerals, chains occur in layers parallel to the **b**–**c** plane and are linked to each other by a single weak hydrogen-bond. In **terskite**, $^1T_2{}^2T_2{}^3T_2$ chains are linked along [010] through sheets of $(NaO_6(OH)_2)^{13-}$-polyhedra (Na1, Na3 and Na4) (Na1 and Na2 in **hydroterskite**) and Zr^{4+}-octahedra, forming an open framework. In **terskite**, framework channels are occupied by Na^+ ions that form $(NaO_6(OH)_2)^{13-}$-polyhedra (Na2 and Na5) which crosslink sheets of Na^+-polyhedra and Zr^{4+}-octahedra along [010] (Figs 95*d*,*e*). In **hydroterskite**, framework channels are occupied by H^+ ions (which substitute for Na^+ at the Na2 and Na5 sites in **terskite**) associated with additional $(OH)^-$ groups. (Figs 95*f*).

The **sapphirine supergroup** includes the **sapphirine-**, **aenigmatite-** and **rhönite-group** minerals, all of which contain $^1T_2{}^2T_2{}^3T_2$ chains (Figs 96*a*–*c*; Table 9). This $^1V_2{}^2V_2{}^3V_2$ chain (Fig. 96*d*) is topologically similar to the chains in **surinamite** (Fig. 91*c*), **saneroite** (Fig. 92*d*) and **terskite** (Fig. 95*e*) as each

https://doi.org/10.1180/mgm.2020.13 Published online by Cambridge University Press

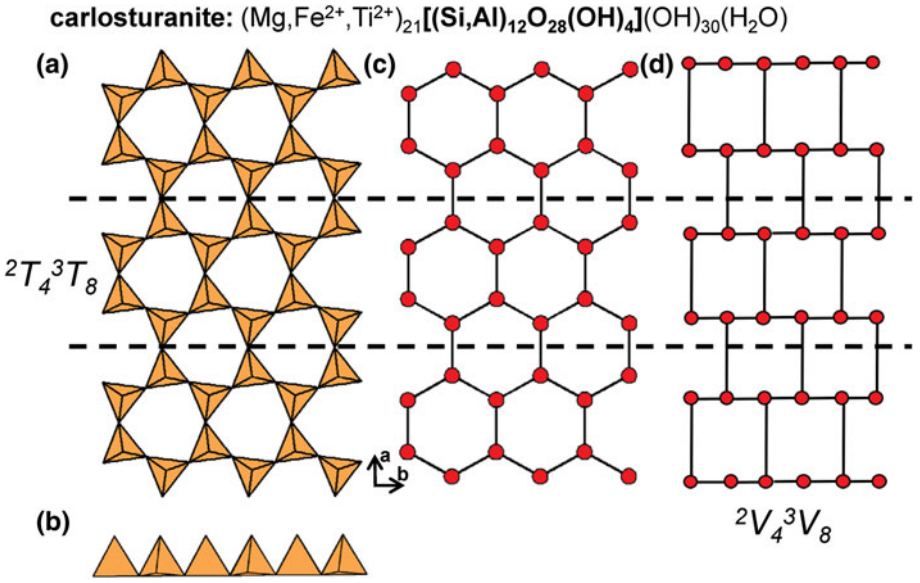

Fig. 84. (*a*, *b*) Tetrahedral representations of the $^{2}T_{4}{}^{3}T_{8}$ ribbon in **carlosturanite** projected (*a*) onto (001), (*b*) along the **a**-axis, (*c*) a ball-and-stick and (*d*) a graphical representation of the ribbon. Dashed black lines outline the geometrical and topological repeat unit of the ribbon.

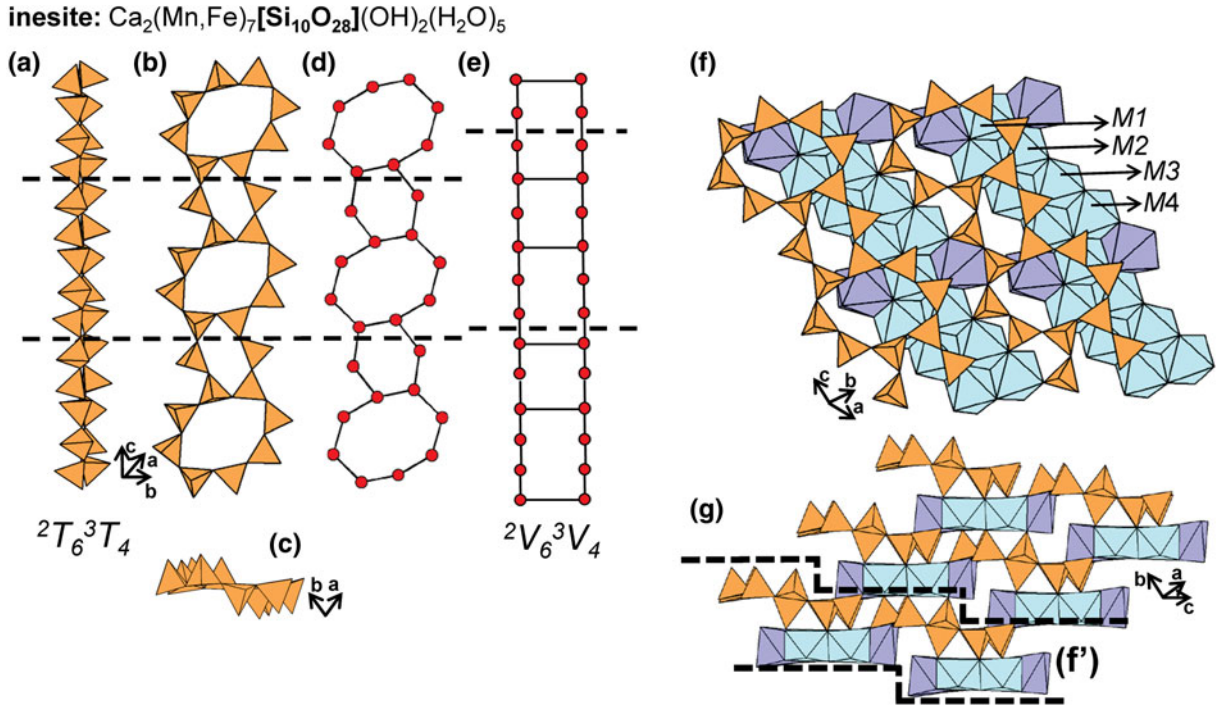

Fig. 85. (*a*, *b*, *c*) Tetrahedral representations of the $^{2}T_{6}{}^{3}T_{4}$ ribbon in **inesite** projected approximately (*a*) orthogonal to the **c**-axis, (*b*) onto (111), (*c*) along the **c**-axis, (*d*) a ball-and-stick and (*e*) a graphical representation of the ribbon. The structure of **inesite** projected (*f*) onto (111) and (*g*) along the **c**-axis. Dashed black lines outline the geometrical and topological repeat unit of the ribbon and H atoms associated with $(OH)^{-}$ and (H_2O) groups are omitted for clarity.

contains $^{2}V_{2}$ chains with 1-connected decorations. Structural similarities are especially noticeable in **surinamite** which forms its own group within the **sapphirine supergroup** (Grew *et al.*, 2008*a*). Due to the crystal-chemical complexity of **sapphirine-supergroup** minerals, we provide only a brief description of each group and readers are referred to McKie (1963), Dornberger-Schiff and Merlino (1974), Higgins and Ribbe (1979), Christy (1988, 1989), Christy and Grew (2004), Christy *et al.* (2002), Burt (1994), Jensen (1996), Kunzmann (1999), Merlino and Zvyagin (1998) and Grew *et al.* (2008*a*) for a more detailed discussion of structure, composition and OD relations. In general, **sapphirine-supergroup** minerals contains six distinct tetrahedra (*T*1–*T*6) (Fig. 96*a*) that polymerise to form $^{1}T_{2}{}^{2}T_{2}{}^{3}T_{2}$ chains that extend along the **a**-axis and link to sheets or ribbons of polyhedra (*M*1–*M*9) that are parallel to (011).

The **sapphirine group** includes **sapphirine-1*A***, **sapphirine-2*M*** and **khmaralite**, although the latter two minerals are not isostructural with the other **sapphirine-supergroup** minerals. The additional 3*A*, 4*M* and 5*A* polytypes are much less abundant and will not be described here (Merlino and Pasero, 1987). In

https://doi.org/10.1180/mgm.2020.13 Published online by Cambridge University Press

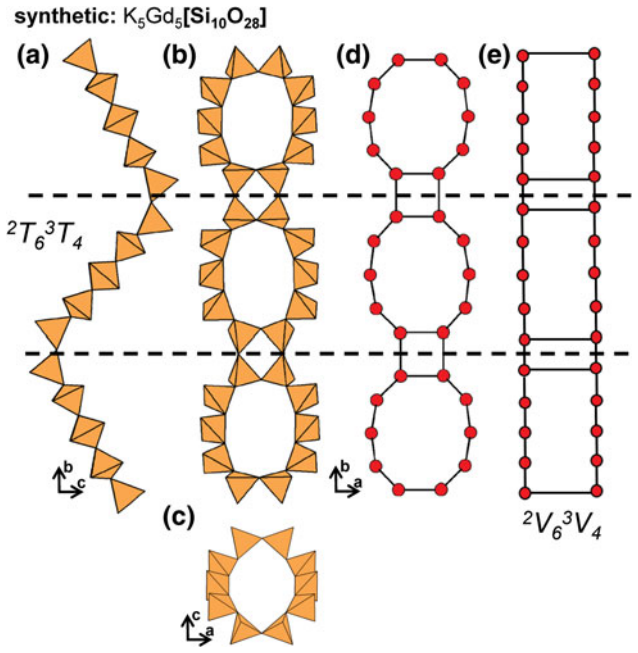

Fig. 86. (*a*, *b*, *c*) Tetrahedral representations of the $^2T_6{}^3T_4$ ribbon in **synthetic $K_5Gd_5[Si_{10}O_{28}]$** projected (*a*) onto (100), (*b*) onto (001), (*c*) along the **b**-axis, (*d*) a ball-and-stick and (*e*) a graphical representation of the ribbon. Dashed black lines outline the geometrical and topological repeat unit of the ribbon.

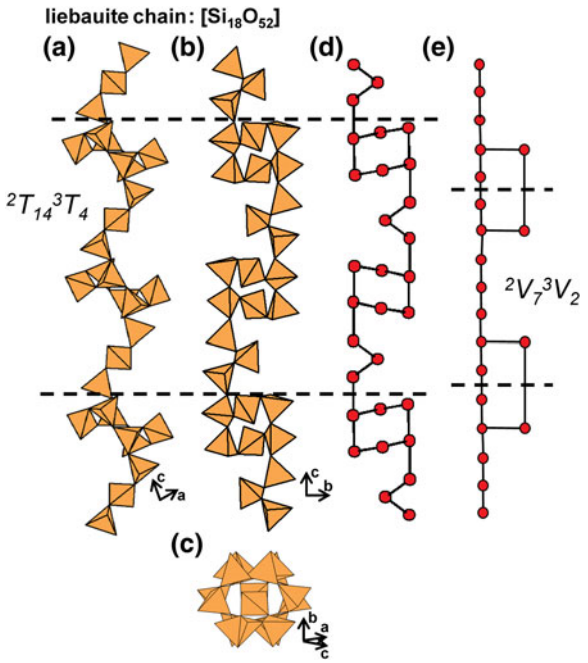

Fig. 88. (*a*, *b*, *c*) Tetrahedral representations of the $^2T_{14}{}^3T_4$ chain in **liebauite** projected (*a*, *b*) orthogonal to [10$\bar{1}$], (*c*) along [10$\bar{1}$], (*d*) a ball-and-stick and (*e*) a graphical representation of the chain. Dashed black lines outline the geometrical and topological repeat unit of the chain.

sapphirine-2*M*, there are eight *M* sites rather than nine, as in most **sapphirine-supergroup** minerals, and **khmaralite** contains 12 *T* sites occupied by Be^{2+}, $Si^{4+}$and Al^{3+} and 16 *M* sites due to a doubled **a**-axis. In **sapphirine-1*A***, all *M* sites (*M*1–*M*9) are octahedrally coordinated and form ribbons parallel to (011) that are linked along [12$\bar{2}$] by $^1T_2{}^2T_2{}^3T_2$ chains (Fig. 96*e*) where *T*1 and *T*4–*T*6 are occupied by $Al^{3+} > Si^{4+}$ and *T*2 and *T*3 are occupied by $Si^{4+} \geq Al^{3+}$ (Fig. 96*a*). In Fig. 96*f*, layer *1* contains

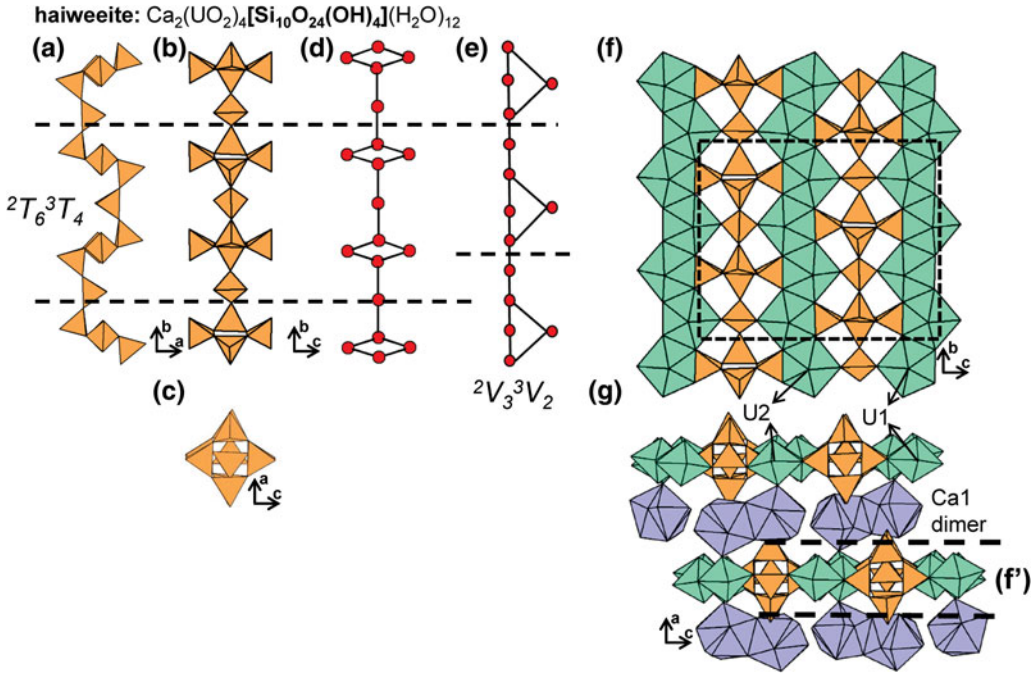

Fig. 87. (*a*, *b*, *c*) Tetrahedral representations of the $^2T_6{}^3T_4$ chain in haiweeite**,** (*d*) a ball-and-stick and (*e*) a graphical representation of the chain. The structure of **haiweeite** projected (*f*) onto (100) and (*g*) along the **b**-axis. Dashed black lines outline the geometrical and topological repeat unit of the ribbon and fine black dashed lines outline the unit cell. The H atoms associated with $(OH)^-$ and (H_2O) groups are omitted for clarity.

https://doi.org/10.1180/mgm.2020.13 Published online by Cambridge University Press

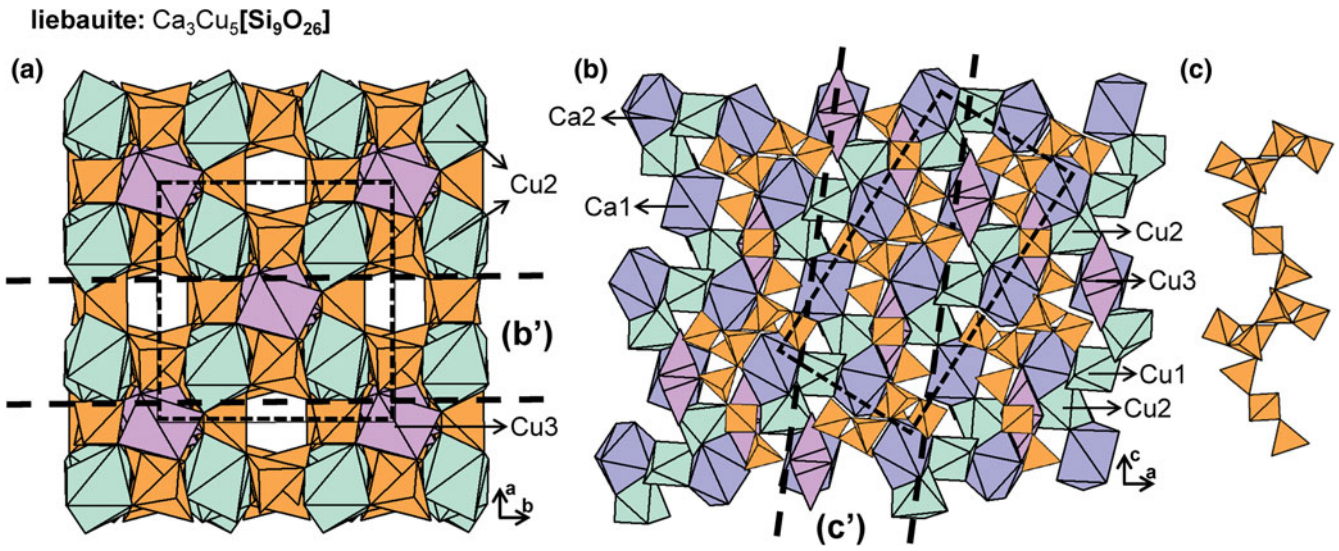

Fig. 89. The structure of **liebauite** projected (*a*) along the **c**-axis, (*b*) onto (010) and (*c*) an isolated $^2T_{14}{}^3T_4$ chain viewed orthogonal to [10$\bar{1}$]. For clarity, Cu^{2+}-octahedra are teal-green and $(CuO_5)^{8-}$-polyhedra are violet. Fine dashed black lines outline the unit cell.

ribbons of edge-sharing Mg^{2+}-octahedra (*M*3–*M*6) and Al^{3+}-octahedra (*M*1, *M*2 and *M*7), layer *2* contains $^1T_2{}^2T_2{}^3T_2$ chains but also contains Al^{3+}-octahedra (*M*8 and *M*9) that link adjacent ribbons perpendicular to [12$\bar{2}$]. In **sapphirine-1*A***, the relatively large *M*5 and *M*6 octahedra are occupied by Mg^{2+}, the sites upon which the **sapphirine-group** is based (Table 9). The *M*8 and *M*9 sites in **aenigmatite-** and **rhönite-group** minerals, which are equivalent to the *M*5 and *M*6 sites in **sapphirine-group** minerals, are occupied by higher coordination Na^+- and Ca^{2+}-polyhedra that link ribbons of octahedra to form sheets parallel to (011). Sabau *et al.* (2002) reported a peraluminous sapphirine where $Al^{3+} > Si^{4+}$ at *T*2 and *T*3 and as a result can be considered an Al^{3+}-analogue of **sapphirine** (Grew *et al.*, 2008*a*).

The **aenigmatite group** includes **aenigmatite**, **krinovite** and **wilkinsonite** in which Si^{4+} fully occupies the *T*1–*T*6 sites (Fig. 97*a*) and Na^+ fully occupies the [8]-coordinated *M*8 and *M*9 sites**.** In **aenigmatite**, the *M*1–*M*6 sites are occupied by Fe^{2+} and the *M*7 site is occupied by Ti^{4+} (Figs 97*b*,*c*). In **krinovite**, the *M*1–*M*2 and *M*7 sites are occupied by Cr^{3+} and the *M*3–*M*6 sites are occupied by Mg^{2+}. In **wilkinsonite**, the *M*1–*M*2 and *M*7 sites are occupied by Fe^{3+} and the *M*3–*M*6 sites are occupied by Fe^{2+}. Grew *et al.* (2008*a*) suggested that chemical data reported by Gaeta and Mottana (1991) represents a Mg^{2+}-analogue of **wilkinsonite**.

The **rhönite group** includes many minerals (Table 9), all of which contain $^{[7-8]}Ca^{2+}$ ions that occupy the *M*8 and *M*9 sites. In **rhönite**, Ti^{4+} occupies the *M*7 site; Mg^{2+}, Fe^{2+} and Fe^{3+} are disordered over the *M*1–*M*6 sites, and Al^{3+} and Si^{4+} occupy the *T*1–*T*6 sites. For the purpose of clarity, in the **rhönite** structure, the *T*1–*T*6 sites are shown as Si^{4+}-tetrahedra and *M*1–*M*6 sites are shown as Mg^{2+}-octahedra (Figs 97*d*,*e*). Fuchs (1971, 1978) reported a Ti^{3+}-bearing, Mg^{2+}-analogue of **rhönite** from the Allende meteorite where Mg^{2+} occupies the *M*7 site instead of Ti^{3+} and $Ti^{3+} > Fe^{3+}$ at the *M* sites (Bonaccorsi *et al.*, 1990; Grew *et al.*, 2008*a*). In Figs 98*a*–*e*, the $^1T_2{}^2T_2{}^3T_2$ chains in **serendibite, addibischoffite (warkite)**, **welshite** and **dorrite** show considerable chemical variation over the *T*1–*T*6 sites. The *M*1–*M*7 sites and *T*1–*T*6 sites in the other **rhönite-group** minerals (Table 9) show complicated chemical variability and OD relations, and detailed discussions are given by Van Derveer *et al.* (1993), Kunzmann (1999), Grew *et al.* (2001, 2007, 2008*a*), Shchipalkina *et al.* (2016*b*) and Ma *et al.* (2017).

$^2T_r{}^3T_r{}^4T_r$ class

$^2T_4{}^3T_2{}^4T_2$ *ribbons*

Revdite contains chains with 4-connected vertices, something that occurs only in **revdite** and **patynite**. The $^2T_2{}^3T_2$ $[Si_4O_6(OH)_5]^{1-}$ chain and the $^2T_4{}^3T_2{}^4T_2$, $[Si_8O_{15}(OH)_6]^{4-}$ ribbon are shown in Figs 99*a*–*d* and 99*e*–*i*, respectively. Here, $^2T_2{}^3T_2$ chains have a geometrical repeat unit that contains three $(SiO_3(OH))^{3-}$-tetrahedra and one $(SiO_2(OH)_2)^{2-}$-tetrahedron. These chains consist of four-membered rings of tetrahedra that link along [001] (Figs 99*a*,*c*) and are topologically identical to the chains in **vlasovite** (Fig. 81*d*) and **synthetic $Li_2Mg_2[Si_4O_{11}]$** and **$Fe_3[BeSi_3O_9OH]_2$** (Fig. 64*f*). The $^2T_4{}^3T_2{}^4T_2$ ribbon (Figs 99*e*–*h*) has a geometrical repeat unit that contains one Si^{4+}-tetrahedron, five $(SiO_3(OH))^{3-}$-tetrahedra, and two $(SiO_2(OH)_2)^{2-}$-tetrahedron and is topologically unique with the vertex degree $^2V_4{}^3V_2{}^4V_2$ (Fig. 99*i*). This ribbon consists of two adjacent $^2T_2{}^3T_2$ chains in which every fourth tetrahedron along the length of each chain links to the equivalent tetrahedron of the adjacent $^2T_2{}^3T_2$ chain. Both chains that comprise the ribbon are offset with respect to each other along [001] (Figs 99*e*,*f*,*h*). In **revdite**, chains and ribbons occur in layers that alternate along [100] and are parallel to (100) (Fig. 100*a*). These layers also contain $(NaO(OH)_3(H_2O))^{4-}$-polyhedra (Na2) and $(NaO_3(OH)_2(H_2O))^{7-}$-octahedra (Na9) that link $^2T_2{}^3T_2$ chains along [010] (Figs 100*a*,*b*). The $(NaO(OH)(H_2O)_3)^{2-}$-polyhedra (Na5), $(NaO_2(OH)_2(H_2O)_2)^{5-}$-octahedra (Na6) and $(NaO_4(H_2O)_2)^{7-}$-octahedra (Na8) occur in layers with $^2T_4{}^3T_2{}^4T_2$ ribbons and link them along [010] (Figs 100*a*,*c*). These complicated Si^{4+}–Na^+–(H_2O) layers are linked to each other along [100] by chains of $(NaO(OH)_3(H_2O)_2)^{4-}$- (Na1), $(Na(OH)_3(H_2O)_3)^{2-}$- (Na3 and Na7)

https://doi.org/10.1180/mgm.2020.13 Published online by Cambridge University Press

Table 9. Minerals with $^{1}T_r{}^{2}T_r{}^{3}T_r{}^{4}T_r$ ribbons and tubes.

$^{c}T_r$	Mineral	Ideal structural formula	Unit stoichiometry	$^{c}V_r$	Space group	O:T	Figs	Refs.
$^{1}T_1{}^{2}T_2{}^{3}T_3$	Synthetic	K_3Eu^{3+}**[$Si_6O_{13}(OH)_4$]**$(H_2O)_2$	$[SiO_{2.16}(OH)_{0.67}]$	$^{1}V_1{}^{2}V_2{}^{3}V_3$	*Pbam*	2.83	90	(1)
$^{1}T_1{}^{2}T_3{}^{3}T_1$	Surinamite	$(Mg,Fe^{2+})_3(Al,Fe^{3+})_3O$**[$AlBeSi_3O_{15}$]**	$[Si_{0.60}Al_{0.2}Be_{0.2}O_3]$	$^{1}V_1{}^{2}V_3{}^{3}V_1$	$P2_1/n$	3.0	91	(2)
$^{1}T_1{}^{2}T_3{}^{3}T_1$	Surinamite-(*Be-free*) *unnamed analogue*	$(Mg,Fe^{2+})_3(Al,Fe^{3+})_3O$**[$Al_2Si_3O_{15}$]**	$[Si_{0.60}Al_{0.4}O_3]$	$^{1}V_1{}^{2}V_3{}^{3}V_1$	$P2_1/n$	3.0	–	(3)
$^{1}T_1{}^{2}T_4{}^{3}T_1$	Saneroite	Na_2Mn_5**[$Si_5O_{14}(OH)(V,Si,As)O_3$]**$(OH)$	$[V_{0.17}Si_{0.83}O_{2.83}(OH)_{0.17}]$	$^{1}V_1{}^{2}V_4{}^{3}V_1$	$P\bar{1}$	3.0	92	(4)
$^{1}T_1{}^{2}T_6{}^{3}T_3$	Scheuchzerite	$Na(Mn,Mg)_9$**[$VSi_9O_{28}(OH)$]**$(OH)_3$	$[V_{0.1}Si_{0.9}O_{2.8}(OH)_{0.1}]$	$^{1}V_1{}^{2}V_6{}^{3}V_3$	$P\bar{1}$	2.90	93,94	(5)
$^{1}T_2{}^{2}T_2{}^{3}T_2$	Terskite	Na_4Zr**[$Si_6O_{14}(OH_4)$]**	$[SiO_2(OH)_{0.67}]$	$^{1}V_1{}^{2}V_1{}^{3}V_1$	Pnc2	3.0	95*a–e*	(6)
$^{1}T_2{}^{2}T_2{}^{3}T_2$	Hydroterskite	Na_2Zr**[$Si_6O_{12}(OH_6)$]**	$[SiO_{2.33}(OH)_{0.33}]$	$^{1}V_1{}^{2}V_1{}^{3}V_1$	Pnc*a*	3.0	95*a–c,f*	(7)
		Sapphirine supergroup						
		Sapphirine group: *M5*/*M6* = Mg						
$^{1}T_2{}^{2}T_2{}^{3}T_2$	Sapphirine-1*A* (2*M*)	$Mg_4(Mg_3Al_9)O_4$**[$Si_3Al_9O_{36}$]**	$[Si_{0.25}Al_{0.75}O_3]$	$^{1}V_2{}^{2}V_2{}^{3}V_2$	$P\bar{1}$ ($P2_1/a$)	3.0	96	(8)
$^{1}T_2{}^{2}T_2{}^{3}T_2$	Khmaralite	$Mg_4(Mg_3Al_9)O_4$**[$Si_5Be_2Al_5O_{36}$]**	$[Si_{0.42}Al_{0.5}Be_{0.08}O_3]$	$^{1}V_2{}^{2}V_2{}^{3}V_2$	$P2_1/c$	3.0	–	(9)
$^{1}T_2{}^{2}T_2{}^{3}T_2$	Sapphirine-(Al) *unnamed analogue*	$Mg_4(Mg_{1.5}Fe^{2+}_{0.3}Fe^{3+}_{1.6}Al_{8.5})O_4$**[$Si_{1.7}Al_{10.3}O_{36}$]**	$[Si_{0.14}Al_{0.86}O_3]$	$^{1}V_2{}^{2}V_2{}^{3}V_2$	$P\bar{1}$	3.0	–	(10)
		Aenigmatite group: *M8*/*M9* = Na						
$^{1}T_2{}^{2}T_2{}^{3}T_2$	Aenigmatite	$Na_4(Fe^{2+}_{10}Ti_2)O_4$**[$Si_{12}O_{36}$]**	$[SiO_3]$	$^{1}V_2{}^{2}V_2{}^{3}V_2$	$P\bar{1}$	3.0	97*a–c*	(11)
$^{1}T_2{}^{2}T_2{}^{3}T_2$	Krinovite	$Na_4(Mg_8Cr^{3+}_4)O_4$**[$Si_{12}O_{36}$]**	$[SiO_3]$	$^{1}V_2{}^{2}V_2{}^{3}V_2$	$P\bar{1}$	3.0	97*a*	(12)
$^{1}T_2{}^{2}T_2{}^{3}T_2$	Wilkinsonite	$Na_4(Fe^{2+}_8Fe^{3+}_4)O_4$**[$Si_{12}O_{36}$]**	$[SiO_3]$	$^{1}V_2{}^{2}V_2{}^{3}V_2$	$P\bar{1}$	3.0	97*a*	(13)
$^{1}T_2{}^{2}T_2{}^{3}T_2$	Wilkinsonite-(Mg) *unnamed analogue*	$Na_4(Mg_5Fe^{3+}_7)O_4$**[$Si_9Fe^{3+}_3O_{36}$]**	$[Si_{0.75}Fe^{3+}_{0.25}O_3]$	$^{1}V_2{}^{2}V_2{}^{3}V_2$	$P\bar{1}$	3.0	97*a*	(14)
		Rhönite group: *M8*/*M9* = Ca						
$^{1}T_2{}^{2}T_2{}^{3}T_2$	Rhönite	$Ca_4(Mg_8Fe^{3+}_2Ti_2)O_4$**[$Si_6Al_6O_{36}$]**	$[Si_{0.5}Al_{0.5})O_3]$	$^{1}V_2{}^{2}V_2{}^{3}V_2$	$P\bar{1}$	3.0	97*d,e*	(15)
$^{1}T_2{}^{2}T_2{}^{3}T_2$	Rhönite-(Ti^{3+}) *unnamed analogue (Allende meteorite)*	$Ca_4(Mg_7AlTi^{3+}_2Ti^{4+})O_4$**[$Si_5Al_7O_{36}$]**	$[Si_{0.42}Al_{0.58})O_3]$	$^{1}V_2{}^{2}V_2{}^{3}V_2$	$P\bar{1}$	3.0	–	(16)
$^{1}T_2{}^{2}T_2{}^{3}T_2$	Kuratite	$Ca_4(Fe^{2+}_{10}Ti_2)O_4$**[$Si_8Al_4O_{36}$]**	$[Si_{0.67}Al_{0.33})O_3]$	$^{1}V_2{}^{2}V_2{}^{3}V_2$	$P\bar{1}$	3.0	–	(17)
$^{1}T_2{}^{2}T_2{}^{3}T_2$	Makarochkinite	$Ca_4(Fe^{2+}_8Fe^{3+}Ti_2)O_4$**[$Be_2Al_2Si_8O_{36}$]**	$[Si_{0.67}Al_{0.17}Be_{0.17}O_3]$	$^{1}V_2{}^{2}V_2{}^{3}V_2$	$P\bar{1}$	3.0	–	(18)
$^{1}T_2{}^{2}T_2{}^{3}T_2$	Serendibite	$Ca_4(Mg_6Al_6)O_4$**[$Si_6B_3Al_3O_{36}$]**	$[Si_{0.5}Al_{0.25}Be_{0.25}O_3]$	$^{1}V_2{}^{2}V_2{}^{3}V_2$	$P\bar{1}$	3.0	98*a*	(19)
$^{1}T_2{}^{2}T_2{}^{3}T_2$	Addibischoffite	$Ca_4(Al_{12})O_4$**[$Al_{12}O_{36}$]**	$[AlO_3]$	$^{1}V_2{}^{2}V_2{}^{3}V_2$	$P\bar{1}$	3.0	98*b*	(20)
$^{1}T_2{}^{2}T_2{}^{3}T_2$	Warkite	$Ca_4(Sc_{12})O_4$**[$Al_{12}O_{36}$]**	$[AlO_3]$	$^{1}V_2{}^{2}V_2{}^{3}V_2$	$P\bar{1}$	3.0	98*b*	(21)
$^{1}T_2{}^{2}T_2{}^{3}T_2$	Welshite	$Ca_4(Mg_9Sb^{5+}_3)O_4$**[$Si_6Be_3Fe^{3+}_2AlO_{36}$]**	$[Si_{0.5}Al_{0.08}Be_{0.25}Fe_{0.17}O_3]$	$^{1}V_2{}^{2}V_2{}^{3}V_2$	$P\bar{1}$	3.0	98*c,d*	(22)
$^{1}T_2{}^{2}T_2{}^{3}T_2$	Dorrite	$Ca_4(Mg_3Fe^{3+}_3)O_4$**[$Si_3Al_8Fe^{3+}O_{36}$]**	$[Si_{0.25}Al_{0.67}Fe^{3+}_{0.08}O_3]$	$^{1}V_2{}^{2}V_2{}^{3}V_2$	$P\bar{1}$	3.0	98*e*	(23)
$^{1}T_2{}^{2}T_2{}^{3}T_2$	Høgtuvaite	$Ca_4(Fe^{2+}_6Fe^{3+}_6)O_4$**[$Si_8Be_2Al_2O_{36}$]**	$[Si_{0.67}Al_{0.17}Be_{0.17}O_3]$	$^{1}V_2{}^{2}V_2{}^{3}V_2$	$P\bar{1}$	3.0	–	(24)
$^{1}T_2{}^{2}T_2{}^{3}T_2$	Khesinite	$Ca_4(Mg_2Fe^{3+}_{10})O_4$**[$Fe^{3+}_{10}Si_2$]**$O_{36}$	$[Fe^{3+}_{0.83}Si_{0.17}]$	$^{1}V_2{}^{2}V_2{}^{3}V_2$	$P\bar{1}$	3.0	–	(25)
$^{1}T_2{}^{2}T_2{}^{3}T_2$	Unnamed Fe-Ga analogue *sapphirine supergroup*	$(Fe,Ga,Sn,Zn)_{16}O_4$**[$(Ga,Ge)_{12}O_{36}$]**	$[Ga,GeO_3]$	$^{1}V_2{}^{2}V_2{}^{3}V_2$	$P\bar{1}$	3.0	–	(26)
$^{2}T_4{}^{3}T_2{}^{4}T_2$	Revdite	Na_{16}**[$Si_4O_6(OH)_5]_2$[$Si_8O_{15}(OH)_6$]** $(OH)_{10}(H_2O)_{28}$	$[SiO_{1.88}(OH)_{0.75}]$ $[SiO_{2.75}]$	$^{2}V_4{}^{3}V_2{}^{4}V_2$ $^{2}V_2{}^{3}V_2$	*B*2	2.69	99,100	(27)
$^{2}T_2{}^{3}T_2{}^{\star}$	〃 〃	〃 〃						
$^{2}T_4{}^{3}T_{12}{}^{4}T_2$	Patynite	$NaKCa_4$**[Si_9O_{23}]**	$[SiO_{2.56}]$	$^{2}V_4{}^{3}V_{12}{}^{4}V_2$	$P\bar{1}$	2.56	101,102	(28)

References: (1) Rastsvetaeva and Aksenov (2011); (2) Barbier *et al.* (2002), De Roever *et al.* (1976), Moore and Araki (1983), Baba *et al.* (2000), Grew *et al.* (2008*a*); (3) Christy and Putnis (1988); (4) Basso and Della Giusta (1980), Lucchetti *et al.* (1981), Nagashima and Armbruster (2010); (5) Brugger *et al.* (2006); (6/7) Pudovkina and Chernitsova (1991), Khomyakov *et al.* (1983*b*), Grice *et al.* (2015); (8) Merlino (1980), Moore (1968,1969*b*), Higgins *et al.* (1979), Moore and Araki (1983), Christy (1988, 1989); (9) Barbier *et al.* (1999), Christy and Grew (2004), Christy *et al.* (2002); (10) Sabau *et al.* (2002), Grew *et al.* (2008*a*); (11) Grew *et al.* (2008*b*), Merlino (1970), Cannillo *et al.* (1971); (12) Merlino (1972), Bonaccorsi *et al.* (1989); (13) Duggan (1990), Burt *et al.* (2007); (14) Gaeta and Mottana (1991); (15) Bonaccorsi *et al.* (1990), Johnston and Stout (1985); (16) Fuchs (1971,1978); (17) Hwang *et al.* (2016), Grew *et al.* (2008*a*); (18) Yakubovich *et al.* (1990), Grew *et al.* (2005); (19) Van Derveer *et al.* (1993), Buerger and Venkatakrishnan (1974), Grice *et al.* (2014); (20) Ma *et al.* (2017); (21) Ma *et al.* (2015), (22) Grew *et al.* (2007), Moore (1978), Grew *et al.* (2001); (23) Cosca *et al.* (1988), Shchipalkina *et al.* (2016*b*); (24) Burt (1994), Grauch *et al.* (1994); (25) Galuskina *et al.* (2017); (26) Johan and Oudin (1986); (27) Rastsvetaeva *et al.* (1992), Khomyakov *et al.* (1980); (28) Kasatkin *et al.* (2019).
*Indicates the $^{c}T_r$ expression of an additional structural unit including a chain, ribbon, tube, cluster or sheet of $[TO_4]^{n-}$ tetrahedra in the respective mineral.

and $(Na(OH)_4(H_2O)_2)^{3-}$-octahedra (*Na*4) that occur in layers parallel to (100) (Fig. 100*a*).

The $^{2}T_4{}^{3}T_{12}{}^{4}T_2$ $[Si_9O_{23}]^{10-}$ silicate unit in **patynite** can be described as a ribbon-tube hybrid with a central tube that consists of five- and eight-membered rings and extends along [100]. This tube is decorated by $^{2}T_2$ chains to form ribbons of eight-membered rings attached to both sides of the tube (Figs 101*a–d*). The graphical representation of this ribbon-tube is shown in Fig. 101*e* with the vertex degree $^{2}V_4{}^{3}V_{12}{}^{4}V_2$. In the structure of **patynite**, $^{2}T_4{}^{3}T_{12}{}^{4}T_2$ ribbon-tubes link adjacent sheets of Ca^{2+}-octahedra along the **c**-axis and $^{[7]}Na^{+}$-polyhedra link ribbon-tubes to each other along the **b**-axis, the channel space of each tube is occupied by $^{[8]}K^{+}$ ions (Fig. 102*a*). The corrugated sheets of Ca^{2+}-octahedra (Ca1–Ca4) (Fig. 102*b*) extend parallel to (100) and resemble the sheets in other tube-silicate minerals such as **tokkoite** (Figs 72*b*,*c*) and **canasite-group** minerals (Figs 49*b*,*d*).

Discussion

Stoichiometric ranges of chain-, ribbon- and tube-silicate minerals

In order to understand the controls on the geometry and topology of silicate units in minerals, it is useful to compare the stoichiometries of these units. Figure 103 shows the ratio between the number of *T*-cations and the corresponding number of coordinating O atoms that comprise the silicate units in all silicate minerals. Cluster structures include nesosilicates, sorosilicates and cyclosilicates, discontinuously spanning the range from TO_4 to TO_3, and do not overlap the range of any other types of single polymerisation. There is a small range of compositions, TO_3 to $TO_{2.87}$, where chain and sheet structures do not overlap, but most of the chain, ribbon and tube compositions overlap with sheet compositions, and the compositions of the framework

https://doi.org/10.1180/mgm.2020.13 Published online by Cambridge University Press

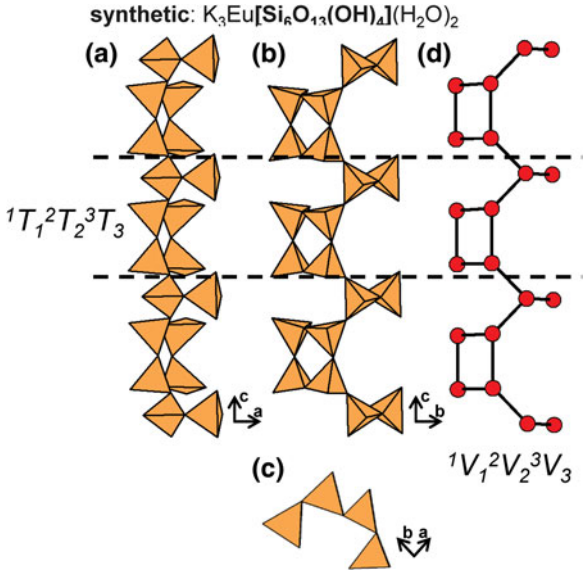

Fig. 90. (*a*, *b*, *c*) Tetrahedral representations of the $^1T_1\ ^2T_2\ ^3T_3$ ribbon in **synthetic $K_3Eu[Si_6O_{13}(OH)_4](H_2O)_2$** projected (*a*) onto (010), (*b*) onto (100), (*c*) along the **c**-axis and (*d*) a ball-and-stick (graphical) representation of the ribbon. Dashed black lines outline the geometrical and topological repeat unit of the ribbon.

structures are completely overlapped by those of the sheet structures. Note that in Fig. 103, the stoichiometric range for framework silicates is outlined by a dashed line as we have not yet examined the compositional limits of partly connected frameworks.

In chain-, ribbon- and tube-silicate minerals, the O:T ratio ranges from 3.0 (i.e. ^2T_r chains) to 2.5 (i.e. ^3T_r tubes). The stoichiometry (O:T) of any chain is controlled by the ratios of *c*-connected tetrahedra, where $c = 1–4$. The relation between stoichiometry and connectivity is shown for $c = 1–4$ in Fig. 104 from which one can determine the chain formula and O:T by counting the number of *c*-connected tetrahedra in the geometrical repeat unit. In Table 10, all chain-, ribbon- and tube-silicates have been listed from $TO_{3.0}$ to $TO_{2.5}$. If the sheet structures of Hawthorne *et al.* (2019) are included, we see a general trend in composition as the degree of polymerisation between $(TO_4)^{n-}$-tetrahedra increases: chains → ribbons → tubes → single sheets → double sheets. This trend is shown in Fig. 105 where we have not included cluster and framework structures as we have not yet examined the stoichiometric ranges of the silicate units in such structures.

Any silicate unit with one direction of infinite polymerisation (1-dimensional) of *T*-tetrahedra is constrained to have a maximum O:T = 3.0. Addition of a 1-connected tetrahedra (O:T = 3.5) to any

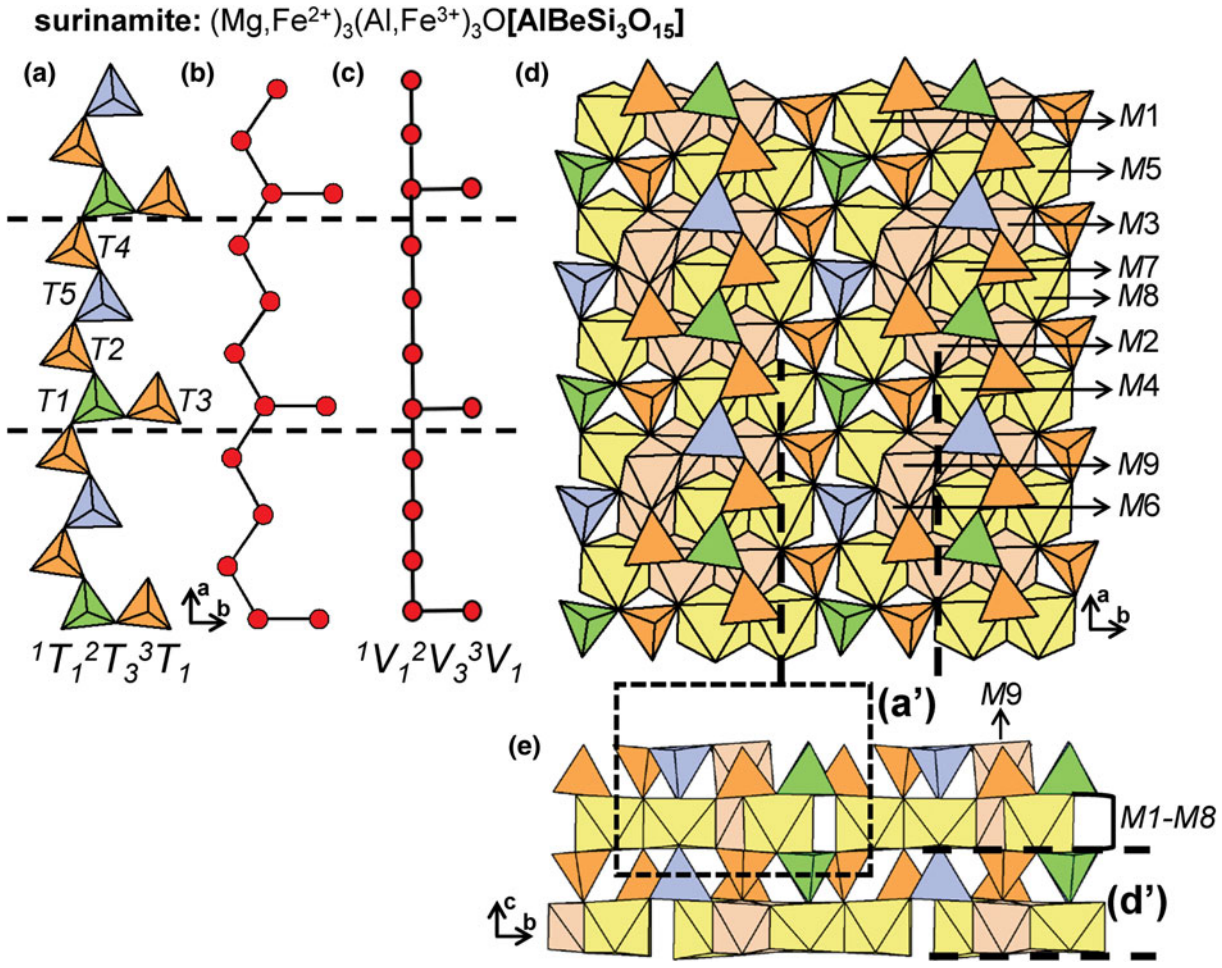

Fig. 91. (*a*) Tetrahedral representation of the chain in **surinamite**, (*b*) a ball-and-stick and (*c*) a graphical representation of the chain. The structure of **surinamite** projected (*d*) onto (001) and (*e*) along the **a**-axis. Dashed black lines outline geometrical and topological repeat unit of the chain and fine dashed black lines outline the unit cell.

https://doi.org/10.1180/mgm.2020.13 Published online by Cambridge University Press

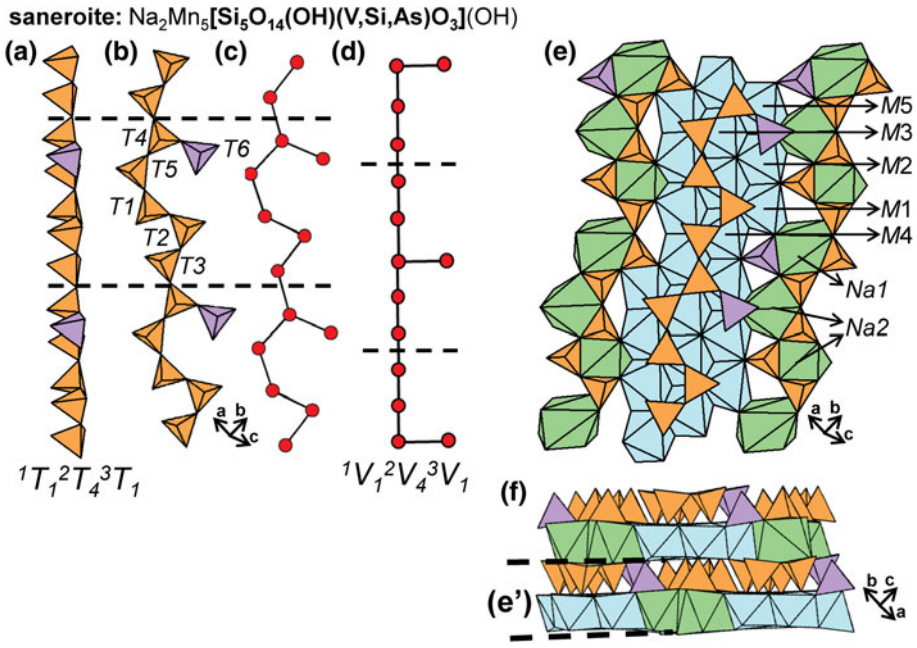

Fig. 92. (*a*, *b*) Tetrahedral representations of the chain in **saneroite** where *T*6 is a $[VO_3(OH)]^{2-}$ tetrahedra, (*c*) a ball-and-stick and (*d*) a graphical representation of the chain. The structure of **saneroite** projected (*e*) orthogonal to [101] and (*f*) along [110]. Dashed black lines outline the geometrical and topological repeat unit of the chain and H atoms associated with $(OH)^-$ groups are omitted for clarity.

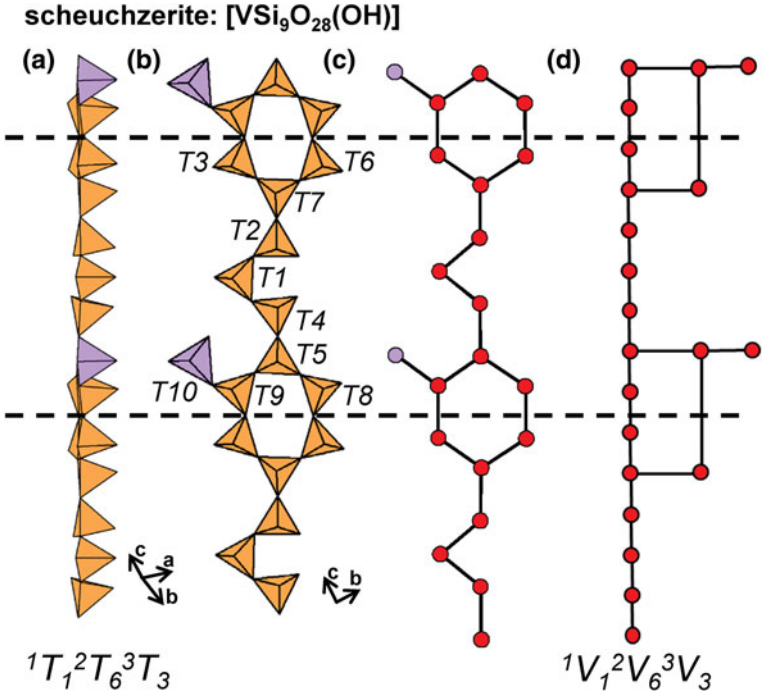

Fig. 93. Tetrahedral representation of the chain in **scheuchzerite** projected (*a*, *b*) orthogonal to [011], where *T*10 is a V^{5+}-tetrahedron, (*c*) a ball-and-stick and (*d*) a graphical representation of the chain. Dashed black lines outline the geometrical and topological repeat unit of the chain.

chain, ribbon or tube in an effort to increase the O:T ratio will result in the generation of a corresponding 3-connected tetrahedron (O:T = 2.5; (3.5 + 2.5)/2 = 3.0) and failure to produce an O:T ratio > 3.0. This situation is in contrast to that in sheet silicates where one can introduce 2-connected tetrahedra into a sheet of 3-connected tetrahedra (Hawthorne, 2015*a*) and increase the O:T ratio above 2.5. The minimum O:T ratio of ribbons and tubes is not constrained to O:T = 2.5, as linkage between any two 3-connected tetrahedra in a ^3T_n chain produces a ribbon or tube in which O:T < 2.5. However, ribbons and tubes with O:T < 2.5 are not observed in chain, ribbon and tube silicates. One may derive ribbons and tubes with stoichiometries that fall within this range. Figure 106 shows examples of ribbons and tubes of tetrahedra with O:T = 2.40, 2.20 and 2.0, respectively. Although the occurrence of the arrangements shown in Fig. 106 may be constrained by the linkage geometry of $(TO_4)^{n-}$-tetrahedra, it is possible to produce arrangements such as the tube structure (Fig. 106*g*) with O:T = 2.0.

Comparison of vertex connectivities for chains and sheets with equal O:T ratios

Of particular interest are the TO_x ranges where two types of structures overlap, such as $[TO_3]$ rings and chains or $[T_4O_{10}]$ tubes and

https://doi.org/10.1180/mgm.2020.13 Published online by Cambridge University Press

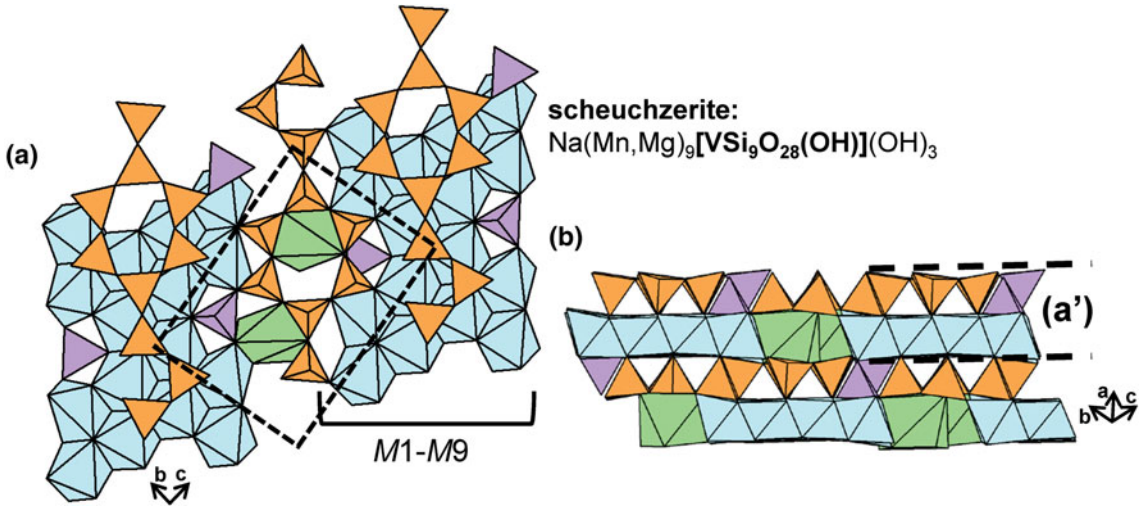

Fig. 94. The structure of **scheuchzerite** projected (*a*) orthogonal to [011] and (*b*) along [111]. Fine dashed black lines outline the unit cell and H atoms associated with $(OH)^-$ groups are omitted for clarity.

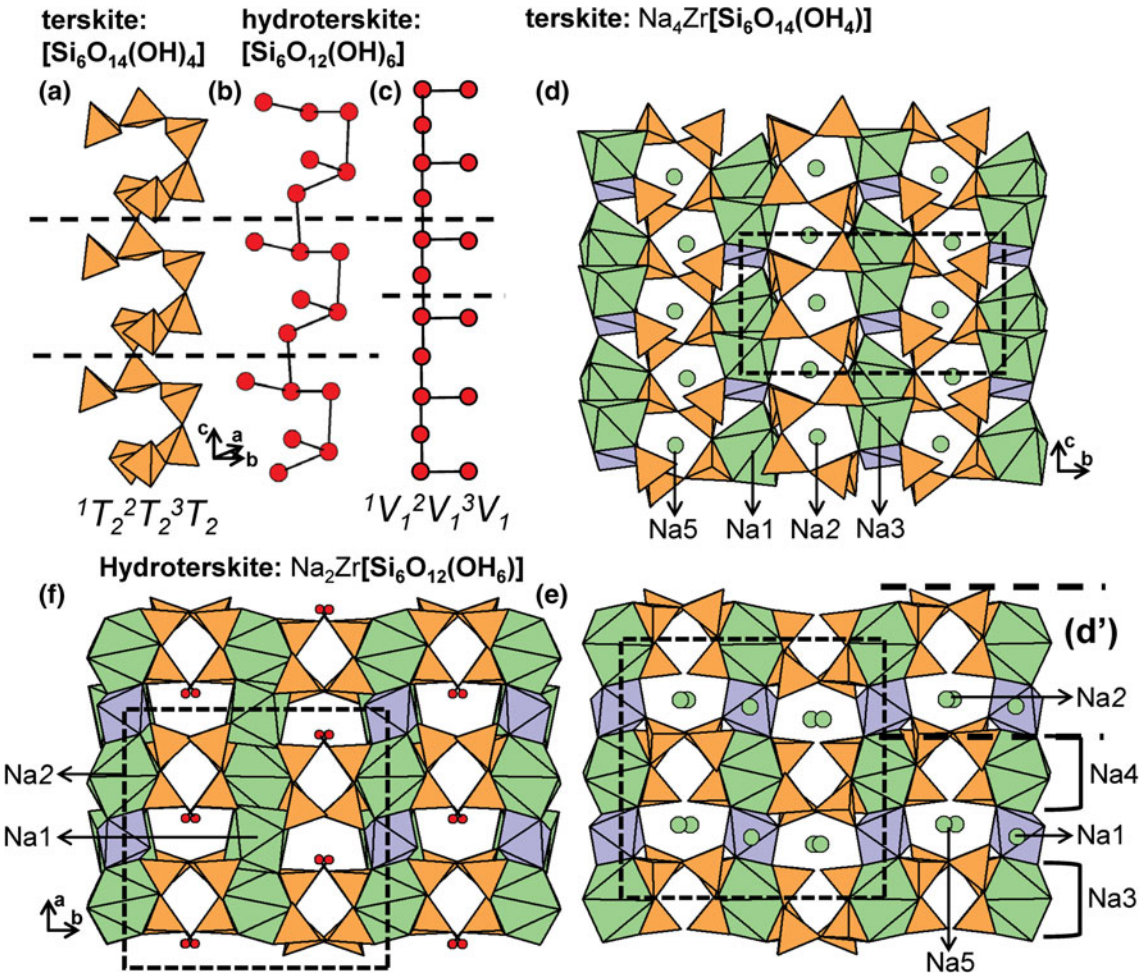

Fig. 95. (*a*) Tetrahedral and (*b*) ball-and-stick representation of the $^1T_2{}^2T_2{}^3T_2$ chain in **terskite** and **hydroterskite** and (*c*) a graphical representation of the $^1V_1{}^2V_1{}^3V_1$ chain. The structure of **terskite** projected (*d*) onto (100) and (*e*) along the **c**-axis where H atoms associated with $(OH)^-$ groups are omitted. The structure of **hydroterskite** projected (*f*) along the **c**-axis where one of three H sites associated with (OH) groups is shown which is replaced by Na^+ ions in **terskite**. Dashed black lines outline the geometrical and topological repeat unit of the chain and fine dashed black lines outline the unit cell.

https://doi.org/10.1180/mgm.2020.13 Published online by Cambridge University Press

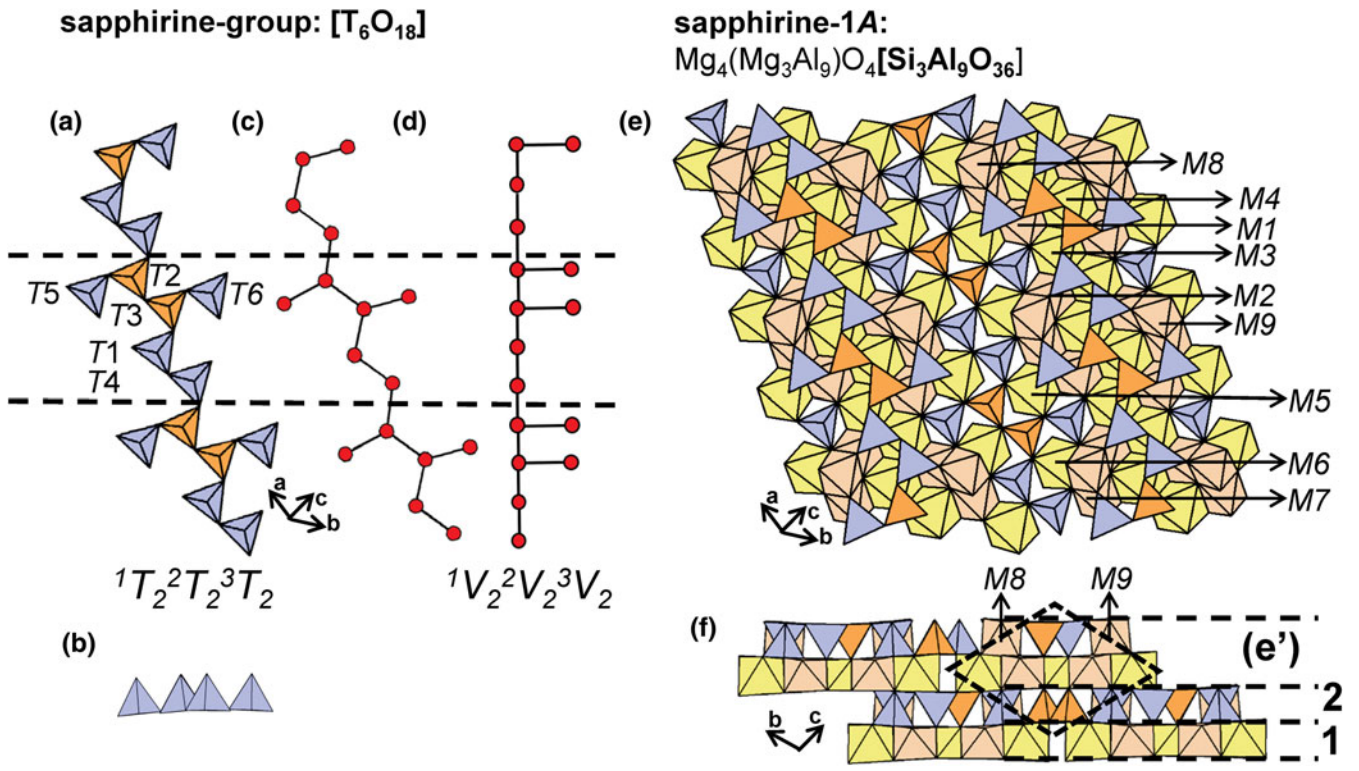

Fig. 96. (*a*, *b*) Tetrahedral representations of the chain in **sapphirine-group** minerals, (*c*) a ball-and-stick and (*d*) a graphical representation of the chain. The structure of **sapphirine-1*A*** projected (*a*) orthogonal to the **a**-axis and (*b*) along the **a**-axis where layer 1 (O-sheet) and layer 2 (H-sheet) are labelled. Dashed black lines outline the geometrical and topological repeat unit of the chain and fine dashed back lines outline the unit cell.

sheets (Fig. 103). As shown in Fig. 104, chain-ribbon stoichiometries overlap with sheet- and double-sheet stoichiometries over the range 3.0 ≥ O:T > 2.50. Table 11 shows the relevant minerals, the vertex connectivities and details of their structure (i.e. chain or ribbon, single-layer or double-layer sheet). The abundance of sheet silicates reaches a minima when O:T = 3 with only a single representative, **hyttsjöite**, and reaches a maxima where O:T = 2.5 with many representative structures including **micas**, **chlorites**

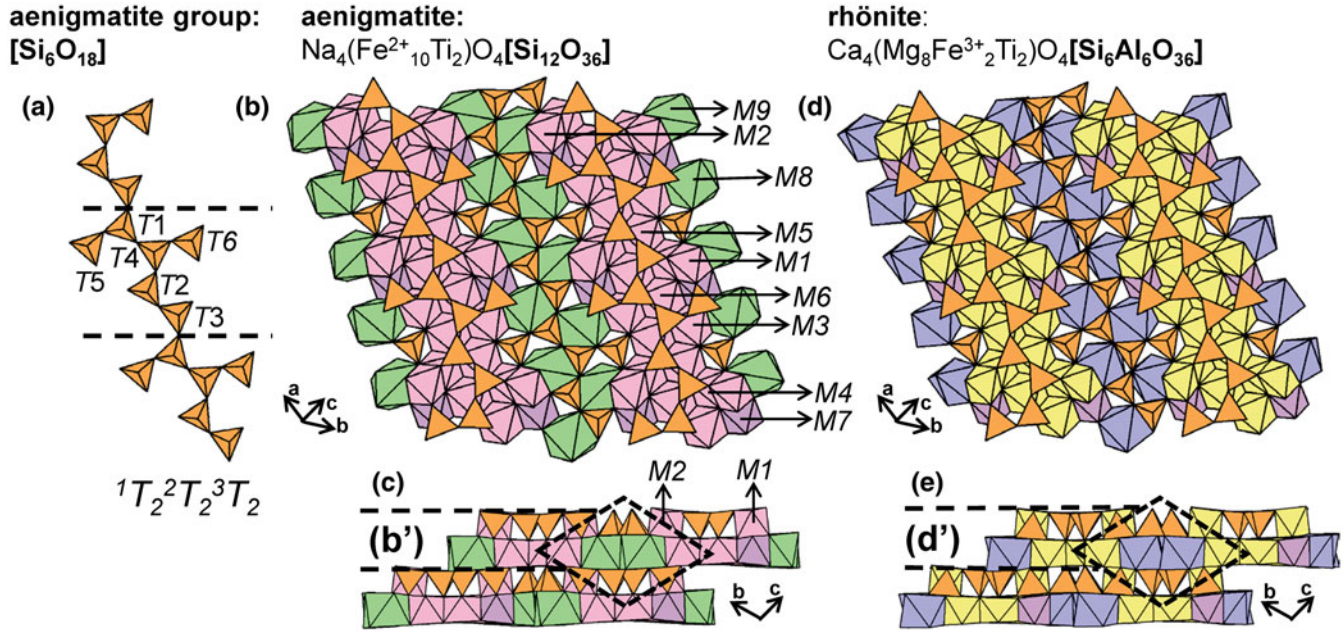

Fig. 97. (*a*) Tetrahedral representation of the chain in **aenigmatite-group** minerals. The structure of (*b*, *c*) **aenigmatite** and (*d*, *e*) **rhönite** projected (*b*, *d*) orthogonal to the **a**-axis and (*c*, *e*) along the **a**-axis. The *M*-site labelling for **aenigmatite** is applicable to **rhönite**. Dashed black lines outline the repeat unit of the chain and fine dashed black lines outline the unit cell.

https://doi.org/10.1180/mgm.2020.13 Published online by Cambridge University Press

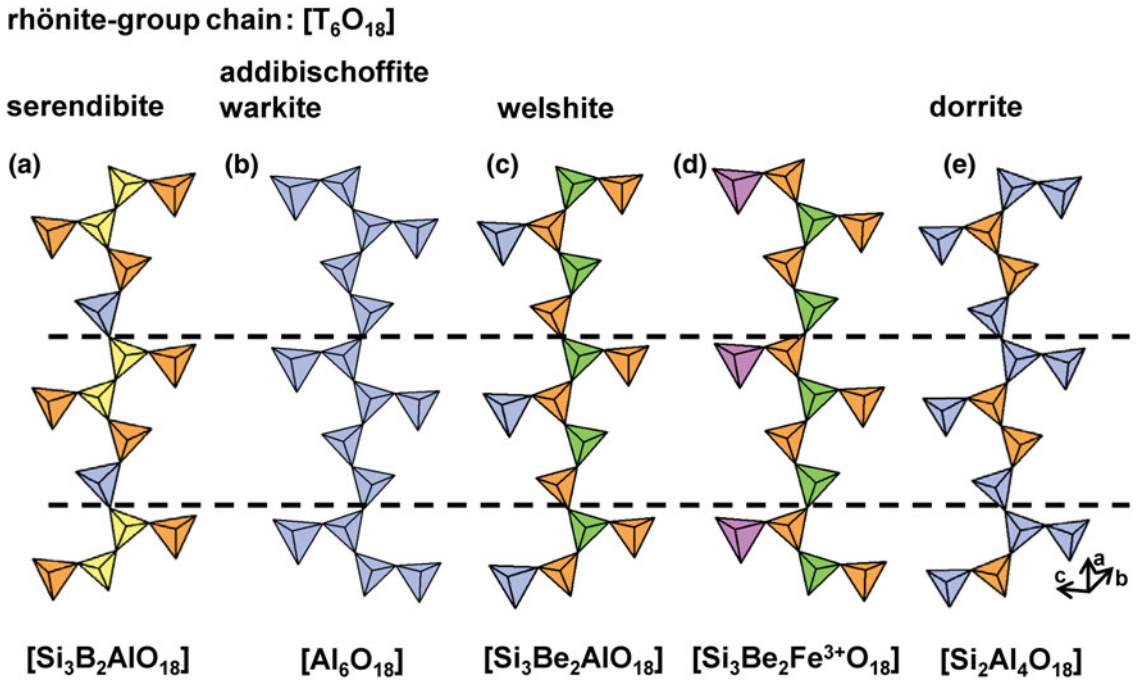

Fig. 98. Tetrahedral representations of the $^{1}T_{2}^{2}T_{2}^{3}T_{2}$ chains in (*a*) **serendibite**, (*b*) **addibischoffite** (**warkite**), (*c*, *d*) **welshite** and (*e*) **dorrite** projected orthogonal to the **a**-axis. Dashed black lines outline the geometrical repeat unit of the chains.

and **clay minerals**. The abundance of sheet silicates progressively decreases as the O:T ratio of the sheet decreases from 2.5–2.0 (Table 11). In general, the opposite trend is seen in chain-silicate minerals in which the abundance is relatively high where O:T = 2.75–3.0, and includes the chain and ribbon arrangements in **pyroxenes**- and, **sapphirine-group** and **amphibole**- and **astrophyllite-supergroup** minerals. For the most part, the abundance of chain silicates decreases as the O:T ratio of the chain decreases from 2.75–2.5 and is zero for O:T < 2.5 (Table 11).

Inspection of Table 11 shows that many chain and sheet structures have the same O:T ratio and the same or different $^{c}V_{r}$ expression. Single-sheet structures and chain and ribbon structures of the same O:T ratio tend to have the same $^{c}V_{r}$ expression (except for a possible difference in multiplicity), whereas double-sheet silicates

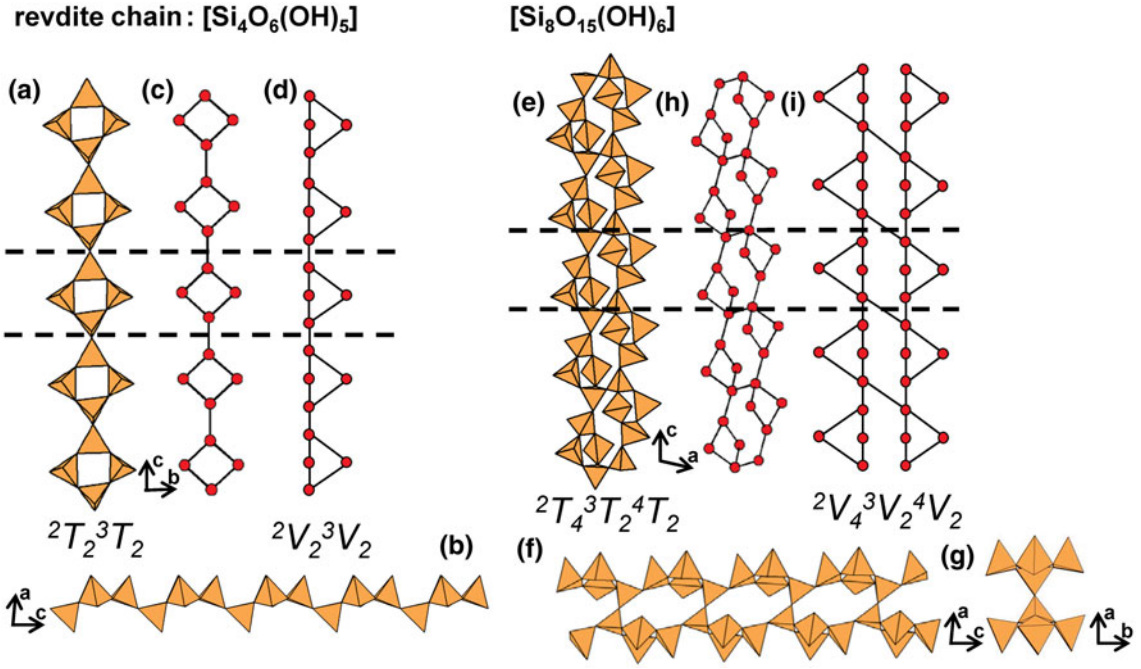

Fig. 99. (*a*, *b*) Tetrahedral representations of the $^{2}T_{2}^{3}T_{2}$ chain in **revdite** projected (*a*) onto (100) and (*b*) onto (010), (*c*) a ball-and-stick and (*d*) a graphical representation of the chain. (*e*, *f*, *g*) Tetrahedral representations of the $^{2}T_{4}^{3}T_{2}^{4}T_{2}$ ribbon in **revdite** projected (*e*, *f*) onto (010), (*g*) along the **c**-axis, (*h*) a ball-and-stick and (*i*) a graphical representation of the ribbon. Dashed black lines outline the geometrical and topological repeat unit of the chain and ribbon.

https://doi.org/10.1180/mgm.2020.13 Published online by Cambridge University Press

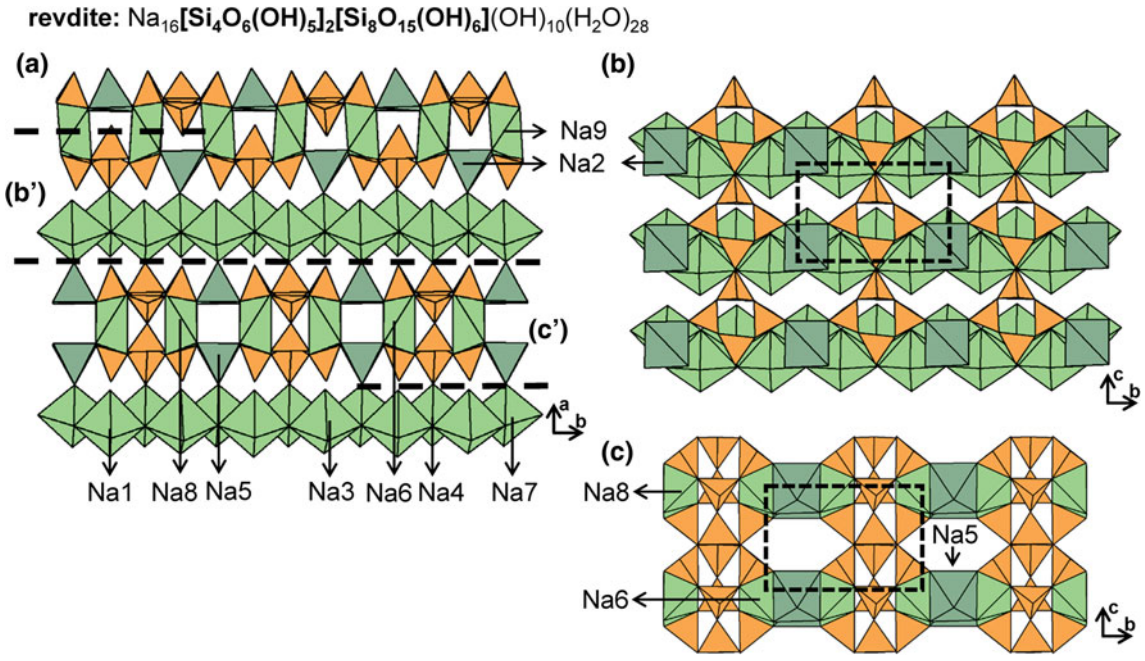

Fig. 100. The structure of **revdite** projected (*a*) along the **c**-axis, (*b*) onto (100), showing the linkage of $^{2}T_{2}{}^{3}T_{2}$ chains to the interstitial structure and (*c*) onto (100), showing the linkage of $^{2}T_{4}{}^{3}T_{2}{}^{4}T_{2}$ ribbons to the interstitial structure. The $^{[5]}Na^{+}$-polyhedra are dark green to differentiate them from Na^{+}-octahedra. Fine dashed black lines outline the unit cell and H atoms associated with $(OH)^{-}$ and (H_2O) groups are omitted for clarity.

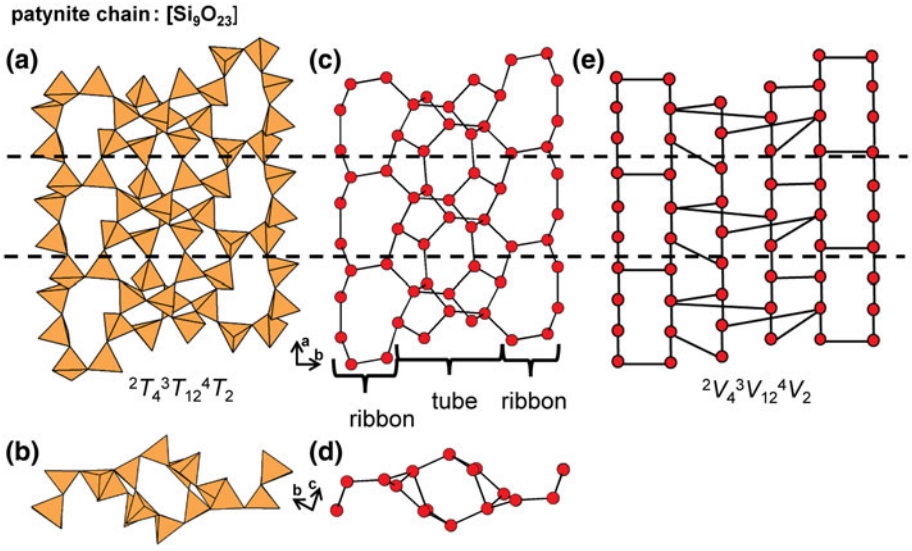

Fig. 101. (*a*, *b*) Tetrahedral representations of the ribbon-tube in **patynite** projected (*a*) onto (001), (*b*) along the **a**-axis, (*c*, *d*) a ball-and-stick and (*e*) a graphical representation of the ribbon-tube. Dashed black lines outline the geometrical and topological repeat unit of the ribbon-tube.

either (1) have different $^{c}V_{r}$ expressions compared to ribbons with the same O:T ratio (e.g. **altisite** and **lemoynite** and **natrolemoynite**), or (2) do not have chain, ribbon or tube analogues (e.g. **samfowlerite**, **tamaite**, **dmisteinbergite**). One-dimensional and two-dimensional polymerisations with the same values of $^{c}V_{r}$ have tetrahedra of the same connectivity but obviously the linkage of those tetrahedra is different. We will examine this issue in more detail in a future paper on the topology of chains, ribbons and tubes.

Structures with mixed polymerisations

Some of the minerals we are dealing with here have more than one type of silicate unit; these are listed in Table 12. We have divided them into two classes: (1) mixed one-dimensional polymerisations: chain, ribbon and tube structures; (2) mixed-dimension polymerisations: clusters, chain-ribbon-tubes and sheets.

In class (1), there are **vinogradovite**, **revdite**, **denisovite** and **charoite** with more than one type of one-dimensional polymerisation. For each $^{c}T_{r}$ expression, we can sum the values of r for each value of c and use the formula shown in Fig. 104 to calculate the net O:T for each mineral in Table 12. In some cases, we must multiply the r values of a given $^{c}T_{r}$ expression to ensure it conforms to the unit-cell contents of the respective mineral. **Vinogradovite** contains $^{2}T_{2}$ chains of stoichiometry $[Si_2O_6]^{4-}$ and $^{3}T_{4}$ ribbons of stoichiometry $[Si_3AlO_{10}]^{5-}$ in the ratio 2:1; there are equal numbers of tetrahedra in each unit: $2 \times [Si_2O_6]^{4-}$

https://doi.org/10.1180/mgm.2020.13 Published online by Cambridge University Press

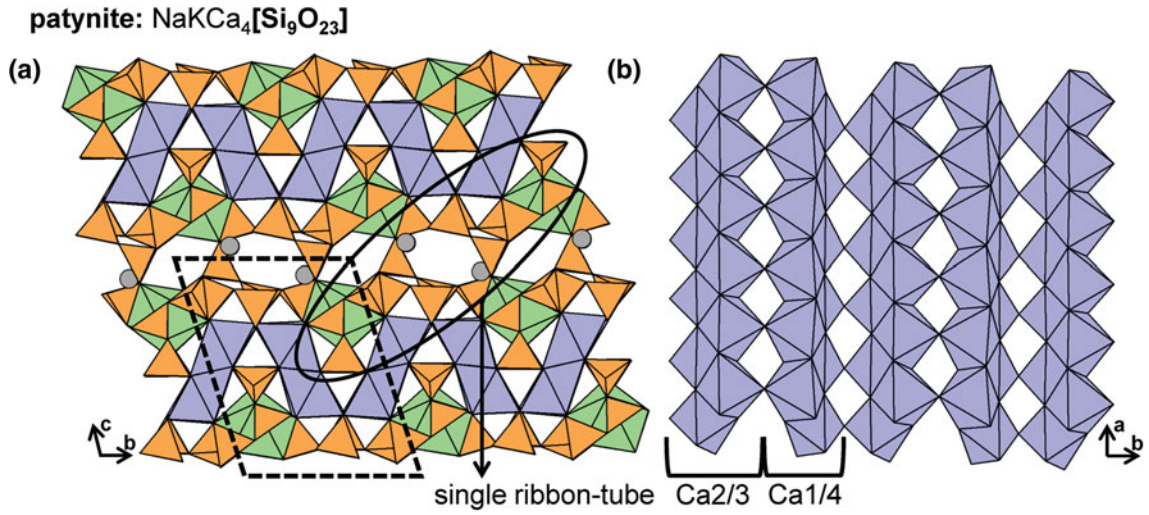

Fig. 102. The structure of **patynite** projected (*a*) along the **a**-axis and (*b*) onto [001]. Fine dashed black lines outline the unit cell.

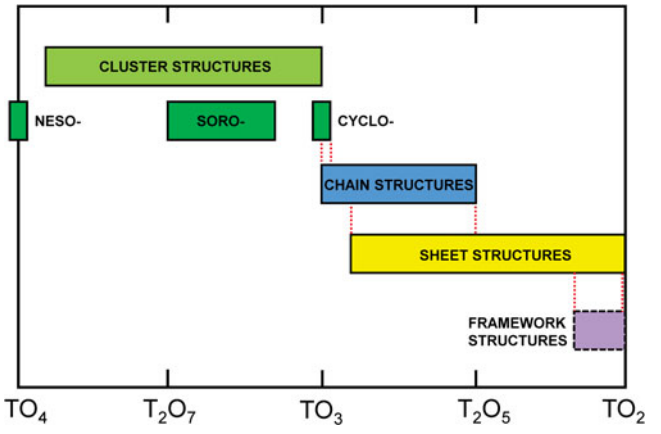

Fig. 103. The stoichiometric range of cluster, chain, sheet, and framework structures. Red dashed lines indicate ranges in which the stoichiometries of silicate units from different groups overlap. Framework-silicates are outlined by a black dashed line as the exact stoichiometric range for these units is unclear as these structures have yet to be described in detail.

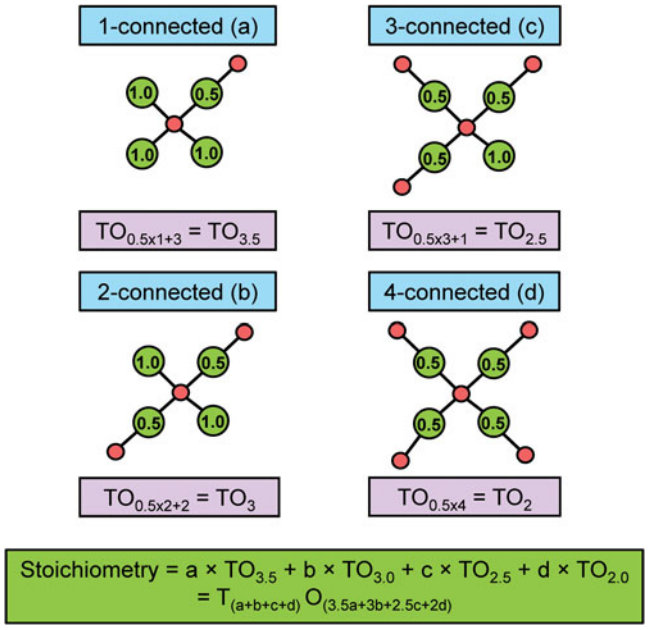

Fig. 104. Schematic illustrating the oxygen anion contribution of 1-, 2-, 3-, 4-connected $[TO_4]^{n-}$ tetrahedra and an associated formula to calculate the stoichiometry of any silicate unit composed of $[TO_4]^{n-}$ tetrahedra.

($^2T_2$) + $[Si_3AlO_{10}]^{5-}$ ($^3T_4$) for a net O:T ratio of $(3.0 \times 4 + 2.5 \times 4) / 8 = 2.75$. **Revdite** contains $^2T_2{}^3T_2$ chains of stoichiometry $[Si_4O_6(OH)_5]^{1-}$ and $^2T_4{}^3T_2{}^4T_2$ ribbons of stoichiometry $[Si_8O_{15}(OH)_6]^{4-}$ in the ratio 2:1; again there are equal numbers of tetrahedra in each unit: $2 \times [Si_4O_6(OH)_5]^{1-}$ ($^2T_2{}^3T_2$) + $[Si_8O_{15}(OH)_6]^{4-}$ ($^2T_4{}^3T_2{}^4T_2$) for a net O:T ratio of $(3.0 \times 8 + 2.5 \times 6 + 2.0 \times 2) / 16 = 2.69$. **Denisovite** contains $^2T_4{}^3T_2$ ribbons of the stoichiometry $[Si_6O_{11}(O,OH)_6]$ and $^3T_{12}$ tubes of the stoichiometry $[Si_{12}O_{30}]^{12-}$ in the ratio 3:1 and there is not equal numbers of tetrahedra in each unit: 3 x $[Si_6O_{11}(O,OH)_6]$ ($^2T_4{}^3T_2$) + $[Si_{12}O_{30}]^{12-}$ ($^3T_{12}$) for a net O:T of $(3.0 \times 12 + 2.5 \times 18) / 30 = 2.70$. **Charoite** contains $^2T_4{}^3T_2$ ribbons and $^3T_{12}$ and $^3T_{17}$ tubes in the ratio 1:1:1 for a net O:T ratio of $(3.0 \times 4 + 2.5 \times 31) / 35 = 2.56$. **Lintisite** is a very interesting structure. It contains $^2T_2$ chains of stoichiometry $[Si_2O_6]^{4-}$ and $^4T_4{}^6T_2$ ribbons of stoichiometry $[Li_2Si_4O_{12}]^{6-}$. As the $(LiO_4)^{7-}$ groups share edges in this ribbon (Fig. 6*d*), the $(LiO_4)^{7-}$-tetrahedron is 6-connected, a possibility not considered in Fig. 104. The result is that the $[Li_2Si_4O_{12}]^{6-}$ ribbon has an O:T ratio of 12:6 = 2.0 and the $[Si_2O_6]^{4-}$ chain has an O:T ratio of 3. Here, each anion associated with the ^6T_r Li^+-tetrahedra contributes 0.33 O^{2-} atoms to the central Li^+ cation and each $(LiO_4)^{7-}$-tetrahedron contributes $4(0.33) = 1.33$ O^{2-} atoms to the net O:T ratio of **lintisite**. The ^4T_r Si^{4+}-tetrahedra contribute 2.33 O^{2-} to the net O:T rather than the typical 2.0 O^{2-} as one of the anions of each Si^{4+}-tetrahedra link to two Li^+-tetrahedra and therefore contributes 0.33 O^{2-} to the central Si^{4+} cation, it follows that the net O:T ratio for **lintisite** is $(3.0 \times 4 + 2.33 \times 4 + 1.33 \times 2) / 10 = 2.4$. **Punkaruaivite** contains a topologically identical $^4T_4{}^6T_2$, $[Li_2Si_4O_{10}(OH)_2]^{4-}$ ribbon and has the same O:T = 2.4 (Table 12), exceeding the minimum O:T = 2.5 in tube silicates.

https://doi.org/10.1180/mgm.2020.13 Published online by Cambridge University Press

Table 10. Minerals and selected synthetic compounds with chains, ribbons and tubes.

O:T	$^{c}T_r$	Mineral	Ideal structural formula	Unit stoichiometry	$^{c}V_r$	C/R/T	Figs
3.06	$^{2}T_4{}^{3}T_2$	Yuksporite	$(Sr,Ba)_2K_4(Ca,Na)_{14}(\square,Mn,Fe)\{(Ti,Nb)_4(O,OH)_4\mathbf{[Si_6O_{17}]_2[Si_2O_7]_3}\}(H_2O,OH)_3$	$[SiO_{2.83}]$	$^{2}V_4{}^{3}V_2$	R	80
	$^{1}T_2{}^{\star}$	〃 〃		$[SiO_{3.5}]$	$^{1}V_2$	Cl	
3.0	$^{2}T_1$	Synthetic	$\mathbf{[GeO_3]}$	$[GeO_3]$	$^{2}V_1$	C	4
3.0	$^{2}T_2$	Pyroxenes opx/cpx	$XY\mathbf{[Si_2O_6]}$	$[SiO_3]$	$^{2}V_1$	C	5
3.0	$^{2}T_2$	Eliseevite	$Na_{1.5}LiTi_2\mathbf{[Si_4O_{10.5}(OH)_{1.5}]}O_2(H_2O)_2$	$[SiO_{2.63}(OH)_{0.37}$	$^{2}V_1$	C	–
3.0	$^{2}T_2$	Kukisvumite	$Na_6ZnTi_4\mathbf{[Si_8O_{24}]}O_4(H_2O)_4$	$[SiO_3]$	$^{2}V_1$	C	–
3.0	$^{2}T_2$	Manganokukisvumite	$Na_6MnTi_4\mathbf{[Si_8O_{24}]}O_4(H_2O)_4$	$[SiO_3]$	$^{2}V_1$	C	–
3.0	$^{2}T_2$	Carpholite	$\square Mn_2Al_4\mathbf{[Si_2O_6]_2}(OH)_4(OH)_4$	$[SiO_3]$	$^{2}V_1$	C	7*a*,*b*
3.0	$^{2}T_2$	Balipholite	$BaMgLiAl_4\mathbf{[Si_2O_6]_2}(OH)_4(OH)_4$	$[SiO_3]$	$^{2}V_1$	C	–
3.0	$^{2}T_2$	Ferrocarpholite	$\square(Fe^{2+},Mg)_2Al_4\mathbf{[Si_2O_6]_2}(OH)_4(OH)_4$	$[SiO_3]$	$^{2}V_1$	C	–
3.0	$^{2}T_2$	Magnesiocarpholite	$\square(Mg,Fe^{2+})_2Al_4\mathbf{[Si_2O_6]_2}(OH)_4(OH)_4$	$[SiO_3]$	$^{2}V_1$	C	–
3.0	$^{2}T_2$	Vanadiocarpholite	$\square Mn_2V_2Al_2\mathbf{[Si_2O_6]_2}(OH)_4(OH)_4$	$[SiO_3]$	$^{2}V_1$	C	–
3.0	$^{2}T_2$	Potassiccarpholite	$KMnLiAl_4\mathbf{[Si_2O_6]_2}(OH)_4F_4$	$[SiO_3]$	$^{2}V_1$	C	–
3.0	$^{2}T_2$	Nchwaningite	$Mn_4^{2+}\mathbf{[Si_2O_6]}(OH)_4\ (H_2O)_2$	$[SiO_3]$	$^{2}V_1$	C	7*c*,*d*
3.0	$^{2}T_2$	Lorenzenite	$Na_2Ti_2\mathbf{[Si_2O_6]}O_3$	$[SiO_3]$	$^{2}V_1$	C	8*a*,*b*
3.0	$^{2}T_2$	Shattuckite	$Cu_5\mathbf{[Si_2O_6]_2}(OH)_2$	$[SiO_3]$	$^{2}V_1$	C	8*c*–*e*
3.0	$^{2}T_2$	Capranicaite	$(K,\square)(Ca,Na)Al_4B_4\mathbf{[Si_2O_6]}O_{12}$	$[SiO_3]$	$^{2}V_1$	C	–
3.0	$^{2}T_2$	Yegorovite	$Na_4\mathbf{[Si_2O_4(OH)_2]_2}(H_2O)_7$	$[SiO_2(OH)]$	$^{2}V_1$	C	9*a*–*f*
3.0	$^{2}T_2$	Aerinite	$Ca_6FeAl(Fe,Mg)_2(Al,Mg)_6\mathbf{[Si_{12}O_{36}]}(OH)_{12}H)(H_2O)_{12}(CO_3)$	$[SiO_3]$	$^{2}V_1$	C	10*a*–*d*
3.0	$^{2}T_2$	Synthetic	$Ba_2\mathbf{[Si_2O_6]}$	$[SiO_3]$	$^{2}V_1$	C	–
3.0	$^{2}T_2$	Synthetic	$Li_4\mathbf{[Si_2O_6]}$	$[SiO_3]$	$^{2}V_1$	C	–
3.0	$^{2}T_2$	Synthetic	$Ag_4\mathbf{[Si_2O_6]}$	$[SiO_3]$	$^{2}V_1$	C	–
3.0	$^{2}T_2$	Synthetic	$Na_4\mathbf{[Si_2O_6]}$	$[SiO_3]$	$^{2}V_1$	C	–
3.0	$^{2}T_2$	Synthetic	$Na_2Zn\mathbf{[Si_2O_6]}$	$[SiO_3]$	$^{2}V_1$	C	–
3.0	$^{2}T_2$	Synthetic	$Na_2Ba\mathbf{[Si_2O_6]}$	$[SiO_3]$	$^{2}V_1$	C	–
3.0	$^{2}T_3$	Wollastonite (1*A*, 3*A*, 4*A*, 5*A*, 7*A*)	$Ca\mathbf{[Si_3O_9]}$	$[SiO_3]$	$^{2}V_1$	C	11
3.0	$^{2}T_3$	Wollastonite (2*M*)	$Ca_3\mathbf{[Si_3O_9]}$	$[SiO_3]$	$^{2}V_1$	C	11
3.0	$^{2}T_3$	Dalnegorskite	$Ca_2Ca_2MnCa\mathbf{[Si_3O_9]_2}$	$[SiO_3]$	$^{2}V_1$	C	–
3.0	$^{2}T_3$	Bustamite	$(Ca,Mn^{2+})_2Ca_2Mn^{2+}Ca\mathbf{[Si_3O_9]_2}$	$[SiO_3]$	$^{2}V_1$	C	12*a*,*b*
3.0	$^{2}T_3$	Ferrobustamite	$(Ca,Fe^{2+})_2Ca_2Fe^{2+}Ca\mathbf{[Si_3O_9]_2}$	$[SiO_3]$	$^{2}V_1$	C	12*c*,*d*
3.0	$^{2}T_3$	Mendigite	$Mn_2^{2+}\ Mn_2^{2+}\ Mn^{2+}Ca\mathbf{[Si_3O_9]_2}$	$[SiO_3]$	$^{2}V_1$	C	12*e*,*f*
3.0	$^{2}T_3$	Pectolite	$NaCa_2\mathbf{[Si_3O_8(OH)]}$	$[SiO_{2.7}(OH)_{0.3}]$	$^{2}V_1$	C	13*a*,*b*
3.0	$^{2}T_3$	Schizolite	$Na(Ca,Mn)_2\mathbf{[Si_3O_8(OH)]}$	$[SiO_{2.7}(OH)_{0.3}]$	$^{2}V_1$	C	13*c*,*d*
3.0	$^{2}T_3$	Murakamiite	$LiCa_2\mathbf{[Si_3O_8(OH)]}$	$[SiO_{2.7}(OH)_{0.3}]$	$^{2}V_1$	C	13*e*,*f*
3.0	$^{2}T_3$	Tanohataite	$LiMn_2^{2+}\mathbf{[Si_3O_8(OH)]}$	$[SiO_{2.7}(OH)_{0.3}]$	$^{2}V_1$	C	13*g*,*h*
3.0	$^{2}T_3$	Serandite	$NaMn_2^{2+}\ \mathbf{[Si_3O_8(OH)]}$	$[SiO_{2.7}(OH)_{0.3}]$	$^{2}V_1$	C	13*i*,*j*
3.0	$^{2}T_3$	Barrydawsonite-(Y)	$Na_2Ca_2(Na,Y)_2\mathbf{[Si_3O_8(OH)]_2}$	$[SiO_{2.7}(OH)_{0.3}]$	$^{2}V_1$	C	–
3.0	$^{2}T_3$	Vistepite	$SnMn_4\mathbf{[B_2Si_4O_{16}(OH)_2]}$	$[(B_{0.3}Si_{0.7})O_{2.7}(OH)_{0.3}]$	$^{2}V_1$	C	14*a*,*b*
3.0	$^{2}T_3$	Cascandite	$CaSc\mathbf{[Si_3O_8(OH)]}$	$[SiO_{2.7}(OH)_{0.3}]$	$^{2}V_1$	C	14*c*,*d*
3.0	$^{2}T_3$	Hilairite	$Na_2Zr\mathbf{[Si_3O_9]}(H_2O)_3$	$[SiO_3]$	$^{2}V_1$	C	15
3.0	$^{2}T_3$	Calciohilairite	$CaZr\mathbf{[Si_3O_9]}(H_2O)_3$	$[SiO_3]$	$^{2}V_1$	C	–
3.0	$^{2}T_3$	Komkovite	$BaZr\mathbf{[Si_3O_9]}(H_2O)_3$	$[SiO_3]$	$^{2}V_1$	C	–
3.0	$^{2}T_3$	Sazykinaite-(Y)	$Na_3YZr\mathbf{[Si_6O_{18}]}(H_2O)_6$	$[SiO_3]$	$^{2}V_1$	C	–
3.0	$^{2}T_3$	Pyatenkoite-(Y)	$Na_3YTi\mathbf{[Si_6O_{18}]}(H_2O)_6$	$[SiO_3]$	$^{2}V_1$	C	–
3.0	$^{2}T_3$	Synthetic	$K_{1.81}Na_{0.09}H_{0.1}Zr\mathbf{[Si_3O_9]}$	$[SiO_3]$	$^{2}V_1$	C	–
3.0	$^{2}T_3$	Synthetic	$Rb_{1.8}Na_{0.2}Zr\mathbf{[Si_3O_9]}(H_2O)_{0.35}$	$[SiO_3]$	$^{2}V_1$	C	–
3.0	$^{2}T_3$	Synthetic	$Pb_{0.6}Na_{0.4}H_{0.4}Zr\mathbf{[Si_3O_9]}(H_2O)_3$	$[SiO_3]$	$^{2}V_1$	C	–
3.0	$^{2}T_3$	Synthetic	$SrZr\mathbf{[Si_3O_9]}(H_2O)_{1.5}$	$[SiO_3]$	$^{2}V_1$	C	–
3.0	$^{2}T_3$	Synthetic	$Na_{1.14}Cs_{0.55}H_{0.31}Zr\mathbf{[Si_3O_9]}(H_2O)_{0.9}$	$[SiO_3]$	$^{2}V_1$	C	–
3.0	$^{2}T_3$	Kamenevite	$K_2Ti\mathbf{[Si_3O_9]}(H_2O)$	$[SiO_3]$	$^{2}V_1$	C	–
3.0	$^{2}T_3$	Umbite	$K_2Zr\mathbf{[Si_3O_9]}(H_2O)$	$[SiO_3]$	$^{2}V_1$	C	16
3.0	$^{2}T_3$	Paraumbite	$K_3HZr_2\mathbf{[Si_6O_{18}]}(H_2O)_3$	$[SiO_3]$	$^{2}V_1$	C	16
3.0	$^{2}T_3$	Kostylevite	$K_2Zr\mathbf{[Si_3O_9]}(H_2O)$	$[SiO_3]$	$^{2}V_1$	C	–
3.0	$^{2}T_3$	Synthetic	$(Cs_{1.37}K_{0.45}H_{0.18})_2\mathbf{[Si_3O_9]}(H_2O)_{0.98}$	$[SiO_3]$	$^{2}V_1$	C	–
3.0	$^{2}T_3$	Foshagite	$Ca_4\mathbf{[Si_3O_9]}(OH)_2$	$[SiO_3]$	$^{2}V_1$	C	17*a*,*b*
3.0	$^{2}T_3$	Hillebrandite	$Ca_6\mathbf{[Si_3O_9]}(OH)_6$	$[SiO_3]$	$^{2}V_1$	C	–
3.0	$^{2}T_3$	Jennite	$Ca_9\mathbf{[Si_3O_9]_2}(OH)_8(H_2O)_8$	$[SiO_3]$	$^{2}V_1$	C	17*c*,*d*
3.0	$^{2}T_3$	'Metajennite'	$Ca_9\mathbf{[Si_3O_9]_2}(OH)_8(H_2O)_2$	$[SiO_3]$	$^{2}V_1$	C	–
3.0	$^{2}T_3$	Plombière (Tobermorite-14Å)	$Ca_5\mathbf{[Si_6O_{16}(OH)_2]}(H_2O)_2{\cdot}(Ca(H_2O)_5)]$	$[SiO_{2.7}(OH)_{0.3}]$	$^{2}V_1$	C	17*e*,*f*
3.0	$^{2}T_3$	Riversideite MDO_1 (Tobermorite-9.3Å)	$Ca_5\mathbf{[Si_6O_{16}(OH)_2]}$	$[SiO_3]$	$^{2}V_1$	C	–
3.0	$^{2}T_3$	Riversideite MDO_2 (Tobermorite-9.3Å)	$Ca_5\mathbf{[Si_6O_{16}(OH)_2]}$	$[SiO_3]$	$^{2}V_1$	C	–
3.0	$^{2}T_3$	Whelanite	$Cu_2Ca_6\mathbf{[Si_6O_{17}(OH)]}(CO_3)(OH)_3(H_2O)_2]$		$^{2}V_1$	C	18*a*,*b*
3.0	$^{2}T_4$	Batisite	$BaNa_2Ti_2\mathbf{[Si_4O_{12}]}O_2$	$[SiO_3]$	$^{2}V_1$	C	19
3.0	$^{2}T_4$	Scherbakovite	$K_2NaTi_2\mathbf{[Si_4O_{12}]}(O,OH)_2$	$[SiO_3]$	$^{2}V_1$	C	–
3.0	$^{2}T_4$	Noonkanbahite	$BaKNaTi_2\mathbf{[Si_4O_{12}]}O_2$	$[SiO_3]$	$^{2}V_1$	C	–

(*Continued*)

https://doi.org/10.1180/mgm.2020.13 Published online by Cambridge University Press

Table 10. (*Continued.*)

O:T	$^{c}T_r$	Mineral	Ideal structural formula	Unit stoichiometry	$^{c}V_r$	C/R/T	Figs
3.0	$^{2}T_4$	Haradaite	$Sr_2V_2^{4+}$**[Si_4O_{12}]**O_2]	[SiO_3]	$^{2}V_1$	C	20*a*,*b*
3.0	$^{2}T_4$	Suzukiite	$Ba_2V_2^{4+}$**[Si_4O_{12}]**O_2]	[SiO_3]	$^{2}V_1$	C	–
3.0	$^{2}T_4$	Ohmilite	$Sr_3(Ti,Fe^{3+})$**[Si_4O_{12}]**$(O,OH)(H_2O)_{2-3}$	[SiO_3]	$^{2}V_1$	C	20*c*,*d*
3.0	$^{2}T_4$	Fukalite (MDO1)	Ca_8**[Si_4O_{12}]**$(OH)_4(CO_3)_2$	[SiO_3]	$^{2}V_1$	C	21
3.0	$^{2}T_4$	Taikanite	$BaSr_2Mn_2^{3+}$**[Si_4O_{12}]**O_2	[SiO_3]	$^{2}V_1$	C	22
3.0	$^{2}T_4$	Krauskopfite	Ba_2**[$Si_4O_{10}(OH)_2$]**$(H_2O)_4$	[$SiO_2(OH)$]	$^{2}V_1$	C	23
3.0	$^{2}T_4$	Balangeroite-*2M(1A)*	$(Mg,Fe^{2+},Fe^{3+})_{42}$**[$Si_4O_{12}$]**$_4O_6(OH)_{40}$	[SiO_3]	$^{2}V_1$	C	24
3.0	$^{2}T_4$	Gageite-*2M(1A)*	$(Mn^{2+},Mg)_{42}$**[Si_4O_{12}]**$_4O_6(OH)_{40}$	[SiO_3]	$^{2}V_1$	C	24
3.0	$^{2}T_5$	Rhodonite	$CaMn_4$**[Si_5O_{15}]**	[SiO_3]	$^{2}V_1$	C	25,26*c*,*d*
3.0	$^{2}T_5$	Vittinkiite	Mn_5**[Si_5O_{15}]**	[SiO_3]	$^{2}V_1$	C	26*a*,*b*
3.0	$^{2}T_5$	Ferrorhodonite	$CaMn_3Fe^{2+}$**[Si_5O_{15}]**	[SiO_3]	$^{2}V_1$	C	25*e*,*f*
3.0	$^{2}T_5$	Marsturite	$NaCaMn_3^{2+}$**[$Si_5O_{14}(OH)$]**	[$SiO_{2.8}(OH)_{0.2}$]	$^{2}V_1$	C	27*a*,*b*
3.0	$^{2}T_5$	Lithiomarsturite	$LiCa_2Mn_2^{2+}$**[$Si_5O_{14}(OH)$]**	[$SiO_{2.8}(OH)_{0.2}$]	$^{2}V_1$	C	27*c*,*d*
3.0	$^{2}T_5$	Nambulite	$(Li,Na)Mn_4^{2+}$**[$Si_5O_{14}(OH)$]**	[$SiO_{2.8}(OH)_{0.2}$]	$^{2}V_1$	C	27*e*,*f*
3.0	$^{2}T_5$	Natronambulite	$(Na,Li)Mn_4^{2+}$**[$Si_5O_{14}(OH)$]**	[$SiO_{2.8}(OH)_{0.2}$]	$^{2}V_1$	C	27*g*,*h*
3.0	$^{2}T_5$	Synthetic	Mn_5^{2+}**[Si_5O_{15}]**	[SiO_3]	$^{2}V_1$	C	–
3.0	$^{2}T_5$	Synthetic	$LiMn_4^{2+}$**[$Si_5O_{14}(OH)$]**	[SiO_3]	$^{2}V_1$	C	–
3.0	$^{2}T_5$	Babingtonite	$Ca_2(Fe^{2+},Mn^{2+})Fe^{3+}$**[$Si_5O_{14}(OH)$]**	[$SiO_{2.8}(OH)_{0.2}$]	$^{2}V_1$	C	28
3.0	$^{2}T_5$	Manganbabingtonite	$Ca_2(Mn^{2+},Fe^{2+})Fe^{3+}$**[$Si_5O_{14}(OH)$]**	[$SiO_{2.8}(OH)_{0.2}$]	$^{2}V_1$	C	28
3.0	$^{2}T_5$	Scandiobabingtonite	$Ca_2(Fe^{2+},Mn^{2+})Sc$**[$Si_5O_{14}(OH)$]**	[$SiO_{2.8}(OH)_{0.2}$]	$^{2}V_1$	C	–
3.0	$^{2}T_5$	Santaclaraite	$CaMn_4^{2+}$**[$Si_5O_{14}(OH)$]**$(OH)(H_2O)$]	[$SiO_{2.8}(OH)_{0.2}$]	$^{2}V_1$	C	–
3.0	$^{2}T_6$	Stokesite	Ca_2Sn_2**[Si_6O_{18}]**$(H_2O)_4$	[SiO_3]	$^{2}V_1$	C	29
3.0	$^{2}T_6$	Gaidonnayite	Na_4Zr_2**[Si_6O_{18}]**$(H_2O)_4$	[SiO_3]	$^{2}V_1$	C	–
3.0	$^{2}T_6$	Georgechaoite	$Na_2K_2Zr_2$**[Si_6O_{18}]**$(H_2O)_4$	[SiO_3]	$^{2}V_1$	C	30
3.0	$^{2}T_6$	Synthetic	Cs_4Zr_2**[Si_6O_{18}]**$(H_2O)_4$	[SiO_3]	$^{2}V_1$	C	–
3.0	$^{2}T_6$	Synthetic	K_8Sr_2**[Si_6O_{18}]**	[SiO_3]	$^{2}V_1$	C	–
3.0	$^{2}T_7$	Pyroxferroite	Fe_7^{2+}**[Si_7O_{21}]**	[SiO_3]	$^{2}V_1$	C	–
3.0	$^{2}T_7$	Pyroxmangite	Mn_7^{2+}**[Si_7O_{21}]**	[SiO_3]	$^{2}V_1$	C	31
3.0	$^{2}T_9$	Synthetic Ferrosilite III	Fe_9^{2+}**[Si_9O_{27}]**	[SiO_3]	$^{2}V_1$	C	32
3.0	$^{2}T_{12}$	Alamosite	Pb_{12}**[$Si_{12}O_{36}$]**	[SiO_3]	$^{2}V_1$	C	33
3.0	$^{2}T_{24}$	Synthetic	$Na_{24}Y_8$**[$Si_{24}O_{72}$]**	[SiO_3]	$^{2}V_1$	C	34
3.0	$^{1}T_2{}^{3}T_2$	Astrophyllite	$K_2NaFe_7^{2+}Ti_2$**[Si_4O_{12}]**$_2O_2(OH)_4F$	[SiO_3]	$^{1}V_1{}^{3}V_1$	C	55,56
3.0	$^{1}T_2{}^{3}T_2$	Bulgakite	$Li_2(Ca,Na)Fe_7^{2+}Ti_2$**[Si_4O_{12}]**$_2O_2(OH)_4(F,O)(H_2O)_2$	[SiO_3]	$^{1}V_1{}^{3}V_1$	C	55
3.0	$^{1}T_2{}^{3}T_2$	Nalivkinite	$Li_2NaFe_7^{2+}Ti_2$**[Si_4O_{12}]**$_2O_2(OH)_4F$	[SiO_3]	$^{1}V_1{}^{3}V_1$	C	55
3.0	$^{1}T_2{}^{3}T_2$	Niobophyllite	$K_2NaFe_7^{2+}(Nb,Ti)_2$**[Si_4O_{12}]**$_2O_2(OH)_4(O,F)$	[SiO_3]	$^{1}V_1{}^{3}V_1$	C	55
3.0	$^{1}T_2{}^{3}T_2$	Tarbagataite	$(K,\square)CaFe_7^{2+}Ti_2$**[$Si_4O_{12}$]**$_2O_2(OH)_4(OH)$	[SiO_3]	$^{1}V_1{}^{3}V_1$	C	55
3.0	$^{1}T_2{}^{3}T_2$	Zircophyllite	$K_2NaFe_7^{2+}Zr_2$**[Si_4O_{12}]**$_2O_2(OH)_4F$	[SiO_3]	$^{1}V_1{}^{3}V_1$	C	55
3.0	$^{1}T_2{}^{3}T_2$	Kupletskite-1*A* (2*M*)	$K_2NaMn_7^{2+}Ti_2$**[Si_4O_{12}]**$_2O_2(OH)_4F$	[SiO_3]	$^{1}V_1{}^{3}V_1$	C	55
3.0	$^{1}T_2{}^{3}T_2$	Kupletskite-(Cs)	$Cs_2NaMn_7^{2+}Ti_2$**[Si_4O_{12}]**$_2O_2(OH)_4F$	[SiO_3]	$^{1}V_1{}^{3}V_1$	C	55
3.0	$^{1}T_2{}^{3}T_2$	Niobokupletskite	$K_2NaMn_7(Nb,Ti)_2$**[Si_4O_{12}]**$_2O_2(OH)_4(O,F)$	[SiO_3]	$^{1}V_1{}^{3}V_1$	C	55
3.0	$^{1}T_2{}^{3}T_2$	Laverovite	$K_2NaMn_7Zr_2$**[Si_4O_{12}]**$_2O_2(OH)_4F$	[SiO_3]	$^{1}V_1{}^{3}V_1$	C	55
3.0	$^{1}T_2{}^{3}T_2$	Devitoite	$Ba_6Fe_7^{2+}Fe_2^{3+}$**[Si_4O_{12}]**$_2(PO_4)_2(CO_3)O_2(OH)_4$	[SiO_3]	$^{1}V_1{}^{3}V_1$	C	55,57
3.0	$^{1}T_2{}^{3}T_2$	Lobanovite	$K_2Na(Fe_4^{2+}Mg_2Na)Ti_2$**[$Si_4O_{12}$]**$_2O_2(OH)_4$	[SiO_3]	$^{1}V_1{}^{3}V_1$	C	55
3.0	$^{1}T_2{}^{3}T_2$	Sveinbergeite	$(H_2O)_2(Ca(H_2O))(Fe_6^{2+}Fe^{3+})Ti_2$**[$Si_4O_{12}$]**$_2O_2(OH)_4((OH)H_2O))$	[SiO_3]	$^{1}V_1{}^{3}V_1$	C	55
3.0	$^{1}T_2{}^{3}T_2$	Heyerdahlite	$Na_3Mn_7Ti_2$**[Si_4O_{12}]**$_2O_2(OH)_4F(H_2O)_2$	[SiO_3]	$^{1}V_1{}^{3}V_1$	C	55
3.0	$^{1}T_1{}^{2}T_3{}^{3}T_1$	Surinamite	$(Mg,Fe^{2+})_3(Al,Fe^{3+})_3O$**[$AlBeSi_3O_{15}$]**	[$Si_{0.60}Al_{0.2}Be_{0.2}O_3$]	$^{1}V_1{}^{2}V_3{}^{3}V_1$	C	91
3.0	$^{1}T_1{}^{2}T_3{}^{3}T_1$	Surinamite-(*Be-free*) *unnamed analogue*	$(Mg,Fe^{2+})_3(Al,Fe^{3+})_3O$**[$Al_2Si_3O_{15}$]**	[$Si_{0.60}Al_{0.4}O_3$]	$^{1}V_1{}^{2}V_3{}^{3}V_1$	C	–
3.0	$^{1}T_1{}^{2}T_4{}^{3}T_1$	Saneroite	Na_2Mn_5**[$Si_5O_{14}(OH)(V,Si,As)O_3(OH)$]**	[$V_{0.17}Si_{0.83}O_{2.83}(OH)_{0.17}$]	$^{1}V_1{}^{2}V_4{}^{3}V_1$	C	92
3.0	$^{1}T_2{}^{2}T_2{}^{3}T_2$	Sapphirine-1*A* (2*M*)	$Mg_4(Mg_3Al_9)O_4$**[$Si_3Al_9O_{36}$]**	[$Si_{0.25}Al_{0.75}O_3$]	$^{1}V_2{}^{2}V_2{}^{3}V_2$	C	96
3.0	$^{1}T_2{}^{2}T_2{}^{3}T_2$	Khmaralite	$Mg_4(Mg_3Al_9)O_4$**[$Si_3Be_2Al_5O_{36}$]**	[$Si_{0.42}Al_{0.5}Be_{0.08}O_3$]	$^{1}V_2{}^{2}V_2{}^{3}V_2$	C	–
3.0	$^{1}T_2{}^{2}T_2{}^{3}T_2$	Sapphirine-(Al) *unnamed analogue*	$Mg_4(Mg_{1.5}\ Fe_{0.3}^{2+}Fe_{1.6}^{3+}Al_{8.5})O_4$**[$Si_{1.7}Al_{10.3}O_{36}$]**	[$Si_{0.14}Al_{0.86}O_3$]	$^{1}V_2{}^{2}V_2{}^{3}V_2$	C	
3.0	$^{1}T_2{}^{2}T_2{}^{3}T_2$	Aenigmatite	$Na_4(Fe_{10}^{2+}Ti_2)O_4$**[$Si_{12}O_{36}$]**	[SiO_3]	$^{1}V_2{}^{2}V_2{}^{3}V_2$	C	97*a*,*c*
3.0	$^{1}T_2{}^{2}T_2{}^{3}T_2$	Krinovite	$Na_4(Mg_8Cr_4^{3+})O_4$**[$Si_{12}O_{36}$]**	[SiO_3]	$^{1}V_2{}^{2}V_2{}^{3}V_2$	C	97*a*
3.0	$^{1}T_2{}^{2}T_2{}^{3}T_2$	Wilkinsonite	$Na_4(Fe_8^{2+}Fe_4^{3+})O_4$**[$Si_{12}O_{36}$]**	[SiO_3]	$^{1}V_2{}^{2}V_2{}^{3}V_2$	C	97*a*
3.0	$^{1}T_2{}^{2}T_2{}^{3}T_2$	Wilkinsonite-(Mg) *unnamed analogue*	$Na_4(Mg_5Fe_7^{3+})O_4$**[$Si_9Fe_3^{3+}O_{36}$]**	[$Si_{0.75}Fe_{0.25}^{3+}O_3$]	$^{1}V_2{}^{2}V_2{}^{3}V_2$	C	97*a*
3.0	$^{1}T_2{}^{2}T_2{}^{3}T_2$	Rhönite	$Ca_4(Mg_8Fe_2^{3+}Ti_2)O_4$**[$Si_6Al_6O_{36}$]**	[$Si_{0.5}Al_{0.5}O_3$]	$^{1}V_2{}^{2}V_2{}^{3}V_2$	C	97*d*,*e*
3.0	$^{1}T_2{}^{2}T_2{}^{3}T_2$	Rhönite-(Ti^{3+}) *unnamed analogue (Allende meteorite)*	$Ca_4(Mg_7AlTi_2^{3+}Ti_2^{4+})O_4$**[$Si_5Al_7O_{36}$]**	[$Si_{0.42}Al_{0.58}O_3$]	$^{1}V_2{}^{2}V_2{}^{3}V_2$	C	–
3.0	$^{1}T_2{}^{2}T_2{}^{3}T_2$	Kuratite	$Ca_4(Fe_{10}^{2+}Ti_2)O_4$**[$Si_8Al_4O_{36}$]**	[$Si_{0.67}Al_{0.33}O_3$]	$^{1}V_2{}^{2}V_2{}^{3}V_2$	C	–
3.0	$^{1}T_2{}^{2}T_2{}^{3}T_2$	Makarochkinite	$Ca_4(Fe_8^{2+}Fe_2^{3+}Ti_2)O_4$**[$Be_2Al_2Si_8O_{36}$]**	[$Si_{0.67}Al_{0.17}Be_{0.17}O_3$]	$^{1}V_2{}^{2}V_2{}^{3}V_2$	C	–
3.0	$^{1}T_2{}^{2}T_2{}^{3}T_2$	Serendibite	$Ca_4(Mg_6Al_6)O_4$**[$Si_6B_3Al_3O_{36}$]**	[$Si_{0.5}Al_{0.25}Be_{0.25}O_3$]	$^{1}V_2{}^{2}V_2{}^{3}V_2$	C	98*a*
3.0	$^{1}T_2{}^{2}T_2{}^{3}T_2$	Addibischoffite	$Ca_4(Al_{12})O_4$**[$Al_{12}O_{36}$]**	[AlO_3]	$^{1}V_2{}^{2}V_2{}^{3}V_2$	C	98*b*
3.0	$^{1}T_2{}^{2}T_2{}^{3}T_2$	Warkite	$Ca_4(Sc_{12})O_4$**[$Al_{12}O_{36}$]**	[AlO_3]	$^{1}V_2{}^{2}V_2{}^{3}V_2$	C	98*b*
3.0	$^{1}T_2{}^{2}T_2{}^{3}T_2$	Welshite	$Ca_4(Mg_9Sb_3^{5+})O_4$**[$Si_6Be_3Fe_2^{3+}AlO_{36}$]**	[$Si_{0.5}Al_{0.08}Be_{0.25}Fe_{0.17}O_3$]	$^{1}V_2{}^{2}V_2{}^{3}V_2$	C	98*c*,*d*

(*Continued*)

https://doi.org/10.1180/mgm.2020.13 Published online by Cambridge University Press

Table 10. (*Continued.*)

O:T	$^{c}T_r$	Mineral	Ideal structural formula	Unit stoichiometry	$^{c}V_r$	C/R/T	Figs
3.0	$^{1}T_2{}^{2}T_2{}^{3}T_2$	Dorrite	$Ca_4(Mg_3Fe^{3+}_9)O_4$**[$Si_3Al_8Fe^{3+}O_{36}$]**	$[Si_{0.25}Al_{0.67}Fe^{3+}_{0.08}O_3]$	$^{1}V_2{}^{2}V_2{}^{3}V_2$	C	98*e*
3.0	$^{1}T_2{}^{2}T_2{}^{3}T_2$	Høgtuvaite	$Ca_4(Fe^{2+}_6Fe^{3+}_6)O_4$**[$Si_8Be_2Al_2O_{36}$]**	$[Si_{0.67}Al_{0.17}Be_{0.17}O_3]$	$^{1}V_2{}^{2}V_2{}^{3}V_2$	C	–
3.0	$^{1}T_2{}^{2}T_2{}^{3}T_2$	Khesinite	$Ca_4(Mg_2Fe^{3+}_{10})O_4$**[$Fe^{3+}_{10}Si_2$]**$O_{36}$	$[Fe^{3+}_{0.83}Si_{0.17}]$	$^{1}V_2{}^{2}V_2{}^{3}V_2$	C	–
3.0	$^{1}T_2{}^{2}T_2{}^{3}T_2$	Unnamed Fe-Ga analogue *sapphirine supergroup*	$(Fe,Ga,Sn,Zn)_{16}O_4$**[$(Ga,Ge)_{12}O_{36}$]**	$[Ga,GeO_3]$	$^{1}V_2{}^{2}V_2{}^{3}V_2$	C	–
3.0	$^{1}T_2{}^{2}T_2{}^{3}T_2$	Terskite	Na_4Zr**[$Si_6O_{14}(OH_4)$]**	$[SiO_2(OH)_{0.67}]$	$^{1}V_1{}^{2}V_1{}^{3}V_1$	C	95*a–e*
3.0	$^{1}T_2{}^{2}T_2{}^{3}T_2$	Hydroterskite	Na_2Zr**[$Si_6O_{12}(OH_6)$]**	$[SiO_{2.33}(OH)_{0.33}]$	$^{1}V_1{}^{2}V_1{}^{3}V_1$	C	95*a–c,f*
2.90	$^{1}T_2{}^{3}T_6$	Veblenite	$KNa(Fe^{2+}_5Fe^{3+}_4Mn_7)Nb_4$**[$Si_2O_7$]$_2$[$Si_8O_{22}$]$_2$** $O_6(OH)_{10}(H_2O)_3$	$[SiO_{2.75}]$	$^{1}V_2{}^{3}V_6$	R	60,61
	$^{1}T_2{}^{\star}$	〃 〃		$[SiO_{3.5}]$	$^{1}V_2$	Cl	
2.90	$^{1}T_1{}^{2}T_6{}^{3}T_3$	Scheuchzerite	$Na(Mn,Mg)_9$**[$VSi_9O_{28}(OH)$]**$(OH)_3$	$[V_{0.1}Si_{0.9}O_{2.8}(OH)_{0.1}]$	$^{1}V_1{}^{2}V_6{}^{3}V_3$	C	93,94
2.89	$^{2}T_{14}{}^{3}T_4$	Liebauite	Ca_3Cu_5**[Si_9O_{26}]**	$[SiO_{2.89}]$	$^{2}V_7{}^{3}V_2$	C	88,89
2.83	$^{1}T_2{}^{3}T_4$	Nafertisite	$Na_3Fe^{2+}_{10}Ti_2$**[Si_6O_{17}]$_2$**$O_2(OH)_6F(H_2O)_2$	$[SiO_{2.83}]$	$^{1}V_2{}^{3}V_4$	R	58,59
2.83	$^{2}T_4{}^{3}T_2$	Howieite	$Na(Fe,Mn)_{10}(Fe,Al)_2$**[$Si_{12}O_{31}(OH)_3$]**$(OH)_{10}$	$[SiO_{2.58}(OH)_{0.25}]$	$^{2}V_4{}^{3}V_2$	C	73*a–e*
2.83	$^{2}T_4{}^{3}T_2$	Taneyamalite	$(Na,Ca)(Mn,Mg,Fe)_{12}$**[$Si_{12}(O,OH)_{34}$]**$(OH)_{10}$	$[Si(OH,O)_{2.83}]$	$^{2}V_4{}^{3}V_2$	C	73*a–c,f,g*
2.83	$^{2}T_4{}^{3}T_2$	Deerite	$(Fe,Mn)_6(Fe,Al)_3$**[Si_6O_{17}]**$O_3(OH)_5$	$[SiO_{2.83}]$	$^{2}V_4{}^{3}V_2$	C	74*a,b*
2.83	$^{2}T_4{}^{3}T_2$	Johninnesite	$Na_2Mn^{2+}_9Mg_7(AsO_4)_2$**[$Si_6O_{17}$]$_2$**$(OH)_8$	$[SiO_{2.83}]$	$^{2}V_4{}^{3}V_2$	C	74*c,d*
2.83	$^{2}T_4{}^{3}T_2$	Kenotobermorite (11Å) 4*O* (anomalous)	Ca_4**[$Si_6O_{15}(OH)_2$]**$(H_2O)_2{\cdot}(H_2O)_3$	$[SiO_{2.5}(OH)_{0.33}]$	$^{2}V_4{}^{3}V_2$	R	75*a,b,e,f*, 76*a,b*
2.83	$^{2}T_4{}^{3}T_2$	Tobermorite (11Å) 2*M* (normal)	Ca_4**[Si_6O_{17}]**$(H_2O)_2){\cdot}(Ca(H_2O)_3$	$[SiO_{2.83}]$	$^{2}V_4{}^{3}V_2$	R	75*a,b,e,f*, 76*c,d*
2.83	$^{2}T_4{}^{3}T_2$	Kenotobermorite (11Å) 2*M* (anomalous)	Ca_4**[$Si_6O_{15}(OH)_2$]**$(H_2O)_2{\cdot}(H_2O)_3$	$[SiO_{2.5}(OH)_{0.33}]$	$^{2}V_4{}^{3}V_2$	R	75*a,b,e,f*, 76*e–f*
2.83	$^{2}T_4{}^{3}T_2$	Clinotobermorite (11Å) 1*A*	Ca_4**[Si_6O_{17}]**$(H_2O)_2){\cdot}(Ca(H_2O)_3$	$[SiO_{2.83}]$	$^{2}V_4{}^{3}V_2$	R	75*c–f* , 77*a,b*
2.83	$^{2}T_4{}^{3}T_2$	Clinotobermorite (11Å) 2*M*	Ca_4**[Si_6O_{17}]**$(H_2O)_2){\cdot}(Ca(H_2O)_3$	$[SiO_{2.83}]$	$^{2}V_4{}^{3}V_2$	R	75*c–f*, 77*c,d*
2.83	$^{2}T_4{}^{3}T_2$	Kenoclinotobermorite (*theoretical*)	Ca_4**[$Si_6O_{15}(OH)_2$]**$(H_2O)_2{\cdot}(H_2O)_3$	$[SiO_{2.5}(OH)_{0.33}]$	$^{2}V_4{}^{3}V_2$	R	75*c–f*
2.83	$^{2}T_4{}^{3}T_2$	Tobermorite (10Å) 4*O*/2*M*	Ca_4**[$Si_6O_{15}(OH)_2$]**$\cdot(H_2O)$	$[SiO_{2.5}(OH)_{0.33}]$	$^{2}V_4{}^{3}V_2$	R	–
2.83	$^{2}T_4{}^{3}T_2$	Kalitobermorite (*theoretical*)	Ca_4**[$AlSi_5O_{15}(OH)_2$]**$(H_2O)_2{\cdot}(K(H_2O)_3$	$[Al_{0.17}Si_{0.83}O_{2.5}(OH)_{0.33}]$	$^{2}V_4{}^{3}V_2$	R	–
2.83	$^{2}T_4{}^{3}T_2$	Xonotlite	Ca_6**[Si_6O_{17}]**$(OH)_2$	$[SiO_{2.83}]$	$^{2}V_4{}^{3}V_2$	R	78
2.83	$^{2}T_4{}^{3}T_2$	Haineaultite	$(Na,Ca)_5Ca(Ti,Nb)_5$**[Si_6O_{17}]$_2$**$(OH,F)_8(H_2O)_5$	$[SiO_{2.83}]$	$^{2}V_4{}^{3}V_2$	R	79*a–d*
2.83	$^{2}T_4{}^{3}T_2$	Zorite	$Na_6Ti(Ti,Nb)_4$**[Si_6O_{17}]$_2$**$(O,OH)_5(H_2O)_{11}$	$[SiO_{2.83}]$	$^{2}V_4{}^{3}V_2$	R	79*a,b,e,f*
2.83	$^{2}T_4{}^{3}T_2$	Synthetic	$Pb_4Ti(Ti,Nb)_4$**[Si_6O_{17}]$_2$**$(O,OH)_5(H_2O)_{10}$	$[SiO_{2.83}]$	$^{2}V_4{}^{3}V_2$	R	–
2.83	$^{2}T_4{}^{3}T_2$	Synthetic	$K_5Na_2Ti(Ti,Nb)_4$**[Si_6O_{17}]$_2$**$(O,OH)_5(H_2O)_{11}$	$[SiO_{2.83}]$	$^{2}V_4{}^{3}V_2$	R	–
2.83	$^{2}T_4{}^{3}T_2$	Synthetic	$Cs_4Na_2Ti(Ti,Nb)_4$**[Si_6O_{17}]$_2$**$(O,OH)_5(H_2O)_5$	$[SiO_{2.83}]$	$^{2}V_4{}^{3}V_2$	R	–
2.83	$^{2}T_4{}^{3}T_2$	Gilalite	Cu_5**[Si_6O_{17}]**$(H_2O)_7$	$[SiO_{2.83}]$	$^{2}V_4{}^{3}V_2$	R	–
2.83	$^{1}T_1{}^{2}T_2{}^{3}T_3$	Synthetic	K_3Eu^{3+}**[$Si_6O_{13}(OH)_4$]**$(H_2O)_2$	$[SiO_{2.16}(OH)_{0.67}]$	$^{1}V_1{}^{2}V_2{}^{3}V_3$	C	90
2.80	$^{2}T_6{}^{3}T_4$	Inesite	$Ca_2(Mn,Fe)_7$**[$Si_{10}O_{28}$]**$(OH)_2(H_2O)_5$	$[SiO_{2.8}]$	$^{2}V_6{}^{3}V_4$	R	85
2.80	$^{2}T_6{}^{3}T_4$	Synthetic	K_5Gd_5**[$Si_{10}O_{28}$]**	$[SiO_{2.8}]$	$^{2}V_6{}^{3}V_4$	R	86
2.80	$^{2}T_6{}^{3}T_4$	Haiweeite	$Ca_2(UO_2)_4$**[$Si_{10}O_{24}(OH)_4$]**$(H_2O)_{12}$	$[SiO_{2.4}(OH)_{0.4}]$	$^{2}V_3{}^{3}V_2$	C	87
2.75	$^{3}T_4$	Vinogradovite	Na_4Ti_4**[Si_2O_6]$_2$[Si_4O_{10}]**$O_4(H_2O,Na,K)_3$	$[SiO_{2.5}]$	$^{3}V_2$	R	35,36*a,b*
	$^{2}T_2{}^{\star}$	〃 〃	〃 〃	$[SiO_3]$	$^{2}V_1$	C	
2.75	$^{3}T_4$	Paravinogradovite	$(Na,\square)_2(Ti^{4+},Fe^{3+})_4$**[$Si_2O_6$]$_2$[$Si_3AlO_{10}$]**$(OH)_4(H_2O)$	$[Si_{0.75}Al_{0.25}O_{2.5}]$	$^{3}V_2$	R	35,36*c,d*
	$^{2}T_2{}^{\star}$	〃 〃	〃 〃	$[SiO_3]$	$^{2}V_1$	C	
2.75	$^{3}T_{12}$	Miserite	$K_2(Ca,Y,REE)_{10}$**[Si_6O_{15}]$_2$[Si_2O_7]$_2$**$(OH,F)_4(H_2O)_2$	$[SiO_{2.5}]$	$^{3}V_{12}$	T	48,49*c,d*
	$^{1}T_2{}^{\star}$	〃 〃	〃 〃	$[SiO_{3.5}]$	$^{1}V_2$	Cl	
2.75	$^{2}T_2{}^{3}T_2$	Amphiboles	$A_{0-1}B_2C_5$**[T_8O_{22}]**$(OH,F)_2$	$[SiO_{2.75}]$	$^{2}V_2{}^{3}V_2$	R	62,63*a,b*
2.75	$^{2}T_2{}^{3}T_2$	Plancheite	Cu_{16}**[Si_8O_{22}]**$(OH)_8(H_2O)_2$	$[SiO_{2.75}]$	$^{2}V_2{}^{3}V_2$	R	62,63*c,d*
2.75	$^{2}T_2{}^{3}T_2$	Lavinskyite-2*O* (1*M*)	$K_2(LiCu^{2+})_2Cu^{2+}_{12}$**[$Si_8O_{22}$]**$(OH)_8$	$[SiO_{2.75}]$	$^{2}V_2{}^{3}V_2$	R	62
2.75	$^{2}T_2{}^{3}T_2$	Synthetic	Li_2Mg_2**[Si_4O_{11}]**	$[SiO_{2.75}]$	$^{2}V_2{}^{3}V_2$	C	64*a,b,e,f*
2.75	$^{2}T_2{}^{3}T_2$	Synthetic	Fe_3**[$BeSi_3O_9(OH)_2$]**	$[Be_{0.25}Si_{0.75}O_{0.82}OH_{0.18}]$	$^{2}V_2{}^{3}V_2$	C	64*c,d,e,f*
2.75	$^{2}T_4{}^{3}T_4$	Vlasovite	Na_2Zr**[Si_4O_{11}]**	$[SiO_{2.75}]$	$^{2}V_2{}^{3}V_2$	C	81,82
2.75	$^{2}T_4{}^{3}T_4$	Synthetic	$HNb(H_2O)$**[Si_4O_{11}]**$\cdot(H_2O)$	$[SiO_{2.75}]$	$^{2}V_2{}^{3}V_2$	R	83
2.75	$^{2}T_4{}^{3}T_4$	Synthetic	$Cs_{0.66}H_{0.33}Nb(H_2O)$**[$Si_4O_{11}$]**	$[SiO_{2.75}]$	$^{2}V_2{}^{3}V_2$	R	83
2.75	$^{2}T_4{}^{3}T_4$	Synthetic	$Na_2H(NbO)$**[Si_4O_{11}]**$\cdot(H_2O)_{1.25}$	$[SiO_{2.75}]$	$^{2}V_2{}^{3}V_2$	R	83
2.71	$^{2}T_3{}^{3}T_4$	Tokkoite	K_2Ca_4**[$Si_7O_{18}(OH)$]**(OH,F)	$[SiO_{2.57}(OH)_{0.14}]$	$^{2}V_3{}^{3}V_4$	R	71,72
2.71	$^{2}T_3{}^{3}T_4$	Senkevichite	$(CsK)Ca_2NaTiO$**[$Si_7O_{18}(OH)$]**	$[SiO_{2.57}(OH)_{0.14}]$	$^{2}V_3{}^{3}V_4$	R	71
2.71	$^{2}T_3{}^{3}T_4$	Tinaksite	K_2Ca_2NaTiO**[$Si_7O_{18}(OH)$]**	$[SiO_{2.57}(OH)_{0.14}]$	$^{2}V_3{}^{3}V_4$	R	71
2.70	$^{3}T_{12}$	Denisovite	$K_{15}(Ca,Na)_{48}$**[Si_6O_{17}]$_6$[$Si_{12}O_{30}$]$_2$**$(F_{16}(OH)_4)(H_2O)_2$	$[SiO_{2.5}]$	$^{3}V_{12}$	T	–
	$^{2}T_4{}^{3}T_2{}^{\star}$	〃 〃	〃 〃	$[SiO_{2.83}]$	$^{2}V_4{}^{3}V_2$	R	
2.69	$^{2}T_4{}^{3}T_2{}^{4}T_2$	Revdite	Na_{16}**[$Si_4O_6(OH)_5$]$_2$[$Si_8O_{15}(OH)_6$]**$(OH)_{10}(H_2O)_{28}$	$[SiO_{1.88}(OH)_{0.75}]$	$^{2}V_4{}^{3}V_2{}^{4}V_2$	R	99,100
	$^{2}T_2{}^{3}T_2{}^{\star}$	〃 〃	〃 〃	$[SiO_{2.75}]$	$^{2}V_2{}^{3}V_2$	C	
2.67	$^{2}T_2{}^{3}T_4$	Jimthompsonite	$(Mg,Fe)_5$**[Si_6O_{16}]**$(OH)_2$	$[SiO_{2.67}]$	$^{2}V_2{}^{3}V_4$	R	65,66
2.67	$^{2}T_2{}^{3}T_4$	Clinojimthompsonite	$(Mg,Fe)_5$**[Si_6O_{16}]**$(OH)_2$	$[SiO_{2.67}]$	$^{2}V_2{}^{3}V_4$	R	65,66
2.67	$^{2}T_2{}^{3}T_4$	Synthetic	Na_2Mg_4**[Si_6O_{16}]**$(OH)_2$	$[SiO_{2.67}]$	$^{2}V_2{}^{3}V_4$	R	–
2.67	$^{2}T_2{}^{3}T_4$	Synthetic	$NaMg_4$**[$Si_6O_{15}(OH)$]**$(OH)_2$	$[SiO_{2.5}(OH)_{0.17}]$	$^{2}V_2{}^{3}V_4$	R	–
2.67	$^{2}T_2{}^{3}T_4$	Synthetic	Ba_4**[Si_6O_{16}]**	$[SiO_{2.67}]$	$^{2}V_2{}^{3}V_4$	R	–
2.67	$^{2}T_2{}^{3}T_4$	Yangite	$PbMn$**[Si_3O_8]**(H_2O)	$[SiO_{2.67}]$	$^{2}V_2{}^{3}V_4$	R	67

(*Continued*)

https://doi.org/10.1180/mgm.2020.13 Published online by Cambridge University Press

Table 10. (*Continued.*)

O:T	$^{c}T_{r}$	Mineral	Ideal structural formula	Unit stoichiometry	$^{c}V_{r}$	C/R/T	Figs
2.67	$^{2}T_{4}{}^{3}T_{8}$	Carlosturanite	$(Mg,Fe^{2+},Ti^{2+})_{21}$**[(Si,Al)$_{12}O_{28}(OH)_{4}$]**$(OH)_{30}(H_2O)$	$[SiO_{2.34}(OH)_{0.33}]$	$^{2}V_{2}{}^{3}V_{4}$	R	84
2.63	$^{2}T_{2}{}^{3}T_{6}$	Synthetic	$K_6Eu_2^{3+}$**[Si$_8$O$_{19}$(OH)$_2$]**$(OH)_2(H_2O)_{11}$	$[SiO_{2.38}(OH)_{0.25}]$	$^{2}V_{2}{}^{3}V_{6}$	R	69*a–d*
2.63	$^{2}T_{2}{}^{3}T_{6}$	Synthetic	Ba_5**[Si$_8$O$_{21}$]**	$[SiO_{2.63}]$	$^{2}V_{2}{}^{3}V_{6}$	R	69*e–h*
2.60	$^{2}T_{2}{}^{3}T_{8}$	Synthetic	Ba_6**[Si$_{10}$O$_{26}$]**	$[SiO_{2.6}]$	$^{2}V_{2}{}^{3}V_{8}$	R	70*a–d*
2.56	$^{3}T_{17}$	Charoite	$(K,Sr)_{15–16}(Ca,Na)_{32}$**[Si$_6O_{11}(O,OH)_6$]$_2$[Si$_{12}O_{18}(O, OH)_{12}$]$_2$[Si$_{17}O_{25}(O,OH)_{18}$]$_2$**$(OH,F)_4(H_2O)_3$	$[SiO_{1.5}(O,OH)]$	$^{3}V_{17}$	T	52
	$^{3}T_{12}$*	〃 〃		$[SiO_{1.83}(O,OH)]$	$^{2}V_{4}{}^{3}V_{2}$	R	
	$^{2}T_{4}{}^{3}T_{2}$*	〃 〃		$[SiO_{2.67}]$	$^{2}V_{2}{}^{3}V_{4}$	R	
2.56	$^{2}T_{2}{}^{3}T_{4}$	Okenite	$Ca_2(H_2O)_9(H_2O)_3Ca_8$**[Si$_6$O$_{16}$][Si$_6$O$_{15}$]$_2$**$(H_2O)_6$	$[SiO_{2.5}]$	$^{3}V_{12}$	S	67,68
	$^{3}T_{12}$*	〃 〃	〃 〃				
2.56	$^{2}T_{4}{}^{3}T_{12}{}^{4}T_{2}$	Patynite	NaKCa$_4$**[Si$_9$O$_{23}$]**	$[SiO_{2.56}]$	$^{2}V_{4}{}^{3}V_{12}{}^{4}V_{2}$	R/T	101,102
2.50	$^{3}T_{4}$	Bigcreekite	Ba_2**[Si$_4$O$_{10}$]**$(H_2O)_8$	$[SiO_{2.5}]$	$^{3}V_{2}$	R	37
2.50	$^{3}T_{4}$	Synthetic	Li_4**[SiGe$_3$O$_{10}$]**	$[(Si_{0.25}Ge_{0.75})O_{2.5}]$	$^{3}V_{2}$	R	–
2.50	$^{3}T_{4}$	Synthetic	Cs_2H_2**[Si$_4$O$_{10}$]**	$[SiO_{2.5}]$	$^{3}V_{2}$	R	–
2.50	$^{3}T_{6}$	Epididymite	Na_2Be_2**[Si$_6$O$_{15}$]**(H_2O)	$[SiO_{2.5}]$	$^{3}V_{2}$	R	38
2.50	$^{3}T_{6}$	Eudidymite	Na_2Be_2**[Si$_6$O$_{15}$]**(H_2O)	$[SiO_{2.5}]$	$^{3}V_{2}$	R	38
2.50	$^{3}T_{6}$	Elpidite	Na_2Zr**[Si$_6$O$_{15}$]**$(H_2O)_3$	$[SiO_{2.5}]$	$^{3}V_{2}$	R	38,39
2.50	$^{3}T_{6}$	Yusupovite	Na_2Zr**[Si$_6$O$_{15}$]**$(H_2O)_3$	$[SiO_{2.5}]$	$^{3}V_{2}$	R	38
2.50	$^{3}T_{6}$	Synthetic	Rb_2Zr**[Si$_6$O$_{15}$]**(H_2O)	$[SiO_{2.5}]$	$^{3}V_{2}$	R	–
2.50	$^{3}T_{6}$	Synthetic	K_2Zr**[Si$_6$O$_{15}$]**(H_2O)	$[SiO_{2.5}]$	$^{3}V_{2}$	R	–
2.50	$^{3}T_{8}$	Caysichite-(Y)	$Y_4(Ca,REE)_4$**[Si$_8$O$_{20}$]**$(CO_3)_6(OH)(H_2O)_7]$	$[SiO_{2.5}]$	$^{3}V_{2}$	R	40,41
2.50	$^{3}T_{8}$	Litidionite	KNaCu**[Si$_4$O$_{10}$]**	$[SiO_{2.5}]$	$^{3}V_{8}$	T	42,43*a,b*
2.50	$^{3}T_{8}$	Fenaksite	KNaFe**[Si$_4$O$_{10}$]$_2$**	$[SiO_{2.5}]$	$^{3}V_{8}$	T	42
2.50	$^{3}T_{8}$	Manaksite	KNaMn**[Si$_4$O$_{10}$]**	$[SiO_{2.5}]$	$^{3}V_{8}$	T	42
2.50	$^{3}T_{8}$	Calcinaksite	KNa[Ca(H$_2$O)]**[Si$_4$O$_{10}$]**	$[SiO_{2.5}]$	$^{3}V_{8}$	T	42
2.50	$^{3}T_{8}$	Agrellite	$NaCa_2$**[Si$_4$O$_{10}$]**(F)	$[SiO_{2.5}]$	$^{3}V_{8}$	T	42,43*c,d*
2.50	$^{3}T_{8}$	Synthetic	K_2Ca**[Si$_4$O$_{10}$]**	$[SiO_{2.5}]$	$^{3}V_{8}$	T	–
2.50	$^{3}T_{8}$	Synthetic	KNa*M***[Si$_4$O$_{10}$]** *M* = Cu^{2+}, Mn^{2+}, Fe^{2+}	$[SiO_{2.5}]$	$^{3}V_{8}$	T	–
2.50	$^{3}T_{8}$	Synthetic	Na_2*M*[Si$_4$O$_{10}$] *M* = Co^{2+}, Ni^{2+}, Cu^{2+}, Mn^{2+}	$[SiO_{2.5}]$	$^{3}V_{8}$	T	–
2.50	$^{3}T_{8}$	Narsarsukite	$Na_4(Ti,Fe)_2$**[Si$_8$O$_{20}$]**$(O,OH,F)_2$	$[SiO_{2.5}]$	$^{3}V_{8}$	T	44,45
2.50	$^{3}T_{8}$	Synthetic	KSc**[Si$_4$O$_{10}$]**F	$[SiO_{2.5}]$	$^{3}V_{8}$	T	
2.50	$^{3}T_{8}$	Synthetic	Pb_6O**(Si$_6$Al$_2$O$_{20}$)**	$[Si_{0.75}Al_{0.25}O_{2.5}]$		T	
2.50	$^{3}T_{8}$	Synthetic	K_2In**[Si$_4$O$_{10}$]**(OH)	$[SiO_{2.5}]$	$^{3}V_{8}$	T	
2.50	$^{3}T_{12}$	Tuhualite	$(Na,K)_2Fe_2^{3+}Fe_2^{2+}$**[Si$_{12}O_{30}$]**$(H_2O)$	$[SiO_{2.5}]$	$^{3}V_{2}$	R	46,47
2.50	$^{3}T_{12}$	Emeleusite	$Na_4Li_2Fe_2^{3+}$**[Si$_{12}$O$_{30}$]**	$[SiO_{2.5}]$	$^{3}V_{2}$	R	46
2.50	$^{3}T_{12}$	Zektzerite	Na_2Li_2Zr2**[Si$_{12}$O$_{30}$]**	$[SiO_{2.5}]$	$^{3}V_{2}$	R	46
2.50	$^{3}T_{12}$	Canasite	$K_3Na_3Ca_5$**[Si$_{12}$O$_{30}$]**$(OH)_4$	$[SiO_{2.5}]$	$^{3}V_{12}$	T	48
2.50	$^{3}T_{12}$	Fluorcanasite	$K_3Na_3Ca_5$**[Si$_{12}$O$_{30}$]**$F_3(OH)(H_2O)$	$[SiO_{2.5}]$	$^{3}V_{12}$	T	48,49*a,b*
2.50	$^{3}T_{12}$	Frankamenite	$K_3Na_3Ca_5$**[Si$_{12}$O$_{30}$]**$F_3(OH)(H_2O)$	$[SiO_{2.5}]$	$^{3}V_{12}$	T	48
2.50	$^{3}T_{16}$	Synthetic	Cs_4Y_2**[Si$_8$O$_{20}$]**F_4	$[SiO_{2.5}]$	$^{3}V_{16}$	R	50
2.50	$^{3}T_{16}$	Synthetic	K_4In_2**[Si$_8$O$_{20}$]**$(OH)_2$	$[SiO_{2.5}]$	$^{3}V_{16}$	R	51
2.50	$^{3}T_{16}$	Synthetic	K_4Lu_2**[Si$_8$O$_{20}$]**$(OH)_2$	$[SiO_{2.5}]$	$^{3}V_{16}$	R	51
2.50	$^{3}T_{16}$	Synthetic	Ru_4Lu_2**[Si$_8$O$_{20}$]**F_2	$[SiO_{2.5}]$	$^{3}V_{16}$	R	51
2.50	$^{3}T_{32}$	Synthetic	Na_{16}**[Si$_{32}$O$_{64}$(OH)$_{16}$]**	$[SiO_2(OH)_{0.5}]$	$^{3}V_{2}$	R	–
2.50	$^{3}T_{56}$	Ashcroftine-(Y)	$K_{10}Na_{10}(Y,Ca)_{24}(OH)_4(CO_3)_{16}$**(Si$_{56}O_{140}$)**$(H_2O)_{16}$	$[SiO_{2.5}]$	$^{3}V_{56}$	T	54
2.40	$^{2}T_{2}$	Lintisite	Na_6Ti_4**[Li$_2$Si$_4$O$_{12}$][Si$_2$O$_6$]$_2$**$O_4(H_2O)_4$	$[SiO_3]$	$^{2}V_{1}$	C	6
	$^{4}T_{4}{}^{6}T_{2}$*	〃 〃	〃 〃	$[Li_{0.33}Si_{0.67}O_2]$	$^{4}V_{2}{}^{6}V_{1}$	R	
2.40	$^{2}T_{2}$	Punkaruaivite	Ti_4**[Li$_2$Si$_4$O$_{10}$(OH)$_2$][Si$_2$O$_6$]$_2$**$(OH)_4(H_2O)_2$	$[SiO_3]$	$^{2}V_{1}$	C	6*d,e*
	$^{4}T_{4}{}^{6}T_{2}$*	〃 〃	〃 〃	$[Li_{0.33}Si_{0.67}O_{1.67}(OH)_{0.33}]$	$^{4}V_{2}{}^{6}V_{1}$	R	

C: chain; R: ribbon; T: tube; Cl: cluster; S: sheet.
*Indicates the $^{c}T_{r}$ expression of an additional structural unit including a chain, ribbon, tube, cluster or sheet of $(TO_4)^{n-}$ tetrahedra in the respective mineral. These minerals are listed in Table 12.

In class (2), minerals contain sheets or clusters of $(TO_4)^{n-}$ tetrahedra in addition to chains, ribbons and/or tubes (Table 12). **Veblenite** contains $^{1}T_{2}{}^{3}T_{6}$ ribbons of stoichiometry $[Si_8O_{22}]^{12-}$ and $^{1}T_{2}$ dimers of stoichiometry $[Si_2O_7]^{6-}$ for a net O:T ratio of $(3.5 \times 4 + 2.5 \times 6)$ / $10 = 2.90$. **Yuksporite** contains $^{2}T_{4}{}^{3}T_{2}$ ribbons of stoichiometry $[Si_6O_{17}]^{10-}$ and $^{1}T_{2}$ dimers of stoichiometry $[Si_2O_7]^{6-}$ in the ratio 2:3 for a net O:T ratio of $(3.5 \times 3 + 3.0 \times 4 + 2.5 \times 2)$ / $9 = 3.06$. Thus, it exceeds the maximum O:T ratio of 3:1 for chain silicates due to the presence of the one-dimensional cluster (i.e. the $[Si_2O_7]$ dimer). **Miserite** contains $^{3}T_{12}$ tubes of stoichiometry $[Si_6O_{15}]^{6-}$ and $^{1}T_{2}$ dimers of stoichiometry $[Si_2O_7]^{6-}$ for a net O:T ratio of $(3.5 \times 4 + 2.5 \times 12)$ / $14 = 2.75$. **Okenite** contains $^{2}T_{2}{}^{3}T_{4}$ ribbons of stoichiometry $[Si_6O_{16}]^{8-}$ and $^{3}T_{12}$ sheets of stoichiometry $[Si_6O_{15}]^{6-}$ in the ratio 1:2 for a net O:T ratio of $(3.0 \times 2 + 2.5 \times 16)$ / $18 = 2.56$. Notably, the inclusion of a sheet in **okenite** does not decrease the O:T ratio below that observed in purely chain-, ribbon- and tube- minerals (Table 10).

Coda

A structure hierarchy organises a large amount of data in a coherent way so as to incorporate new structures and to correlate topological and chemical variations in these structures with mineral paragenesis. A corollary of such work is the recognition of patterns and trends that emerge during the development of a structure hierarchy for chain-, ribbon- and tube-silicates. Here we list some of these observations and the questions that they raise with regard to chain-, ribbon- and tube-silicate minerals:

https://doi.org/10.1180/mgm.2020.13 Published online by Cambridge University Press

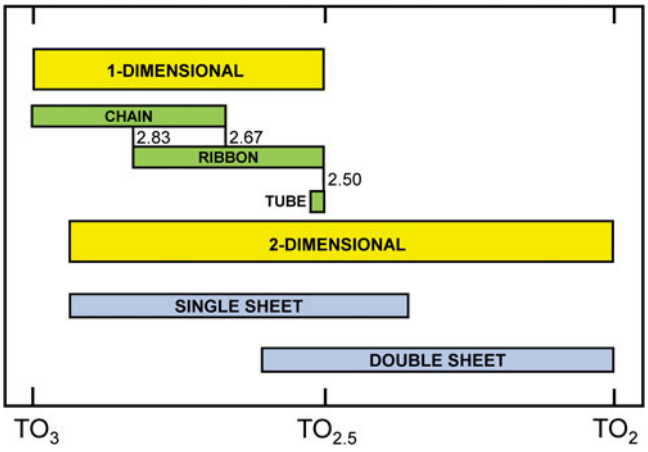

Fig. 105. The stoichiometric range of 1-dimesional structures; chains, ribbons, and tubes and 2-dimensional structures; single and double sheets.

[1] The majority of chain and ribbon arrangements in minerals correspond to only a small number of graphs: of the 450 minerals, 375 correspond to 4 graphs, whereas the other 75 minerals correspond to 46 graphs. Why are certain chain, ribbon and/or tube arrangements favoured over others (i.e. $^{2}T_{2}$,$^{2}T_{2}{}^{3}T_{2}$)?

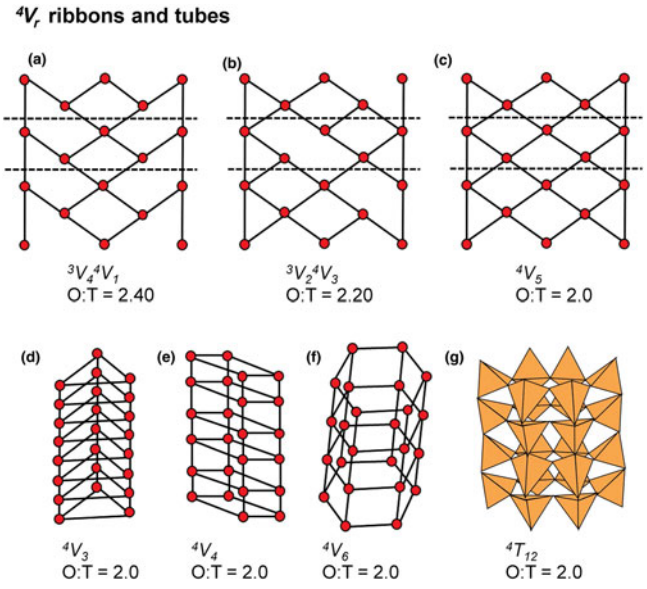

Fig. 106. The graphical representation of ribbons and tubes with O:T = 2.0 ≤ × ≤ 2.5 that are not observed in minerals. (*a*) $^{3}V_{4}{}^{4}V_{1}$ (O:T = 2.40), (*b*) $^{3}V_{2}{}^{4}V_{3}$ (O:T = 2.20), and (*c*) $^{4}V_{5}$ (O:T = 2.0) ribbon graphs. (*d*) $^{4}V_{3}$ (triangles), (e) $^{4}V_{4}$ (squares), and (*f*) $^{4}V_{6}$ (hexagons) tube graphs where O:T = 2.0 and (*g*) a tetrahedral representation of a $^{4}T_{12}$ tube that is topologically identical to the tube shown in (*f*). Dashed black lines outline the repeat unit of the graphs in (*a*), (*b*) and (*c*).

Table 11. Comparison of vertex connectivities in chain, ribbon and sheet structures with the same O:T ratio.

O:T	Sheet mineral	S/D	$^{c}V_{r}$ *(net)*	Chain mineral	C/R/T	$^{c}V_{r}$ *(graph)*
3.0	----	--	----	Pyroxene	C	$^{2}V_{1}$
3.0	----	--	----	Pyroxenoids	C	$^{2}V_{1}$
3.0	----	--	----	Astrophyllite	C	$^{1}V_{1}{}^{3}V_{1}$
3.0	Hyttsjöite	S	$^{1}V_{6}{}^{2}V_{18}{}^{3}V_{6}$	Sapphirine	C	$^{1}V_{2}{}^{2}V_{2}{}^{3}V_{2}$
2.90	----	--	----	Scheuchzerite	C	$^{1}V_{1}{}^{2}V_{6}{}^{3}V_{3}$
2.89	----	--	----	Liebauite	C	$^{2}V_{7}{}^{3}V_{2}$
2.83	----	--	----	Howieite	C	$^{2}V_{4}{}^{3}V_{2}$
2.83	----	--	----	Tobermorite	R	$^{2}V_{4}{}^{3}V_{2}$
2.80	Zeophyllite	S	$^{2}V_{3}{}^{3}V_{2}$	Inesite	R	$^{2}V_{6}{}^{3}V_{4}$
2.80	Britvinite	S	$^{2}V_{3}{}^{3}V_{2}$	Syn. $K_5Gd_5[Si_{10}O_{28}]$	R	$^{2}V_{6}{}^{3}V_{4}$
2.80	Molybdophyllite	S	$^{2}V_{3}{}^{3}V_{2}$	Haiweeite	C	$^{2}V_{3}{}^{3}V_{2}$
2.75	Tumchaite	S	$^{2}V_{4}{}^{3}V_{4}$	Amphibole	R	$^{2}V_{2}{}^{3}V_{2}$
2.67	Kvanefjeldite	S	$^{2}V_{4}{}^{3}V_{8}$	Carlosturanite	R	$^{2}V_{2}{}^{3}V_{4}$
〃 〃	〃 〃	〃	〃 〃	Jimthompsonite	R	$^{2}V_{2}{}^{3}V_{4}$
2.60	Altisite	D	$^{2}V_{4}{}^{3}V_{4}{}^{4}V_{2}$	Syn. $Ba_6[Si_{10}O_{26}]$	R	$^{2}V_{2}{}^{3}V_{8}$
2.60	Lemoynite	D	$^{2}V_{4}{}^{3}V_{4}{}^{4}V_{2}$	〃 〃	〃	〃 〃
2.60	Natrolemoynite	D	$^{2}V_{4}{}^{3}V_{4}{}^{4}V_{2}$	〃 〃	〃	〃 〃
2.56	Okenite*	S/R	$(^{3}V_{12})(^{2}V_{2}{}^{3}V_{4})$	Patynite	R-T	$^{2}V_{4}{}^{3}V_{12}{}^{4}V_{2}$
2.50	Mica	S	$^{3}V_{2}$	Vinogradovite	R	$^{3}V_{2}$
2.50	Gyrolite	S	$^{3}V_{2}$	Eudidymite	R	$^{3}V_{2}$
2.50	Antigorite	S	$^{3}V_{2}$	Caysichite-(Y)	R	$^{3}V_{2}$
2.50	Prehnite	S	$^{2}V_{2}{}^{4}V_{2}$	Tuhualite	R	$^{3}V_{2}$
2.50	Amstallite	S	$^{2}V_{4}{}^{4}V_{4}$	Syn. $Cs_4Y_2[Si_8O_{20}]F_4$	R	$^{3}V_{8}$
2.50	Apophyllite	S	$^{3}V_{8}$	Litidionite	T	$^{3}V_{8}$
2.50	Datolite	S	$^{3}V_{8}$	Narsarsukite	T	$^{3}V_{8}$
2.50	Varennesite	S	$^{3}V_{10}$	Canasite	T	$^{3}V_{12}$
2.50	Armstrongite	S	$^{3}V_{12}$	Charoite (tube 1)**	T	$^{3}V_{12}$
2.50	Pyrosmalite-(Fe), -(Mn)	S	$^{3}V_{12}$	Syn. $K_4In_2[Si_8O_{20}](OH)_4$	T	$^{3}V_{16}$
2.50	Intersilite	S	$^{3}V_{20}$	Charoite (tube 2)**	T	$^{3}V_{17}$
2.50	Bementite	S	$^{3}V_{23}$	Ashcroftine-(Y)	T	$^{3}V_{56}$
2.42	Samfowlerite	S	$^{3}V_{40}{}^{4}V_{8}$	----	--	----
2.40	Tamaite	D	$^{3}V_{16}{}^{4}V_{4}$	----	--	----
2.38	Rhodesite	D	$^{3}V_{6}{}^{4}V_{2}$	----	--	----
2.33	Stilpnomelane	D	$^{3}V_{24}{}^{4}V_{12}$	----	--	----
2.20	Tuscanite	D	$^{2}V_{2}{}^{4}V_{8}$	----	--	----
2.17	Esquireite	D	$^{3}V_{2}{}^{4}V_{4}$	----	--	----
2.0	Dmisteinbergite	D	$^{4}V_{4}$	----	--	----

S = single sheet, D = double sheet; C = chain, R = ribbon, T = Tube.
*Includes both a sheet and a ribbon; **O:T ratio of isolated $^{2}V_{12}$ and $^{3}V_{17}$ tubes in charoite.

https://doi.org/10.1180/mgm.2020.13 Published online by Cambridge University Press

Table 12. Chain-, ribbon- and tube-silicates that contain more than one type of structural unit of $[TO_4]^{n-}$ tetrahedra.

Mineral	Formula	Unit formula	O:T	Unit type	${}^{c}T_r$	${}^{c}V_r$	Figs
Class 1: structures with mixed chains and ribbons							
Vinogradovite	Na_4Ti_4**$[Si_2O_6]_2[Si_3AlO_{10}]$**$O_4(H_2O,Na,K)_3$	$[Si_2O_6]^{4-}$	3.0	C	${}^{2}T_2$**	${}^{2}V_1$	36
〃 〃	〃 〃	$[Si_3AlO_{10}]^{5-}$	2.50	R	${}^{3}T_4$	${}^{3}V_2$	35,36
			<2.75>				
Revdite	Na_{16}**$[Si_4O_6(OH)_5]_2[Si_8O_{15}(OH)_6]$**$(OH)_{10}(H_2O)_{28}$	$[Si_4O_6(OH)_5]^{1-}$	2.75	C	${}^{2}T_2{}^{3}T_2$**	${}^{2}V_2{}^{3}V_2$	99*a–d*,100
〃 〃	〃 〃	$[Si_8O_{15}(OH)_6]^{4-}$	2.63	R	${}^{2}T_4{}^{3}T_2{}^{4}T_2$	${}^{2}V_4{}^{3}V_2{}^{4}V_2$	99*e–l*,100
			<2.69>				
Lintisite	Na_6Ti_4**$[Li_2Si_4O_{12}][Si_2O_6]_2$**$O_4(H_2O)_4$	$[Si_2O_6]^{4-}$	3.0	C	${}^{2}T_2$**	${}^{2}V_1$	6
〃 〃	〃 〃	$[Li_2Si_4O_{12}]^{6-}$	2.0	R	${}^{4}T_4{}^{6}T_2$	${}^{4}V_2{}^{6}V_1$	6*a,d,e*
			<2.40>				
Punkaruaivite	Ti_4**$[Li_2Si_4O_{10}(OH)_2][Si_2O_6]_2$**$(OH)_4(H_2O)_2$	$[Si_2O_6]^{4-}$	3.0	C	${}^{2}T_2$**	${}^{2}V_1$	
〃 〃	〃 〃	$[Li_2Si_4O_{10}(OH)_2]^{4-}$	2.0	R	${}^{4}T_4{}^{6}T_2$	${}^{4}V_2{}^{6}V_1$	6*d,e*
			<2.40>				
Denisovite	$K_{15}(Ca,Na)_{48}$**$[Si_6O_{17}]_6[Si_{12}O_{30}]_2$**$(F_{16}(OH)_4)(H_2O)_2$	$[Si_6O_{17}]$	2.83	R	${}^{2}T_4{}^{3}T_2$***	${}^{2}V_4{}^{3}V_2$	–
〃 〃	〃 〃	$[Si_{12}O_{30}]$	2.5	T	${}^{3}T_{12}$	${}^{3}V_{12}$	–
			<2.70>				
Charoite	$(K,Sr)_{15-16}(Ca,Na)_{32}$**$[Si_6O_{11}(O,OH)_6]_2[Si_{12}O_{18}(O,OH)_{12}]_2$** **$[Si_{17}O_{25}(O,OH)_{18}]_2$**$(OH,F)_4(H_2O)_3$	$[Si_6O_{11}(O,OH)_6]$	2.83	R	${}^{2}T_4{}^{3}T_2$	${}^{2}V_4{}^{3}V_2$	52*g–l*,53
〃 〃	〃 〃	$[Si_{12}O_{18}(O,OH)_{12}]$	2.50	T	${}^{3}T_{12}$	${}^{3}V_{12}$	52*d–f*,53
〃 〃	〃 〃	$[Si_{17}O_{25}(O,OH)_{18}]$	2.53	T	${}^{3}T_{17}$	${}^{3}V_{17}$	52*a–c*,53
			<2.56>				
Class 2: structures with mixed clusters, chain-ribbon-tubes and sheets							
Veblenite	$KNa(Fe^{2+}_5Fe^{3+}_4Mn_7)Nb_3Ti$**$[Si_2O_7]_2[Si_8O_{22}]_2$**$O_6(OH)_{10}(H_2O)_3$	$[Si_2O_7]^{6-}$	3.50	Cl	${}^{1}T_2$	${}^{1}V_2$	61
〃 〃	〃 〃	$[Si_8O_{22}]^{12-}$	2.75	R	${}^{1}T_2{}^{3}T_6$	${}^{1}V_2{}^{3}V_6$	60,61
			<2.90>				
Yuksporite	$(Sr,Ba)_2K_4(Ca,Na)_{14}(□,Mn,Fe)\{(Ti,Nb)_4(O,OH)_4$**$[Si_6O_{17}]_2[Si_2O_7]_3$**$\}$ $(H_2O,(OH))_3$	$[Si_2O_7]^{6-}$	3.50	Cl	${}^{1}T_2$*	${}^{1}V_2$	80*d,f*
〃 〃	〃 〃	$[Si_6O_{17}]^{10-}$	2.83	R	${}^{2}T_4{}^{3}T_2$	${}^{2}V_4{}^{3}V_2$	80*a–d*
			<3.06>				
Miserite	$K_2(Ca,Y,REE)_{10}$**$[Si_6O_{15}]_2[Si_2O_7]_2$**$(OH,F)_4(H_2O)_2$	$[Si_2O_7]^{6-}$	3.50	Cl	${}^{1}T_2$**	${}^{1}V_2$	49*d*
〃 〃	〃 〃	$[Si_6O_{15}]^{6-}$	2.50	T	${}^{3}T_{12}$	${}^{3}V_{12}$	48,49
			<2.75>				
Okenite	$Ca_2(H_2O)_9(H_2O)_3)(Ca_8$**$[Si_6O_{16}][Si_6O_{15}]_2$**$(H_2O)_6$	$[Si_6O_{16}]^{8-}$	2.67	R	${}^{2}T_2{}^{3}T_4$	${}^{2}V_2{}^{3}V_4$	67,68
〃 〃	〃 〃	$[Si_6O_{15}]^{6-}$	2.50	S	${}^{3}T_{12}$	${}^{3}V_{12}$	68*b*
			<2.56>				

Structure type: Cl: cluster, C: chain, R: ribbon, T: tube, S: single sheet.
* *r* values of ${}^{c}T_r$ expression multiplied or by 1.5 to conform to unit cell contents of mineral;
** *r* values of ${}^{c}T_r$ expression multiplied or by 2 to conform to unit cell contents of mineral;
*** *r* values of ${}^{c}T_r$ expression multiplied or by 3 to conform to unit cell contents of mineral.

[2] The maximum O:T ratio for any arrangement of tetrahedra that extends infinitely in a single direction is topologically constrained to 3.0. However, it is topologically possible to derive ribbon, and tube arrangements with O:T = 2.5–2.0 (Fig. 106) yet no such arrangements are observed in minerals; why?

[3] Are there specific topological characteristics that influence the abundance of a mineral with that topology? 4-connected vertices (${}^{4}V_r$) are extremely rare (**revdite** and **patynite**) and ${}^{4}V_n$ ribbons and tubes do not occur in chain-, ribbon- and tube-silicate minerals but occur in sheet-silicate minerals.

[4] Why is the abundance of chain-silicate minerals so much greater when O:T = 2.75–3.0?

[5] To what extent do the stoichiometries of the silicate units in cluster- and framework-silicates overlap with those of chain- and sheet-silicates? Are the general trends in mineral abundance as a function of the O:T similar to those observed in chain- and sheet-silicates minerals?

[6] Are there geometrical or topological relations between chain and sheet structures with the same tetrahedra and/or vertex connectivity?

[7] To what extent do the composition and structure of the rest of a mineral influence the geometry and topology of the chains, ribbons and/or tubes to which they link?

There are two major issues to pursue in the future: (1) examine the topological details of chains in order to derive all possible chain-ribbon-tube topologies (subject to reasonable boundary conditions such as a maximum value of the number of tetrahedra) such that we may characterise the aspects of chain, ribbon and tube topologies that dictate whether or not they correspond to observed chain arrangements in minerals; (2) look for general correlations between connectivity and paragenesis. Broad correlations between silicate stoichiometry, paragenesis and degree of fractionation were derived almost a century ago (Bowen, 1928); are these relations part of a more detailed connection between silicate structure and paragenesis? Hints at such detailed relations are apparent in the small amount of work that has been done for other oxyanions (e.g. pegmatitic phosphates, Moore, 1970, 1973; evaporitic Mg-sulfates, Hawthorne, 1992; secondary Te-oxysalt minerals, Christy *et al.*, 2016*a*,*b*). Furthermore, it will be interesting to compare paragenesis in igneous, hydrothermal/metasomatic and metamorphic environments where the structure of magmas and speciation in hydrothermal/metasomatic fluids almost certainly affect mineral structure and sequence of crystallisation.

Acknowledgements. We thank one anonymous reviewer and Sergey Krivovichev for suggestions that significantly improved this paper. The work was supported by a Graduate Fellowship to MCD from the University of

https://doi.org/10.1180/mgm.2020.13 Published online by Cambridge University Press

Manitoba and a Discovery Grant to FCH from the Natural Sciences and Engineering Research Council of Canada.

Supplementary material. To view supplementary material for this article, please visit https://doi.org/10.1180/mgm.2020.13

References

Abdu Y.A. and Hawthorne F.C. (2013) Local structure in *C*2/*c* clinopyroxenes on the hedenbergite ($CaFeSi_2O_6$)-ferrosilite ($Fe_2Si_2O_6$) join: A new interpretation for the Mössbauer spectra of Ca-rich *C*2/*c* clinopyroxenes and implications for pyroxene exsolution. *American Mineralogist*, **98**, 1227–1234.

Agakhanov A.A., Pautov L.A., Uvarova Y.A., Sokolova E.V., Hawthorne F.C. and Karpenko V.Y. (2005) Senkevichite $CsKNaCa_2TiO[Si_7O_{18}(OH)]$, a new mineral. *New Data on Minerals*, **40**, 17–22.

Agakhanov A.A., Pautov L.A., Uvarova Y.A., Sokolova E., Hawthorne F.C. and Karpenko V.Yu. (2008) Nalivkinite, $Li_2NaFe_7^{2+}Ti_2(Si_8O_{24})O_2(OH)_4F$, a new mineral of the astrophyllite group from the Darai-Pioz massif, Tadjikistan. *New Data on Minerals*, **43**, 5–12.

Agakhanov A.A., Pautov L.A., Karpenko V.Y., Sokolova E., Abdu Y.A., Hawthorne F.C., Pekov I.V. and Siidra O.I. (2015) Yusupovite, $Na_2Zr(Si_6O_{15})(H_2O)_3$, a new mineral species from the Darai-Pioz alkaline massif and its implications as a new microporous filter for large ions. *American Mineralogist*, **100**, 1502–1508.

Agakhanov A.A., Pautov L.A., Sokolova E., Abdu Y.A. and Karpenko V.Y. (2016) Two astrophyllite-supergroup minerals: bulgakite, a new mineral from the Darai-Pioz Alkaline Massif, Tajikistan and revision of the crystal structure and chemical formula of nalivkinite. *The Canadian Mineralogist*, **54**, 33–48.

Agrell S.O., Brown M.G. and McKie D. (1965) Deerite, howieite, and zussmanite, three new minerals from the Franciscan of the Laytonville district, Mendocino County, California. *American Mineralogist*, **50**, 278.

Akasaka M., Kimura T. and Nagashima M. (2013) X-ray Rietveld and ^{57}Fe Mössbauer study of babingtonite from Kouragahana, Shimane Peninsula, Japan. *Journal of Mineralogical and Petrological Sciences*, **108**, 121–130.

Aksenov S.M., Rastsvetaeva R.K., Chukanov N.V. and Kolitsch U. (2014) Structure of calcinaksite $KNa[Ca(H_2O)Si_4O_{10}]$, the first hydrous member of the litidionite group of silicates with $[Si_8O_{20}]^{8-}$ tubes. *Acta Crystallographica*, **B70**, 768–775.

Aksenov S.M., Shipalkina N.V., Rastsvetaeva R.K., Rusakov V.S., Pekov I.V., Chukanov N.V. and Yapaskurt V.O. (2015) Iron-rich bustamite from Broken Hill, Australia: the crystal structure and cation-ordering features. *Kristallografiya*, **60**, 340–345.

Alfors J.T., Stinson M.C., Matthews R.A. and Pabst A. (1965) Seven new barium minerals from eastern Fresno County, California. *American Mineralogist*, **50**, 314–340.

Amami J., Fend M. and Trabelsi-Ayedi M. (2005) Crystal structure and spectroscopic studies of $NaGd(PO_3)_4$. *Materials Research Bulletin*, **40**, 2144–2152.

Ams B.E., Jenkins D.M., Boerio-Goates J., Morcos R.M., Navrotsky A. and Bozhilov K.N. (2009) Thermochemistry of a synthetic Na-Mg-rich triple-chain silicate: determination of thermodynamic variables. *American Mineralogist*, **94**, 1242–1254.

Aoki Y., Akasako H. and Ishida K. (1981) Taneyamalite, a new manganese silicate mineral from the Taneyama mine, Kumamoto Prefecture, Japan. *Mineralogical Journal*, **10**, 385–395.

Araki T. and Zoltai T. (1972) Crystal structure of babingtonite. *Zeitschrift für Kristallographie*, **135**, 355–373.

Armbruster T. (2000) Cation distribution in Mg, Mn-bearing babingtonite from Arvigo, Val Calanca, Grisons, Switzerland. *Schweizerische Mineralogische und Petrographische Mitteilungen*, **80**, 279–284.

Armbruster T., Oberhänsli R. and Kunz M. (1993) Taikanite, $BaSr_2Mn_2^{3+}O_2[Si_4O_{12}]$, from the Wessels mine, South Africa: A chain silicate related to synthetic $Ca_3Mn_2^{3+}O_2[Si_4O_{12}]$. *American Mineralogist*, **78**, 1088–1095.

Baba S., Grew E.S., Shearer C.K. and Sheraton J.W. (2000) Surinamite: a high-temperature metamorphic beryllosilicate from Lewisian sapphirine-bearing kyanite-orthopyroxene-quartz-potassium feldspar gneiss at South Harris, N.W. Scotland. *American Mineralogist*, **85**, 1474–1484.

Bagiński B., Macdonald R., White J.C. and Jeżak L. (2018) Tuhualite in a peralkaline rhyolitic ignimbrite from Pantelleria, Italy. *European Journal of Mineralogy*, **30**, 367–373.

Bakakin V.V. and Soloveva L.P. (1970) The crystal structure of $Fe_3BeSi_3O_9(F,OH)_2$ the example of the wollastonitelike silicate chain on the basis of Fe. *Kristallografiya*, **15**, 1144–1151.

Barbier J., Grew E.S., Moore P.B. and Su S. (1999) Khmaralite, a new beryllium-bearing mineral related to sapphirine: a superstructure resulting from partial ordering of Be, Al, and Si on tetrahedral sites. *American Mineralogist*, **84**, 1650–1660.

Barbier J., Grew E.S., Hålenius E., Hålenius U. and Yates M.G. (2002) The role of Fe and cation order in the crystal chemistry of surinamite, $(Mg,Fe^{2+})_3(Al,Fe^{3+})_3O[AlBeSi_3O_{15}]$: a crystal structure, Mössbauer spectroscopic, and optical spectroscopic study. *American Mineralogist*, **87**, 501–513.

Basciano L.C., Groat L.A., Roberts A.C., Gault R.A., Dunning G.E. and Walstrom R.E. (2001) Bigcreekite: a new barium silicate mineral species from Fresno County, California. *The Canadian Mineralogist*, **39**, 761–768.

Basso R. and Carbone C. (2010) Relationships between crystal data and crystal chemistry of carpholite-group minerals. *Periodico di Mineralogia*, **79**, 91–98.

Basso R. and Della Giusta A. (1980) The crystal structure of a new manganese silicate. *Neues Jahrbuch für Mineralogie, Abhandlungen*, **138**, 333–342.

Basso R., Lucchetti G., Palenzona A. and Zefiro L. (1995) Haradaite from the Gambatesa mine, eastern Liguria, Italy. *Neues Jahrbuch für Mineralogie, Monatshefte*, 281–288.

Basso R., Cabella R., Lucchetti G., Martinelli A. and Palenzona A. (2005) Vanadiocarpholite, $Mn^{2+}V^{3+}Al(Si_2O_6)(OH)_4$, a new mineral from the Molinello mine, northern Apennines, Italy. *European Journal of Mineralogy*, **17**, 501–507.

Battocchio F., Monteiro P.J.M. and Wenk H.-R. (2012) Rietveld refinement of the structures of 1.0 C-S-H and 1.5 C-S-H. *Cement and Concrete Research*, **42**, 1534–1548.

Belluso E. and Ferraris G. (1991) New data on balangeroite and carlosturanite from alpine serpentinites. *European Journal of Mineralogy*, **3**, 559–566.

Belokoneva E.L. (2005) Symmetry and topological analysis of the OD nenadkevichite-labuntsovite-zorite family. *Kristallografiya*, **50**, 19–26.

Belov N.V. (1961) *Crystal Chemistry of Silicates with Large Cations*. Akademia Nauk SSSR, Moscow.

Berger T. and Range K.J. (1996) Zwei Metasilicate mit Vierer-einfach-Ketten: Hochdrucksynthese und Strukturverfeinerung von $Sr_2(VO)_2Si_4O_{12}$ (Haradait) und $Sr_2(TiO)_2Si_4O_{12}$. *Zeitschrift für Naturforschung, B: A Journal of Chemical Sciences*, **51**, 1099–1103.

Berman H. (1937) Constitution and classification of the natural silicates. *American Mineralogist*, **22**, 341–408.

Biagioni C., Bonaccorsi E., Lezzerini M., Merlini M. and Merlino S. (2012*a*) Thermal behaviour of tobermorite from N'Chwaning II mine (Kalahari Manganese Field, Republic of South Africa). I. Thermo-gravimetric and X-ray diffraction studies. *European Journal of Mineralogy*, **24**, 981–989.

Biagioni C., Bonaccorsi E., Merlino S., Bersani D. and Forte C. (2012*b*) Thermal behaviour of tobermorite from N'Chwaning II mine (Kalahari Manganese Field, Republic of South Africa) II. Crystallographic and spectroscopic study of tobermorite 10 Å. *European Journal of Mineralogy*, **24**, 991–1004.

Biagioni C., Merlino S. and Bonaccorsi E. (2015) The tobermorite supergroup: a new nomenclature. *Mineralogical Magazine*, **79**, 485–495.

Biagioni C., Bonaccorsi E., Lezzerini M. and Merlino S. (2016) Thermal behaviour of Al-rich tobermorite. *European Journal of Mineralogy*, **28**, 23–32.

Bissert G. (1980) Verfeinerung der struktur von tinaksit, $Ca_2K_2NaTiO[Si_7O_{18}(OH)]$. *Acta Crystallographica*, **B36**, 259–263.

Boggs R.C. (1988) Calciohilairite: $CaZrSi_3O_9(H_2O)_3$, the calcium analogue of hilairite from the Golden Horn batholith, northern Cascades, Washington. *American Mineralogist*, **73**, 1191–1194.

Boggs R.C. and Ghose S. (1985) Georgechaoite $NaKZrSi_3O_9{\cdot}2H_2O$, a new mineral species from Wind Mountain, New Mexico. *The Canadian Mineralogist*, **23**, 1–4.

Bonaccorsi E., Merlino S. and Pasero M. (1989) The crystal structure of the meteoritic mineral krinovite, $NaMg_2CrSi_3O_{10}$. *Zeitschrift für Kristallographie*, **187**, 133–138.

Bonaccorsi E., Merlino S. and Pasero M. (1990) Rhönite: structural and microstructural features, crystal chemistry and polysomatic relationships. *European Journal of Mineralogy*, **2**, 203–218.

Bonaccorsi E., Merlino S. and Taylor H.F.W. (2004) The crystal structure of jennite, $Ca_9Si_6O_{18}(OH)_6(H_2O)_8$. *Cement and Concrete Research*, **34**, 1481–1488.

Bonaccorsi E., Merlino S. and Kampf A.R. (2005) The crystal structure of tobermorite 14Å (plombierite), a C-S-H phase. *Journal of the American Ceramics Society*, **88**, 505–512.

Bonaccorsi E., Ferraris G. and Merlino S. (2012) Crystal structure of 2*M* and 1*A* polytypes of balangeroite. *Zeitschrift für Kristallographie*, **227**, 460–467.

Boucher M.L. and Peacor D.R. (1968) The crystal structure of alamosite, $PbSiO_3$. *Zeitschrift für Kristallographie*, **126**, 98–111.

Bowen N.L. (1928) *Evolution of Igneous Rocks*. Princeton University Press, Princeton, New Jersey, USA.

Bragg W.L. (1930) The structure of silicates. *Zeitschrift für Kristallographie*, **74**, 237–305.

Brandão P., Rocha J., Reis M.S., dos Santos A.M. and Jin R. (2009) Magnetic properties of $KNaMSi_4O_{10}$ compounds (M = Mn, Fe, Cu). *Journal of Solid State Chemistry*, **182**, 253–258.

Brugger J. and Berlepsch P. (1997) Johninnesite, $Na_2(Mn^{2+})_9(Mg,Mn)_7(AsO_4)_2(Si_6O_{17})_2(OH)_8$: a new occurrence in Val Ferrera (Graubünden, Switzerland). *Schweizerische Mineralogische und Petrographische Mitteilungen*, **77**, 449–455.

Brugger J., Krivovichev S., Meisser N., Ansermet S. and Armbruster T. (2006) Scheuchzerite, $Na(Mn,Mg)_9[VSi_9O_{28}(OH)](OH)_3$, a new single-chain silicate. *American Mineralogist*, **91**, 937–943.

Bruno E., Carbonin S. and Molin G. (1982) Crystal structures of Ca-rich clinopyroxenes on the $CaMgSi_2O_6$–$Mg_2Si_2O_6$ join. *Tschermaks Mineralogische und Petrographische Mitteilungen*, **29**, 223–240.

Buerger M.J. (1956) The determination of the crystal structure of pectolite, $Ca_2NaHSi_3O_8$. *Zeitschrift für Kristallographie*, **108**, 248–261.

Buerger M.J. and Venkatakrishnan V. (1974) Serendibite, a complicated, new, inorganic crystal structure. *Proceedings of the National Academy of Sciences of the United States of America*, **71**, 4348–4351.

Burnham C.W. (1971) The crystal structure of pyroxferroite from Mare Tranquillitatis. *Proceedings of the Second Lunar Science Conference*, **1**, 47–57.

Burns P.C. (1999) The crystal chemistry of uranium. Pp. 23–90 in: *Uranium: Mineralogy, Geochemistry, and the Environment* (P.C. Burns and R. Finch, editors). Reviews in Mineralogy, **38**. Mineralogical Society of America, Washington, DC.

Burns P.C. (2001) A new uranyl silicate sheet in the structure of haiweeite and comparison to other uranyl silicates. *The Canadian Mineralogist*, **39**, 1153–1160.

Burns P.C. (2005) U^{6+} minerals and inorganic compounds: insights into an expanded structural hierarchy of crystal structures. *The Canadian Mineralogist*, **43**, 1839–1894.

Burns P.C., Grice J.D. and Hawthorne F.C. (1995) Borate minerals. I. Polyhedral clusters and fundamental building blocks. *The Canadian Mineralogist*, **33**, 1131–1151.

Burt D.M. (1994) Vector representation of some mineral compositions in the aenigmatite group, with special reference to hogtuvaite. *The Canadian Mineralogist*, **32**, 449–457.

Burt J.B., Downs R.T. and Costin G. (2007) Single-crystal X-ray refinement of wilkensonite, $Na_2Fe_4^{2+}Fe_2^{3+}Si_6O_{20}$. *Acta Crystallographica*, **E63**, 122–124.

Cadoni M. and Ferraris G. (2011) Synthesis and crystal structure of $Na_2MnSi_4O_{10}$: relationship with the manaksite group. *Rendiconti Lincei*, **22**, 225–234.

Callegari A.M., Boiocchi M., Bellatreccia F., Caprilli E., Medenbach O. and Cavallo A. (2011) Capranicaite, $(K,\square)(Ca,Na)Al_4B_4Si_2O_{18}$: a new inosilicate from Capranica, Italy, with a peculiar topology of the periodic single chain $[Si_2O_6]$. *Mineralogical Magazine*, **75**, 33–43.

Cámara F., Sokolova E., Abdu Y. and Hawthorne F.C. (2010) The crystal structures of niobophyllite, kupletskite-(Cs) and Sn-rich astrophyllite: revisions to the crystal chemistry of the astrophyllite-group minerals. *The Canadian Mineralogist*, **48**, 1–16.

Cámara F., Sokolova E., Hawthorne F.C., Rowe R., Grice J.D. and Tait K.T. (2013) Veblenite, $K_2\square_2Na(Fe_5^{2+}Fe_4^{3+}Mn_7^{2+}\square)Nb_3Ti(Si_2O_7)_2(Si_8O_{22})_2O_6(OH)_{10}(H_2O)_3$, a new mineral from Seal Lake, Newfoundland and Labrador: mineral description, crystal structure, and a new veblenite Si_8O_{22} ribbon. *Mineralogical Magazine*, **77**, 2955–2974.

Cámara F., Sokolova E., Abdu Y.A. and Hawthorne F.C. (2014) Nafertisite, $Na_3Fe_{10}^{2+}Ti_2(Si_6O_{17})_2O_2(OH)_6F(H_2O)_2$, from Mt. Kukisvumchorr, Khibiny alkaline massif, Kola peninsula, Russia: Refinement of the crystal structure and revision of the chemical formula. *European Journal of Mineralogy*, **26**, 689–700.

Cameron M. and Papike J.J. (1979) Amphibole crystal chemistry: a review. *Fortschritte der Mineralogie*, **57**, 28–67.

Cameron M. and Papike J.J. (1981) Structural and chemical variations in pyroxenes. *American Mineralogist*, **66**, 1–50.

Cannillo E., Mazzi F., Fang J.H., Robinson P.D. and Ohya Y. (1971) The crystal structure of aenigmatite. *American Mineralogist*, **56**, 427–446.

Cannillo E., Rossi G. and Ungaretti L. (1973) The crystal structure of elpidite. *American Mineralogist*, **58**, 106–109.

Carpenter A.B., Chalmers R.A., Gard J.A., Speakman K. and Taylor H.F.W. (1966) Jennite, a new mineral. *American Mineralogist*, **51**, 56–74.

Celestian A.J., Lively J. and Xu W. (2019) In situ Cs and H exchange into gaidonnayite and proposed mechanisms of ion diffusion. *Inorganic Chemistry*, **58**, 1919–1928.

Cesbron F.P. and Williams S.A. (1980) Apachite and gilalite, two new copper silicates from Christmas, Arizona. *Mineralogical Magazine*, **43**, 639–641.

Chao G.Y. (1985) The crystal structure of gaidonnayite $Na_2ZrSi_3O_9{\cdot}2H_2O$. *The Canadian Mineralogist*, **23**, 11–15.

Chao G.Y. and Watkinson D.H. (1974) Gaidonnayite, $Na_2ZrSi_3O_9{\cdot}2H_2O$, a new mineral from Mont St. Hilaire, Quebec. *The Canadian Mineralogist*, **12**, 316–319.

Chao G.Y., Watkinson D.H. and Chen T.T. (1974) Hilairite, $Na_2ZrSi_3O_9(H_2O)_3$, a new mineral from Mont St. Hilaire, Quebec. *The Canadian Mineralogist*, **12**, 237–240.

Chiragov M.I. and Shirinova A.F. (2004) Crystal structure of charoite; relations to structures of miserite, canasite and okenite. *Mineralogicheskiy Zhurnal*, **26**, 5–9.

Chisholm J.E. (1981) Pyribole structure types. *Mineralogical Magazine*, **44**, 205–216.

Christiansen C.C., Johnsen O. and Stahl K. (1998) Crystal structure of kupletskite from the Kangerdlugssuaq intrusion, East Greenland. *Neues Jahrbuch für Mineralogie, Monatshefte*, 253–264.

Christy A.G. (1988) A new 2c superstructure in beryllian sapphirine from Casey Bay, Enderby Land, Antarctica. *American Mineralogist*, **73**, 1134–1137.

Christy A.G. (1989) The effect of composition, temperature and pressure on the stability of the 1*Tc* and 2*M* polytypes of sapphirine. *Contributions to Mineralogy and Petrology*, **103**, 203–215.

Christy A.G. and Grew E.S. (2004) Synthesis of beryllian sapphirine in the system MgO–BeO–Al_2O_3–SiO_2–H_2O and comparison with naturally occurring beryllian sapphirine and khmaralite, Part 2: A chemographic study of Be content as a function of P, T, assemblage and FeMg-1 exchange. *American Mineralogist*, **89**, 327–338.

Christy A.G. and Putnis A. (1988) Planar and line defects in the sapphirine polytypes. *Physics and Chemistry of Minerals*, **15**, 548–558.

Christy A.G., Tabira Y., Hölscher A., Grew E.S. and Schreyer W. (2002) Synthesis of beryllian sapphirine in the system MgO–BeO–Al_2O_3–SiO_2–H_2O and comparison with naturally occurring beryllian sapphirine and khmaralite. Part 1: experiments, TEM, and XRD. *American Mineralogist*, **87**, 1104–1112.

Christy A.G., Mills S.J., Kampf A.R., Housley R.M., Thorne B. and Marty J. (2016*a*) The relationship between mineral composition, crystal structure and paragenetic sequence: the case of secondary Te mineralization at the Bird Nest drift, Mountain, California, USA. *Mineralogical Magazine* **80**, 291–310.

Christy A.G., Mills S.J. and Kampf A.R. (2016*b*) A review of the structural architecture of tellurium oxycompounds. *Mineralogical Magazine*, **80**, 415–545.

Chukanov N.V., Aksenov S.M., Rastsvetaeva R.K., Van K.V., Belakovskiy D.I., Pekov I.V., Gurzhiy V.V., Schüller W. and Ternes B. (2015*a*) Mendigite, $Mn_2Mn_2MnCa(Si_3O_9)_2$, a new mineral species of the bustamite group from the Eifel Volcanic region, Germany. *Geology of Ore Deposits*, 57, 721–731.

https://doi.org/10.1180/mgm.2020.13 Published online by Cambridge University Press

Chukanov N.V., Aksenov S.M., Rastsvetaeva R.K., Blass G., Varlamov D.A., Pekov I.V., Belakovskiy D.I. and Gurzhiy V.V. (2015*b*) Calcinaksite, $KNaCa(Si_4O_{10})H_2O$, a new mineral from the Eifel volcanic area, Germany. *Mineralogy and Petrology*, **109**, 397–404.

Churakov S.V. (2009) Structural position of H_2O molecules and hydrogen bonding in anomalous 11Å tobermorite. *American Mineralogist*, **94**, 156–165.

Churakov S.V. and Mandaliev P. (2008) Structure of the hydrogen bonds and silica defects in the tetrahedral double chain of xonotlite. *Cement and Concrete Research*, **38**, 300–311.

Coda A., Dal Negro A. and Rossi G. (1967) The crystal structure of krauskopfite. *Atti della Accademia Nazionale dei Lincei*, **42**, Ser. B, 859–873.

Compagnoni R., Ferraris G. and Fiora L. (1983) Balangeroite, a new fibrous silicate related to gageite from Balangero, Italy. *American Mineralogist*, **68**, 214–219.

Compagnoni R., Ferraris G. and Mellini M. (1985) Carlosturanite, a new asbestiform rock-forming silicate from Val Varaita, Italy. *American Mineralogist*, **70**, 767–772.

Cong X. and Kirkpatrick R.J. (1996) ^{29}Si and ^{17}O NMR investigation of the structure of some crystalline calcium silicate hydrates. *Advanced Cement Based Materials*, **3**, 133–143.

Cooper M.A. and Hawthorne F.C. (1998) The crystal structure of blatterite, $Sb_3^{5+}(Mn^{3+},Fe^{3+})_9$ $(Mn^{2+},Mg)_{35}(BO_3)_{16}O_{32}$, and structural hierarchy in Mn^{3+}-bearing zigzag borates. *The Canadian Mineralogist*, **36**, 1171–1193.

Cosca M.A., Rouse R.R. and Essene E.J. (1988) Dorrite $[Ca_2(Mg_2Fe_4^{3+})(Al_4Si_2)O_{20}]$, a new member of the aenigmatite group from a pyrometamorphic melt-rock. *American Mineralogist*, **73**, 1440–1448.

Cruciani G., De Luca P., Nastro A. and Pattison P. (1998) Rietveld refinement of the zorite structure of ETS-4 molecular sieves. *Microporous and Mesoporous Materials*, **21**, 143–153.

Czank M. (1981) Chain periodicity faults in babingtonite, $Ca_2Fe^{2+}Fe^{3+}H[Si_5O_{15}]$. *Acta Crystallographica*, **A37**, 617–620.

Czank M. and Bissert G. (1993) The crystal structure of $Li_2Mg_2[Si_4O_{11}]$, a loop-branched dreier single chain silicate. *Zeitschrift für Kristallographie*, **204**, 129–142.

Dai Y. and Post J.E. (1995) Crystal structure of hillebrandite: A natural analogue of calcium silicate hydrate (CSH) phases in Portland cement. *American Mineralogist*, **80**, 841–844.

Deriu A., Ferraris G. and Belluso E. (1994) ^{57}Fe Mössbauer study of the asbestiform silicates balangeroite and carlosturanite. *Physics and Chemistry of Minerals*, **21**, 222–227.

De Roever E.W.F., Kieft C., Murray E., Klein E., Drucker W.H. and Moore P.B. (1976) Surinamite, a new Mg–Al silicate from the Bakhuis Mountains, western Surinam I. Description, occurrence, and conditions of formation II. X-ray crystallography and proposed crystal structure. *American Mineralogist*, **61**, 193–199.

Donnay G. and Chao G.Y. (1986) Hydrogen bonding in gaidonnayite. *The Canadian Mineralogist*, **24**, 417–419.

Dorfman M.D., Rogachev D.D., Goroshchenko Z.I. and Uspenskaya E.I. (1959) Canasite, a new mineral. *Trudy Mineralogicheskogo Muzeya Akademiya Nauk SSSR*, **9**, 158–166.

Dornberger-Schiff K. and Merlino S. (1974) Order-disorder in sapphirine, aenigmatite and aenigmatite-like minerals. *Acta Crystallographica*, **A30**, 168–173.

Dörsam G., Kahlenberg V. and Fischer R.X. (2003) Single crystal X-ray diffraction study of $CsHSi_2O_5$. *Zeitschrift für Anorganische und Allgemeine Chemie*, **629**, 981–984.

Downs R.T., Pinch W.W., Thompson R.M., Evans S.H. and Megaw L. (2016) Yangite, $PbMnSi_3O_8{\cdot}H_2O$, a new mineral species with double wollastonite silicate chains from the Kombat mine, Namibia. *American Mineralogist*, **101**, 2539–2543.

Duggan M.B. (1990) Wilkinsonite, $Na_2Fe_4^{2+}Fe_2^{3+}Si_6O_{20}$, a new member of the aenigmatite group from the Warrumbungle Volcano, New South Wales, Australia. *American Mineralogist*, **75**, 694–701.

Dunn P.J. (1979) The chemical composition of gageite: an empirical formula. *American Mineralogist*, **64**, 1056–1058.

Dunn P.J., Rouse R.C., Cannon B. and Nelen J.A. (1977) Zektzerite: a new lithium sodium zirconium silicate related to tuhualite and the osumilite group. *American Mineralogist*, **62**, 416–420.

Dunn P.J., Peacor D.R., Su S.C., Nelen J.A. and von Knorring O. (1986) Johninnesite, a new sodium manganese arsenosilicate from the Kombat Mine, Namibia. *Mineralogical Magazine*, **50**, 667–670.

Durand G., Vilminot S., Richard-Plouet M., Derory A., Lambour J.P. and Drillon M. (1997) Magnetic behavior of $Na_2MSi_4O_{10}$ (M = Co, Ni) compounds. *Journal of Solid State Chemistry*, **131**, 335–340.

Erd R.C. and Ohashi Y. (1984) Santaclaraite, a new calcium-manganese silicate hydrate from California. *American Mineralogist*, **69**, 200–206.

Evans B.W. and Kuehner S.M. (2011) A nickel-iron analogue of balangeroite and gageite (Sasaguri, Kyushu, Japan). *European Journal of Mineralogy*, **23**, 717–720.

Evans Jr. H.T. and Mrose M.E. (1966) Shattuckite and planchéite: a crystal chemical study. *Science*, **154**, 506–507.

Evans Jr. H.T. and Mrose M.E. (1977) The crystal chemistry of the hydrous copper silicates, shattuckite and planchéite. *American Mineralogist*, **62**, 491–502.

Evans Jr. H.T. and Hughes J.M. (1990) Crystal chemistry of the natural vanadium bronzes. *American Mineralogist*, **75**, 508–521.

Fang J.H., Robinson P.D. and Ohya Y. (1972) Redetermination of the crystal structure of eudidymite and its dimorphic relationship to epididymite. *American Mineralogist*, **57**, 1345–1354.

Ferraris G., Mellini M. and Merlino S. (1987) Electron-diffraction and electron-microscopy study of balangeroite and gageite: Crystal structures, polytypism, and fiber texture. *American Mineralogist*, **72**, 382–391.

Ferraris G., Ivaldi G., Khomyakov A.P., Sobolova S.V., Belluso E. and Pavese A. (1996) Nafertisite, a layer titanosilicate member of a polysomatic series including mica. *European Journal of Mineralogy*, **8**, 241–249.

Fewox C.S., Clearfield A. and Celestian A.J. (2011) In situ X-ray diffraction study of cesium exchange in synthetic umbite. *Inorganic Chemistry*, **50**, 3596–3604.

Filatov S.K., Semenova T.F. and Vergasova L.P. (1992) Types of polymerization of $[OCu_4]^{6+}$ tetrahedra in compounds with 'additional' oxygen atoms. *Proceedings of the USSR Academy of Sciences*, **322**, 536–539 [in Russian].

Filipenko O.S., Pobedimskaya E.A., Ponomarev V.I. and Belov N.V. (1971) Cristaline structure of synthetic barium silicate $Ba_4Si_6O_{16}$ new band oxysilicic radical (Si_6O_{16}). *Doklady Akademii Nauk SSSR*, **196**, 1337–1340.

Finger L.W. and Hazen R.M. (1978) Refined occupancy factors for synthetic Mn–Mg pyroxmangite and rhodonite. *Carnegie Institution of Washington Year Book*, **77**, 850–853.

Fleet M.E. (1977) The crystal structure of deerite. *American Mineralogist*, **62**, 990–998.

Fuchs L.H. (1971) Occurrence of wollastonite, rhoönite, and andradite in the Allende meteorite. *American Mineralogist*, **56**, 2053–2068.

Fuchs L.H. (1978) The mineralogy of a rhoönite-bearing calcium aluminum rich inclusion in the Allende meteorite. *Meteoritics*, **13**, 73–88.

Fuchs I., Mellini M. and Memmi I. (2001) Crystal-chemistry of magnesiocarpholite: controversial X-ray diffraction, Mössbauer, FTIR and Raman results. *European Journal of Mineralogy*, **13**, 533–543.

Gaeta M. and Mottana A. (1991) Phase relations of aenigmatite minerals in a syenitic ejectum, Wonchi volcano, Ethiopia. *Mineralogical Magazine*, **55**, 529–534.

Gagné O. and Hawthorne F.C. (2015) Comprehensive derivation of bond-valence parameters for ion pairs involving oxygen. *Acta Crystallographica*, **B71**, 562–578.

Gagné O. and Hawthorne F.C. (2016) Chemographic exploration of the milarite-type structure. *The Canadian Mineralogist*, **54**, 1229–1247.

Gagné O. and Hawthorne F.C. (2017) Empirical Lewis-acid strengths for 135 cations bonded to oxygen. *Acta Crystallographica*, **B73**, 956–961.

Galuskina I.O., Galuskin E.V., Pakhomova A.S., Widmer R., Armbruster T., Krüger B., Grew E.S., Vapnik Y., Dzierażanowski P. and Murashko M. (2017) Khesinite, $Ca_4Mg_2Fe_{10}^{3+}O_4[(Fe_{10}^{3+}Si_2)O_{36}]$, a new rhönite-group (sapphirine supergroup) mineral from the Negev Desert, Israel – natural analogue of the SFCA phase. *European Journal of Mineralogy*, **29**, 101–116.

Garbev K. (2004) *Struktur, Eigenschaften und quantitative Rietveldanalyse von hydrothermal kristallisierten Calciumsilikathydraten (C-S-H-Phasen)*. Dissertation, Institut fur Technische Chemie, Ruprecht-Karls-Universität Heidelberg, Germany. Forschungzentrum Karlsruhe GmbH Wissenschaftliche Berichte FZKA6877.

Gard J.A. and Taylor H.F.W. (1958) Foshagite: composition, unit cell and dehydration. *American Mineralogist*, **43**, 1–15.

https://doi.org/10.1180/mgm.2020.13 Published online by Cambridge University Press

Gard J.A. and Taylor H.F.W. (1960) The crystal structure of foshagite. *Acta Crystallographica*, **13**, 785–793.

Gard J.A. and Taylor H.F.W. (1976) Calcium silicate hydrate (II) (C-S-H(II)). *Cement and Concrete Research*, **6**, 667–678.

Gard J.A., Taylor H.F.W., Cliff G. and Lorimer G.W. (1977) A re-examination of jennite. *American Mineralogist*, **62**, 365–368.

Gatta G.D., Rotiroti N., McIntyre G.J., Guastoni A. and Nestola F. (2008) New insights into the crystal chemistry of epididymite and eudidymite from Malosa, Malawi: a single-crystal neutron diffraction study. *American Mineralogist*, **93**, 1158–1165.

Gault R.A., Ercit T.S., Grice J.D. and Velthuizen J.V. (2004) Manganokukisvumite, a new mineral species from Mont Saint-Hilaire, Quebec. *The Canadian Mineralogist*, **42**, 781–785.

Gay P. and Rickson K.O. (1960) X-ray data on stokesite. *Mineralogical Magazine*, **32**, 433–435.

George A.M., Richet P. and Stebbins J.F. (1998) Cation dynamics and premelting in lithium metasilicate (Li_2SiO_3) and sodium metasilicate (Na_2SiO_3): A high-temperature NMR study. *American Mineralogist*, **83**, 1277–1284.

Ghent E.D., Stout M.Z. and Erdmer P. (1990) Howieite in blueschists, Pinchi Lake, British Columbia. *The Canadian Mineralogist*, **28**, 855–858.

Ghose S. and Thakur P. (1985) The crystal structure of georgechaoite $NaKZrSi_3O_9{\cdot}2H_2O$. *The Canadian Mineralogist*, **23**, 5–10.

Ghose S. and Wan C. (1978) Zektzerite, $NaLiZrSi_6O_{15}$: a silicate with six-tetrahedral-repeat double chains. *American Mineralogist*, **63**, 304–310.

Ghose S. and Wan C. (1979) Agrellite, $Na(Ca,RE)_2Si_4O_{10}F$: a layer structure with silicate tubes. *American Mineralogist*, **64**, 563–572.

Ghose S., Sen Gupta P.K., Boggs R.C. and Schlemper E.O. (1989) Crystal chemistry of a nonstoichiometric carpholite, $K_x(Mn_{2-x}Li_x)Al_4Si_4O_{12}(OH)_4F_4$: A chain silicate related to pyroxenes. *American Mineralogist*, **74**, 1084–1090.

Gittins J., Gasparrini E.L. and Fleet S.G. (1973) The occurrence of vlasovite in Canada. *The Canadian Mineralogist*, **12**, 211–214.

Gobechiya E.R., Pekov I.V., Pushcharovsky D.Y., Ferraris G., Gula A., Zubkova N.V. and Chukanov N.V. (2003) New data on vlasovite: refinement of the crystal structure and the radiation damage of the crystal during the X-ray diffraction experiment. *Kristallografiya*, **48**, 808–812.

Golovachev V.P., Drozdov Y.N., Kuz'min E.A. and Belov N.V. (1971) The crystal structure of phenaxite $FeNaK(Si_4O_{10})(KNaFe[Si_4O_{10}])$. *Doklady Akademii Nauk SSSR*, **15**, 902–904.

Grauch R.I., Lindahl I., Evans H.T., Burt D.M., Fitzpatrick J.J., Foord E.E., Graff P. and Hysingjord J. (1994) Høgtuvaite, a new beryllian member of the aenigmatite group from Norway, with new X-ray data on aenigmatite. *The Canadian Mineralogist*, **32**, 439–448.

Grew E.S., Hålenius U., Kritikos M. and Shearer C.K. (2001) New data on welshite, e.g. $Ca_2Mg_{3.8}Mn^{2+}_{0.6}Fe^{2+}_{0.1}Sb^{5+}_{1.5}O_2[Si_{2.8}Be_{1.7}Fe^{3+}_{0.65}Al_{0.7}As_{0.17}O_{18}]$, an aenigmatite-group mineral. *Mineralogical Magazine*, **65**, 665–674.

Grew E.S., Barbier J., Britten J., Yates M.G., Polyakov V.O., Shcherbakova E.P., Hålenius U. and Shearer C.K. (2005) Makarochkinite, $Ca_2Fe^{2+}_4Fe^{3+}TiSi_4BeAlO_{20}$, a new beryllosilicate member of the aenigmatite-sapphirine-surinamite group from the Il'men mountains (souther Urals), Russia. *American Mineralogist*, **90**, 1402–1412.

Grew E.S., Barbier J., Britten J., Halenius U. and Shearer C.K. (2007) The crystal chemistry of welshite, a non-centrosymmetric (P1) aenigmatite-sapphirine-surinamite group mineral. *American Mineralogist*, **92**, 80–90.

Grew E.S., Hålenius U., Pasero M. and Barbier J. (2008*a*) Recommended nomenclature for the sapphirine and surinamite group (sapphirine supergroup). *Mineralogical Magazine*, **72**, 839–876.

Grew E.S., Hålenius U. and Pasero M. (2008*b*) The crystal-chemistry of aenigmatite revisited: electron microprobe data, structure refinement and Mössbauer spectroscopy of aenigmatite from Vesterøya (Norway). *European Journal of Mineralogy*, **20**, 983–991.

Grice J.D. and Dunn P.J. (1994) Johninnesite: Crystal-structure determination and its relationship to other arsenosilicates. *American Mineralogist*, **79**, 991–995.

Grice J.D., Belley P.M. and Fayek M. (2014) Serendibite, a complex chemical borosilicate mineral from Pontiac, Quebec: Description, chemical composition, and crystallographic data. *The Canadian Mineralogist*, **52**, 1–14.

Grice J.D., Rowe R. and Poirier G. (2015) Hydroterskite: A new mineral species from the Saint-Amable Sill, Quebec, and a comparison with terskite and elpidite. *The Canadian Mineralogist*, **53**, 821–832.

Grice J.D., Burns P.C. and Hawthorne F.C. (1999) Borate minerals II. A hierarchy of structures based on the borate fundamental building block. *The Canadian Mineralogist*, **37**, 731–762.

Grigor'eva A.A., Zubkova N.V., Pekov I.V. and Pushcharovsky D.Y. (2009) Crystal structure of hilairite from Khibiny Alkaline Massif (Kola Peninsula). *Doklady Earth Sciences*, **428**, 1051–1053.

Grigor'eva A.A., Zubkova N.V., Pekov I.V., Kolitsch U., Pushcharovsky D.Y., Vigasina M.F., Giester G., Dordević T., Tillmanns E. and Chukanov N.V. (2011) Crystal chemistry of elpidite from Kahn Bogdo (Mongolia) and its K- and Rb-exchanged forms. *Kristallografiya*, **56**, 832–841.

Grosse H.P. and Tillmanns E. (1974) Bariummetasilicate, $BaSiO_3$ (hT). *Crystal Structure Communications*, **3**, 603–605.

Gunawardane R.P., Cradwick M.E. and Dent Glasser L.S. (1973) Crystal structure of $Na_2BaSi_2O_6$. *Journal of the Chemical Society, Dalton Transactions, Inorganic Chemistry*, 2397–2400.

Haile S.M. and Wuensch B.J. (1997) Comparison of the crystal chemistry of selected MSi_6O_{15}-based silicates. *American Mineralogist*, **82**, 1141–1149.

Hamid S.A. (1981) The crystal structure of the 11Å natural tobermorite $Ca_{2.25}[Si_3O_{7.5}(OH)_{1.5}]H_2O$. *Zeitschrift für Kristallographie*, **154**, 189–198.

Hang C., Simonov M.A. and Belov N.V. (1969) The crystalline structure of ramsayite $Na_2Ti_2Si_2O_9 = Na_2Ti_2O_3(Si_2O_6)$. *Doklady Akademii Nauk SSSR*, **186**, 820–823.

Hawthorne F.C. (1981) Crystal chemistry of the amphiboles. Pp. 1–102 in: *Amphiboles and Other Hydrous Pyriboles: Mineralogy* (D.R. Veblen and P.H. Ribbe, editors). Reviews in Mineralogy, **9A**. Mineralogical Society of America, Washington, DC.

Hawthorne F.C. (1983*a*) Graphical enumeration of polyhedral clusters. *Acta Crystallographica*, **A39**, 724–736.

Hawthorne F.C. (1983*b*) Characterization of the average structure of natural and synthetic amphiboles. *Periodico di Mineralogia*, **52**, 543–581.

Hawthorne F.C. (1983*c*) The crystal chemistry of the amphiboles. *The Canadian Mineralogist*, **21**, 173–480.

Hawthorne F.C. (1984) The crystal structure of stenonite and the classification of the aluminofluoride minerals. *The Canadian Mineralogist*, **22,** 245–251.

Hawthorne F.C. (1985) Towards a structural classification of minerals: The VIMIVT2On minerals. *American Mineralogist*, **70**, 455–473.

Hawthorne F.C. (1986) Structural hierarchy in $^{VI}M_x^{III}T_y\varphi_z$ minerals. *The Canadian Mineralogist*, **24**, 625–642.

Hawthorne F.C. (1990) Structural hierarchy in $M^{[6]}T^{[4]}\varphi_n$ minerals. *Zeitschrift für Kristallographie*, **192**, 1–52.

Hawthorne F.C. (1992) The role of OH and H_2O in oxide and oxysalt minerals. *Zeitschrift für Kristallographie*, **201**, 183–206.

Hawthorne F.C. (1998) Structure and chemistry of phosphate minerals. *Mineralogical Magazine*, **62**, 141–164.

Hawthorne F.C. (2002) The use of end-member charge-arrangements in defining new mineral species and heterovalent substitutions in complex minerals. *The Canadian Mineralogist*, **40**, 699–710.

Hawthorne F.C. (2012*a*) A bond-topological approach to theoretical mineralogy: crystal structure, chemical composition and chemical reactions. *Physics and Chemistry of Minerals*, **39**, 841–874.

Hawthorne F.C. (2012*b*) Bond topology and structure-generating functions: Graph-theoretic prediction of chemical composition and structure in polysomatic T–O–T (biopyribole) and H–O–H structures. *Mineralogical Magazine*, **76**, 1053–1080.

Hawthorne F.C. (2014) The structure hierarchy hypothesis. *Mineralogical Magazine*, **78**, 957–1027.

Hawthorne F.C. (2015*a*) Generating functions for stoichiometry and structure of single- and double-layer sheet-silicates. *Mineralogical Magazine*, **79**, 1675–1709.

Hawthorne F.C. (2015*b*) Toward theoretical mineralogy: a bond-topological approach. *American Mineralogist*, **100**, 696–713.

Hawthorne F.C. (2018) A bond-topological approach to borate minerals: A brief review. *Physics and Chemistry of Glasses – European Journal of Glass Science and Technology*, **59B**, 121–129.

https://doi.org/10.1180/mgm.2020.13 Published online by Cambridge University Press

Hawthorne F.C. and Oberti R. (2007) Amphiboles: crystal chemistry. Pp. 1–54 in: *Amphiboles: Crystal Chemistry, Occurrence, and Health Issues* (F.C. Hawthorne, R. Oberti, G. Della Ventura and A. Mottana, editors). Reviews in Mineralogy & Geochemistry, **67**. Mineralogical Society of America and the Geochemical Society, Chantilly, Virginia, USA.

Hawthorne F.C. and Schindler M. (2008) Understanding the weakly bonded constituents in oxysalt minerals. *Zeitschrift für Kristallographie*, **223**, 41–68.

Hawthorne F.C. and Smith J.V. (1986*a*) Enumeration of 4-connected 3-dimensional nets and classification of framework silicates. 3D nets based on insertion of 2-connected vertices onto 3- connected plane nets. *Zeitschrift für Kristallographie*, **175**, 15–30.

Hawthorne F.C. and Smith J.V. (1986*b*) Enumeration of 4-connected 3-dimensional nets and classification of framework silicates. Body-centred cubic nets based on the rhombicuboctahedron. *The Canadian Mineralogist*, **24**, 643–648.

Hawthorne F.C. and Smith J.V. (1988) Enumeration of 4-connected 3-dimensional nets and classification of framework silicates. Combination of zigzag and saw chains with 6^3, 3.12^2, 4.8^2, 4.6.12 and $(5^2.8)_2(5.8^2)_1$ nets. *Zeitschrift für Kristallographie*, **183**, 213–231.

Hawthorne F.C. and Sokolova E. (2012) The role of H_2O in controlling bond topology: The $^{[6]}Mg(SO_4)(H_2O)_n$ ($n = 0$–6) structures. *Zeitschrift für Kristallographie*, **227**, 594–603.

Hawthorne F.C., Burns P.C. and Grice J.D. (1996) The crystal chemistry of boron. Pp. 41–115 in: *Boron: Mineralogy, Petrology, and Geochemistry* (L.M. Anovitz and E.S. Grew, editors). Reviews in Mineralogy, **33**. Mineralogical Society of America, Washington, DC.

Hawthorne F.C., Krivovichev S.V. and Burns P.C. (2000) The crystal chemistry of sulfate minerals. Pp. 1–112 in: *Sulfate Minerals: Crystallography, Geochemistry, and Environmental Significance* (C.N. Alpers, J.L. Jambor, and D.K. Nordstrom, editors). Reviews in Mineralogy & Geochemistry, **40**. Mineralogical Society of America, Washington, DC.

Hawthorne F.C., Oberti R., Della Ventura G. and Mottana A. (editors)(2007) *Amphiboles: Crystal Chemistry, Occurrence and Health Issues*. Reviews in Mineralogy & Geochemistry, **67**. Mineralogical Society of America and the Geochemical Society, Chantilly, Virginia, USA.

Hawthorne F.C., Oberti R., Harlow G.E., Maresch W.V., Martin R.F., Schumacher J.C. and Welch M.D. (2012) Nomenclature of the amphibole group. *American Mineralogist*, **97**, 2031–2048.

Hawthorne F.C., Sokolova E., Pautov, L.A., Agakhanov A.A. and Karpenko V.Y. (2016) Refinement of the crystal structure of berezanskite, $Ti_2\square_2KLi_3(Si_{12}O_{30})$. *Mineralogical Magazine*, **80**, 733–737.

Hawthorne F.C., Uvarova Y.A. and Sokolova E. (2019) A structure hierarchy for silicate minerals: sheet silicates. *Mineralogical Magazine*, **83**, 3–55.

Hejny C. and Armbruster T. (2001) Polytypism in xonotlite $Ca_6Si_6O_{17}(OH)_2$. *Zeitschrift für Kristallographie*, **216**, 396–408.

Henmi C. and Kusachi I. (1992) Clinotobermorite, $Ca_5Si_6(O,OH)_{18}\cdot 5H_2O$, a new mineral from Fuka, Okayama Prefecture, Japan. *Mineralogical Magazine*, **56**, 353–358.

Henmi C., Kusachi I., Kawahara A. and Henmi K. (1977) Fukalite, a new calcium carbonate silicate hydrate mineral. *Mineralogical Journal*, **8**, 374–381.

Henmi C., Kawahara A., Henmi K., Kusachi I. and Takéuchi Y. (1983) The 3*T*, 4*T* and 5*T* polytypes of wollastonite from Kushiro, Hiroshima Prefecture, Japan. *American Mineralogist*, **68**, 156–163.

Hesse K.F. (1984) Refinement of the crystal structure of wollastonite–2*M* (parawollastonite). *Zeitschrift für Kristallographie*, **168**, 93–98.

Hesse K.F. and Liebau F. (1980) Crystal chemistry of silica-rich barium silicates refinement of the crystal structures of $Ba_4(Si_6O_{16})$, $Ba_5(Si_8O_{21})$ and $Ba_6(Si_{10}O_{26})$, silicates with triple quadruple and quintuple chains. *Zeitschrift für Kristallographie*, **153**, 3–17.

Higgins J.B. and Ribbe P.H. (1979) Sapphirine II. A neutron and X-ray diffraction study of (Mg–Al)VI and (Si–Al)IV ordering in monoclinic sapphirine. *Contributions to Mineralogy and Petrology*, **68**, 357–368.

Higgins J.B., Ribbe P.H. and Herd R.K. (1979) Sapphirine I. Crystal chemical contributions. *Contributions to Mineralogy and Petrology*, **68**, 349–356.

Hoffmann C. and Armbruster T. (1997) Clinotobermorite, $Ca_5(Si_3O_8(OH))_2(H_2O)_4Ca_5(Si_6O_{17})(H_2O)_5$, a natural C–S–H(I) type cement mineral determination of the substructure. *Zeitschrift für Kristallographie*, **212**, 863–873.

Hogarth D.D., Chao G.Y., Plant A.G. and Steacy H.R. (1974) Caysichite, a new silico-carbonate of yttrium and calcium. *The Canadian Mineralogist*, **12**, 293–298.

Huminicki D.M.C. and Hawthorne F.C. (2002*a*) The crystal chemistry of the phosphate minerals. Pp. 123–253 in: *Phosphates* (M.L. Kohn, J. Rakovan and J.M. Hughes, editors). Reviews in Mineralogy & Geochemistry, **48**. Mineralogical Society of America, Washington, DC.

Hung L.-I., Wang S.-L., Kao H.-M. and Lii K.-H. (2003) Hydrothermal synthesis, crystal structure, and solid-state NMR spectroscopy of a new indium silicate: $K_2In(OH)(Si_4O_{10})$. *Inorganic Chemistry*, **42**, 4057–4061.

Hwang S.L., Shen P., Chu H.T., Yui T.F., Varela M.E. and Iizuka Y. (2016) Kuratite, $Ca_4(Fe^{2+}_{10}Ti_2)O_4[Si_8Al_4O_{36}]$, the Fe^{2+}-analogue of rhönite, a new mineral from the D'Orbigny angrite meteorite. *Mineralogical Magazine*, **80**, 1067–1076.

Hybler J., Petříček V., Jurek K., Skála R. and Císařová I. (1997) Structure determination of vistepite $SnMn_4B_2Si_4O_{18}(OH)_2$: isotypism with bustamite, revised crystallographic data and composition. *The Canadian Mineralogist*, **35**, 1283–1292.

Ilyukhin V.V., Pudovkina Z.V., Voronkov A.A., Khomyakov A.P. and Pyatenko J.A. (1981) The crystal structure of the new natural modification of $K_2ZrSi_3O_9H_2O$. *Doklady Akademii Nauk SSSR*, **257**, 608–610.

Ilyushin G.D., Khomyakov A.P., Shumyatskaya N.V., Voronkov A.A., Nevskii N.N., Ilyukhin V.V. and Belov N.V. (1981) Crystal structure of a new natural zirconosilicate, $K_4Zr_2Si_6O_{18}\cdot 2H_2O$. *Doklady Akademii Nauk SSSR*, **256**, 860–863

Imaoka T., Nagashima M., Kano T., Kimura J-I., Chang Q. and Fukuda C. (2017) Murakamiite, $LiCa_2Si_3O_8(OH)$, a Li-analogue of pectolite, from the Iwagi Islet, southwest Japan. *European Journal of Mineralogy*, **29**, 1045–1053.

Ito J. (1972) Synthesis and crystal chemistry of Li-hydro-pyroxenoids. *Mineralogical Journal*, **7**, 45–65.

Ito M., Matsubara S., Yokoyama K., Momma K., Miyawaki R., Nakai I. and Kato A. (2014) Crystal structure of suzukiite from the Mogurazawa mine, Gunma Prefecture, Japan. *Journal of Mineralogical and Petrological Sciences*, **109**, 222–227.

Jansen M., Heidebrecht K., Matthes R. and Eysel W. (1991) Silber (I)-catena-Polysilicat Kristallzüchtung und Strukturanalyse. *Zeitschrift für Anorganische und Allgemeine Chemie*, **601**, 5–11.

Jenkins D.M., Gilleaudeau G.J., Kawa C., Dibiase J.M. and Fokin M. (2012) Compositional limits and analogs of monoclinic triple-chain silicates. *Contributions to Mineralogy and Petrology*, **164**, 229–244.

Jensen B.B. (1996) Solid solution among members of the aenigmatite group. *Mineralogical Magazine*, **60**, 982–986.

Johan Z. and Oudin E. (1986) Présence de grenats, $Ca_3Ga_2(GeO_4)_3$, $Ca_3Al_2[Ge,Si)O_4]_3$ et d'un équivalent ferrifère, germanifère et gallifère de la sapphirine $Fe_4(Ga,Sn,Fe)_4(Ga,Ge)_6O_{20}$, dans la blende des gisements de la zone axiale pyrénéenne. Conditions de formation des phases germanifères et gallifères. *Compte Rendus de l'Académie des Sciences, Paris*, **303**, Series II, 811–816.

Johnsen O., Nielsen K. and Sotofte I. (1978) The crystal structure of emeleusite, a novel example of sechser-doppelkette. *Zeitschrift für Kristallographie*, **147**, 297–306.

Johnston A.D. and Stout J.H. (1985) Compositional variation of naturally occurring rhoenite. *American Mineralogist*, **70**, 1211–1216.

Kahlenberg V. and Manninger T. (2014) $Rb_2Lu[Si_4O_{10}]F$, a tubular chain silicate. *Acta Crystallographica*, **E70**, i14, 1–15.

Kahlenberg V., Kaindl R. and Sartory B. (2007) On the existence of a second modification of $K_4SrSi_3O_9$ – X-ray single crystal diffraction, Raman spectroscopical and high temperature studies. *Solid State Sciences*, **9**, 65–71.

Kalinin V.V., Dauletkulov A.B., Gorshkov A.I. and Troneva N.V. (1985) Taikanite – a new silicate of strontium, barium and manganese. *Zapiski Vsesoyuznogo Mineralogicheskogo Obshchestva*, **114**, 635–641.

Kalsbeek N. and Rønsbo J.G. (1992) Refinement of the vinogradovite structure, positioning of Be and excess Na. *Zeitschrift für Kristallographie*, **200**, 237–245.

Kampf A.R., Rossman G.R., Steele I.M., Pluth J.J., Dunning G.E. and Walstrom R.E. (2010) Devitoite, a new heterophyllosilicate mineral with astrophyllite-

https://doi.org/10.1180/mgm.2020.13 Published online by Cambridge University Press

like layers from eastern Fresno County, California. *The Canadian Mineralogist*, **48**, 29–40.

Kampf A.R., Mills S.J., Merlino S., Pasero M., McDonald A.M., Wray W.B. and Hindman J.R. (2012) Whelanite, $Cu_2Ca_6[Si_6O_{17}(OH)](CO_3)(OH)_3(H_2O)_2$, an (old) new mineral from the Bawana mine, Milford, Utah. *American Mineralogist*, **97**, 2007–2015.

Kaneva E., Lacalamita M., Mesto E., Schingara E., Scordari F. and Vladykin N. (2014) Structure and modeling of disorder in miserite from the Murun (Russia) and Dara-i-Pioz (Tajikistan) massifs. *Physics and Chemistry of Minerals*, **41**, 49–63.

Kaneva E.V., Vladykin N.V., Mesto E., Lacalamita M., Scordari F. and Schingaro E. (2018) Refinement of the crystal structure of vlasovite from Burpala Massif (Russia). *Kristallografiya*, **63**, 1092–1098.

Kapustin Y.L. (1973) Zircophyllite, the zirconium analog of astrophyllite. *International Geology Review*, **15**, 621–625.

Karimova O. and Burns P.C. (2007) Silicate tubes in the crystal structure of manaksite. Pp. 153–156 in: *Minerals as Advanced Materials*. Springer-Verlag.

Kasatkin A.V., Cámara F., Chukanov N.V., Škoda R., Nestola F., Agakhanov A.A., Belakovskiy D.I. and Lednyov V.S. (2019) Patynite, $NaKCa_4[Si_9O_{23}]$, a new mineral from the Patynskiy Massif, Southern Siberia, Russia. *Minerals*, **9**, 611.

Kawamura K. and Kawahara A. (1976) Crystal structure of synthetic copper sodium silicate: $Cu_3Na_2(Si_4O_{12})$. *Acta Crystallographica*, **32**, 2419–2422.

Kawamura K. and Kawahara A. (1977) The crystal structure of synthetic copper sodium silicate: $CuNa_2Si_4O_{10}$. *Acta Crystallographica*, **B33**, 1071–1075.

Khomyakov A.P., Cherepivskaya G.E., Kurova T.A. and Vlasyuk V.P. (1980) Revdite, a new mineral. *Zapiski Vsesoyuznogo Mineralogicheskogo Obshchestva*, **109**, 566–579.

Khomyakov A.P., Voronkov A.A., Kobyashev Y.S. and Polezhaeva L.I. (1983*a*) Umbite and paraumbite, new potassium zirconosilicates from the Khibina alkalic massif. *Zapiski Vsesoyuznogo Mineralogicheskogo Obshchestva*, **112**, 461–469.

Khomyakov A.P., Semenov E.I., Voronkov A.A. and Nechelyustov G.N. (1983*b*) Terskite, $Na_4ZrSi_6O_{16}{\cdot}2H_2O$, a new mineral. *Zapiski Vsesoyuznogo Mineralogicheskogo Obshchestva*, **112**, 226–232.

Khomyakov A.P., Voronkov A.A., Polezhaeva L.I. and Smolyaninova N.N. (1983*c*) Kostylevite, $K_4Zr_2Si_6O_{18}{\cdot}2H_2O$, a new mineral. *Zapiski Vsesoyuznogo Mineralogicheskogo Obshchestva*, **112**, 469–474.

Khomyakov A.P., Kurova T.A. and Nechelyustov G.N. (1992) Manaksite $NaKMnSi_4O_{10}$: a new mineral. *Zapiski Vserossijskogo Mineralogicheskogo Obshchestva*, **121**, 112–114.

Khomyakov A.P., Nechelustov G.N. and Rastsvetaeva R.K. (1993) Sazykinaite-(Y) $Na_5YZrSi_6O_{18}{\cdot}6H_2O$ – a new mineral. *Zapiski Vserossijskogo Mineralogicheskogo Obshchestva*, **122**, 76–82.

Khomyakov A.P., Nechelyustov G.N. and Rastsetaeva R.K. (1996) Pyatenkoite-(Y) $Na_5(Y,Dy,Gd)\,TiSi_6O_{18}{\cdot}6H_2O$ – a new mineral. *Zapiski Vserossijskogo Mineralogicheskogo Obshchestva*, **125**, 72–79.

Khomyakov A.P., Kulikova I.E., Sokolova E., Hawthorne F.C. and Kartashov P.M. (2003) Paravinogradovite (Na, $\square)_2[(Ti^{4+},Fe^{3+})_4\{Si_2O_6\}_2\{Si_3AlO_{10}\}(OH)_4]H_2O$, a new mineral species from the Khibina alkaline massif, Kola Peninsula, Russia: description and crystal structure. *The Canadian Mineralogist*, **41**, 989–1002.

Khomyakov A.P., Nechelyustov G.N., Krivokoneva G.K., Rastsvetaeva R.K., Rozenberg K.A. and Rozhdestvenskaya I.V. (2009) Fluorcanasite, $K_3Na_3Ca_5Si_{12}O_{30}(F,OH)_4(H_2O)$, a new mineral species from the Khibiny alkaline pluton, Kola Peninsula, Russia, and new data on canasite. *Geology of Ore Deposits*, **51**, 757–766.

Khomyakov A.P., Cámara F., Sokolova E., Abdu Y. and Hawthorne F.C. (2011) Sveinbergeite, $Ca(Fe^{2+}_6Fe^{3+})Ti_2(Si_4O_{12})_2O_2(OH)_5(H_2O)_4$, a new astrophyllite-group mineral from the Larvik Plutonic Complex, Oslo Region, Norway: description and crystal structure. *Mineralogical Magazine*, **75**, 2687–2702.

Kolitsch U. (2008) Implications for the nomenclature of p-p hydropyroxenoids: the crystal structure of marsturite from the Molinello mine, Liguria, Italy. *Annual Meeting of the Deutsche Mineralogische Gesellschaft*, Abs. No. 120, Berlin, Germany.

Kolitsch U. and Tillmanns E. (2004) The structural relation between the new synthetic silicate $K_2ScFSi_4O_{10}$ and narsarsukite, $Na_2(Ti,Fe^{3+})(O,F)Si_4O_{10}$. *European Journal of Mineralogy*, **16**, 143–149.

Kolitsch U., Merlino S., Belmonte D., Carbone C., Cabella R., Lucchetti G. and Ciriotti M. E. (2018) Lavinskyite-1*M*, $K(LiCu)Cu_6(Si_4O_{11})_2(OH)_4$, the monoclinic MDO equivalent of lavinskyite-2*O* (formerly lavinskyite), from the Cerchiara manganese mine, Liguria, Italy. *European Journal of Mineralogy*, **30**, 811–820.

Komatsu M., Chihara K. and Mizota T. (1973) A new strontium hydrous silicate mineral from Ohmi, Niigata Prefecture, Central Japan. *Mineralogical Journal*, **7**, 298–301.

Konev A.A., Vorobiev E.I., Paradina L.F. and Sapozhnikov A.N. (1987) Denisovite from Murunskii Massif – the 2nd find in the world. *Doklady Akademii Nauk SSSR*, **293**, 196–198.

Konishi H., Akai J. and Kurokawa K. (1993) Calcic analog of clinojimthompsonite from the Oeyama Ophiolite, Southwest Japan. *Journal of the Geological Survey of Japan*, **99**, 679–682.

Kornev A.N., Maksimov B.A., Lider V.V., Ilyukhin V.V. and Belov N.V. (1972) Crystal structure of $Na_2Cu[Si_4O_{10}]$. *Doklady Akademii Nauk SSSR*, **17**, 735–737.

Kosoi A.L. (1975) Structure of babingtonite. *Kristallografiya*, **20**, 730–739.

Kostov I. and Breskovska V. (1989) *Phosphate, Arsenate and Vanadate Minerals. Crystal Chemistry and Classification*. Kliment Ohridski University Press, Sofia, Bulgaria.

Krivovichev S.V. (2008) *Structural Crystallography of Inorganic Oxysalts*. International Union of Crystallography Monographs on Crystallography **22**. Oxford University Press, UK

Krivovichev S.V. (2009) *Structural Mineralogy and Inorganic Crystal Chemistry*. St. Petersburg University Press, Russia, 398 pp.

Krivovichev S.V. and Burns P.C. (2004) Crystal structure of synthetic alamosite Pb$[SiO_3]$. *Zapiski Vserossijskogo Mineralogicheskogo Obshchestva*, **133**, 70–76.

Krivovichev S.V. and Filatov S.K. (1999*a*) Structural principles for minerals and inorganic compounds containing anion-centered tetrahedra. *American Mineralogist*, **84**, 1099–1106.

Krivovichev S.V. and Filatov S.K. (1999*b*) Metal arrays in structural units based on anion-centered metal tetrahedra. *Acta Crystallographica*, **B55**, 664–676.

Krivovichev S.V., Filatov S.K. and Semenova T.F. (1998) Types of cationic complexes on the base of oxocentered tetrahedra [OM4] in crystal structures of inorganic compounds. *Russian Chemical Reviews*, **67**, 137–155.

Krivovichev S.V., Yakovenchuk V.N., Armbruster T., Döbelin N., Pattison P., Weber H.P. and Depmeier W. (2004*a*) Porous titanosilicate nanorods in the structure of yuksporite, $(Sr,Ba)_2K_4(Ca,Na)_{14}(\square,Mn,Fe)\{(Ti,Nb)_4(O,OH)_4[Si_6O_{17}]_2[Si_2O_7]_3\}(H_2O,OH)_n$, resolved using synchrotron radiation. *American Mineralogist*, **89**, 1561–1565.

Krivovichev S.V., Yakovenchuk V.N. and Pakhomovsky Y.A. (2004*b*) Topology and symmetry of titanosilicate framework in the crystal structure of shcherbakovite, $Na(K,Ba)_2(Ti,Nb)_2[Si_4O_{12}]$. *Zapiski Vserossijskogo Mineralogicheskogo Obshchestva*, **133**, 55–63.

Krivovichev S.V., Mentré O., Siidra O.I., Colmont M. and Filatov S.K. (2013) Anion-centered tetrahedra in inorganic compounds. *Chemical Reviews*, **113**, 6459–6535.

Kudoh Y. and Takéuchi Y. (1979) Polytypism in xonotlite: (I) Structure of an A-1 polytype. *Mineralogical Journal*, **9**, 349–373.

Kunzmann T. (1999) The aenigmatite-rhönite mineral group. *European Journal of Mineralogy*, **11**, 743–756.

Lacalamita M., Mesto E., Kaneva E., Scordari F., Pedrazzi G., Vladykin N. and Schingaro E. (2017) Structure refinement and crystal chemistry of tokkoite and tinaksite from the Murun massif. *Mineralogical Magazine*, **81**, 251–272.

Larsen A.O. and Raade G. (1991) Gaidonnayite from nepheline syenite pegmatite on Siktesøya in the southern part of the Oslo Region, Norway. *Norsk Geologisk Tidsskrift*, **71**, 303–306.

Law A.D. and Whittaker E.J.W. (1980) Rotated and extended model structures in amphiboles and pyroxenes. *Mineralogical Magazine*, **43**, 565–574.

Leverett P., Williams P.A. and Hibbs D.E. (2008) Ca-Mg-Fe-rich rhodonite from the Morro da Mina mine, Conselheiro Lafaiete, Minas Gerais, Brazil. *The Mineralogical Record*, **39**, 125–130.

Liebau F. (1957) The crystal structures of rhodonite, $CaMn_4[Si_5O_{15}]$, and pyroxmangite, $(Ca,Mg)(Mn,Fe)_6[Si_7O_{21}]$. *Acta Crystallographica*, **10**, 761–761.

Liebau F. (1980) The role of cationic hydrogen in pyroxenoid crystal chemistry. *American Mineralogist*, **65**, 981–985.

https://doi.org/10.1180/mgm.2020.13 Published online by Cambridge University Press

Liebau F. (1985) *Structural Chemistry of Silicates*. Springer-Verlag, Berlin.
Lindsley D.H. and Burnham C.W. (1970) Pyroxferroite: stability and X-ray crystallography of synthetic $Ca_{0.15}Fe_{0.85}SiO_3$ pyroxenoid. *Science*, **168**, 364–367.
Lópes A., Frost R.L., Scholz R., Xi Y. and Amaral A. (2014) Infrared and raman spectroscopic characterization of the silicate mineral gilalite $Cu_5SI_6O_{17}(H_2O)_7$. *Spectroscopy Letters*, **47**, 488–493.
Lucchetti G., Penco A.M. and Rinaldi R. (1981) Saneroite, a new natural hydrated Mn-silicate. *Neues Jahrbuch für Mineralogie, Monatshefte*, 161–168.
Lussier A.L., Lopez R.A.K. and Burns P.C. (2016) Revised and expanded structure hierarchy of natural and synthetic hexavalent uranium compounds. *The Canadian Mineralogist*, **54**, 177–283.
Ma C., Krot A.N., Beckett J.R., Nagashima K. and Tschauner O. (2015) Discovery of warkite, $Ca_2Sc_6Al_6O_{20}$, a new Sc-rich ultra-refractory mineral in Murchison and Vigarano. *Meteoritics and Planetary Science*, **50** (S1), Abstract No. 5025.
Ma C., Krot A.N. and Nagashima K. (2017) Addibischoffite, $Ca_2Al_6Al_6O_{20}$, a new calcium aluminate mineral from the Acefer 214 CH carbonaceous chondrite: A new refractory phase from the solar nebula. *American Mineralogist*, **102**, 1556–1560.
MacGillavry C.H., Korst W.L., Moore E.J.W. and Van Der Plas H.J. (1956) The crystal structure of ferrocarpholite. *Acta Crystallographica*, **9**, 773–776.
Machatschki F. (1928) Zur Frage der Struktur und Konstitution der Feldspate. *Zentralblatt für Mineralogie, Geologie und Palaeontologie*, **A3**, 97–104.
Majzlan J., Drahota P. and Filippi M. (2014) Paragenesis and crystal chemistry of arsenic minerals. Pp. 17–184 in: *Arsenic: Environmental Geochemistry, Mineralogy, and Microbiology* (R.J. Bowell, C.N. Alpers, H.E. Jamieson, D.K. Nordstrom and J. Majzlan, editors). Reviews in Mineralogy & Geochemistry, **79**. Mineralogical Society of America, Washington, DC.
Maksimov B.A., Kalinin V.P., Merinov B.V., Ilyukhin V.V. and Belov N.V. (1980) The crystal structure of rare-earth Na, Y-metasilicate $Na_3YSi_3O_9$. *Doklady Akademii Nauk SSSR*, **252**, 875–879.
Mamedov K.S. and Belov N.V. (1956) Crystal structure of wollastonite. *Doklady Akademii Nauk SSSR*, **107**, 463–466.
Maresch W.V., Welch M.D., Gottschalk M., Ruthmann W., Czank M. and Ashbrook S.E. (2009) Synthetic amphiboles and triple-chain silicates in the system Na_2O–MgO–SiO_2–H_2O: phase characterization, compositional relations and excess H. *Mineralogical Magazine*, **73**, 957–996.
Mason B. (1975) Compositional limits of wollastonite and bustamite. *American Mineralogist*, **60**, 209–212.
Matesanz E., Garcia-Guinea J., Crespo-Feo E., Lopez-Arce P., Valle-Fuentes F.J. and Correcher V. (2008) The high-temperature behavior of charoite. *The Canadian Mineralogist*, **46**, 1207–1213.
Matsubara S. (1981) Taneyamalite, $(Na,Ca)(Mn^{2+},Mg,Fe^{3+},Al)_{12}Si_{12}(O,OH)_{44}$, a new mineral from the Iwaizawa mine, Saitama Prefecture, Japan. *Mineralogical Magazine*, **44**, 51–53.
Matsubara S., Kato A. and Yui S. (1982) Suzukiite, $Ba_2V_2^{4+}[O_2|Si_4O_{12}]$, a new mineral from the Mogurazawa mine, Gumma Prefecture, Japan. *Mineralogical Journal*, **11**, 15–20.
Matsubara S., Kato A. and Tiba T. (1985) Natronambulite, $(Na,Li)(Mn,Ca)_4Si_5O_{14}OH$, a new mineral from the Tanohata mine, Iwate Prefecture, Japan. *Mineralogical Journal*, **12**, 332–340.
McBurney T.C. and Murdoch J. (1959) Haiweeite, a new uranium mineral from California. *American Mineralogist*, **44**, 839–843.
McConnell J.D.C. (1954) The hydrated calcium silicates riversideite, tobermorite and plombierite. *Mineralogical Magazine*, **30**, 293–305.
McDonald A.M. and Chao G.Y. (2004) Haineaultite, a new hydrated sodium calcium titanosilicate from Mont Saint-Hilaire, Quebec: description, structure determination and genetic implications. *The Canadian Mineralogist*, **42**, 769–780.
McDonald W.S. and Cruickshank D.W.J. (1967) A reinvestigation of the structure of sodium metasilicate, Na_2SiO_3. *Acta Crystallographica*, **22**, 37–43.
McKie D. (1963) Order-disorder in sapphirine. *Mineralogical Magazine*, **33**, 635–645.
Meller N., Kyritsis K. and Hall C. (2009) The mineralogy of the CaO–Al_2O_3–SiO_2–H_2O (CASH) hydroceramic system from 200 to 350°C. *Cement and Concrete Research*, **39**, 45–53.
Mellini M. and Merlino S. (1978) Cayschite: a double crankshaft chain structure. *The Canadian Mineralogist*, **16**, 81–88.
Mellini M. and Merlino S. (1982) The crystal structure of cascandite, $CaScSi_3O_8(OH)$. *American Mineralogist*, **67**, 604–609.
Mellini M., Ferraris G. and Compagnoni R. (1985) Carlosturanite: HRTEM evidence of a polysomatic series including serpentine. *American Mineralogist*, **70**, 773–781.
Mellini M., Merlino S., Orlandi P. and Rinaldi R. (1982) Cascandite and jervisite, two new scandium silicates from Baveno, Italy. *American Mineralogist*, **67**, 599–603.
Men'shikov Y.P. (1984) Denisovite $Ca_4(K_{1.4}Na_{0.6})_2Si_6O_{16}(F,OH)_2$ – a new mineral from the Khibina massif. *Zapiski Vsesoyuznogo Mineralogicheskogo Obshchestva*, **113**, 718–723.
Men'shikov Y.P., Khomyakov A.P., Ferraris O., Bellusa E., Gula A. and Kulchitskaya E.A. (2003) Eveslogite, $(Ca,K,Na,Sr,Ba)_{48}[(Ti,Nb,Fe,Mn)_{12}(OH)[Si_{48}O_{144}](F,OH,Cl)_{14}$ a new mineral from Khibiny alkaline massif, Kola peninsula, Russia. *Zapiski Vserossijskogo Mineralogicheskogo Obshchestva*, **132**, 59–67.
Merlino S. (1969) Tuhualite crystal structure. *Science*, **166**, 1399–1401.
Merlino S. (1970) Crystal structure of aenigmatite. *Journal of the Chemical Society. Section D: Chemical Communications*, **20**, 1288–1289.
Merlino S. (1972) X-ray crystallography of krinovite. *Zeitschrift für Kristallographie*, **136**, 81–88.
Merlino S. (1980) Crystal structure of sapphirine-1*Tc*. *Zeitschrift für Kristallographie*, **151**, 91–100.
Merlino S. (1983) Okenite, $Ca_{10}Si_{18}O_{46}{\cdot}18H_2O$: the first example of a chain sheet silicate. *American Mineralogist*, **68**, 614–622.
Merlino S. and Biagioni C. (2018) Tuhualite revisited: new crystal data and structure refinements on specimens from two localities. *Periodico di Mineralogia*, **87**, 257–267.
Merlino S. and Bonaccorsi E. (2008) Double wollastonite chains: topological/conformational varieties, polytypic forms, isotypic compounds. *Zeitschrift für Kristallographie*, **223**, 85–97.
Merlino S. and Pasero M. (1987) Studio HRTEM della saffirina: relazioni tra politipi 1*Tc* e 2*M* e nuovo politipo 4*M*. *Rendiconti della Societá Italiana di Mineralogia e Petrologia*, **42**, 310.
Merlino S. and Zvyagin B.B. (1998) Modular features of sapphirine-type structures. *Zeitschrift für Kristallographie*, **213**, 513–521.
Merlino S., Pasero M. and Khomyakov A.P. (1990) The crystal structure of lintisite, $Na_3LiTi_2[Si_2O_6]_2O_2(H_2O)_2$, a new titanosilicate from Lovozero (USSR). *Zeitschrift für Kristallographie*, **193**, 137–148.
Merlino S., Bonaccorsi E. and Armbruster T. (1999) Tobermorites: Their real structure and order–disorder (OD) character. *American Mineralogist*, **84**, 1613–1621.
Merlino S., Bonaccorsi E. and Armbruster T. (2000*a*) The real structure of clinotobermorite and tobermorite 9Å: OD character, polytypes, and structural relationships. *European Journal of Mineralogy*, **12**, 411–429.
Merlino S., Pasero M. and Ferro O. (2000*b*) The crystal structure of kukisvumite, $Na_6ZnTi_4(Si_2O_6)_4O_4{\cdot}4H_2O$. *Zeitschrift für Kristallographie*, **215**, 352–356.
Merlino S., Bonaccorsi E. and Armbruster T. (2001) The real structure of tobermorite 11Å: normal and anomalous forms, OD character and polytypic modification. *European Journal of Mineralogy*, **13**, 577–590.
Merlino S., Bonaccorsi E., Grabezhev A.I., Zadov A.E., Pertsev N.N. and Chukanov N.V. (2009) Fukalite: An example of an OD structure with two-dimensional disorder. *American Mineralogist*, **94**, 323–333.
Mills S.J., Hatert F., Nickel E.H. and Ferraris G. (2009) The standardisation of mineral group hierarchies: application to recent nomenclature proposals. *European Journal of Mineralogy*, **21**, 1073–1080.
Mitchell R.H., Welch M.D., Kampf A.R., Chakhmouradian A.K. and Spratt J. (2015) Barrydawsonite-(Y), $Na_{1.5}CaY_{0.5}Si_3O_9H$: a new pyroxenoid of the pectolite–serandite group. *Mineralogical Magazine*, **79**, 671–686.
Mitsuda T. and Taylor H.F.W. (1978) Normal and anomalous tobermorites. *Mineralogical Magazine*, **42**, 229–235.
Mizota T., Komatsu M. and Chihara K. (1973) On the crystal structure of $Sr_3TiSi_4O_{12}(OH)(H_2O)_2$, a new mineral. *Mineralogical Journal*, **7**, 302–305.
Mizota T., Komatsu M. and Chihara K. (1983) A refinement of the crystal structure of ohmilite, $Sr_3(Ti,Fe^{3+})(O,OH)(Si_2O_6)_2(H_2O)_{2-3}$. *American Mineralogist*, **68**, 811–817.

https://doi.org/10.1180/mgm.2020.13 Published online by Cambridge University Press

Moore P.B. (1968) Crystal structure of sapphirine. *Nature*, **218**, 81–82.
Moore P.B. (1969*a*) A novel octahedral framework: Gageite. *American Mineralogist*, **54**, 1005–1017.
Moore P.B. (1969*b*) The crystal structure of sapphirine. *American Mineralogist*, **54**, 31–49.
Moore P.B. (1970) Crystal chemistry of the basic iron phosphates. *American Mineralogist*, **55**, 135–169.
Moore P.B. (1973) Pegmatite phosphates. Descriptive mineralogy and crystal chemistry. *Mineralogical Record*, **4**, 103–130.
Moore P.B. (1978) Welshite, $Ca_2Mg_4Fe^{3+}Sb^{5+}O_2[Si_4Be_2O_{18}]$, a new member of the aenigmatite group. *Mineralogical Magazine*, **42**, 129–132.
Moore P.B. and Araki T. (1974) Pinakiolite, $Mg_2Mn^{3+}O_2[BO_3]$; warwickite, $Mg(Mg_{0.5}Ti_{0.5})O[BO_3]$; wightmanite, $Mg_5(O)(OH)_5[BO_3]\cdot nH_2O$: crystal chemistry of complex 3 Å wallpaper structures. *American Mineralogist*, **59**, 985–1004.
Moore P.B. and Araki T. (1979) Crystal structure of synthetic $Ca_3Mn_2O_2(Si_4O_{12})$. *Zeitschrift für Kristallographie*, **150**, 287–297.
Moore P.B. and Araki T. (1983) Surinamite, ca. $Mg_3Al_4Si_3BeO_{16}$: its crystal structure and relation to sapphirine, ca. $Mg_{2.8}Al_{7.2}Si_{1.2}O_{16}$. *American Mineralogist*, **68**, 804–810.
Moore P.B., Sen Gupta P.K., Schlemper E.O. and Merlino S. (1987) Ashcroftine, ca. $K_{10}Na_{10}(Y,Ca)_{24}(OH)_4(CO_3)_{16}(Si_{56}O_{140})\cdot 16H_2O$, a structure with enormous polyanions. *American Mineralogist*, **72**, 1176–1189.
Mukhopadhyay S., Das K. and Fukuoka M. (2005) Nambulite, (Li,Na) $Mn_4Si_5O_{14}(OH)$, in the Sausar Group of rocks in Central India. *Journal of Mineralogical and Petrological Sciences*, **100**, 26–30.
Murakami T., Takéuchi Y., Tagai T. and Koto K. (1977) Lithium-hydrorhodonite. *Acta Crystallographica*, **B33**, 919–921.
Nagase T., Hori H., Kitamine M., Nagashima M., Abduriyim A. and Kuribayashi T. (2012) Tanohataite, $LiMn_2Si_3O_8(OH)$: a new mineral from the Tanohata mine, Iwate Prefecture, Japan. *Journal of Mineralogical and Petrological Sciences*, **107**, 149–154.
Nagashima M. and Armbruster T. (2010) Saneroite: chemical and structural variations of manganese pyroxenoids with hydrogen bonding in the silicate chain. *European Journal of Mineralogy*, **22**, 393–402.
Nagashima M., Armbruster T., Kolitsch U. and Pettke T. (2014*a*) The relation between Li ↔ Na substitution and hydrogen bonding in five-periodic single-chain silicates nambulite and marsturite: A single-crystal X-ray study. *American Mineralogist*, **99**, 1462–1470.
Nagashima M., Mitani K. and Akasaka M. (2014*b*) Structural variation of babingtonite depending on cation distribution at the octahedral sites. *Mineralogy and Petrology*, **108**, 287–301.
Nagashima M., Imaoka T., Fukuda C. and Pettke T. (2018) Relationship between cation substitution and hydrogen-bond system in hydrous pyroxenoids with three-periodic single chain of SiO_4 tetrahedra: pectolite, murakamiite, marshallsussmanite, serandite and tanohataite. *European Journal of Mineralogy*, **30**, 451–463.
Narita H., Koto K., Morimoto N. and Yoshii M. (1975) The crystal structure of nambulite (Li,Na)$Mn_4Si_5O_{14}(OH)$. *Acta Crystallographica*, **B31**, 2422–2426.
Narita H., Koto K. and Morimoto N. (1977) The crystal structures of $MnSiO_3$ polymorphs (rhodonite and pyroxmangite-type). *Mineralogical Journal*, **8**, 329–342.
Naumova I.S., Pobedimskaya E.A. and Belov N.V. (1974) Crystal structure of carpholite $MnAl_2(Si_2O_6)(OH)_4$. *Kristallografiya*, **19**, 1155–1160.
Nelson W.R. and Griffen D.T. (2005) Crystal chemistry of Zn-rich rhodonite ("fowlerite"). *American Mineralogist*, **90**, 969–983.
Nestola F., Tribaudino M., Boffa Ballaran T., Liebske C. and Bruno M. (2007) The crystal structure of pyroxenes along the jadeite-hedenbergite and jadeite-aegirine joins. *American Mineralogist*, **92**, 1492–1501.
Newberg D.W. (1964) X-ray study of shattuckite. *American Mineralogist*, **49**, 1234–1239.
Nickel E.H., Rowland J.F. and Charette D.J. (1964) Niobophyllite – the niobium analogue of astrophyllite; a new mineral from Seal Lake, Labrador. *The Canadian Mineralogist*, **8**, 40–52.
Nikishova L.V., Lazebnik K.A., Rozhdestvenskaya I.V., Emelyanova N.N. and Lazebnik Y.D. (1996) Frankamenite $K_3Na_3Ca_5(Si_{12}O_{30})F_3(OH)\cdot H_2O$ – a new mineral, triclinic vareity of canasite from charoitites. *Zapiski Vserossijskogo Mineralogicheskogo Obshchestva*, **125**, 106–108.
Nikitin A.V. and Belov N.V. (1962) Crystal structure of batisite, $Na_2BaTi_2Si_4O_{14} = Na_2BaTi_2O_2[Si_4O_{12}]$. *Doklady Akademii Nauk SSSR*, **146**, 1401–1403.
Nyfeler D., Armbruster T., Dixon R. and Bermanec V. (1995) Nchwaningite, $Mn_2^{2+}SiO_3(OH)_2H_2O$, a new pyroxene-related chain silicate from the N'chwaning mine, Kalahari manganese field, South Africa. *American Mineralogist*, **80**, 377–386.
Oberti R., Hawthorne F.C., Ungaretti L. and Cannillo E. (1993) The behaviour of Mn in amphiboles: Mn in richterite. *European Journal of Mineralogy*, **5**, 43–51.
Oberti R., Hawthorne F.C., Cannillo E. and Cámara F. (2007) Long-range order in amphiboles. Pp. 125–171 in: *Amphiboles: Crystal Chemistry, Occurrence, and Health Issues* (F.C. Hawthorne, R. Oberti, G. Della Ventura and A. Mottana, editors). Reviews in Mineralogy & Geochemistry, **67**. Mineralogical Society of America and the Geochemical Society, Chantilly, Virginia, USA.
Ohashi Y. and Finger L.W. (1974) The effect of cation substitution on the symmetry and the tetrahedral chain configuration in pyroxenes. *Carnegie Institution of Washington Year Book*, **73**, 522–525.
Ohashi Y. and Finger L.W. (1975) Pyroxenoids: a comparison of refined structures of rhodonite and pyroxmangite. *Carnegie Institution of Washington Year Book*, **74**, 564–569.
Ohashi Y. and Finger L.W. (1976) Stepwise cation ordering in bustamite and disordering in wollastonite. *Carnegie Institution of Washington Year Book*, **75**, 746–753.
Ohashi Y. and Finger L.W. (1978) The role of octahedral cations in pyroxenoid crystal chemistry. I. Bustamite, wollastonite, and the pectolite-schizolite-serandite series. *American Mineralogist*, **63**, 274–288.
Ohashi Y. and Finger L.W. (1981) The crystal structure of santaclaraite, $CaMn_4[Si_5O_{14}(OH)](OH)\cdot H_2O$: the role of hydrogen atom in the pyroxenoid structure. *American Mineralogist*, **66**, 154–168.
Orlandi P., Pasero M. and Vezzalini G. (1998) Scandiobabingtonite, a new mineral from the Baveno pegmatite, Piedmont, Italy. *American Mineralogist*, **83**, 1330–1334.
Papike J.J. and Ross M. (1970) Gedrites: crystal structures and intracrystalline cation distributions. *American Mineralogist*, **55**, 1945–1972.
Papike J.J., Prewitt C.T., Sueno S. and Cameron M. (1973) Pyroxenes: comparisons of the real and ideal structural topologies. *Zeitschrift für Kristallographie*, **138**, 254–273.
Pautov L.A., Belakovsku D.I., Skála R., Sokolova E.V., Ignatenko K.I. and Mokhov A.V. (1992) Vistepite $Mn_5SnB_2Si_5O_{20}$ – a new borosilicate of manganese and tin. *Zapiski Vsesoyuznogo Mineralogicheskogo Obshchestva*, **121**, 107–112.
Peacor D.R. and Buerger M.J. (1962*a*) Determination and refinement of the crystal structure of bustamite, $CaMnSi_2O_6$. *Zeitschrift für Kristallographie*, **117**, 331–343.
Peacor D.R. and Buerger M.J. (1962*b*) The determination and refinement of the structure of narsarsukite, $Na_2TiOSi_4O_{10}$. *American Mineralogist*, **47**, 539–556.
Peacor D.R. and Niizeki N. (1963) The redetermination and refinement of the crystal structure of rhodonite, $(Mn,Ca)SiO_3$. *Zeitschrift für Kristallographie*, **119**, 98–116.
Peacor D.R. and Prewitt C.T. (1963) Comparison of the crystal structure of bustamite and wollastonite. *American Mineralogist*, **48**, 588–596.
Peacor D.R., Essene E.J., Brown P.E. and Winter G.A. (1978*a*) The crystal chemistry and petrogenesis of a magnesian rhodonite. *American Mineralogist*, **63**, 1137–1142.
Peacor D.R., Dunn P.J. and Sturman B.D. (1978*b*) Marsturite, $Mn_3CaNaHSi_5O_{15}$, a new mineral of the nambulite group from Franklin, New Jersey. *American Mineralogist*, **63**, 1187–1189.
Peacor D.R., Dunn P.J., White Jr. J.S., Grice J.D. and Chi P.H. (1990) Lithiomarsturite, a new member of the pyroxenoid group, from North Carolina. *American Mineralogist*, **75**, 409–414.
Pekov I.V., Chukanov N.V., Kononkova N.N. and Pushcharovsky D.Y. (2003) Rare-metal zeolites of the hilairite group. *New Data on Minerals*, **38**, 20–33.
Pekov I.V., Grigorieva A.A., Zubkova N.V., Turchkova A.G. and Pushcharovsky D.Y. (2010*a*) Crystal chemistry of cation-exchanged forms of hilairite: new experimental data and chemical composition -structure-genesis relations. *Kristallografiya*, **55**, 1091–1100.
Pekov I.V., Zubkova N.V., Chukanov N.V., Zadov A.E., Grishin V.G. and Pushcharovsky D.Y. (2010*b*) Yegorovite, $Na_4[Si_4O_8(OH)_4]\cdot 7H_2O$, a new

https://doi.org/10.1180/mgm.2020.13 Published online by Cambridge University Press

mineral from the Lovozero Alkaline Pluton, Kola Peninsula. *Geology of Ore Deposits*, **52**, 584–590.

Pekov I.V., Zubkova N.V., Yapaskurt V.O., Belakovskiy D.I., Lykova I.S., Britvin S.N., Turchkova A.G. and Pushcharovsky D.Y. (2017) Kamenevite, IMA 2017–021. CNMNC Newsletter No. 38, *Mineralogical Magazine*, **81**, 1033–1038.

Pertlik F. and Zahiri R. (1999) Rhodonite with a low calcium content: crystal structure determination and crystal chemical calculations. *Monatshefte für Chemie*, **130**, 257–265.

Piilonen P.C., Lalonde A.E., Mcdonald A.M. and Gault R.A. (2000) Niobokupletskite, a new astrophyllite-group mineral from Mont Saint-Hilaire, Quebec, Canada: description and crystal structure. *The Canadian Mineralogist*, **38**, 627–639.

Piilonen P.C., McDonald A.M. and Lalonde A.E. (2001) Kupletskite polytypes from the Lovozero massif, Kola Peninsula, Russia: kupletskite-1*A* and kupletskite-*Ma2b2c*. *European Journal of Mineralogy*, **13**, 973–984.

Piilonen P.C., LaLonde A.E., McDonald A.M., Gault R.A. and Larsen A.O. (2003*a*) Insights into astrophyllite-group minerals. I. Nomenclature, composition and development of a standardized general formula. *The Canadian Mineralogist*, **41**, 1–26.

Piilonen P.C., McDonald A.M. and LaLonde A.E. (2003*b*) Insights into astrophyllite-group minerals. II. Crystal chemistry. *The Canadian Mineralogist*, **41**, 27–54.

Piilonen P.C., Pekov I.V., Back M., Steede T. and Gault R.A. (2006) Crystal-structure refinement of a Zn-rich kupletskite from Mont Saint-Hilaire, Quebec, with contributions to the geochemistry of zinc in peralkaline environments. *Mineralogical Magazine*, **70**, 565–578.

Pinckney L.R. and Burnham C.W. (1988) Effects of compositional variation on the crystal structures of pyroxmangite and rhodonite. *American Mineralogist*, **73**, 798–808.

Plaisier J.R., Ijdo D.J.W., de Mello Donego C. and Blasse G. (1995) Structure and luminescence of barium uranium disilicate ($BaUO_2Si_2O_6$). *Chemistry of Materials*, **7**, 738–743.

Plášil J., Fejfarová K., Čejka J., Dušek M., Škoda R. and Sejkora J. (2013) Revision of the crystal structure and chemical formula of haiweeite, $Ca(UO_2)_2(Si_5O_{12})(OH)_2{\cdot}6H_2O$. *American Mineralogist*, **98**, 718–723.

Pozas J.M.M., Rossi G. and Tazzoli V. (1975) Re-examination and crystal structure analysis of litidionite. *American Mineralogist*, **60**, 471–474.

Prewitt C.T. (1967) Refinement of the structure of pectolite, $Ca_2NaHSi_3O_9$. *Zeitschrift für Kristallographie*, **125**, 298–316.

Prewitt C.T. and Buerger M.J. (1963) Comparison of the crystal structures of wollastonite and pectolite. *Mineralogical Society of America Special Paper* **1**, 293–302. International Mineralogical Association Papers and Proceedings of the Third General Meeting, Washington, DC, April 17-20, 1962.

Prewitt C.T. and Peacor D.R. (1964) Crystal chemistry of the pyroxenes and pyroxenoids. *American Mineralogist*, **49**, 1527–1542.

Prider R.T. (1965) Noonkanbahite, a potassic batisite from the lamproites of Western Australia. *Mineralogical Magazine*, **34**, 403–405.

Pudovkina Z.V. and Chernitsova N.M. (1991) The crystal structure of terskite $Na_4Zr[H_4Si_6O_{18}]$. *Doklady Akademii Nauk SSSR*, **316**, 645–649.

Pushcharovsky D.Y., Pekov I.V., Pasero M., Gobechiya E.R., Merlino S. and Zubkova N.V. (2002) Crystal structure of cation-deficient calciohilairite and possible mechanisms of decationization in mixed-framework minerals. *Kristallografiya*, **47**, 814–81.

Pyatenko Y.A. and Pudovkina Z.V. (1960) Crystal structure of narsarsukite. *Kristallografiya*, **5**, 563–573.

Rapoport P.A. and Burnham C.W. (1973) Ferrobustamite: the crystal structures of two Ca,Fe bustamite-type pyroxenoids. *Zeitschrift für* Kristallographie, **138**, 419–438.

Rastsvetaeva R.K. and Aksenov S.M. (2011) New phases of K, Eu-silicate in the family of compounds with the orthorhombic pellyite-like unit cell. *Bulgarian Chemical Communications*, **43**, 308–315.

Rastsvetaeva R.K. and Andrianov V.I. (1984) Refined crystal structure of vinogradovite. *Kristallografiya*, **29**, 403–406.

Rastsvetaeva R.K. and Khomyakov A.P. (1992) Crystal structure of a rare earth analog of hilairite. *Kristallografiya*, **37**, 1561–1563.

Rastsvetaeva R.K. and Khomyakov A.P. (1996) Pyatenkoite-(Y) $Na_5YTiSi_6O_{18}{\cdot}6H_2O$, a new mineral of the hilairite group: crystal structure. *Doklady Chemistry*, **351**, 283–286.

Rastsvetaeva R.K., Simonov V.I. and Belov N.V. (1968) Crystal structure of vinogradovite $Na_4Ti_4[Si_2O_6]_2[Si_4O_{10}]O_4{\cdot}nH_2O$. *Doklady Akademii Nauk SSSR*, **12**, 1090–1092.

Rastsvetaeva R.K., Mikheeva M.G., Yamnova N.A., Pushcharovskii D.Y. and Khomyakov A.P. (1992) Crystal structure of revdite $Na_{16}[Si_4O_6(OH)_5]_2[Si_8O_{15}(OH)_6](OH)_{10}{\cdot}28H_2O$. *Kristallografiya*, **37**, 632–636.

Rastsvetaeva R.K., Pushcharovskii D.Yu., Konev A.A. and Evsunin V.G. (1997*a*) The crystal structure of K-containing batisite. *Kristallografiya*, **42**, 837–840.

Rastsvetaeva R.K., Arakcheeva A.V., Pushcharovsky D.Yu., Atencio D. and Menezes Filho L.A.D. (1997*b*) A new silicon band in the haiweete [sic] structure. *Kristallografiya*, **42**, 927–933.

Rastsvetaeva R.K., Rozenberg K.A., Khomyakov A.P. and Rozhdestvenskaya I.V. (2003) Crystal structure of F-canasite. *Doklady Chemistry*, **391**, 177–180.

Rastsvetaeva R.K., Bolotina N.B., Zadov A.E., and Chukanov N.V. (2005) Crystal structure of fukalite dimorph $Ca_4(Si_2O_6)(CO_3)(OH)_2$ from the Gumeshevsk deposit, the Urals. *Doklady Earth Sciences*, **405**, 1347–1351.

Redhammer G.J., Amthauer G., Roth G., Tippelt G. and Lottermoser W. (2006) Single crystal X-ray diffraction and temperature dependent ^{57}Fe Mössbauer spectroscopy on the hedenbergite-aegirine $(Ca,Na)(Fe^{2+},Fe^{3+})Si_2O_6$ solid solution. *American Mineralogist*, **91**, 1271–1292.

Richardson I.G. (2008) The calcium silicate hydrates. *Cement and Concrete Research*, **38**, 137–158.

Richmond W.E. (1942) Inesite, $Mn_7Ca_2Si_{10}O_{28}(OH)_2(H_2O)_5$. *American Mineralogist*, **27**, 563–569.

Rius J., Elkaim E. and Torrelles X. (2004) Structure determination of the blue mineral pigment aerinite from synchrotron powder diffraction data: The solution of an old riddle. *European Journal of Mineralogy*, **16**, 127–134.

Rius J., Crespi A., Roig A. and Melgarejo J.C. (2009) Crystal-structure refinement of Fe^{3+}-rich aerinite from synchrotron powder diffraction and Mössbauer data. *European Journal of Mineralogy*, **21**, 233–240.

Robinson P.D. and Fang J.H. (1970) The crystal structure of epididymite. *American Mineralogist*, **55**, 1541–1549.

Rogov Y.G., Rogova V.P., Voronkov A.A. and Moleva V.A. (1965) Tinaksite $NaK_2Ca_2TiSi_7O_{19}(OH)$, a new mineral. *Doklady Akademii Nauk SSSR*, **162**, 658–661.

Rossi G., Smith D.C., Ungaretti L. and Domeneghetti M.C. (1983) Crystal-chemistry and cation ordering in the system diopside-jadeite: A detailed study by crystal structure refinement. *Contributions to Mineralogy and Petrology*, **83**, 247–258.

Rozhdestvenskaya I.V. and Krivovichev S.V. (2011) Tubular chains in the structures of natural and synthetic silicates. *Kristallografiya*, **56**, 1076–1087.

Rozhdestvenskaya I.V. and Nikishova L.V. (1998) Crystal structure of $Na(Ca,Sr)_2Si_4O_{10}F$ strontium agrellite from yakutian charoitites: agrellite polytypes. *Kristallografiya*, **43**, 637–645.

Rozhdestvenskaya I.V. and Nikishova L.V. (2002) Crystallochemical characteristics of alkali calcium silicates from charoites. *Kristallografiya*, **47**, 545–554

Rozhdestvenskaya I.V. and Vasilieva V.A. (2014) Cation ordering and structural deformations in pectolite $HNaCaSi_3O_9$-serandite $HNaMn_2Si_3O_9$. *Journal of Structural Chemistry*, **55**, 1268–1276.

Rozhdestvenskaya I.V., Nikishova L.V., Bannova I.I. and Lasebnik Y.D. (1987) Canasite: The refinement of crystal structure and comparison with that of miserite. *Acta Crystallographica Supplement*, **A43**, C159.

Rozhdestvenskaya I.V., Nikishova L.V., Lazebnik Yu.D. and Lazebnik K.A. (1989) The crystal structure of tokkoite and its relation to the structure of tinaksite. *Zeitschrift für Kristallographie*, **189**, 195–204.

Rozhdestvenskaya I.V., Nikishova L.V. and Lazebnik K.A. (1996) The crystal structure of frankamenite. *Mineralogical Magazine*, **60**, 897–905.

Rozhdestvenskaya I.V., Bannova I.I., Nikishova L.V. and Soboleva T.V. (2004) The crystal structure of fenaksite $K_2Na_2Fe_2Si_8O_{20}$. *Doklady Earth Sciences*, **398**, 524–528.

Rozhdestvenskaya I.V. and Evdokimov M.D. (2006) Refinement of miserite crystal structure $(K_{1.29}\square_{0.21})[Ca_{5.51}M^{3+}_{0.49}](Si_6(O,OH)_{15})(Si_2O_7)(F,OH)_2(H_2O)_{0.25}$ (M = Y, *REE*, Fe, Ti, Mn, Mg, Na) from the Dara-i-Pioz occurrence, Pamir, Tajikistan. *Doklady Earth Sciences*, **406**, 74–78.

Rozhdestvenskaya I.V., Kogure T., Abe E. and Drits V.A. (2009) A structural model for charoite. *Mineralogical Magazine*, **73**, 883–890.

https://doi.org/10.1180/mgm.2020.13 Published online by Cambridge University Press

Rozhdestvenskaya I.V., Mugnaioli E., Czank M., Depmeier W., Kolb U., Reinholdt A. and Weirich T. (2010) The structure of charoite, (K,Sr,Ba,Mn)$_{15-16}$(Ca,Na)$_{32}$[(Si$_{70}$(O,OH)$_{180}$)](OH,F)$_{4.0}$·nH$_2$O, solved by conventional and automated electron diffraction. *Mineralogical Magazine*, **74**, 159–177.

Rozhdestvenskaya I.V., Mugnaioli E., Czank M., Depmeier W., Kolb U. and Merlino S. (2011) Essential features of the polytypic charoite-96 structure compared to charoite-90. *Mineralogical Magazine*, **75**, 2833–2846.

Rozhdestvenskaya I.V., Mugnaioli E., Schowalter M., Schmidt M.U., Czank M., Depmeier W. and Rosenauer A. (2017) The structure of denisovite, a fibrous nanocrystalline polytypic disordered 'very complex' silicate, studied by a synergistic multi-disciplinary approach employing methods of electron crystallography and X-ray powder diffraction. *IUCrJ*, **4**, 223–242.

Ryall W.R. and Threadgold I.M. (1966) Evidence for [(SiO3)5]$_\infty$ type chains in inesite as shown by X-ray and infrared absorption studies. *American Mineralogist*, **51**, 754–761.

Sabau G., Alberico A. and Negulescu E. (2002) Peraluminous sapphirine in retrogressed kyanite-bearing eclogites from the South Carpathians: status and implications. *International Geology Review*, **44**, 859–876.

Sabelli C. and Trosti-Ferroni T. (1985) A structural classification of sulfate minerals. *Periodico di Mineralogia*, **54**, 1–46.

Salvadó M.A., Pertierra P., Garcia-Granda S., Khainakov S.A., Garcia J.R., Bortun A.I. and Clearfield A. (2001) Novel silicate anion: $Si_8O_{22}^{12-}$. Hydrothermal synthesis and X-ray powder structure of three new niobium silicates. *Inorganic Chemistry*, **40**, 4368–4373.

Sandomirskii P.A. and Belov N.V. (1979) The OD structure of zorite. *Kristallografiya*, **24**, 1198–1210.

Sandomirskii P.A. and Belov N.V. (1984) *Crystal Chemistry of Mixed Anionic Radicals*. Nauka, Moscow.

Sassi M., Gramlich V., Miéhé-Brendié J., Josien L., Paillaud J-L., Benggedach A. and Patarin J. (2003) Synthesis and characterization of a new one-dimensional sodium silicate named Mu-29. *Microporous and Mesoporous Materials*, **64**, 51–61.

Schäfer M.C. and Schleid T. (2007) Synthese und kristallstruktur des fluorid-ino-oxosilicats Cs$_2$YFSi$_4$O$_{10}$. *Zeitschrift für anorganische chemie*, **633**, 1018–1023.

Schaller W.T. (1955) The pectolite–schizolite–serandite series. *American Mineralogist*, **40**, 1022–1031.

Schindler M. and Hawthorne F.C. (2001*a*) A bond-valence approach to the structure, chemistry and paragenesis of hydroxy-hydrated oxysalt minerals: I. Theory. *The Canadian Mineralogist*, **39**, 1225–1242.

Schindler M. and Hawthorne F.C. (2001*b*) A bond-valence approach to the structure, chemistry and paragenesis of hydroxy-hydrated oxysalt minerals: II. Crystal structure and chemical composition of borate minerals. *The Canadian Mineralogist*, **39**, 1243–1256.

Schindler M. and Hawthorne F.C. (2001*c*) A bond-valence approach to the structure, chemistry and paragenesis of hydroxy-hydrated oxysalt minerals: III. Paragenesis of borate minerals. *The Canadian Mineralogist*, **39**, 1257–1274.

Schindler M. and Hawthorne F.C. (2004) A bond-valence approach to the uranyl-oxide hydroxy-hydrate minerals: Chemical composition and occurrence. *The Canadian Mineralogist*, **42**, 1601–1627.

Schindler M. and Hawthorne F.C. (2008) The stereochemistry and chemical composition of interstitial complexes in uranyl-oxysalt minerals. *The Canadian Mineralogist*, **46**, 467–501.

Schindler M., Hawthorne F.C. and Baur W.H. (2000) A crystal-chemical approach to the composition and occurrence of vanadium minerals. *The Canadian Mineralogist*, **38**, 1443–1456.

Schindler M., Huminicki D.M.C. and Hawthorne F.C. (2006) Sulfate minerals: I. Bond topology and chemical composition. *The Canadian Mineralogist*, **44**, 1403–1429.

Schingaro E., Mesto E., Lacalamita M., Scordari F., Kaneva E. and Vladykin F.N. (2017) Single-crystal X-ray diffraction, EMPA, FTIR and X-ray photoelectron spectroscopy study of narsarsukite from Murun Massif, Russia. *Mineralogical Magazine*, **81**, 339–354.

Schmahl W.W. and Tillmanns E. (1987) Isomorphic substitutions, straight Si–O–Si geometry, and disorder of tetrahedral tilting in batisite, (Ba,K)(K,Na)Na(Ti,Fe,Nb,Zr)Si$_4$O$_{14}$. *Neues Jahrbuch für Mineralogie, Monatshefte*, 107–118.

Schmidmair D., Kahlenberg V. and Grießer A. (2018) K$_2$CaSi$_4$O$_{10}$: A novel phase in the ternary system K$_2$O–CaO–SiO$_2$ and member of the litidionite group of crystal structures. *Journal of the American Ceramic Society*, **101**, 919–927.

Scott J.D. (1976) Crystal structure of miserite, a zoltai type 5 structure. *The Canadian Mineralogist*, **14**, 515–528.

Sebastián V., DÍaz I., Téllez C., Coronas J. and SantamarÍa J. (2008) Spheres of microporous titanosilicate umbite with hierarchical pore systems. *Advanced Functional Materials*, **18**, 1314–1320.

Shchipalkina N.V., Aksenov S.M., Chukanov N.V., Pekov I.V., Rastsvetaeva R.K., Schäfer C., Ternes B. and Shüller W. (2016*a*) Pyroxenoids of pyroxmangite-pyroxferroite series from xenoliths of Bellerberg Paleovolcano (Eifel, Germany): chemical variations and specific features of cation distribution. *Kristallografiya*, **61**, 896–904.

Shchipalkina N.V., Zubkova N.V., Pekov I.V. and Koshlyakova N.N. (2016*b*) Dorrite from Kopeisk, South Urals, Russia: crystal structure and cation ordering. *Neues Jahrbuch für Mineralogie, Abhandlungen*, **193**, 275–282.

Shchipalkina N.V., Chukanov N.V., Pekov I.V., Aksenov S.M., McCammon C., Belakovskiy D.I., Britvin S.N., Koshlyakova N.N., Schäfer C., Scholz R. and Rastsvetaeva R.K. (2017) Ferrorhodonite, CaMn$_3$Fe[Si$_5$O$_{15}$], a new mineral species from Broken Hill, New South Wales, Australia. *Physics and Chemistry of Minerals*, **44**, 323–334.

Shchipalkina N.V., Pekov I.V., Ksenofontov D.A., Chukanov N.V., Belakovskiy D.I. and Koshlyakova N.N. (2018) Dalnegorskite, IMA 2018-007. CNMNC Newsletter, *Mineralogical Magazine*, **82**, 779–785.

Shchipalkina N.V., Chukanov N.V., Rusakov V.S., Pekov I.V., Koshlyakova N.N. and Scholz R. (2019*a*) Iron distribution in Fe-rich bustamite-type minerals. *Physics and Chemistry of Minerals*, **46**, 133–142.

Shchipalkina N.V., Pekov I.V., Chukanov N.V., Biagioni C. and Pasero M. (2019*b*) Crystal chemistry and nomenclature of rhodonite-group minerals. *Mineralogical Magazine*, **83**, 829–835.

Shi, N.-C., Ma Z.S., Li G.W., Yamnova N.A. and Pushcharovskii D.Y. (1998) Structure refinement of monoclinic astrophyllite. *Acta Crystallographica*, **B54**, 109–114.

Siidra, O.I., Krivovichev S.V. and Depmeier W. (2009) Crystal structure of Pb$_6$O[(Si$_6$Al$_2$)O$_{20}$]. *Glass Physics and Chemistry*, **35**, 406–410.

Simonov M.A., Belokoneva E.L. and Belov N.L. (1980) Refined crystal structure determination of synthetic Zn chkalovite Na$_2$Zn(Si$_2$O$_6$). *Kristallografiya*, **25**, 1282–1284.

Smith J.V. (1977) Enumeration of 4-connected 3-dimensional nets and classification of framework silicates; I, Perpendicular linkage from simple hexagonal net. *American Mineralogist*, **62**, 703–709.

Smith J.V. (1978) Enumeration of 4-connected 3-dimensional nets and classification of framework silicates, II, Perpendicular and near-perpendicular linkages from 4.8^2, 3.12^2 and 4.6.12 nets. *American Mineralogist*, **63**, 960–969.

Smith J.V. (1988) Topochemistry of zeolites and related materials. I. Topology and geometry. *Chemical Reviews*, **188**, 149–182.

Sokolova E. (2006) From structure topology to chemical composition. I. Structural hierarchy and stereochemistry in titanium disilicate minerals. *The Canadian Mineralogist*, **44**, 1273–1330.

Sokolova E. (2012) Further developments in the structure topology of the astrophyllite-group minerals. *Mineralogical Magazine*, **76**, 863–882.

Sokolova E. and Cámara F. (2008) Re-investigation of the crystal structure of magnesium astrophyllite. *European Journal of Mineralogy*, **20**, 253–260.

Sokolova E. and Cámara F. (2017) The seidozerite supergroup of TS-block minerals: nomenclature and classification, with change of the following names: rinkite to rinkite-(Ce), mosandrite to mosandrite-(Ce), hainite to hainite-(Y) and innelite-1*T* to innelite-1*A*. *Mineralogical Magazine*, **81**, 1457–1484.

Sokolova E. and Hawthorne F.C. (2016) The crystal structure of zircophyllite, K$_2$NaFe$_7^{2+}$Zr$_2$(Si$_4$O$_{12}$)$_2$O$_2$(OH)$_4$F, an astrophyllite-supergroup mineral from Mont Saint-Hilaire, Quebec, Canada. *The Canadian Mineralogist*, **54**, 1539–1547.

https://doi.org/10.1180/mgm.2020.13 Published online by Cambridge University Press

Sokolova E.V., Arakcheeva A.V. and Voloshin A.V. (1991) Crystal structure of komkovite. *Doklady Akademii Nauk SSSR*, **320**, 1384–1388.

Sokolova E.V., Hawthorne F.C. and Pautov L.A. (2000) The crystal chemistry of Li-bearing minerals with the milarite-type structure: The crystal structure of end-member sogdianite. *The Canadian Mineralogist*, **38**, 853–859.

Sokolova E., Hawthorne F.C., Ball N.A., Mitchell R.H. and Della Ventura G. (2006) Vlasovite, $Na_2Zr(Si_4O_{11})$, from the Kipawa alkaline complex, Quebec, Canada: crystal-structure refinement and infrared spectroscopy. *The Canadian Mineralogist*, **44**, 1349–1356.

Sokolova E., Cámara F., Hawthorne F.C. and Ciriotti M.E. (2017*a*) The astrophyllite supergroup: nomenclature and classification. *Mineralogical Magazine*, **81**, 143–153.

Sokolova E., Cámara F., Hawthorne F.C., Semenov E.I. and Ciriotti M.E. (2017*b*) Lobanovite, $K_2Na(Fe_4^{2+}Mg_2Na)Ti_2(Si_4O_{12})_2O_2(OH)_4$, a new mineral of the astrophyllite supergroup and its relation to magnesioastrophyllite. *Mineralogical Magazine*, **81**, 175–181.

Sokolova E., Cámara F., Hawthorne F.C. and Ciriotti M.E. (2018*a*) Redefinition of zircophyllite, ideally $K_2NaMn_7Zr_2(Si_4O_{12})_2O_2(OH)_4F$, a kupletskite-group mineral of the astrophyllite supergroup (in accord with IMA 15-B) as an astrophyllite-group mineral, ideally $K_2NaFe_7^{2+}Zr_2(Si_4O_{12})O_2(OH)_4F$ (IMA 17-D). *The Canadian Mineralogist*, **56**, 3–5.

Sokolova E., Day M.C., Hawthorne F.C. and Kristiansen, R. (2018*b*) Heyerdahlite, $Na_3Mn_7Ti_2(Si_4O_{12})_2O_2(OH)_4F(H_2O)_2$, a new mineral of the astrophyllite supergroup from the Larvik Plutonic complex, Norway: description and crystal structure. *Mineralogical Magazine*, **82**, 243–255.

Sokolova E., Day M.C., Hawthorne F.C., Kasatkin A.V., Downs R.T., Horváth L. and Pfenninger-Horváth E. (2019) Laverovite, $K_2NaMn_7Zr_2(Si_4O_{12})_2O_2(OH)_4F$, a new astrophyllite-super-group mineral from Mont Saint-Hilaire, Québec, Canada. *The Canadian Mineralogist*, **57**, 201–213.

Stepanov A.V., Bekenova G.K., Levin V.L., Sokolova E., Hawthorne F.C. and Dobrovol'skaya E.A. (2012) Tarbagataite, $(K,\square)_2(Ca,Na)(Fe^{2+},Mn)_7Ti_2(Si_4O_{12})_2O_2(OH)_4(OH,F)$, a new astrophyllite-group mineral species from the Verkhnee Espe Deposit, Akjailyautas Mountains, Kazakhstan: description and crystal structure. *The Canadian Mineralogist*, **50**, 159–168.

Strunz H. (1938) Stereochemie der Silikatmineralien. *Zeitschrift für die gesamte Naturwissenschaft*, **5**, 181–189.

Sundberg M.R., Lehtinen M. and Kivekäs R. (1987) Refinement of the crystal structure of ramsayite (lorenzenite). *American Mineralogist*, **72**, 173–177.

Tait K.T., Hawthorne F.C., Grice J.D., Jambor J.L. and Pinch W.W. (2004) Potassic-carpholite, a new mineral species from the sawtooth batholith, Boise County, Idaho, U.S.A. *The Canadian Mineralogist*, **42**, 121–124.

Takéuchi Y. and Joswig W. (1967) The structure of haradaite and a note on the Si–O bond lengths in silicates. *Mineralogical Journal*, **5**, 98–123.

Takéuchi Y. and Kudoh Y. (1977) Hydrogen bonding and cation ordering in Magnet Cove pectolite. *Zeitschrift für Kristallographie*, **146**, 281–292.

Takéuchi Y., Koto K. and Yamanaka T. (1976*a*) Crystal-chemical aspects of pyroxenoids. *The Journal of the Japanese Association of Mineralogists, Petrologists and Economic Geologists Special Paper*, **1**, 41–64.

Takéuchi Y., Kudoh Y. and Yamanaka T. (1976*b*) Crystal chemistry of the serandite-pectolite series and related minerals. *American Mineralogist*, **61**, 229–237.

Tateyama H., Shimoda S. and Sudo T. (1978) Synthesis and crystal structure of a triple chain silicate, $Na_2Mg_4Si_6O_{16}(OH)_2$. *Contributions to Mineralogy and Petrology*, **66**, 149–156.

Taylor H.F.W. (1953) Crestmoreite and riversideite. *Mineralogical Magazine*, **30**, 155–165.

Taylor H.F.W. (1964) The calcium silicate hydrates. *Chemistry of Cements*, **1**, 167–232.

Taylor H.F.W. (1992) Tobermorite, jennite, and cement gel. *Zeitschrift für Kristallographie*, **202**, 41–50.

Thompson Jr. J.B. (1978) Biopyriboles and polysomatic series. *American Mineralogist*, **63**, 239–249.

Thompson R.M., Yang H. and Downs R.T. (2016) Ideal wollastonite and the structural relationship between the pyroxenoids and pyroxenes. *American Mineralogist*, **101**, 2544–2553.

Toebbens D.M., Kahlenberg V. and Kaindi R. (2005) Characterization and ab-initio XRPD structure determination of a novel silicate with vierer single chains: the crystal structure of $NaYSi_2O_6$. *Inorganic Chemistry*, **44**, 9554–9560.

Tribaudino M., Benna P. and Bruno E. (1989) Average structure and M2 site configurations in *C*2/*c* clinopyroxenes along the Di-En join. *Contributions to Mineralogy and Petrology*, **103**, 452–456.

Upton B.G.J., Hill P.G., Johnsen O. and Petersen O.V. (1978) Emeleusite: a new LiNaFeIII silicate from south Greenland. *Mineralogical Magazine*, **42**, 31–34.

Uvarova Y.A., Sokolova E., Hawthorne F.C., Liferovich R.P. and Mitchell R.H. (2003) The crystal chemistry of shcherbakovite from the Khibina Massif, Kola Peninsula, Russia. *The Canadian Mineralogist*, **41**, 1193–1201.

Uvarova Y.A., Sokolova E., Hawthorne F.C., Agakhanov A.A., Pautov L.A. and Karpenko V.Y. (2006) The crystal chemistry of senkevichite, $CsKNaCa_2TiO[Si_7O_{18}(OH)]$, from the Dara-i-Pioz alkaline massif, northern Tajikistan. *The Canadian Mineralogist*, **44**, 1341–1348.

Uvarova Y.A., Sokolova E., Hawthorne F.C., Agakhanov A.A. and Pautov L.A. (2008) The crystal structure of nalivkinite, a new lithium member of the astrophyllite group. *The Canadian Mineralogist*, **46**, 651–659.

Uvarova Y.A., Sokolova E., Hawthorne F.C., Liferovich R.P., Mitchell R.H., Pekov I.V. and Zadov A.E. (2010) Noonkanbahite, $BaKNaTi_2(Si_4O_{12})O_2$, a new mineral species: description and crystal structure. *Mineralogical Magazine*, **74**, 441–450.

Van Derveer D.G., Swihart G.H., Sen Gupta P.K. and Grew E.S. (1993) Cation occupancies in serendibite: a crystal structure study. *American Mineralogist*, **78**, 195–203.

Veblen D.R. and Burnham, C.W. (1978*a*) New biopyriboles from Chester, Vermont: I. descriptive mineralogy. *American Mineralogist*, **63**, 1000–1009.

Veblen D.R. and Burnham C.W. (1978*b*) New biopyriboles from Chester, Vermont: II. The crystal chemistry of jimthompsonite, clinojimthompsonite, and chesterite, and the amphibole-mica reaction. *American Mineralogist*, **63**, 1053–1073.

Vigfusson V.A. (1931) The hydrated calcium silicates. I. The system CaO–SiO2–H2O. II. Hillebrandite and Foshagite. *American Journal of Science*, **21**, 67–78.

Vinogradova R.A., Sychkova V.A. and Kabalov Y.K. (1966) Manganiferous babingtonite from the Rudnyi Kaskad deposit, Eastern Sayan. *Doklady Akademii Nauk SSSR*, **169**, 434–437.

Viswanathan K. (1981). The crystal structure of a Mg-rich carpholite. *American Mineralogist*, **66**, 1080–1085.

Viswanathan K. and Seidel E. (1979) Crystal chemistry of Fe-Mg-carpholites. *Contributions to Mineralogy and Petrology*, **70**, 41–47.

Völlenkle H., Wittmann A. and Nowotny H. (1968) Die Kristallstruktur von $Li_2(Si_{0.25}Ge_{0.75})_2O_5$. *Zeitschrift für Kristallographie*, **126**, 37–45.

Voloshin A.V., Pakhomovskiy Y.Y., Men'shikov Y.P., Sokolova Y.V. and Yegorov-Tismenko Y.K. (1990) Komkovite – a new hydrous barium zirconosilicate from the carbonatites of Vuoriyarvi (Kola Peninsula). *Mineralogiceskij Zhurnal*, **12**, 69–73.

Vorma A. (1963) Crystal structure of stokesite, $CaSnSi_3O_9{\cdot}2H_2O$. *Mineralogical Magazine*, **33**, 615–617.

Voronkov A.A. and Pyatenko Y.A. (1962) The crystal structure of vlasovite. *Kristallografiya*, **6**, 755–760.

Voronkov A.A., Ilyukhin V.V. and Belov N.V. (1974) Principles of the formation of mixed frameworks and their formula. *Doklady Akademii Nauk SSSR*, **219**, 600–603.

Voronkov A.A., Ilyukhin V.V. and Belov N.V. (1975) Basic microblocks of mixed frameworks. *Koordinatsionnaya Khimiya*, **1**, 244–247.

Wagner C., Parodi G.C., Semet M., Robert J.L., Berrahma M. and Velde D. (1991) Crystal chemistry of narsarsukite. *European Journal of Mineralogy*, **3**, 575–585.

Wan C. and Ghose S. (1978) Inesite, a hydrated calcium manganese silicate with five-tetrahedral-repeat double chains. *American Mineralogist*, **63**, 563–571.

Wang P., Xu X., Zhou D., Yu X. and Qiu J. (2015) Sunlight activated long-lasting luminescence from $Ba_5Si_8O_{21}$: Eu^{2+}, Dy^{3+} phosphor. *Inorganic Chemistry*, **54**, 1690–1697.

Warren B.E. and Bragg W.L. (1928) The structure of diopside, $CaMg(SiO_3)_2$. *Zeitschrift für Kristallographie*, **69**, 168–193.

https://doi.org/10.1180/mgm.2020.13 Published online by Cambridge University Press

Watanabe T., Kato A., Ito J., Yoshimura T., Momoi H. and Fukuda K. (1982) Haradaite, $Sr_2V_2^{4+}[O_2Si_4O_{12}]$, from the Noda Tamagawa mine, Iwate Prefecture and the Yamato mine, Kagoshima Prefecture, Japan. *Proceedings of the Japan Academy*, **58**, Ser. B, 21–24.

Weber H-P. (1983) Ferrosilite, the high-temperature polymorph of $FeSiO_3$. *Acta Crystallographica*, **C39**, 1–3.

Wells A.F. (1962) *Structural Inorganic Chemistry*. 3rd Ed. Oxford University Press, UK.

Wells A.F. (1977) *Three-Dimensional Nets and Polyhedra*. Wiley, *New York*.

Wenk H.R. (1973) The crystal structure of howieite. *Naturwissenschaften*, **60**, 254–255.

Wenk H.R. (1974) Howieite, a new type of chain silicate. *American Mineralogist*, **59**, 86–97.

Wenk H.-R., Biagioni R.N., Hsiao J., Lee D.L., Tanzella F.L., Yeh S.M., Hodgson K. and Nissen H.U. (1976) Deerite, $(Fe,Mn)_{12}Si_8(O,OH)_{32}$, yet another type of chain silicate. *Naturwissenschaften*, **63**, 433–434.

Williams E.R. and Weller M.T. (2014) A variable-temperature neutron diffraction study of serandite: a Mn-silicate framework with a very strong, two-proton site, hydrogen bond. *American Mineralogist*, **99**, 1755–1760.

Woodrow P.J. (1967) The crystal structure of astrophyllite. *Acta Crystallographica*, **22**, 673–678.

Worthing M.A. (1987) Deerite from Papua New Guinea. *Mineralogical Magazine*, **51**, 689–693.

Xu H. and Boggs P.R. (1996) TEM investigation of the domain structure and superstructure in hillebrandite, $Ca_2SiO_3(OH)_2$. *American Mineralogist*, **81**, 1371–1374.

Yakovenchuk V.N., Ivanyuk G.Y., Pakhomovsky Y.A., Selivanova E.A., Men'shikov Y.P., Korchak J.A., Krivovichev S.V., Spiridonova D.V. and Zalkind O.A. (2010) Punkaruaivite, $LiTi_2[Si_4O_{11}(OH)](H_2O)$, a new mineral species from hydrothermal assemblages, Khibiny and Lovozero Alkaline Massifs, Kola Peninsula, Russia. The *Canadian Mineralogist*, **48**, 41–50.

Yakovenchuk V.N., Ivanyuk G.Y., Krivovichev S.V., Pakhomovsky Y.A., Selivanova E.A., Korchak J.A., Men'shikov Y.P., Drogobuzhskaya S.V. and Zalkind O.A. (2011) Eliseevite, $Na_{1.5}Li[Ti_2Si_4O_{12.5}(OH)_{1.5}]\cdot 2H_2O$, a new microporous titanosilicate from the Lovozero alkaline massif (Kola Peninsula, Russia). *American Mineralogist*, **96**, 1624–1629.

Yakovenchuk V.N., Krivovichev S.V., Pakhomovsky Y.A., Selivanova E.A. and Ivanyuk G.Y. (2012) Microporous titanosilicates of the lintisite–kukisvumite group and their transformation in acidic solutions. Pp. 229–238 in: *Minerals as Advanced Materials II* (S.V. Krivovichev, editor). Springer.

Yakubovich O.V., Malinovskii Y.A. and Polyakov V.O. (1990) Crystal structure of makarochkinite. *Kristallografiya*, **35**, 1388–1394.

Yamanaka T., Sadanaga R. and Takeuchi Y. (1977) Structural variation in the ferrobustamite solid solution. *American Mineralogist*, **62**, 1216–1224.

Yang H., Downs R.T. and Yang Y.W. (2011) Lithiomarsturite, $LiCa_2Mn_2Si_5O_{14}(OH)$. *Acta Crystallographica*, **E67**, i73.

Yang H., Downs R.T., Evans S.H. and Pinch W.W. (2014) Lavinskyite, $K(LiCu)Cu_6(Si_4O_{11})_2(OH)_4$, isotypic with planchéite, a new mineral from the Wessels mine, Kalahari Manganese Fields, South Africa. *American Mineralogist*, **99**, 525–530.

Yoshii M., Aoki Y. and Maeda K. (1972) Nambulite, a new lithium- and sodium-bearing manganese silicate from the Funakozawa mine, north-eastern Japan. *Mineralogical Journal*, **7**, 29–44.

Yuan X., Guowu L. and Guangming Y. (2017) Mineralogy and crystallography of stokesite from inner Mongolia, China. *The Canadian Mineralogist*, **55**, 63–74.

Zanazzi P.F., Nestola F., Nazzareni S. and Comodi P. (2008) Pyroxmangite: A high pressure single-crystal study. *American Mineralogist*, **93**, 1921–1928.

Zhao X., Li J., Chen P., Li Y., Chu Q., Liu X., Yu J. and Xu R. (2010) New lanthanide silicates based on anionic silicate chain, layer, and framework prepared under high-temperature and high-pressure conditions. *Inorganic Chemistry*, **49**, 9833–9838.

Zhitova E.S., Krivovichev S.V., Hawthorne F.C., Krzhizhanovskaya M.G., Zolotarev A.A., Abdu Y.A., Yakovenchuk V.N., Pakhomovsky Y.A. and Goncharov A.G. (2017) High-temperature behaviour of astrophyllite, $K_2NaFe_7^{2+}Ti_2(Si_4O_{12})_2O_2(OH)_4F$. A combined X-ray diffraction and Mossbauer spectroscopic study. *Physics and Chemistry of Minerals*, **44**, 595–613.

Zhizhong P., Zhesheng M. and Shaoxu H. (1987) The refinement of the crystal structure of balipholite. *Scientia Sinica Series B*, **30**, 779–784.

Zöller M.H., Tillmanns E. and Hentschel G. (1992) Liebauite, $Ca_3Cu_5Si_9O_{26}$: A new silicate mineral with 14er single chain. *Zeitschrift für Kristallographie*, **200**, 115–126.

Zolotarev Jr. A.A., Zhitova E.S., Gabdrakhmanova F.A., Krzhizhanovskaya M.G., Zolotarev A.A. and Krivovichev S.V. (2017) Batisite, $Na_2BaTi_2(Si_4O_{12})O_2$, from Inagli massif, Aldan, Russia: crystal-structure refinement and high-temperature X-ray diffraction study. *Mineralogy and Petrology*, **111**, 843–851.

Zoltai T. (1960) Classification of silicates and other minerals with tetrahedral structures. *American Mineralogist*, **45**, 960–973.

Zubkova N.V., Pushcharovsky D.Y., Giester G., Pekov I.V., Turchkova A.G., Chukanov N.V. and Tillmanns E. (2005) Crystal structures of K- and Cs-exchanged forms of zorite. *Kristallografiya*, **50**, 411–417.

Zubkova N.V., Pushcharovsky D.Y., Giester G., Pekov I.V., Turchkova A.G., Tillmanns E. and Chukanov N.V. (2006) Crystal structure of Pb-exchanged form of zorite. *Kristallografiya*, **51**, 413–416.

Zubkova N.V., Pekov I.V., Turchkova A.G., Pushcharovskii D.Y., Merlino S., Pasero M. and Chukanov N.V. (2007) Crystal structures of potassium-exchanged forms of catapleiite and hilairite. *Kristallografiya*, **52**, 65–70.

Zubkova N.V., Kolitsch U., Pekov I.V., Turchkova A.G., Vigasina M.F., Pushcharovsky D.Y. and Tillmans E. (2009*a*) Crystal chemistry of Rb-, Sr-, Ba-, Ca- and Pb-exchanged forms of natural hilairite. *European Journal of Mineralogy*, **21**, 495–506.

Zubkova N.V., Pekov I.V., Pushcharovskii D.Y. and Kazantsev S.S. (2009*b*) Crystal structure of yegorovite $Na_4[Si_4O_8(OH)_4](H_2O)_7$. *Doklady Earth Sciences*, **426**, 797–801.

Zubkova N.V., Ksenofontov D.A., Kabalov Yu.K., Chukanov N.V., Nedelko V.V., Pekov I.V. and Pushcharovsky D.Yu. (2011) Dehydration-induced structural transformations of the microporous zirconosilicate elpidite. *Neorganicheskie Materialy*, **47**, 575–581.

https://doi.org/10.1180/mgm.2020.13 Published online by Cambridge University Press